FIRE RESISTANCE OF ULTRA-HIGH STRENGTH

CONCRETE FILLED STEEL TUBULAR COLUMNS

XIONG MINGXIANG

NATIONAL UNIVERSITY OF SINGAPORE

2013

FIRE RESISTANCE OF ULTRA-HIGH STRENGTH CONCRETE FILLED STEEL TUBULAR COLUMNS

XIONG MINGXIANG

(B.ENG. Wuhan University of Science and Technology

M.ENG. Huazhong University of Science and Technology)

A THESIS SUBMITTED

FOR THE DEGREE OF DOCTOR OF PHILOSOPHY

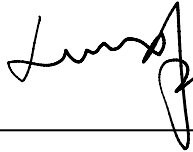**DEPARTMENT OF CIVIL AND ENVIRONMENTAL ENGINEERING**

NATIONAL UNIVERSITY OF SINGAPORE

2013

DECLARATION

I hereby declare that this thesis is my original work and it has been written by me in its entirety. I have duly acknowledged all the sources of information which have been used in the thesis.

This thesis has also not been submitted for any degree in any university previously.

Xiong Mingxiang

06 June 2013

Acknowledgements

Table of Content

Summary

The aim of this research is to evaluate the fire resistance of high strength tubular steel columns infilled with ultra-high strength concrete with compressive strength up to 160MPa. Although research work has been done on concrete filled steel tubular (CFST) columns and design codes are available for fire resistant design, guidelines on high strength steel and concrete on CFST is not available. The present research aims to extend the design codes by investigating the behaviors of these high strength materials at elevated temperatures by means of experiments and analytical methods.

High strength steel (HSS) is heat-treated from mild steel. A total of 73 specimens were tested in axial tension in order to obtain the temperature dependent mechanical properties of high strength steel. The tests were carried out based on both steady-state and transient-state methods. Compared with normal strength steel (NSS) in EN 1993-1-2, the relative thermal elongations of HSS were smaller. Elastic modulus and effective yield strength of HSS were reduced faster than NSS beyond 400°C. Thermal creep exhibited significant effect on the elastic modulus but it was not significant on the effective yield strengths. The mechanical properties obtained from the experiment were essential to determine the critical temperature and then the fire resistance time of columns with HSS.

UHSC is prone to spalling when it is subject to high temperature. Spalling behavior and residual properties of UHSC after elevated temperatures were experimentally investigated based on types of fiber, dosages of polypropylene fiber, heating rates, and curing conditions. Test results revealed that steel fiber was not effective to prevent spalling of UHSC but polypropylene (PP) fiber with dosage of 0.1% in volume was effective. Residual compressive strength and residual elastic modulus of

UHSC were affected by dosages of polypropylene fiber and heating rates but not by the curing conditions.

A total of 27 cylindrical specimens were tested to measure the temperature dependent compressive strength and elastic modulus of UHSC at elevated temperatures. Experimental evidence showed that both compressive strength and elastic modulus experienced sharp deteriorations at temperature around 100°C and then were partly recovered after heating to 300°C. Compared with normal strength concrete (NSC) and high strength concrete (HSC) in EN 1992-1-2, the compressive strength and elastic modulus of UHSC were reduced slower beyond 300°C. The tested strength and elastic modulus could be used to calculate the fire resistance of CFST columns with UHSC.

A total of 22 CFST columns of 3.81m were tested including both single-tube columns and double-tube columns. These columns were heated in accordance with ISO-834 fire. The experimental investigation focused on the varied thickness of fire protection material, cross-sectional size, boundary condition, load level, and eccentricity of load. Temperature profiles, axial deformations, fire resistance time, and failure modes were obtained from tests. The experimental observations showed that most columns were failed by the overall buckling, except for three columns by the cross-sectional failure. Transversal cracks on concrete were observed for columns failed by the overall buckling; whereas longitudinal splitting were found on columns with the cross-sectional failure. Welding tearing failure was found in one column due to the poor welding quality.

Existing simple calculation model (SCM) in EN 1994-1-2 and proposed M-N interaction model (MNIM) were used to predict the fire resistance time of CFST columns and their validity was verified by comparing test data from present research

with data from the literature. By using SCM and MNIM, the effective length of the CFST column in the fire test was derived by solving the 4th-order differential equation of the lateral displacement. The temperature profiles of columns were calculated based on finite difference method (FDM). The comparisons between tested and calculated fire resistance time indicated that MNIM exhibited more conservative and less scattered calculation data than SCM due to more reasonable consideration for the second-order effect under fire.

Parametric analyses were carried out based on the validated MNIM method and aimed to investigate the effects of strengths of steel and concrete on the fire resistance time of CFST columns. Analysis results showed that the fire resistance time of columns with UHSC was slightly higher than that of columns with NSC and HSC. The fire resistance time of columns with HSS was shorter than that of columns with NSS. The parametric analyses further indicated that the circular and square columns with single-tube would exhibit same fire resistance time if they have equal section factors. However, the circular columns exhibited slightly higher fire resistance time than the square columns in terms of equal section factors and double-tube. In addition, it is difficult to determine the superiority between the single-tube columns and the double-tube columns in fire situations. Larger section factor makes the double-tube columns exhibited shorter fire resistance time. However, the double-tube columns have smaller non-dimensional slenderness ratio which resulted in higher buckling capacity and thus higher fire resistance time.

x

List of Publications

Xiong M.X, Liew J.Y.R, Zhang M.H. Fire behavior of high strength steel tubular columns infilled with ultra-high strength concrete. The 23th KKCNN Symposium on Civil Engineering, Taipei, China, 13-15 November, 2010.

Liew J.Y.R, Xiong M.X, Xiong D.X. Ultra-high strength composite columns for high-rise buildings. The 3rd International Symposium on Innovative Design of Steel Structures, Singapore, 28 June, 2011.

Xiong M.X, Liew J.Y.R, Zhang M.H. Fire resistance of high strength steel (steady-state tests). The 7th International Conference on Steel and Aluminum Structures, Sarawak, Malaysia, 13-15 July, 2011.

Xiong M.X, Liew J.Y.R. Experimental investigation on mechanical properties of high strength steel at elevated temperatures (transient-state tests). The 10th International Conference on Advances in Steel Concrete Composite and Hybrid Structures, Singapore, 2-4 July, 2012.

Liew J.Y.R, Xiong D.X, Xiong M.X, Yu X. Design of concrete filled steel tube with high strength materials. The 9th World Congress, CTBUH, Shanghai, China, 19-21 September, 2012.

List of Tables

List of Figures

xviii

Chapter 1   Introduction

1.1 Background

1.1.1   Concrete Filled Steel Tubular Column

It is well known that concrete and steel are the most widely used construction materials in civil engineering works. The steel members have high load capacity to weight ratio, but buckling will reduce the structural efficiency as the full section capacity cannot be utilized. In addition, steel members need protection for corrosion and fire. The advantage of concrete structure is low cost. However, the concrete members are relative bulky and heavy. Due to low tensile strength, concrete members are prone to cracking under tension and to spalling at high temperature.

Steel-concrete composite structure is deemed to integrate the respective advantages of steel and concrete materials. In the present research, steel-concrete composite column is studied. There are three conventional types of steel-concrete composite columns given in EN 1994-1-1 (2004): Concrete Encased Steel (CES) column, Partially Concrete Encased Steel (PCES) column and Concrete Filled Steel Tubular (CFST) column. The types of CFST column are shown in Figure 1.1.

Compared with CFST columns, CES and PCES columns may have smaller moment capacity since the steel sections are encased by concrete, thus producing a smaller second moment of area. However, fire protection material may not be necessary for CES and PCES columns due to their inherent fire resistances from the concrete cover.

CFST columns have many advantages over conventional steel and reinforced concrete columns, such as high load bearing capacity and ductility due to confinement effect

and convenience for fabrication and construction due to permanent formwork of steel tubes (Liew, 2004&2004; Liew and Xiong, 2009).

CFST column is an economical load bearing system. Webb and Peyton (1990) investigated the costs of steel, concrete and CFST structures. These costs were calculated on a cost/meter basis. It was found that for a 10-storey building, the cost of CFST structure was around 10% higher than that of concrete structure, but only half of that of steel structure. When it comes to a 30-storey building, the cost of CFST structure was almost same with that of concrete structure, but only 40% of that of steel structure. Thus CFST structures will be more economical for high-rise buildings.

CFST column has better fire resistance than pure steel column. This is because the concrete can absorb the heat from the steel tube whereas the steel tube can prevent the concrete from spalling. Due to the retarded temperature elevation of the steel tube by infilled concrete, less fire protection material, compared with bare steel member, is applicable to achieve the required fire resistance time. Thus, the cost for fire protection is reduced (Han and Yang, 2007). CFST column also has good post-fire resistance, since the residual capacity after fire can still maintain 50%~90% of that under ambient temperature (Han and Huo, 2002).

Recently, a new type of CFST column has been developed. It is known as the concrete filled double-skin tubular (CFDST) column. The CFDST column comprises two concentrically placed steel hollow tubes. Concrete is filled into the gap between the external tube and internal tube and/or into the inner tube. The CFDST columns have good fire resistance since the inner tube can take over the load from the external tube which would be sacrificed in fire. The CFDST columns are used in building structures, piers, electricity transmission tower, lampstandard, and cable-stayed

bridges. In the current research, the CFST columns with both single-tube and double-tube are studied.

1.1.2 Fire Hazard

Fire is the rapid oxidation of a combustible material releasing heat, light, and various reaction products such as carbon dioxide and water. Fire starts when a combustible material with an adequate supply of oxygen is subjected to enough heat and is able to sustain a chain reaction. Combustible material, oxygen and heat are commonly called as a fire tetrahedron. Fire can be extinguished by removing any one of the element of the fire tetrahedron. For example, fire extinguishing by application of water is to remove heat from the fuel since the heat is depressed by water faster than the combustion generates it. Fire extinguishing by application of carbon dioxide is to starve the fire of oxygen. Fire extinguishing by removal of the fuel is to starve the fire of combustible material. In fire engineering, the hazard is typically prevented by the following means.

(1) Education

This is to ensure that building owners and operators understand the applicable building and fire codes, have a purpose-designed fire safety, and know the building's weak spots and strengths to ensure the highest possible level of safety.

(2) Active fire protections

These are manual and automatic detection and suppression of fires, such as fire sprinkler system, fire extinguisher, fire alarm or smoking detector.

(3) Passive fire protection.

These are fire-resistance rated wall and floor assemblies that form fire compartments to limit the spread of fire. There are fire insulation materials to protect structural members. There are novel materials to improve the inherent fire resistance of structural members.

1.1.3 Concrete Filled Steel Tubular Column in Fire Hazard

As mentioned above, fire protection materials may not be necessary for CES or PCES columns since the steel section is well insulated by the covering concrete. However, for CFST columns, fire protection material could be required and the thickness of fire protection material depends on the required fire rating (FR).

Generally, the fire behavior of CFST columns depends on the external force and the duration of the fire. The typical longitudinal displacement of CFST column, changing with fire exposure time, is shown in Figure 1.2.

Before the column is heated, the loads, carried by the steel tube and concrete core, are distributed based on the steel contribution ratio. During the stage I of fire exposure, the temperature of steel tube rises faster than concrete due to its direct exposure to fire and higher thermal conductivity. Higher temperature gives higher thermal expansion. As a result, the steel tube tends to take more external load than concrete.

At stage II of fire exposure, the strength of the steel tube is gradually reduced as temperature increases. As a result, the column contracts, and the load taken by the steel tube is gradually redistributed to the concrete and/or inner tube. This contraction

is often accompanied by a local bulging of the steel tube and sometimes weld tearing for welded steel tubes.

At stage III of fire exposure, the concrete and/or inner tube fully takes over the load from the external steel tube. The strengths of concrete and/or inner tube decreases as fire exposure time increases. Ultimately the column fails when the concrete and/or inner tube can no longer bear the external load. The ultimate failure modes can be either buckling failure or cross-section failure. Accordingly, the crack on the surface of concrete can be either transverse cracking or longitudinal splitting.

The fire resistance of CFST column depends on a number of factors, such as the load level, the cross-sectional dimensions, concrete strength, steel strength, thickness of steel tube, type of fire protection material, thickness of fire protection material, boundary conditions, and so on.

1.2 Motivation and Objectives

The need for sustainable construction is hastened around the world aiming to reduce the consumptions of construction materials. Especially in Singapore, the situation is to reduce concrete consumption by 50% in a 5-year's timeframe according to Ministry of National Development after the ban on Indonesia's export of sand in recent years. Some ways to achieve this is to replace the conventional concrete with more sustainable non-concrete alternatives such as steel, or to use higher strength concrete. Regarding concrete, the production of ultra-high strength concrete (UHSC) with compressive strength greater than 140MPa becomes possible with the development of concrete technology and availability of a variety of materials such as silica fume and high-range water-reducing admixtures. However, its application has been currently

limited to special applications such as offshore and marine structures, industrial floors, pavements, and security barriers. In terms of steel, the production of high strength steel (HSS) with tensile strength around 800MPa becomes possible with the development of metallurgical technology and availability of a variety of alloy elements. However, HSS are mostly used in cars, trucks, cranes, bridges, roller coasters and other structures that are designed to handle large amounts of stress or need a good strength-to-weight ratio.

UHSC and HSS have not been used in building structures. Because there are some concerns relating to the use of HSS, such as fire-safety requirements, corrosion protection, long term durability and maintenance issues which have a significant impact on sustainable development. Also, there are concerns on the brittleness and spalling behavior of UHSC. These concerns may be attributed to the current state-of-the art design codes only allow the use of normal strength steel with a grade not higher than S460 and concrete strength only up to C50/C60 (EN 1994-1-1, 2004).

UHSC is deemed to be prone to spalling under high temperatures; whereas the strength of HSS deteriorates very fast under fire, especially for heat-treated HSS. Therefore, research is necessary to evaluate the behaviors of HSS and UHSC under high temperatures. In addition, the fire behavior of composite columns with UHSC and HSS also needs to be investigated when it is used as load bearing systems in high-rise building structures. Overall, the motivation of this research is to extend the design code to the application of UHSC and HSS for column construction in high-rise buildings. The research objectives are given as follows.

(1) Determine the mechanical properties of UHSC at elevated temperatures

(2) Determine the residual mechanical properties of UHSC after heating

(3)   Determine the mechanical properties of HSS at elevated temperatures

(4)   Investigate experimentally the fire resistance of CFST columns with UHSC and HSS

(5)   Calibrate the existing method in the design code and develop a new method to calculate the fire resistance of CFST columns with UHSC and HSS

(6)   Provide design recommendations on the application of CFST columns with UHSC and HSS

1.3 Overview of Contents

Chapter 1 gives the background knowledge about CFST columns, fire hazards, and the behavior of CFST columns under fire hazards. The research motivation and objectives are also introduced.

Chapter 2 presents the literature review on the mechanical properties of UHSC at and after exposure to elevated temperatures, mechanical properties of HSS at elevated temperatures, and the fire behavior of CFST columns.

Chapter 3 introduces the experimental study on the mechanical properties of HSS at elevated temperatures and the comparisons with those of normal strength steels (NSS) as given in EN 1994-1-2. The investigated mechanical properties include relative thermal elongations, elastic modulus, effective yield strengths, and stress-strain curves. The critical temperature of HSS is also discussed.

Chapter 4 introduces the experimental investigation on the mechanical properties of UHSC after exposure to elevated temperatures. The investigated mechanical properties are residual elastic modulus, residual cylindrical compressive strength. The

spalling behavior of UHSC under fire is also investigated. Accordingly, the effective dosage of polymer fiber for prevention of spalling is recommended.

Chapter 5 presents the experimental study on the mechanical properties of UHSC at elevated temperatures and comparisons with those of NSC and HSC as given in EN 1992-1-2. The investigated mechanical properties include elastic modulus and cylindrical compressive strength.

Chapter 6 presents the experimental results of CFST columns under standard ISO-834 fire. The details of tested CFST columns and supports, concrete casting, steaming holes, thermocouples, test setup, test procedure and failure criteria are introduced. The test results including temperature profiles of columns, axial deformation, fire resistance time, and failure modes are discussed.

Chapter 7 introduces the existing simple calculation model (SCM) in EN 1994-1-2 and the proposed M-N interaction model (MNIM) for fire resistant design of CFST columns. The effective lengths of CFST columns in fire test are derived. Finite difference method (FDM) is introduced for calculating the temperature profiles of CFST columns. The validations for FDM, SCM and MNIM are presented. Parametric analysis is introduced and the design recommendations are given.

Chapter 8 draws the conclusions for the current research, and proposes the future work to be done.

concrete
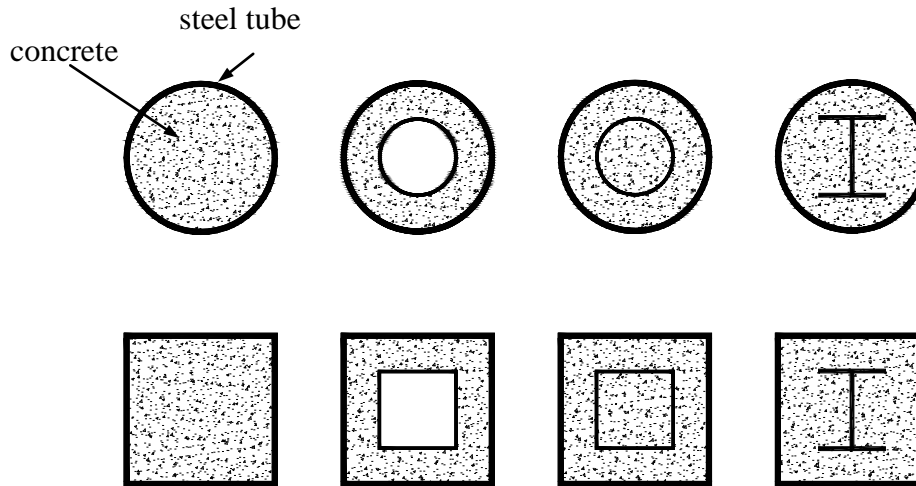
steel tube

Figure 1.1: Types of concrete filled steel tubular columns

Stage I   Stage II   Stage III

Longitudinal displacement of column under fire

Contraction | Expansion

Fire exposure time
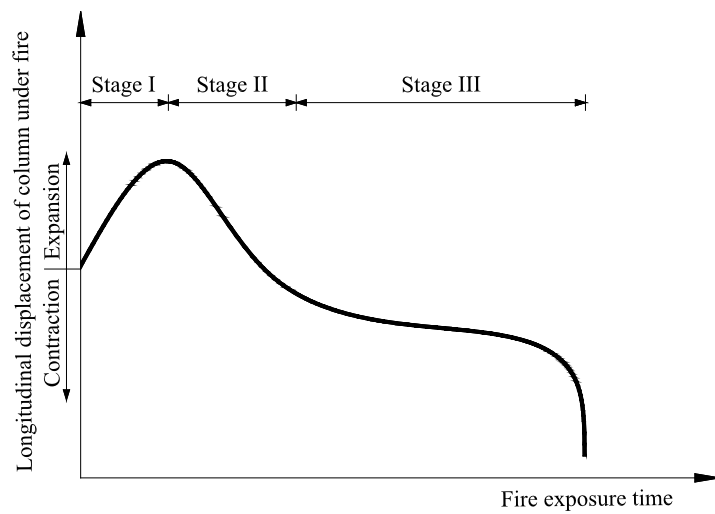
Figure 1.2: Typical longitudinal displacement of CFST column exposed to fire

Chapter 2   Literature Review

2.1 Overview

The literature review presents the mechanical properties of concrete at/after elevated temperatures, mechanical properties of steel at elevated temperatures, spalling behavior of high strength concrete (HSC) at high temperature. The reviewed mechanical properties of both concrete and steel include compressive strength, tensile strength, elastic modulus, and stress-strain curves. Then, the previous studies on the fire behavior of concrete filled steel tubular columns are reviewed, including both experimental studies and numerical analyses. Finally, the current guidelines for fire resisting design of CFST columns are introduced.

2.2 Mechanical Properties of Concrete at Elevated Temperatures

The compressive strength under high temperatures has been investigated since the 1940s (Menzel, 1943; Binner, 1949; Malhotra, 1956; Saemann, 1957). Since then, a number of tests have been done. Through these tests, it was found that the compressive strength under high temperature was affected by the type of aggregate (Abrams, 1971; Sullivan and Shanshar, 1992; Hammer, 1995). Siliceous aggregate concrete had greater strength loss than concrete with carbonate aggregate, whereas firebrick aggregate resulted in superior performance. The replacement of normal weight coarse aggregate with light-weight aggregate did not seem to affect the strength loss.

The strength was also found to be affected by heating rate (Diederichs et al., 1988). Higher heating rate normally induced lower strength and was more likely to induce

10

spalling of concrete. Furthermore, the strength loss of HSC was larger than that of NSC (Lie, 1992; Furumura et al., 1995; Felicetti et al., 1996; EN 1992-1-2, 2004).

The elastic modulus is normally governed by aggregate type and water/cement ratio (Li et al., 2006). The higher the water/cement ratio is, the larger the modulus loss is. The curing condition also affected the modulus loss. The specimen cured in humidity room had larger modulus loss than that cured in air (Castillo and Durani, 1990). Furthermore, the modulus loss of NSC was larger than that of HSC (Diederichs et al., 1988; Hammer, 1995; Furumura et al., 1995).

Some test results of compressive strength and elastic modulus at elevated temperatures are shown in Figure 2.1, Figure 2.2 and Figure 2.3. There are two tests with concrete strength higher than 100MPa plotted in Figure 2.2. It can be seen that the reduction factors of compressive strength with strength equal to 118MPa at room temperature are smallest. Its reduction factor is about 0.15 which is about one third of that of NSC with siliceous aggregate as given in EN 1992-1-2 (2004). The reduction factors of compressive strength with strength equal to 106.6MPa at temperatures higher than 400°C even could not be obtained in Diederich's test (1988) due to spalling. Regarding elastic modulus as shown in Figure 2.3, HSC with compressive strength higher than 100MPa shows similar reduction factors to those of NSC.

For stress-strain curves of concrete at elevated temperatures, it includes three stages:

(1)　The stress linearly increases before half of the peak stress is achieved.

(2)　The stress further increases, but with changed modulus. Compared with stress-strain curves at higher temperatures, the peak stress is reduced and the strain corresponding to peak stress is increased due to the developed cracks.

(3)   The stress is gradually reduced after peak stress. Because of the development of

cracks, normally there is no obvious brittle failure under high temperature. The

higher the temperature is, the more ductile the failure is; the higher the strength

is, the more brittle the failure is.

Some experimental work has been done on the stress-strain curves of concrete at

elevated temperatures in literature. Among those researches, the stress-strain curves

from Lie and Allen (1974), Cheng and Kodur (2004) and EN 1992-1-2 (2004) are

mostly used in numerical analyses.

The comparison between the stress-strain curves of NSC at elevated temperatures in

Lie and Allen's test and those as given in EN 1992-1-2 is shown in Figure 2.4. It can

be seen that the compressive strength is not reduced until 400°C in Lie and Allen's

model, whereas the strength decreases from 200°C in EN 1992-1-2. Overall, Lie and

Allen's model shows the slower reductions of strengths and larger strains

corresponding to peak stresses.

The comparison between the stress-strain curves at elevated temperatures of HSC in

Cheng and Kodur's tests and those as given in EN 1992-1-2 is shown in Figure 2.5. It

can be seen that the elastic modulus and compressive strength of HSC in both Cheng

and Kodur' model and EN 1992-1-2 are similar when the temperature is lower than

200°C. Beyond 200°C, both elastic modulus and compressive strength as given in EN

1992-1-2 are smaller than those shown in Cheng and Kodur' model. It can also be

seen that the compressive stress after peak strength in Cheng and Kodur's model

drops faster than that as given in EN 1992-1-2, which shows more brittle behavior.

2.3 Spalling of High Strength Concrete at Elevated Temperature

It is well known that HSC is prone to spall under high temperature. The spalling is caused by thermal stress due to temperature gradient during heating, and the splitting force by release of vapor water around 100°C. It is reported that the addition of metal fiber or polymer fiber is effective to prevent spalling of HSC under high temperatures (Kalifa et al., 2001; Chen and Liu, 2004; Han et al., 2005&2009; Zeiml et al., 2006; Xiao and Falkner, 2006; Hadi, 2007).

However, the effect of fiber on spalling has not been reported for UHSC. Since UHSC is more likely to spall than HSC, it is necessary to investigate its spalling behavior and then give recommendations for the prevention of spalling.

2.4 Mechanical properties of Concrete after Heating

The residual strength and elastic modulus of concrete are measured after the specimen is cooled down to room temperature. There are three types of residual strength/modulus: unstressed without pre-load, heated-stressed, stressed-heated (RILEM, 2007). The unstressed residual properties are mostly investigated.

Through the previous research, it was found that the residual strength and modulus were affected by the type of aggregate, heating rate, cooling process, cylinder size, concrete grade (Abrams, 1971; Hertz, 1984&1991; Morita et al., 1992; Sullivan and Shanshar, 1992; Felicetti et al., 1996).

Siliceous aggregate had the largest loss of residual strength and elastic modulus; whereas higher heating rate affects in the same way. Furthermore, smaller size of

cylinder gives larger loss of residual strength. For the effect of concrete grade, the residual strength and elastic modulus of HSC were reduced faster than those of NSC.

Some experimental results are given in Figure 2.6 and Figure 2.7. It is found in Figure 2.6 that the residual compressive strength of HSC is generally reduced faster than NSC, except that from Hertz's tests where concrete strength was about 150MPa. Compared with the reduction factors of compressive strength at elevated temperatures as given in Figure 2.1, the residual compressive strength shows faster degradation.

The elastic modulus of concrete after elevated temperatures as plotted in Figure 2.7. It is found that the reduction factors of elastic modulus are similar for concrete of different grades, except those from Hertz's tests.

2.5 Mechanical Properties of Steel at Elevated Temperatures

Fire has significant influence on the mechanical properties of steel due to its good conductivity. In literature, Kirby and Preston (1988), Lie and Chabot (1990), Outinen et al. (2001), Poh (2001) and Schneider (2010) investigated the high temperature mechanical properties of hot rolled steel plates with grades less than S460. Cold-formed steels have been studied by Outinen et al. (2001) and Chen and Young (2007), and fire resistant steel by Kelly and Sha (1999). Generally, the yield stress and elastic modulus are reduced with elevating temperature.

For normal strength steel (NSS), the length of the plastic plateau is shortened with increasing temperature; and there is no obvious plastic plateau after 500°C. The post-yield stress increases in the range of 180°C~370°C due to the blue brittleness as shown in Figure 2.8 (Harmathy, 1970).

Due to the disappearance of plastic plateau, proof stress is defined as yield stress. In BS5950: Part 8 (2003), there are three proof stresses provided: 2% proof stress is used for protected flexural composite members; 1.5% proof stress is used for unprotected flexural members; 0.5% proof stress for others. In EN 1993-1-2 (2005) and EN 1994-1-2(2005), 2% proof stress is used for all steel members under fire.

In order to investigate the behavior of steel structures under fire, various stress-strain-temperature (σ-ε-T) relationships are used in the world. These relationships could be bilinear (Jeane, 1985; Contro et al., 1988), tri-linear (Corraddi et al., 1990), or quadrolinear (Ianizzi et al., 1991). There are also models using an elliptical curve to approximate the transition between proportional stress and yield stress (Furumura, 1986; Purkiss, 1988; Rubert and Schaumann, 1988). The most widely used models for NSS are from Lie and Chabot (1990), Poh (2001) and EN 1993-1-2 (2005). The comparisons are shown in Figure 2.9.

The Lie and Chabot's model was developed for hollow steel tubes without concrete infill. It implicitly includes the effects of creep at elevated temperatures. For the model as given in EN 1993-1-2, there is no strain-hardening stage, and is more complicated than Lie and Chabot's model because more parameters are involved. The Poh's model was developed by rigorous testing of steel coupons. Hence the curves are more close to realistic situations as shown in Figure 2.9. However, it focused on the short-term behavior, and creep was not included.

It is noted that the design guildlines for applications of hot-finished carbon steels with grades up to S460 at ambient temperature are presented in EN 1993-1-1 (2005). Accordingly their mechanical properties under high temperatures are given in EN 1993-1-2 (2005). Although EN 1993-1-12 (2007) gives some supplementary rules for

the applications of steels with grades greater than S460 up to S700 at ambient temperature, their mechanical properties at elevated are not provided. Therefore, further investigations of HSS materials at elevated temperatures are essential to fill the research gap and then to extend their use in building construction.

HSS is conventionally taken as having a minimum yield strength greater than $460N/mm^2$ (Graham, 2006). The main advantages of HSS are savings in costs of steel material and welding consumables by means of reducing material consumption. There are limited research on the fire behavior of HSS. Kirby (1995) and Li et al. (2002) tested high strength bolt (HST) at high temperatures to gain knowledge on bolted connections in fire. Chen et al. (2006) tested heat-treated high strength steels. The yield strength of steel in tests conducted by Chen et al. (2006), named BISPLATE 80, was about 790 MPa. It was quenched and tempered from mild steel, and tested in both steady-state and transient-state methods. The test results showed a lower reduction in elastic modulus and yield strength at elevated temperatures than NSS as in EN 1993-1-2. However, the adverse effect on strength due to high temperatures as described in the technical manual of BISPLATE (2006) was not observed when the tempering temperature of the steel was exceeded.

2.6 Fire Resistance of Concrete Filled Steel Tubular Columns

2.6.1   Experimental Studies

The experimental investigations on the fire resistance of concrete filled steel tubular columns were started from 1970s. The National Research Council of Canada (NRCC) is one of such research groups. In their tests, sizes of column, types of concrete and

steel, load ratios and boundary conditions were considered. After that, some papers, reports and design guides have been published.

For instance, Lie and Caron (1988 & 1988) experimentally investigated the fire resistances of circular hollow steel columns filled with carbonate or siliceous aggregate Concrete. Lie and Iwin (1991&1992), Lie and Dawod (1992), Lie and Denham (1993, 1993), and Kodur (1996&1996) carried out experimental and theoretical studies to predict the fire resistances of circular, square and circular hollow steel section columns filled with plain concrete, bar-reinforced concrete, and steel-fiber-reinforced concrete. It can be obtained from their research that, of the various variables, the column section size and the load ratio have the greatest influence on the fire resistance of the column. The effective length, concrete strength, type of aggregate, and the concrete cover to steel reinforcement for longer columns have a moderate influence. The influence of steel reinforcement is small, and the concrete cover to steel reinforcement for shorter columns as well as that of the thickness of steel wall is insignificant.

The research group of Han (2007) started fire research of composite columns from 1990s in China. The considered parameters included the perimeter of the cross section, slenderness ratio, steel contribution ratio, percentage of steel reinforcement, eccentricity, strengths of concrete and steel, and ratio between height and width of the cross section. The research results showed that the size of cross section and slenderness ratio had greatest influence on the fire resistance of composite columns. These conclusions were similar to that obtained by NRCC.

The researchers in Japan (Sakumoto Y, et al., 1994) have carried out the standard fire tests on square CFST columns made from fire-resistant (FR) steel and insulated with

different types of fire protection. The experimental investigations focused on the effects of axial load ratio and eccentricity. The authors reported that the unprotected FR steel CFST columns failed by inelastic buckling after 30min, whereas fire protected FR steel CFST columns sustained for more than 120 min. Furthermore, the fire protected FR steel and conventional steel CFST columns had comparable fire resistance times.

Recently, sixteen tests on slender circular hollow section columns filled with NSC and HSC, subjected to concentric axial loads and standard fire, have been conducted by Romero et al. (2011). The concrete strength ranged from 30MPa to 80MPa. The results evidenced some limitations in the simple calculation model given in EN 1994-1-2 when predicting the axial buckling load of slender CFST columns under fire, for both NSC and HSC. It was recommended that the simple calculation model should be revised based on their findings.

Currently, high strength concrete is more and more widely used in civil constructions. Hence, its fire behavior becomes a concern for engineers. It was reported (Kodur, 1998, Patterson et al., 1999; Feng et al., 2001) that the fire resistance time of CFST column with NSC is nearly three times that of HSC when other conditions are the same. The addition of steel fibers into HSC can significantly improve fire behavior.

Self-consolidating high strength concrete has now been developed and investigated due to its high workability and flowability. For construction of self-consolidating concrete, no vibration is needed during construction. When it comes to the fire behavior of CFST column with high strength self-consolidating concrete, it is found that the fire resistance is comparable to that of conventional CFST column with NSC (Lu et al., 2009 & 2010).

18

As the concrete filled double-skin tubular (CFDST) column is developed, its fire behavior has been studied (Lu et al., 2010). It was found that CFDST columns can have higher critical temperatures on outer steel tubes than CFST columns. Thus, CFDST columns may have better fire endurance. The outer perimeter and cavity ratio are the main factors to govern the fire resistance of CFDST columns.

2.6.2   Numerical Studies

Besides the experimental work mentioned above, many numerical analyses have been done with the increasing development of computer technology (Kodur, 1996; Wang, 2000; Zha, 2003; Tan et al., 2004; Ding and Wang, 2005&2008; Hong and Varma, 2008; Yu et al., 2009; Schaumann et al., 2006 & 2009; Espinos, 2010). Numerical analysis is getting more and more popular since it can greatly save material costs, labor costs, and time consuming.

EN 1994-1-2 (2004) gives the guidelines to calculate the fire resistance of composite columns, with the assumptions that the buckling curve "c" is adopted. The coefficient of effective length is 1.0 for a simply supported column and 0.5 for a fixed one respectively. However, it was reported that the buckling curve "a" seemed to give more accurate results (Wang, 1997). And the coefficient of effective length could be 0.75 for fixed-fixed columns, 0.8 for pin-fixed columns due to the local buckling at the ends of the column (Colin, 2000).

2.6.3   Design Codes

With regard to Eurocodes, the guidance for fire resistance design of CFST columns is provided in EN 1994-1-2 (2004). There are two methods: simple calculation model

(SCM) and advanced calculation model (ACM). SCM is similar to the simplified design method for CFST columns under axial compression at room temperature design situations, except that the mechanical properties of materials at elevated temperatures are used. SCM is only used for columns in braced frames and for concrete filled hollow sections exposed to fire all around the column according to standard temperature-time curve. In addition, it is only applicable for square and circular sections at the following conditions:

Buckling length			$\leq$	4.5m
140mm	$\leq$	depth or diameter of cross-section	$\leq$	400mm
C20/C25	$\leq$	concrete grades	$\leq$	C40/C50
0%	$\leq$	percentage of reinforcing steel	$\leq$	5%
Standard fire resistance			$\leq$	120min

It is applicable for CFST columns under axial compression and the eccentricity of axial compression not greater than 0.5 times the side length or diameter of the cross-section. It is also applicable for CFST columns infilled with reinforced concrete. The load eccentricity and reinforcing bars inside concrete are taken into account through amplifying the external axial load by two parameters which can be obtained by charts given in Figure H.1 and Figure H.2 of EN 1994-1-2. There is a contradiction from using these two parameters. The external axial load is amplified by 2.5 times even when there are no load eccentricity and reinforcing bars inside concrete. The SCM is not applicable for CFST columns with both external bending moment and axial load.

ACM is capable of providing a realistic analysis of structures exposed to fire. It is based on fundamental physical behavior in such a way as to lead to a reliable approximation of the expected behavior of the relevant structural component under fire situation. Compared with SCM, ACM gives an improved approximation of the actual structural behavior under fire situations. Especially, it can provide information concerning stress and strain evolution, deformations and/or temperature fields. ACM is a more general method since it is applicable for individual members, subassemblies, or entire structures with any type of cross-section. However, it may resort to advanced computation technology such as commercial finite element softwares and involve more complicated geometric and material models compared with SCM. ACM is not used in current research because the detailed material stress-strain models of UHSC have not been obtained through experiments which were limited by testing facilities.

When it comes to American codes, the guidance for fire resistance design of CFST columns is provided in ASCE/SFPE 29-99 (2000). The fire resistance time is calculated based on an empirical equation which is regressed from column tests done by the National Research Council of Canada (Kodur and Lie, 1995; Kodur and Lie, 1997; Kodur and Makinnon, 2000). Since the equation is based on actual column tests, its application is limited. Following restrictions are placed on the use of the equation:

(1) The calculation is limited to columns requiring a fire resistance rating of 2 hours or less.

(2) The 28 day compressive strength of the fill concrete must be between 20MPa and 40MPa.

(3) The column effective length must be between 2m and 4m.

21

(4) Circular sections must have a diameter between 140mm and 406 mm.

(5) Square and rectangular sections must have a side length between 140mm and 305mm.

(6) Compressive force shall not exceed the design strength of the concrete core at ambient temperatures determined in accordance with the AISC LRFD "Specification for Structural Steel Buildings".

(7) Vent holes must be provided at the top and bottom of the column section to relieve steam pressure.

The equation is not applicable for high strength materials and for CFST columns with both bending moment and axial compression. The advanced method of analysis is also provided in ANSI/SISC 360-05 (2005) which is similar to the advanced calculation model given in EN 1994-1-2.

2.7 Summary

Based on the forgoing literature review on high temperature mechanical properties of concrete and steel, fire behavior of CFST columns, and design guildelines, some findings can be summarized as follows.

(1) Strength and elastic modulus of concrete decrease with increasing temperature. Strength and elastic modulus of HSC are reduced faster than NSC. HSC is prone to spall under high temperature. However, this can be prevented by the addition of metal or polymer fibers.

(2) As temperature increases, the peak stress of concrete is reduced and the strain corresponding to peak stress increases due to the developed cracks. Both for NSC and HSC, the stress-strain model given in EN 1992-1-2 generally shows faster reductions of elastic modulus and strength than Lie and Allen's model (NSC) and Cheng and Kodur' model (HSC).

(3) Residual compressive strength of HSC is reduced faster than NSC. Residual strength after exposure to high temperature shows faster degradation than the strength at high temperature. The reduction factors of elastic modulus are similar for concrete of various grades.

(4) As temperature increases, yield stress and elastic modulus of steel decreases. For NSS, the post-yield stress increases at temperatures $180^{o}C \sim 370^{o}C$ due to blue brittleness. Creep has a significant effect on the performance of steel in fire.

(5) UHSC and HSS are innovative construction materials. There is little information about their fire behaviors which have not been incorporated into design codes.

(6) Eurocodes and American codes provide methods for the design of CFST columns in fire situations. However, they are not applicable for columns with high strength materials and subjected to both bending moment and axial compression.

(7) CFST columns under fire have been broadly investigated based on both experiments and numerical analyses. CFDST columns are innovative and only a few columns have been tested under fire. Overall, CFST and CFDST columns with UHSC and HSS have not been studied. Thus, it is necessary to carry out research to propose guidelines for incorporation into design codes.
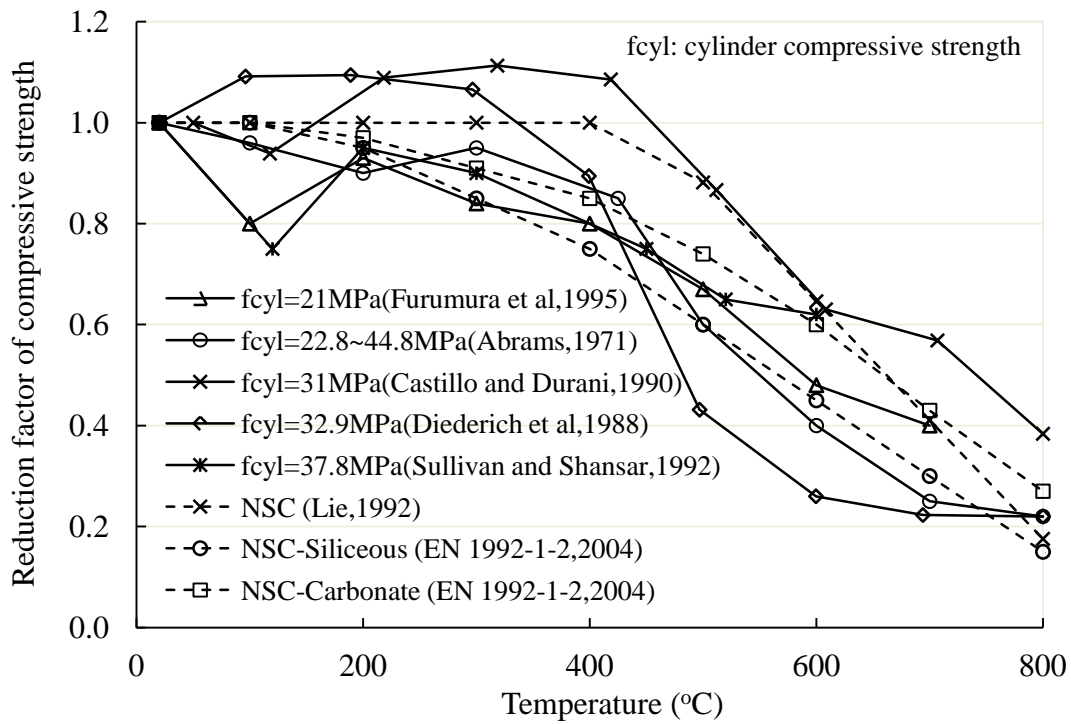
Figure 2.1: Reduction factor of compressive strength of NSC at elevated temperatures
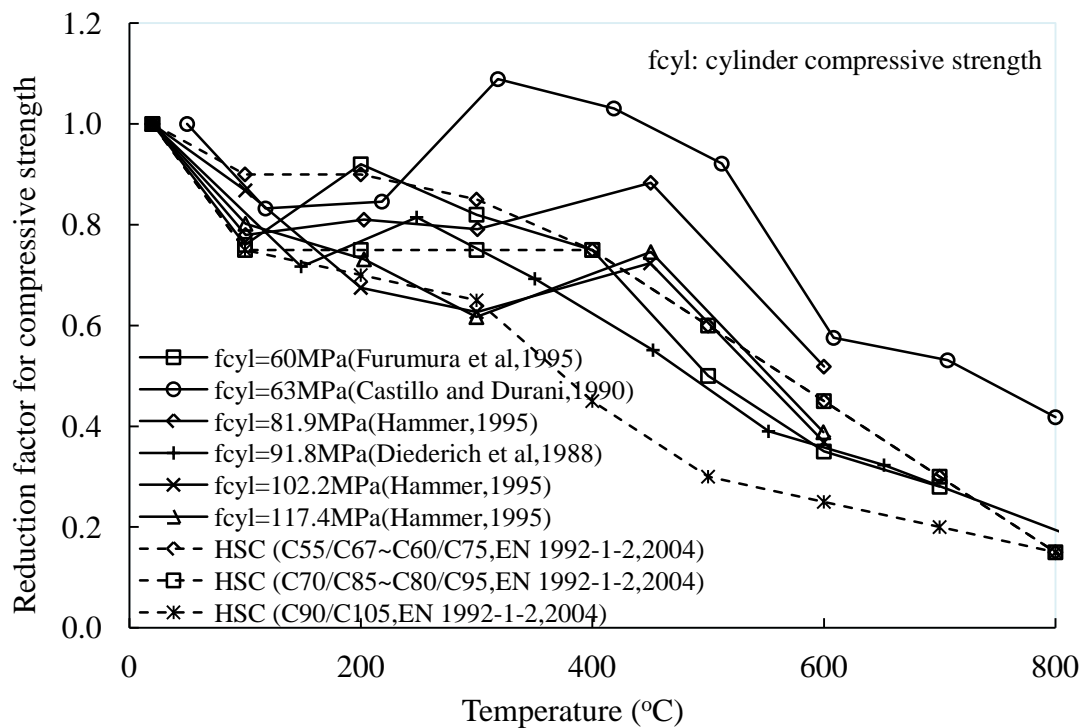
Figure 2.2: Reduction factor of compressive strength of HSC at elevated temperatures
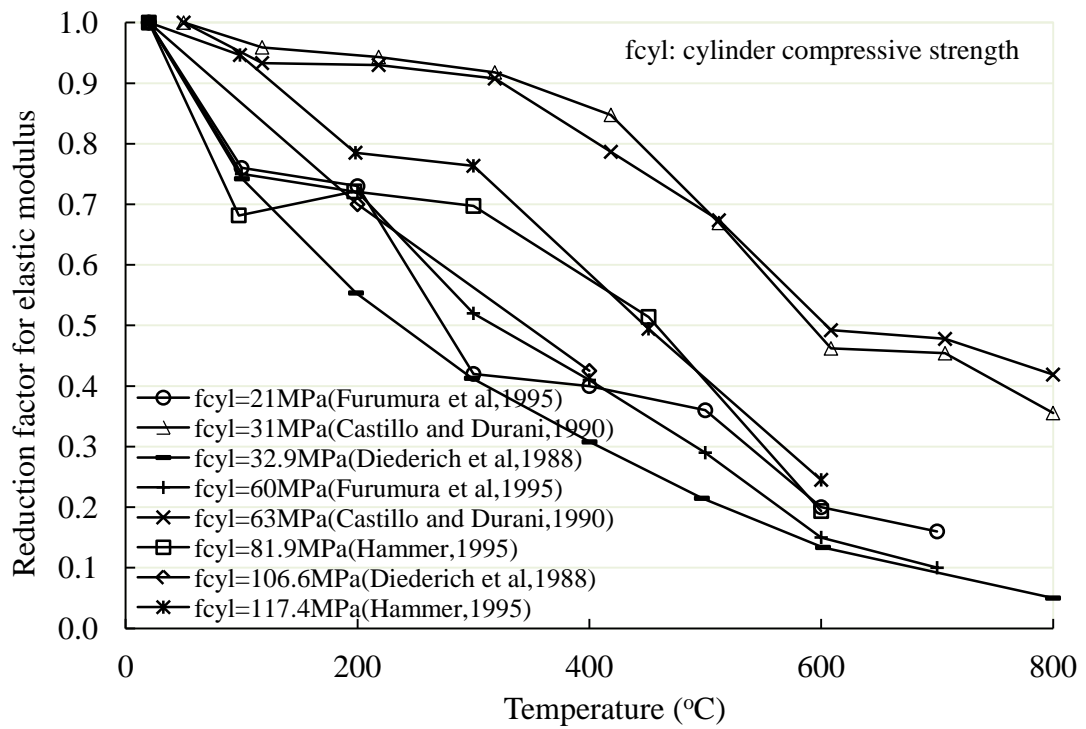
Figure 2.3: Reduction factor of elastic Modulus of concrete at elevated temperatures
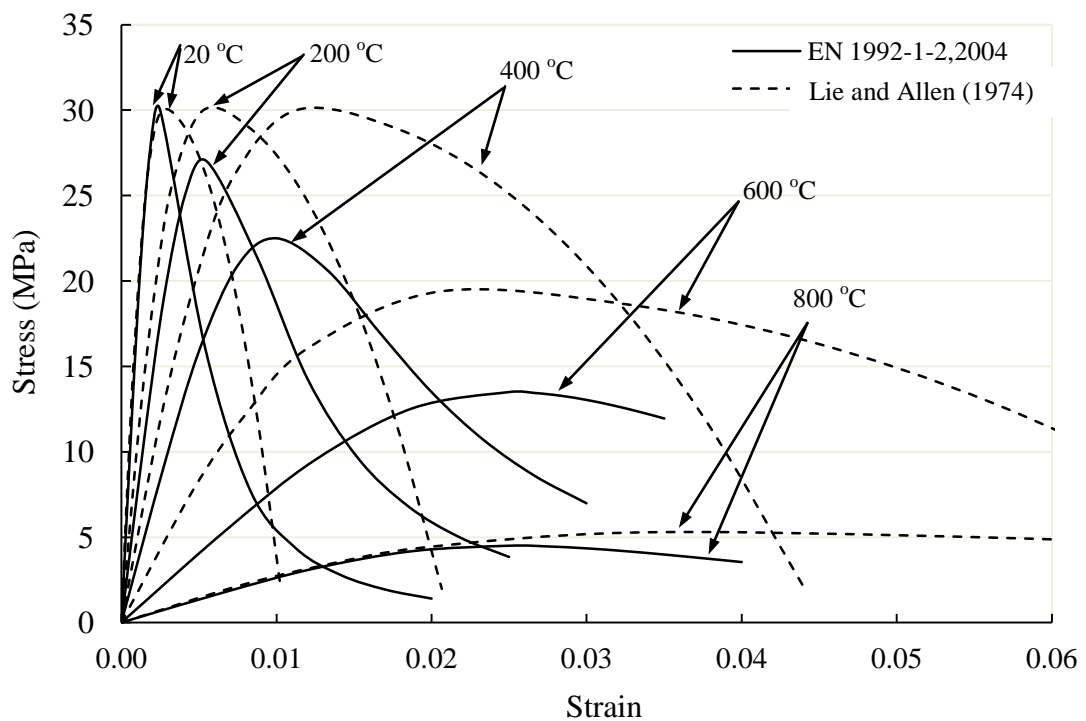
Figure 2.4: Stress-strain curves of NSC at high temperatures
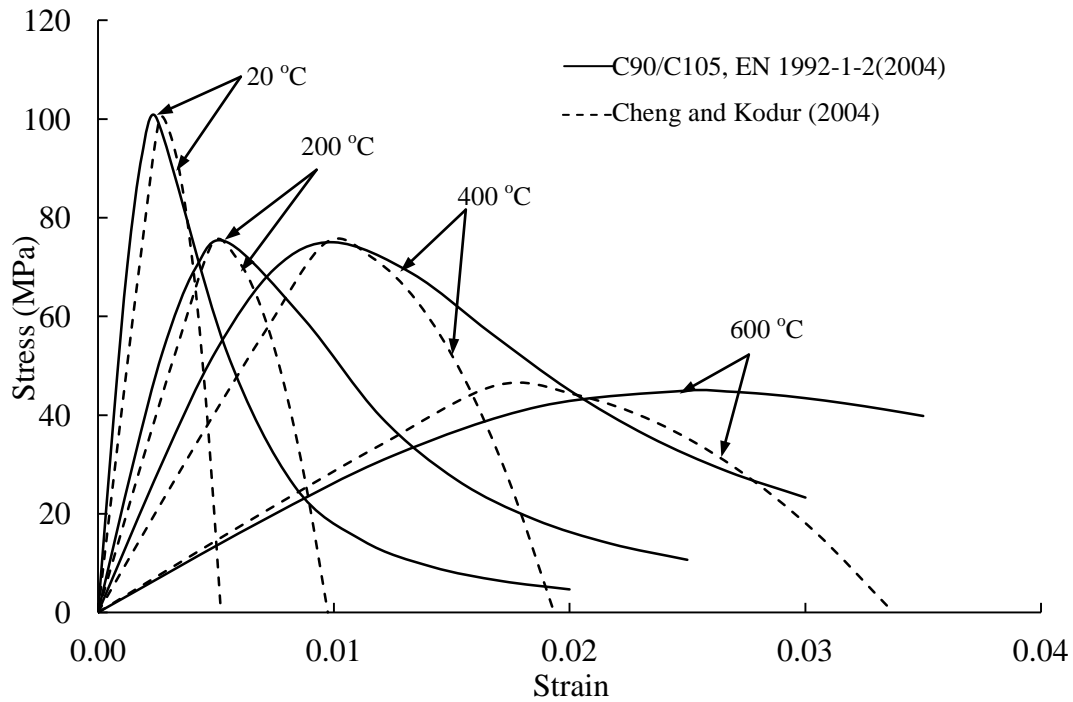
Figure 2.5: Stress-strain curves for HSC at high temperatures
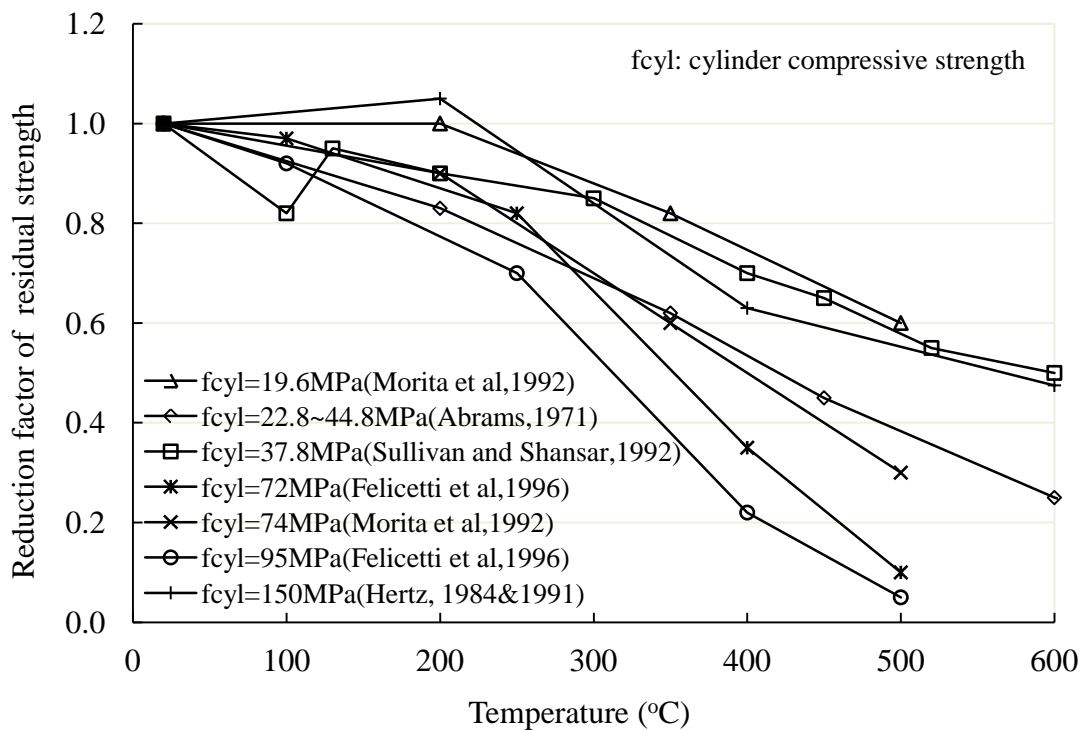
Figure 2.6: Reduction factors of unstressed residual compressive strength
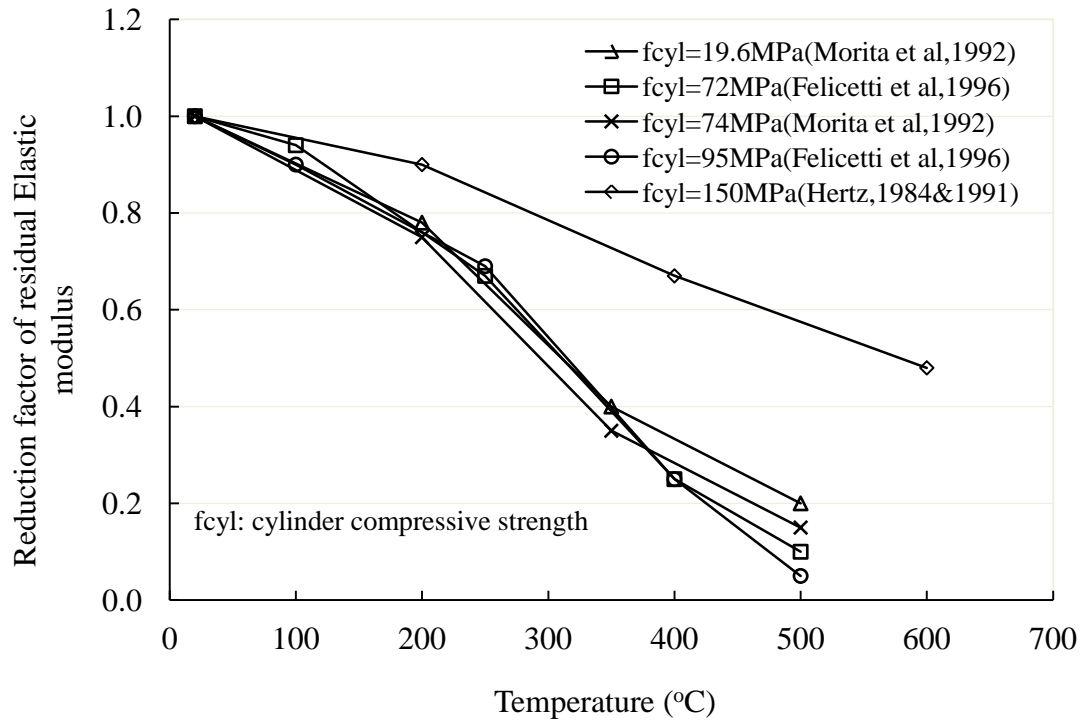
Figure 2.7: Reduction factors for unstressed residual elastic modulus
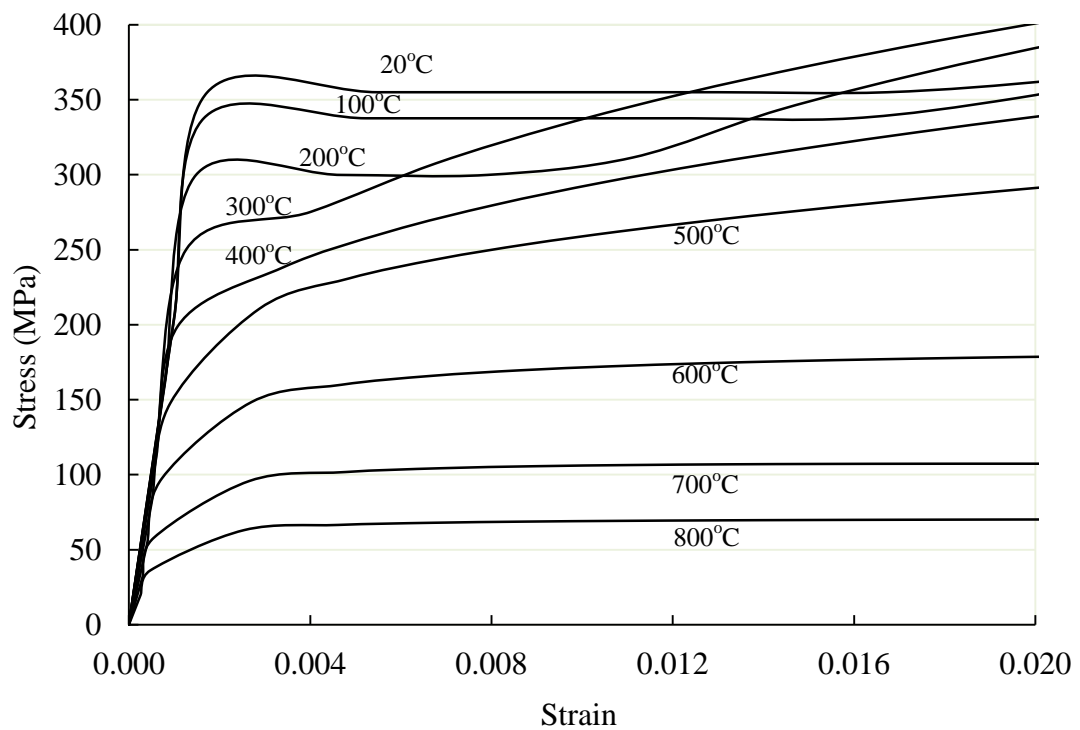
Figure 2.8: Typical stress-strain curves for ASTM A36 steel at high temperatures
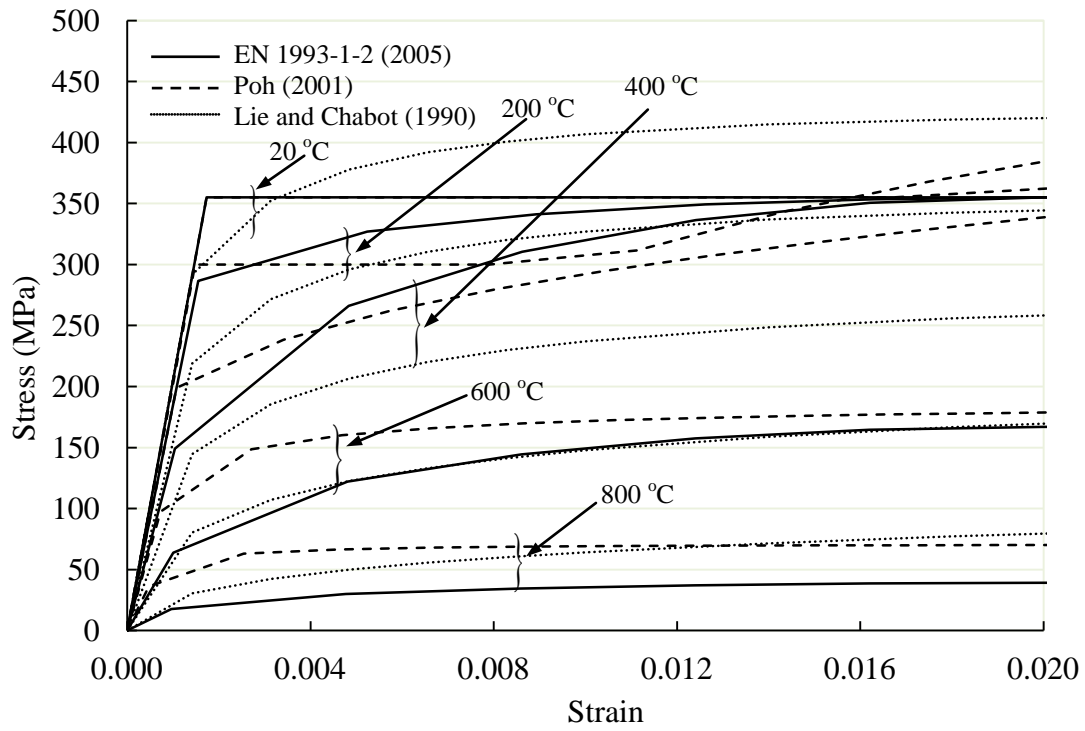
Figure 2.9: Comparison between stress-strain curves of steel at elevated temperatures

Chapter 3 Behavior of High Strength Steel at Elevated Temperatures

3.1 Overview

This chapter introduces the experimental investigations on mechanical properties of a new high strength low alloy steel, RQT701, at elevated temperatures. The investigated parameters were relative thermal elongation, elastic modulus, effective yield strengths, and stress-strain relations. Axial tensile tests were carried out at elevated temperature by both steady-state and transient-state methods. The test results were compared with those for unheat-treated carbon steels (NSS) with grades up to S460 as in EN 1993-1-2. The critical temperatures of steel columns of various grades were also investigated. The relative elongations and the reduction factors of effective yield strengths and elastic modulus are proposed for fire resistance design and numerical simulation of structural members made from HSS RQT701.

3.2 Chemical Compositions of High Strength Steel

HSS RQT701 is a quenched and tempered structural steel, combining high strength with excellent forming and welding performance. The chemical compositions of HSS RQT701 and NSS are compared in Table 3.1. The chemical compositions of NSS are taken from EN 10025-2 (2004). It can be seen that the carbon content of HSS RQT701 is similar to that of NSS. HSS RQT701 has lower content of sulfur, which implies larger resistance to lamellar tearing and better notch impact toughness and weldability, but poorer machinability. Besides, the content of nitrogen of HSS RQT701 is lower, which indicates less likelihood of blue brittleness where a blue

oxide film is formed on the surface of steel at temperature $180^{o}C \sim 370^{o}C$. It can also be found that it is stricter for HSS RQT701 with regard to the addition of copper since the copper is detrimental in heat-treatment and leads to poor surface quality.

3.3 Microstructure of High Strength Steel at High Temperature

HSS RQT701 is manufactured from mild steel plates through heat-treatment. The process of heat-treatment is that the mild steel plate is heated above a temperature where phase transformation occurs. Then it is quenched with specified cooling rate. After that it is tempered to the specified temperature in order to achieve the required strength and ductility. The changes of mechanical properties are actually due to the change of microstructure during heat-treatment. Hence, in order to investigate the behavior of HSS RQT701 under elevated temperatures, it is important to understand the phase transformations.

Over the decades, the mechanisms of phase transformations have been investigated and illustrated in a simple *Fe-C* diagram as shown in Figure 3.1. It can be seen that the microstructure of unheat-treated NSS with carbon content of about 0.2% by weight is morphologically characterized by α-ferrite and θ-cementite below a critical temperature of $727^{o}C$ at which the specific heat value approaches infinity as provided in EN 1993-1-2. Beyond this critical temperature, α-ferrite and θ-cementite transform into γ-austenite. Heat-treated high strength steel is generally processed by heating the mild steel to a temperature higher than $727^{o}C$ where it is characterized by austenite. Then it is annealed or quenched under various cooling rates to achieve the required strength and ductility. Cooling rate affects phase transformations (Totten, 2006). A microstructure with lamellar mixture of ferrite and cementite is obtained if the cooling

rate is slow. Medial cooling rate results in a microstructure mainly characterized by bainite. A hard martensite microstructure with retained austenite can be observed under rapid cooling.

HSS RQT701 is quenched by water at $880^oC \sim 900^oC$ where the microstructure, as mentioned above, is fully characterized by austenite. As stated in the fabrication manual of HSS RQT701 (Corus construction & Industrial, 2006), during quenching, large volumes of high pressure water are sprayed across the full width of the plate and to both the top and bottom surfaces to ensure that the plate is uniformly cooled down. The cooling rate is very high. Therefore after it is quenched, the microstructure of HSS RQT701 is mainly characterized by martensite structure rather than α-ferrite and θ-cementite. Martensite structure is hard and brittle. It can lead to distortion and cracking. Hence, it is necessary to modify its mechanical properties by tempering (Bhadeshia and Honeycombe, 2006).

HSS RQT701 is tempered at $560^oC \sim 640^oC$. Tempering relieves tight crystals and leads to improved ductility but reduced strength (Tubal, 1984). The transformation of microstructure during tempering depends on the tempering temperature. As a rule of thumb, coagulation and spheroidization of cementite and recrystallization of ferrite will be finally achieved with the increasing tempering temperature (Bhadeshia and Honeycombe, 2006; Callister, 2007). This transformation of microstructure implies that the microstructure of HSS RQT701, with increasing tempering temperature, gradually approaches the mixture of cementite and ferrite which characterize the microstructure of NSS at room temperature. In other words, HSS RQT701 may have similar mechanical properties to NSS at high temperatures. That is why it is specified in the fabrication manual that heating HSS RQT701 in excess of 560^oC is not

generally recommended since it can cause some deterioration in mechanical properties, because most hard martensite has transformed into the mixture of ferrite and cementite after tempering temperature. Testing HSS RQT701 in fire is actually another tempering process. Thus, the measured mechanical properties can be reasonably interpreted based on the microstructure transformation in tempering.

3.4 Tensile Test at Elevated Temperature

3.4.1 Test Specimens

The coupon specimens were prepared in accordance with ASTM E 8M-04 (2004) and ASTM E 21-09 (2009) standards. The dimensions of the test specimens are shown in Figure 3.2. High pressure water jet cutting machine was used to cut the coupon shape to avoid unnecessary heat built up which may affect its mechanical properties.

The specimens were generally longer than those tested at room temperature since the shoulder ends of specimens were elongated so that they can be pin-connected to the tensile test machine outside the heating furnace (ASTM E 21-09, 2009). The thickness of the coupon specimens was 12mm. Before carring out the tests the reduced sections of the specimens were grinded to make the surfaces flat. Then the dimensions of the reduced sections and gauge lengths were measured.

3.4.2 Test Equipment and Instrumentation

Axial tensile tests were conducted on an INSTRON 1334 servo-hydraulic testing machine, with a maximum 75mm stroke displacement and 500kN capacity.

The heat apparatus was a model of SF-16 split-tube furnace with three-zone configuration and an optional side entry extensometer port. The furnace is constructed with a brushed stainless steel shell and terminal covers. Heating elements are slurried windings. A type K thermocouple is mounted in the center of each heating zone. The external sizes (diameter x height) are 254 x 330mm and internal heating sizes are 76 x 280mm. The furnace can heat up to a maximum temperature of 1250°C.

For ambient temperature tests, both extensometer and strain gauges were used to measure the strain. The strain gauge readings were used to calibrate the extensometer. For elevated temperature tests, only the extensometer was used. The arms of the extensometer are ceramic rods with quartz chisel ends which pass through the side entry port of the furnace to contact the specimen. It is specified for a gauge length of 25mm and can travel 2.5mm. Thus the maximum measurable strain is 10%. During testing, the displacement of the specimen is detected and transmitted by the rods to the strain gauges placed within the extensometer body. A cooling fan mounted close to the extensometer is provided to maintain the temperature of the extensometer at below 150°C.

3.4.3   Test Setup

The specimen was first attached to the servo-hydraulic testing machine with a built-in load cell. Then the split-tube the furnace was moved in to enclose the specimen. After that, the extensometer was inserted into the furnace to touch the specimen. Finally the furnace was closed and sealed with fire resistant wools. The specimen was lightly tensioned to about 1kN to ensure full contact between the pins and the pin holes. The test setup is shown in Figure 3.3.

3.4.4 Test Methods

There are generally two test methods to conduct the tensile tests of steel materials at high temperatures: transient-state and steady-state tests. In the transient-state tests, the specimen was heated under a constant pre-load until it fails. As a result, a temperature-strain curve is recorded during the testing, which can be converted into stress-strain curve. However, the thermal strain should be subtracted from the total strain recorded, thus another test for thermal strain is needed. In steady-state tests, the specimen is first heated up to the target temperature and then loaded to failure. The stress-strain curves can be obtained directly from the tests.

The steady-state test method is easier to carry out than the transient-state method; therefore it is more widely used (Outinen et al., 2001). However, the transient-state method may give more realistic test results because it simulates the true loading conditions including the thermal creep effect of a loaded component exposed to fire. In the literature, numerous coupon tests have been conducted on NSS at elevated temperature using both test methods. There is enough evidence to show that the transient-state test is the preferred method whereas the steady-state test may yield similar results at small strains of steel (Kirby and Preston, 1988).

In this paper, both steady-state and transient-state tests were conducted on HSS RQT701. In steady-state tests, the heating rate was 10°C/min and the loading rate was 0.15mm/min. In addition to ambient temperature which is about 30°C, the target high temperatures ranged from 100°C~800°C with increments of 100°C. These target high temperatures were held for one hour to obtain uniform temperature distributions in both furnace and specimen. Three specimens were tested at each target temperature. A

total of 27 specimens were required to complete the steady-state tests for HSS RQT701.

In the transient-state tests, the preload levels are applied as percentages of the effective yielding strength at 2% strain at ambient temperature. The applied preload levels range from 5%~100% with increments of 5% with three exceptions of 7.5%, 67%, 92%. The preloads were applied under load control. Load control mode was adopted since it could maintain the preloads during the following heating. The loading rate was 1.5kN/min. The heating rate was then applied at 10^oC/min to specimen failure. The strain-temperature relations were recorded at temperature increments of 100^oC. At each increment of temperature, it was held for 20 minutes before taking the readings (EN 10002-5, 1992; ASTM E21-09, 2009). The relative thermal elongations, measured in the steady-state tests, were deducted from strain-temperature relations obtained from the transient-state tests. Two specimens were tested for each preload level. A total of 46 specimens were required to complete the transient-state tests for HSS RQT701.

3.5 Test Results

3.5.1 Relative Thermal Elongation

The relative thermal elongation of steel was measured during the heating stage in the steady-state tests. It was calculated from the expansion in gauge length divided by the gauge length. The comparison between relative thermal elongations of HSS RQT701 and NSS as in EN 1993-1-2 is shown in Figure 3.4.

The comparison shows that the relative thermal elongations of HSS RQT701 are slightly smaller than the values in EN1993-1-2 for NSS. This could be due to the different microstructure of RQT701 mainly characterized by the presence of martensite, which is harder than the microstructure of NSS characterized by ferrite and cementite. Thermal expansion is a tendency to change the separation between the atoms with the changed temperature. Hence, it is dominated by the inter-atom forces. Hardness is defined as a means to resist permanent deformation. It is also strongly characterized by inter-atom bonds. The greater the hardness of the metal, the greater resistance it has to deform (ASM handbook, 2000). Hence the harder martensite has stronger inter-atom bonds, and thus has smaller thermal expansion.

3.5.2 Elastic Modulus

The elastic modulus is determined based on the initial linear part of the stress-strain curve. The elasic moduli of HSS RQT701 at ambient temperature are 200GPa and 208GPa measured by the strain gauge and extensometer respectively. The small difference of measurements could be due to the lateral imperfections of the specimens. Strain gauges were attached on both sides of specimen and hence the effect of imperfections could be averaged out. However, this may not be eliminated by the extensometer since it only touched one side of the specimen.

The comparisons between reduction factors of elastic moduli of HSS RQT701 and NSS as in EN 1993-1-2 are shown in Figure 3.5. The modulus reduction factor is the ratio of the elastic modulus at elevated temperature $E_{a,\theta}$ divided by that at ambient temperature E_a, both measured by the extensometer.

It can be seen that the elastic moduli of HSS RQT701 are reduced slower than NSS for temperatures lower than 400°C. That could be attributed to the martensite structure of HSS RQT701 which is harder than ferrite and cementite in NSS. The reduction factors from transient-state tests are slightly smaller than those from the steady-state tests when the temperature is lower than 400°C, but dramatically smaller beyond 400°C. This is due to the effect of thermal creep which becomes noticeable only after about one third of the melting temperature of steel which is around 1200°C~1500°C (Fessler and Hyde, 1978; Kodur et al, 2010). Compared with the elastic modulus from steady-state tests, the elastic modulus from transient-state tests was reduced by 45%~65% beyond 400°C.

3.5.3   Effective Yield Strength

The effective yield strengths of steels can be classified by different post-yield strains. Different yield strengths are used at different situations in fire engineering of members. In BS 5950-8 (2003), the effective yield strengths corresponding to 0.5% and 1.5% strains are used for members in compression according to different slenderness ratios; for 3-side heated steel beams, the effective yield strength of 2.0% strain is adopted; the effective yield strengths of 0.5% and 2.0% strains are applied for composite beams based on whether it is protected or not. However, in EN 1993-1-2, the effective yield strength, corresponding to 2.0% strain, is adopted for all fire situations. The effective yield strength with 0.2% offset strain is normally taken as the yield strength in ambient design situations.

The effective yield strengths of HSS RQT701 at different strain levels at ambient temperatures are shown in Table 3.2. It can be found that the effective yield strengths

measured by strain gauge and extensometer are similar. The effective yield strength with 0.5% strain is smaller than that with 0.2% offset strain. This is contrary for NSS with grades not greater than S460. Generally, for a given elastic modulus of 210GPa, $f_{y,0.2\% \text{offset}}$ equals $f_{y,0.5\%}$ at 633MPa.

The comparisons between the reduction factors for effective yield strengths of HSS RQT701 and NSS as in EN 1993-1-2 are shown in Figure 3.6~Figure 3.9. The reduction factors of HSS RQT701 are also based on the effective yield strengths at ambient temperatures measured by extensometer. The symbols $f_{y,0.2\%\text{offset}}$, $f_{y,0.2\%\text{offset},\theta}$, $f_{y,0.5\%}$, $f_{y,0.5\%,\theta}$, $f_{y,1.5\%}$, $f_{y,1.5\%,\theta}$, $f_{y,2.0\%}$, $f_{y,2.0\%,\theta}$ stands for the effective yield strengths at ambient and high temperatures respectively.

The comparison of results shows that the effective yield strengths of HSS RQT701 from transient-state tests are slightly lower than those from steady-state tests for temperature less than 400$^{\text{o}}$C. It could be due to the fact that there is strain hardening after yielding, and the elastic moduli of transient-state tests, as mentioned above, are slightly smaller than those of steady-state tests in this range of temperature. As a result, the stress after yielding increases less by strain hardening in transient-state tests. However, there is almost no strain hardening after 400$^{\text{o}}$C (shown in afftermentioned stress-strain curves). Hence, there is no increase of stress after yielding no matter how different the elastic moduli are. As a result, the effective yield strengths and their reduction factors for steady-state and transient-state tests are similar after 400$^{\text{o}}$C.

The effective yield strengths of HSS RQT701 reduce faster than NSS after 400$^{\text{o}}$C. This is because in the temperature range between 400$^{\text{o}}$C to 800$^{\text{o}}$C, the martensite structure of HSS RQT701 is transforming slowly into ferrite and cementite which characterize the microstructure of NSS. Thus HSS RQT701 steel may have similar

effective yield strengths at this temperature range as NSS. However, the effective yield strength of HSS RQT701 at ambient temperature is higher and hence their reduction factors are smaller.

3.5.4 Stress-Strain Relation

The stress-strain curves from steady-state tests are shown in Figure 3.10. Due to the limited travel distance of extensometer, most tests were terminated before the specimens failed. Hence, the ultimate strains were not obtained. But the results shown are sufficient for design purposes.

It can be seen that the elastic modulus decreases with increasing temperature, but the post-yield stresses (strain>1%) are not monotonically reduced. The post-yield stresses at 100°C are smaller than those at 200°C and 300°C. And the post-yield stresses at 200°C and 300°C almost catch up with those at ambient temperature (30°C). It is doubted this is due to the blue brittleness of steel (Li, 2006). Blue brittleness is mainly caused by the dislocated nitrogen atoms in the range of 180°C~370°C. As a result, the strength increases, but the ductility decreases (Dolzhenkov, 1971). The blue brittleness can be eliminated if alloy elements, such as aluminum or titanium, react with nitrogen, or by reducing the content of nitrogen. However, the blue brittleness was not captured in the stress-strain curves from the transient-state tests as shown in Figure 3.11. This may due to the fact that the stress-strain curves in the transient-state tests are converted from temperature-strain curves. The converted curves are plotted using limited data (each specimen contributed only one data point). Thus, the curves are not smooth and the minor variations by blue brittleness were not captured.

3.6 Critical Temperature

In the prescriptive method of fire engineering design, critical temperature is used to determine the fire resistance time of individual steel elements. Table 4.1 in EN 1993-1-2 gives the critical temperatures based on different load levels. These tabulated critical temperatures are calculated as:

$$\theta_{cr} = 39.19 \ln\left(\frac{1}{0.9674\mu_0^{3.833}} - 1\right) + 482 \qquad (3.1)$$

Where θ_{cr} and μ_0 are critical temperature and load level respectively. This formula is actually obtained by regression of the reduction factors of the effective yield strength. It implies that the critical temperature is not related to the deteriorated elastic modulus which in turn will affect the non-dimensional column slenderness ratio $\bar{\lambda}_{fi}$ at elevated temperatures. As a result, it may give a higher critical temperature and an unsafe estimation of fire resistance time.

The simple calculation model (SCM) as given in EN 1993-1-2 can be used to take into account the effect of slenderness on critical temperature. The critical temperature is calculated based on the equilibrium between the external fire load and the internal fire resistance of steel members. The critical temperature is obtained as the following equation is satisfied.

$$E_{fi} = G_k + \psi_{fi}G_{k,1} = \chi_{fi} R_{fi} / \gamma_{M,fi} \qquad (3.2)$$

E_{fi} is the external fire load of the steel element. G_k and $G_{k,1}$ are the characteristic values of the permanent action and leading variable action. ψ_{fi} is a combination factor which is taken as 0.3 for domestic, residential and office buildings (EN 1990, 2002;

EN 1991-1-2, 2002). χ_{fi} is the reduction factor of buckling under high temperature. $\gamma_{M,fi}$ is partial factor of the steel material at fire situations. R_{fi} is the cross-sectional resistance of the steel element, such as moment and compression capacity at fire situations. In the following equations, subscript "r" represents their counterparts at room temperature.

At room temperature, the external load can be obtained as shown in the following equation, assuming the steel element is fully loaded to its ultimate state.

$$E_r = \gamma_G G_k + \gamma_{Q,1} G_{k,1} = \chi_r R_r / \gamma_{M,r} \qquad (3.3)$$

γ_G and $\gamma_{Q,1}$ are partial factors of permanent action and variable action, which are 1.35 and 1.5 respectively (EN 1990, 2002). The cross-sectional resistances R_r and R_{fi} are only related to the effective yield strength of steel. Hence, their ratio can be calculated as given by:

$$\frac{R_{fi}}{R_r} = \frac{f_{y,fi}}{f_{y,r}} = k_{y,\theta} \qquad (3.4)$$

The reduction factor for the load combination is shown as:

$$\eta_{fi} = \frac{G_k + \psi_{fi} G_{k,1}}{\gamma_G G_k + \gamma_{Q,1} G_{k,1}} \qquad (3.5)$$

After rearranging, the critical temperature is calculated when the following equation is satisfied.

$$\frac{\eta_{fi}}{k_{y,\theta}} \frac{\gamma_{M,fi}}{\gamma_{M,r}} \frac{\chi_r}{\chi_{fi}} = 1 \qquad (3.6)$$

η_{fi} is the reduction factor of load combination which is recommended as 0.65 (EN 1993-1-2, 2005). It represents the load level in fire situations. The parameters χ_r and χ_{fi} are the reduction factor of buckling at ambient temperature design situations and of fire design situations respectively. The parameter $k_{y,\theta}$ is the reduction factor of the effective yield strength of steel at high temperature. The partial factors of material $\gamma_{M,r}$ and $\gamma_{M,fi}$ are equal to 1.0.

The non-dimension slenderness ratio at fire design situation can be written as shown in the following equation (EN 1993-1-2, 2005).

$$\overline{\lambda}_{fi} = \overline{\lambda} \sqrt{k_{y,\theta} \Big/ k_{E,\theta}} \tag{3.7}$$

Hence, the reduction factor of buckling at ambient design situations and fire design situations can be calculated as given in following two equations.

$$\chi_r = \frac{1}{\varphi_r + \sqrt{\varphi_r^2 - \overline{\lambda}_r^2}} \leq 1 \tag{3.8}$$

Where $\varphi_r = 0.5\left[1 + \alpha_r\left(\overline{\lambda}_r - 0.2\right) + \overline{\lambda}_r^{\,2}\right]$,

α_r is imperfection factor depending on buckling curve

$$\chi_{fi} = \frac{1}{\varphi_{fi} + \sqrt{\varphi_{fi}^2 - \overline{\lambda}_{fi}^2}} \leq 1 \tag{3.9}$$

Where $\varphi_{fi} = 0.5\left(1 + \alpha_{fi}\overline{\lambda}_{fi} + \overline{\lambda}_{fi}^{\,2}\right)$,

$\alpha_{fi} = 0.65\sqrt{235/f_y}$ irrespective of buckling curve

The reduction factors of elastic modulus $k_{E,\theta}$ and effective yield strength $k_{y,\theta}$ are shown in Table 3.3. For HSS RQT701, in which, the effective yield strength with 2.0% strain from transient-state tests is adopted.

Substituting the reduction factors of elastic modulus $k_{E,\theta}$ and effective yield strength $k_{y,\theta}$ into Eqn.(3.6) ~ Eqn.(3.9), the critical temperatures for buckling of steel columns with HSS RQT701 and NSS with respect to the non-dimensional slenderness $\bar{\lambda}_r$ at ambient temperature are shown in Figure 3.12. The imperfection factor α_r is taken as 0.21 which corresponds to buckling curve "a" for all steel grades at ambient temperature. For the purpose of comparison, it is assumed that the simple calculation model as given in EN 1993-1-2 is also applicable to HSS RQT701.

It can be seen that the critical temperature decreases with the non-dimensional slenderness $\bar{\lambda}_r$ for all steel grades. When $\bar{\lambda}_r$ is smaller than 0.5, the critical temperature of HSS RQT701 is smaller than those of NSS. This could be due to the fact that the failure of steel column is governed by the cross-sectional capacity, rather than the buckling capacity. As a result, HSS RQT701 fails faster due to lower reduction factors of effective yield strength.

When $\bar{\lambda}_r$ is greater than 0.5, the critical temperature of HSS RQT701 gradually becomes higher than those of NSS. This is due to the imperfection factor α_{fi} as shown in Eqn.(3.9). The higher the steel grade is, the smaller the value of α_{fi}. Since HSS RQT701 has the smallest α_{fi}, its reduction factor of buckling χ_{fi} in fire design situations is the largest of the other steel grades. Similarly for NSS, the critical temperature gradually increases with steel grade from S275 to S460, due to the effect of the imperfection factor α_{fi}.

It also can be found in Figure 3.12 that the critical temperature gradually increases when the slenderness $\bar{\lambda}_r$ is greater than 1.0. This is attributed to the parabolic shape of $\varphi_{fi}/\bar{\lambda}_{fi}$ in Eqn. (3.9) which has a minimum value at $\bar{\lambda}_{fi} = 1.0$.

It is difficult to select a reasonable buckling curve for the design of column made from HSS at ambient temperature, since the buckling curves are generally summarized from thousands of testing specimens. In the preliminary study, the effects of various buckling curves on critical temperatures of columns with HSS RQT 701 are presented as shown in Figure 3.13. It can be seen that the critical temperature increases as the buckling curve at room temperature varies from "a_0" to "d". The reason is due to the fact that the critical temperature is calculated based on the equilibrium between the external fire load and the internal fire resistance. The external fire load is a fraction (η_{fi}) of the buckling capacity of column at room temperature design which decreases as the buckling curve varies from "a_0" to "d". Thus, the external fire load is smallest when the buckling curve is "d". However, the buckling capacities in fire situations are the same for all columns irrespective of the buckling curves. As a result, the highest critical temperature is produced when buckling curve is "d". This phenomenon has also been observed on NSS (Access Steel, 2006).

3.7 Summary

In this paper, the temperature dependent mechanical properties of high strength steel RQT701, such as relative thermal elongation, elastic modulus, effective yield strengths at different strain levels, critical temperature and stress-strain curves are

presented. The test results are compared with those of NSS as in EN 1993-1-2. The following conclusions can be drawn.

(1) Relative thermal elongations of HSS RQT701 are smaller than those of NSS as in EN 1993-1-2, due to different microstructures under high temperatures.

(2) Elastic moduli of HSS RQT701 are reduced slower than those of NSS for temperatures lower than 400°C, attributed to the martensite structure of HSS RQT701 which is harder than ferrite and cementite in NSS. But beyond 400°C, elastic moduli of NSS are similar to those of HSS from steady-state tests but reduced slower than those from transient-state tests.

(3) The reduction factors of elastic moduli of HSS RQT701 from transient-state tests are slightly smaller than those from steady-state tests when the temperature is lower than 400°C, but dramatically smaller beyond 400°C. This is due to the thermal creep effect which is noticeable at temperatures reaching about one third of steel melting temperature.

(4) Reduction factors of effective yield strength of HSS RQT701 obtained from transient-state tests are slightly smaller than those from steady-state tests when the temperatures are lower than 400°C, but they become similar beyond 400°C. This is due to the effect of strain hardening after yielding.

(5) Effective yield strengths of HSS RQT701 steel are reduced faster than NSS after 400°C. This is because of the transformation of the microstructure of HSS RQT701 which gradually approaches that of NSS. As a result, they have similar effective yield strengths at high temperatures, but different ones at ambient temperature.

(6) In EN 1993-1-2, the tabulated critical temperatures are obtained through regression of the reduction factors of yield strength. It is not related to the deteriorated elastic modulus at elevated temperatures. As a result, it gives an unsafe estimation of fire resistance time of a steel member.

(7) Critical temperatures, calculated based on the simple calculation model in EN 1993-1-2, generally decrease with increasing non-dimensional column slenderness. The critical temperatures increase with increasing steel grade.

(8) For a given load level, critical temperature of a steel column made from HSS RQT701 increases as its buckling curve at room temperature varies from "a_0" to "d", due to the decreasing external fire load.

Table 3.1: Typical chemical compositions of HSS RQT701 and NSS (%)

	RQT701 (8≤t≤30)		S235J0	S275J0	S335J0	S450J0
	Typical	Max.	Max. (≤16)	Max. (≤16)	Max. (≤16)	Max. (≤16)
C	0.14	0.20	0.17	0.18	0.20	0.20
Si	0.44	0. 50	-	-	0.55	0.55
Mn	1.44	1.60	1.40	1.50	1.60	1.70
S	0.003	0.01	0.03	0.03	0.03	0.03
P	0.011	0.025	0.03	0.03	0.03	0.03
Cr	0.022	0.25	-	-	-	-
Mo	0.003	0.2	-	-	-	-
Nb	0.032	0.06	-	-	-	-
V	0.059	0.08	-	-	-	-
Ni	0.023	0.7	-	-	-	-
Ti	0.029	0.04	-	-	-	-
N	0.003	-	0.012	0.012	0.012	0.025
Cu	0.018	0.2	0.55	0.55	0.55	0.55
Al	0.038	0.06	-	-	-	-
B	0.002	0.004	-	-	-	-

Table 3.2: Effective yield strengths of HSS RQT701 at ambient temperature (MPa)

	$f_{y,0.2\%offset}$	$f_{y,0.5\%}$	$f_{y,1.5\%}$	$f_{y,2.0\%}$
Strain gauge	740	725	775	781
Extensometer	740	729	775	780

Table 3.3: Reduction factors of elastic modulus and effective yield strengths

Temp. (^{o}C)	HSS RQT701		EN 1993-1-2	
	$k_{E,\theta}$ (GPa)	$k_{y,\theta}$ (MPa)	$k_{E,\theta}$ (GPa)	$k_{y,\theta}$ (MPa)
30	1	1	1	1
100	0.962	0.967	1	1
200	0.921	0.949	0.90	1
300	0.853	0.926	0.80	1
400	0.800	0.902	0.70	1
500	0.353	0.660	0.60	0.78
600	0.116	0.308	0.31	0.47
700	0.053	0.120	0.13	0.23
800	-	-	0.09	0.11
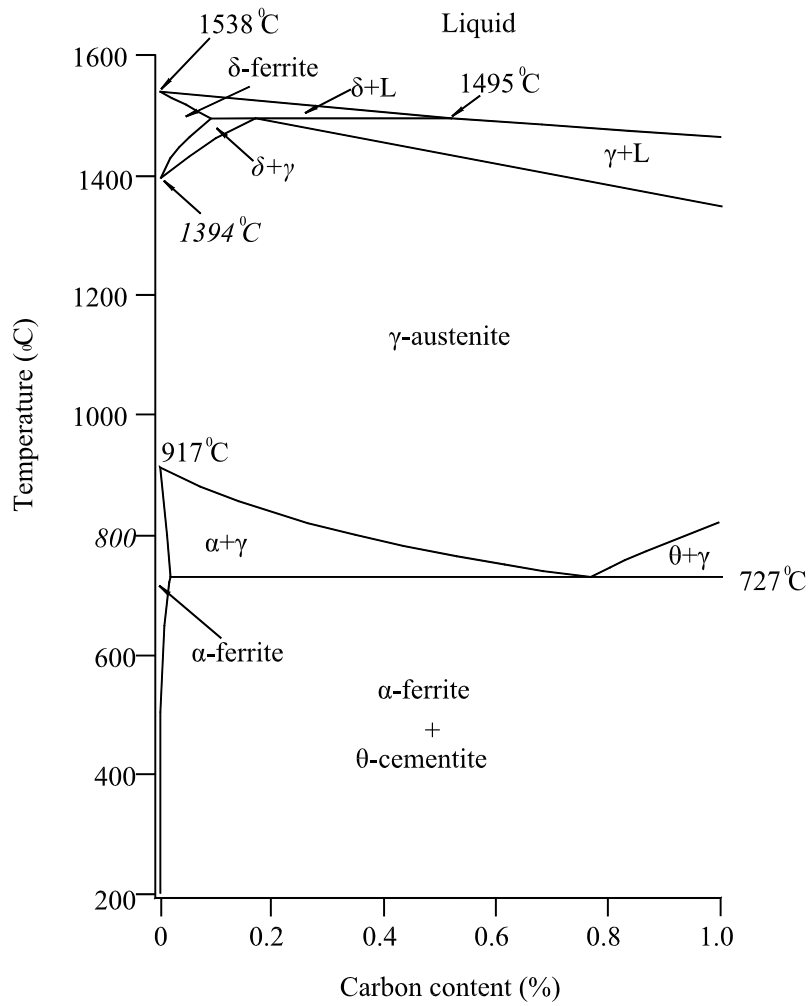
Figure 3.1: Phase transformation of steel at elevated temperature
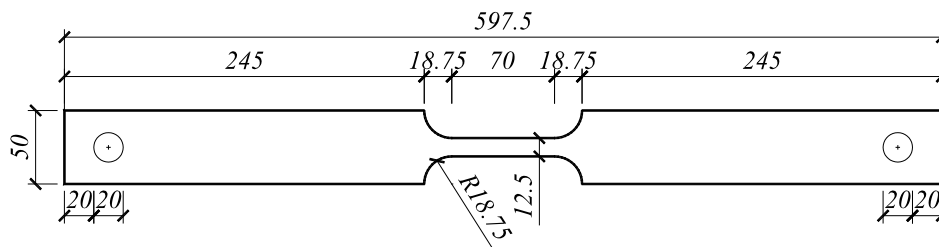
Figure 3.2: Dimensions of coupon specimen (units in mm)
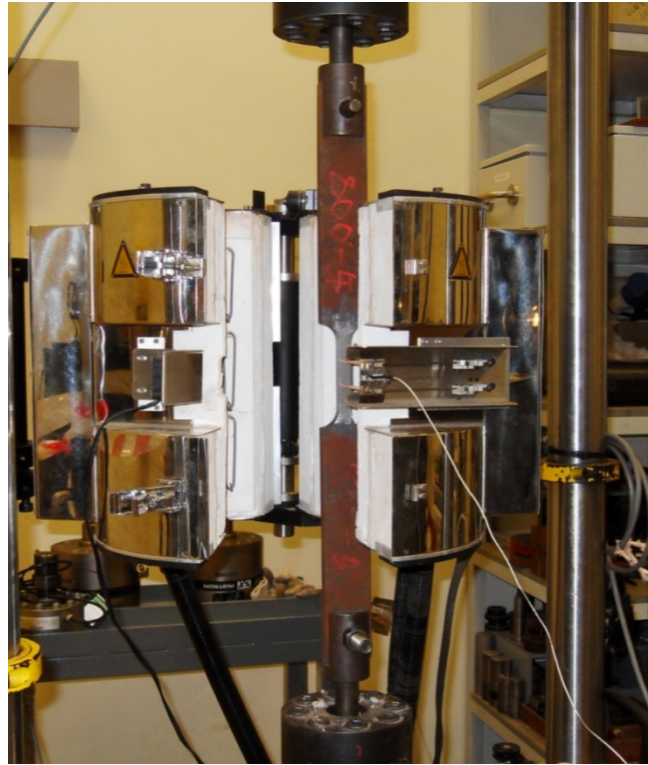
Figure 3.3: Test setup
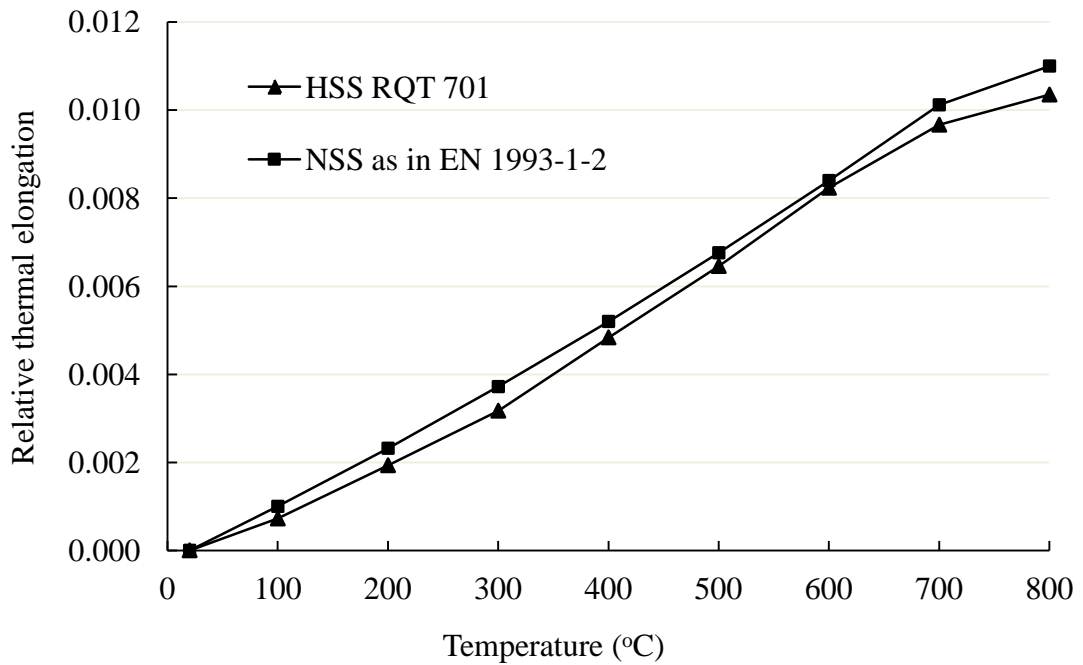
Figure 3.4: Relative thermal elongations of HSS RQT701 and NSS at elevated

temperature
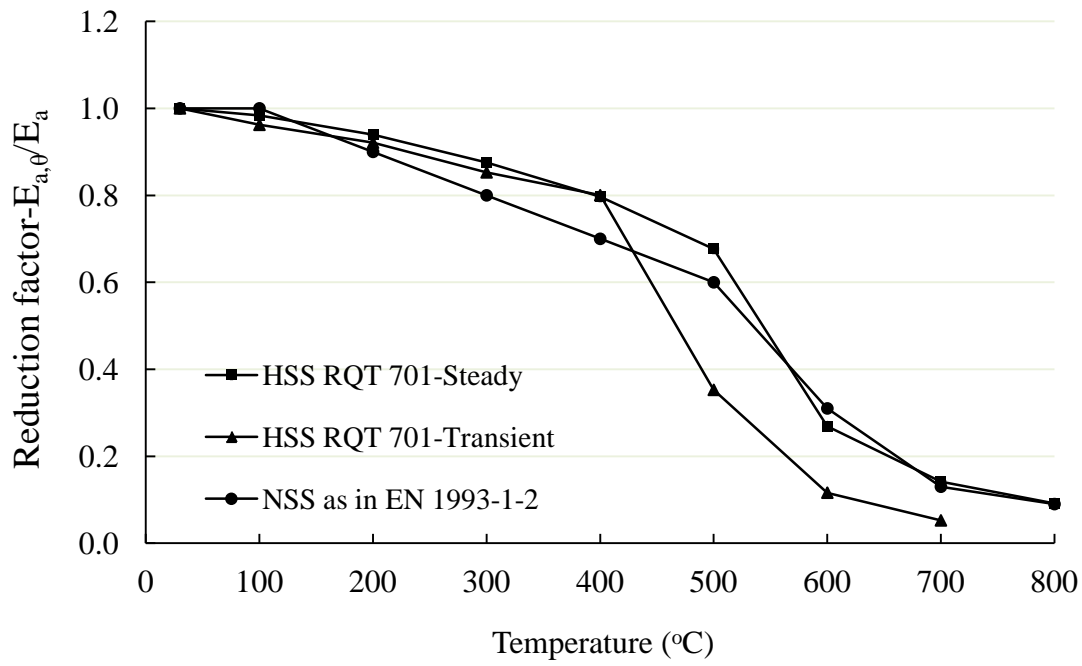
Figure 3.5: Comparison of $E_{a,\theta}/E_a$ ratio and temperature relation of HSS RQT 701 and NSS
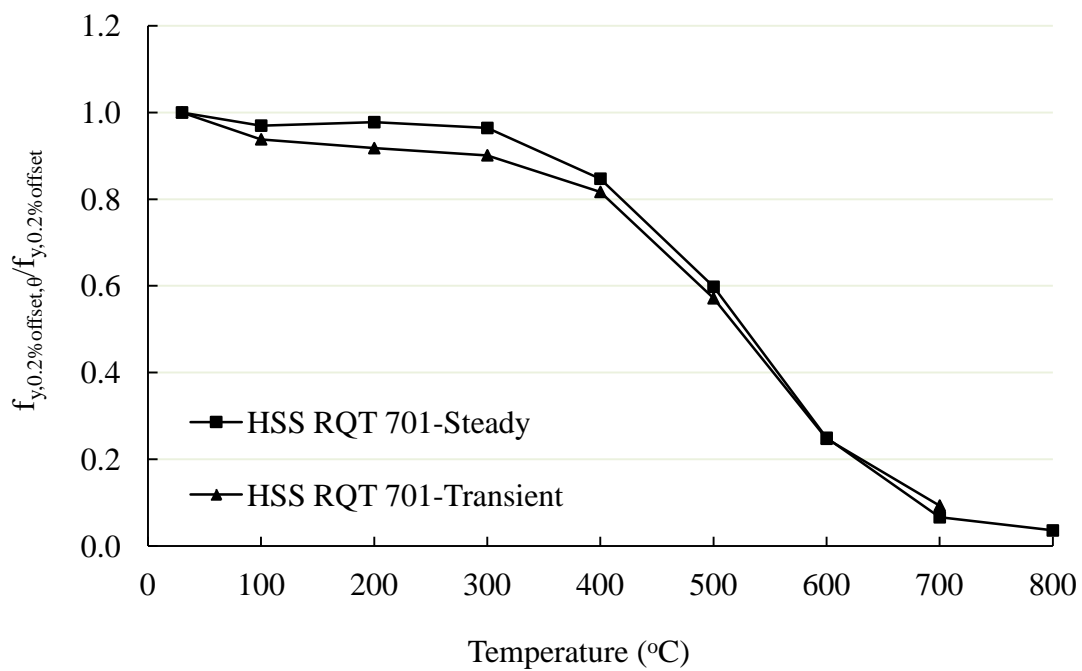
Figure 3.6: Reduction factor of effective yield strength at 0.2% offset strain at elevated temperature
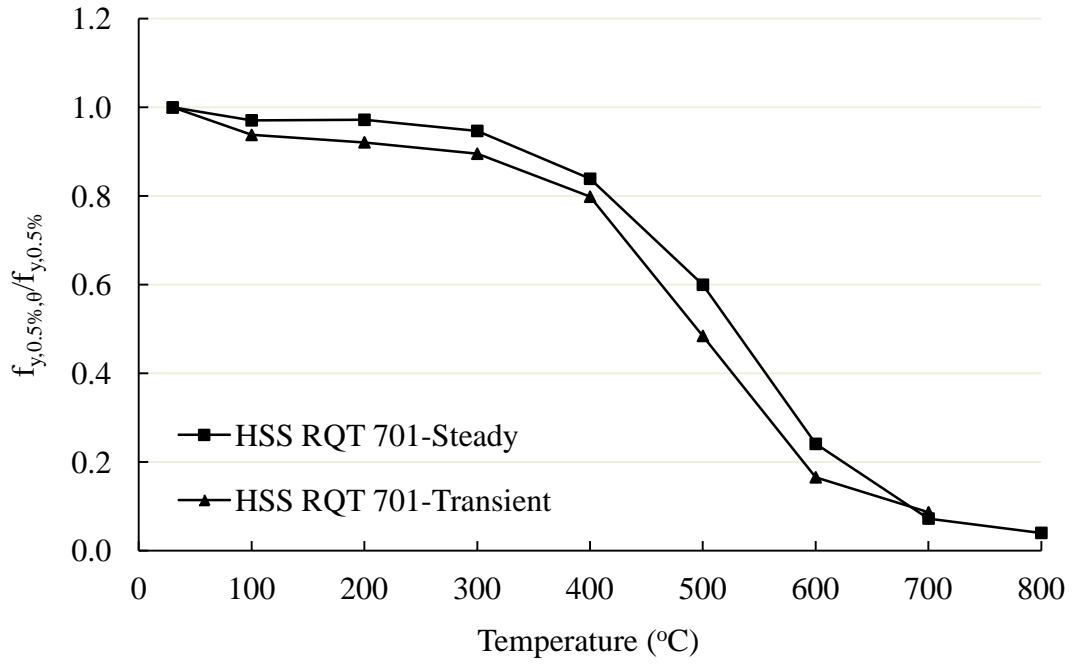
Figure 3.7: Reduction factors of effective yield strengths at 0.5% strain at elevated
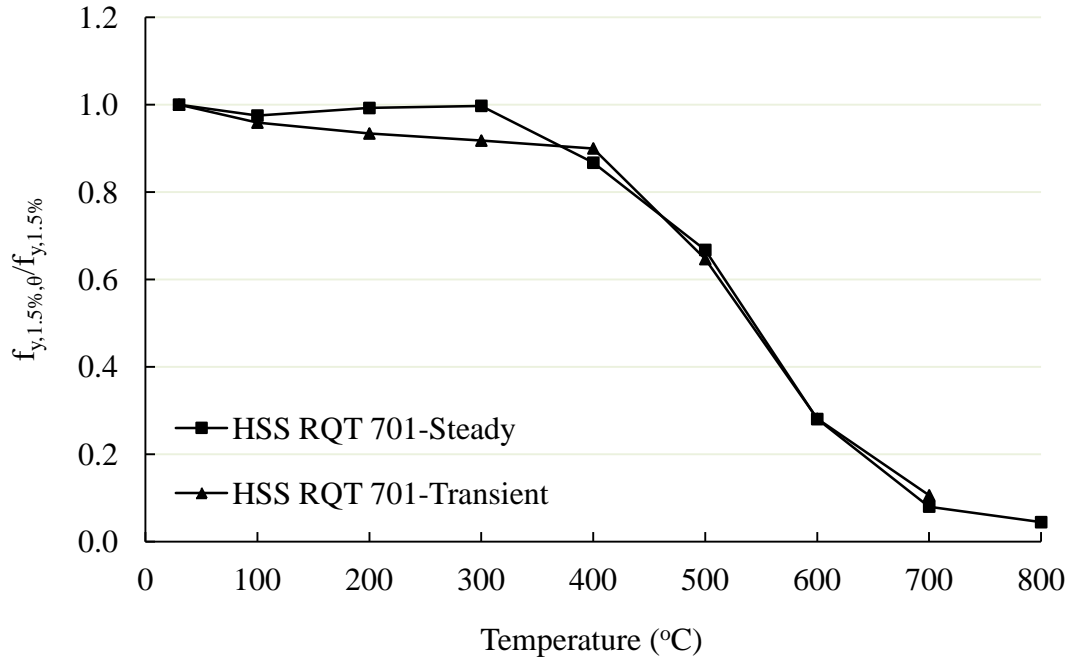
temperature

Figure 3.8: Reduction factors of effective yield strengths at 1.5% strain at elevated
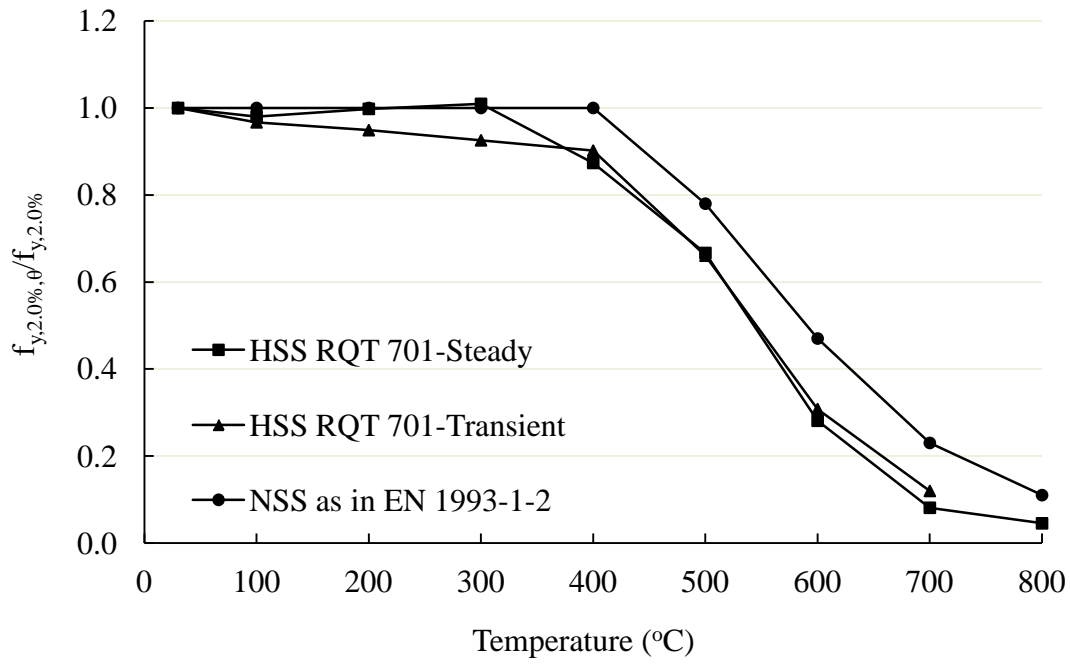
temperature

Figure 3.9: Reduction factors of effective yield strengths at 2.0% strain at elevated temperature
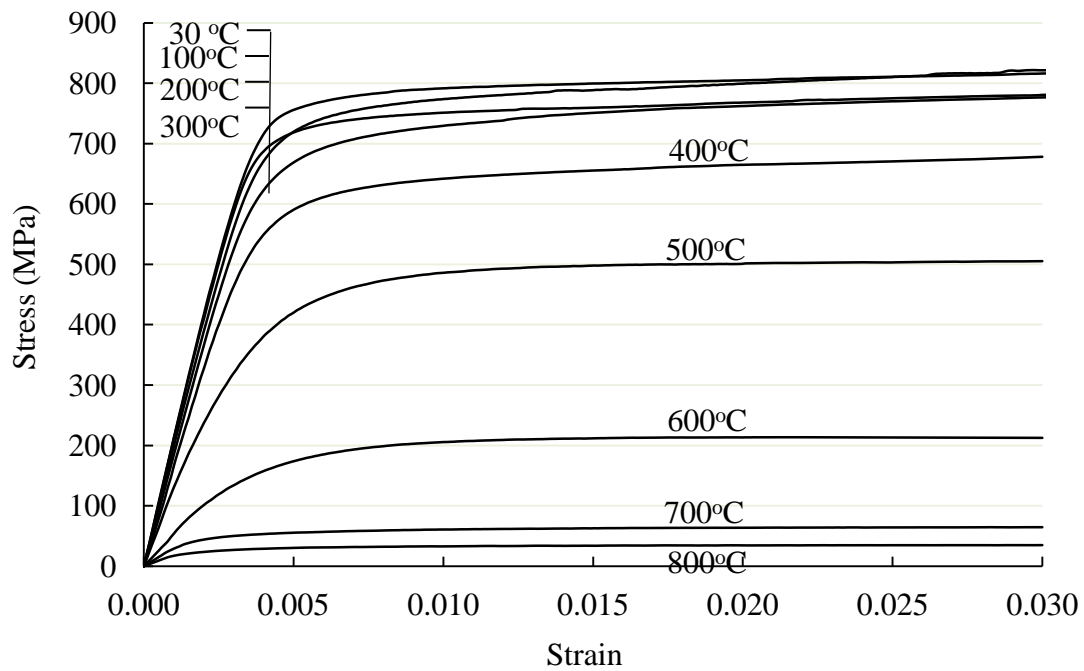
Figure 3.10: Stress-strain curves of HSS RQT701 from steady-state tests at elevated temperature
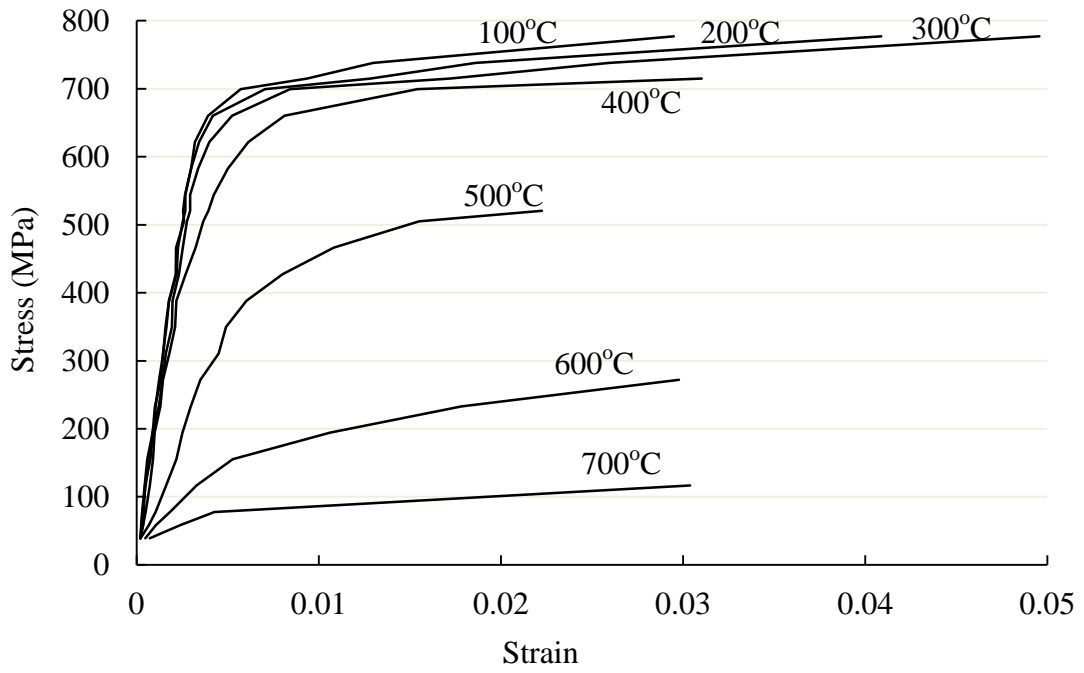
Figure 3.11: Stress-strain curves of HSS RQT701 from transient-state tests at elevated
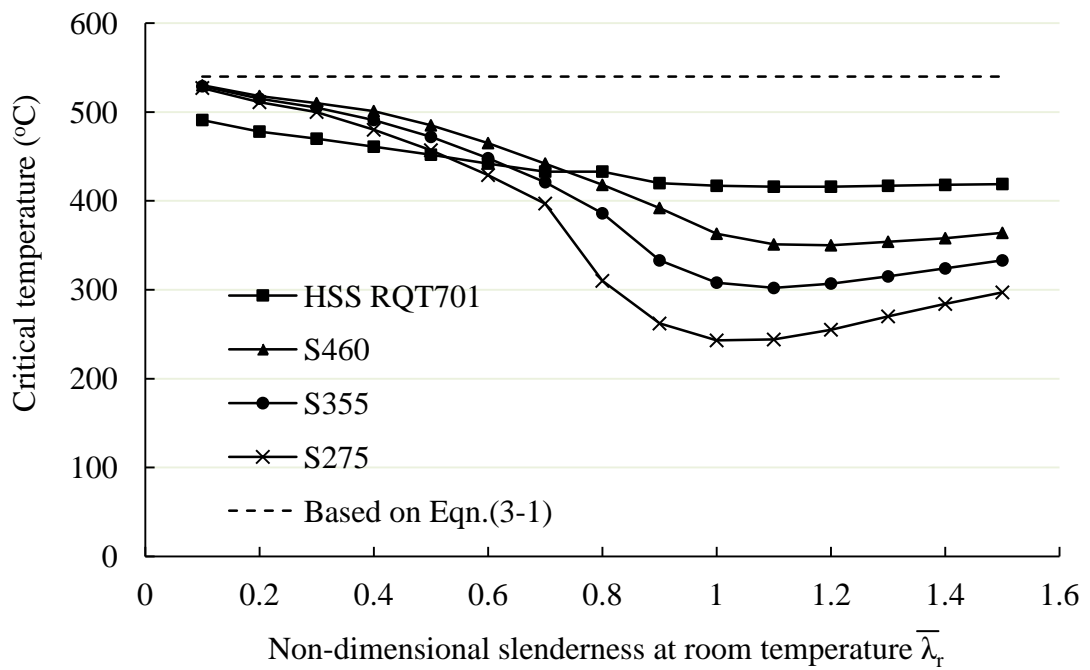
temperature

Figure 3.12: Critical temperatures of columns with HSS RQT 701, S460, S355 and

S275
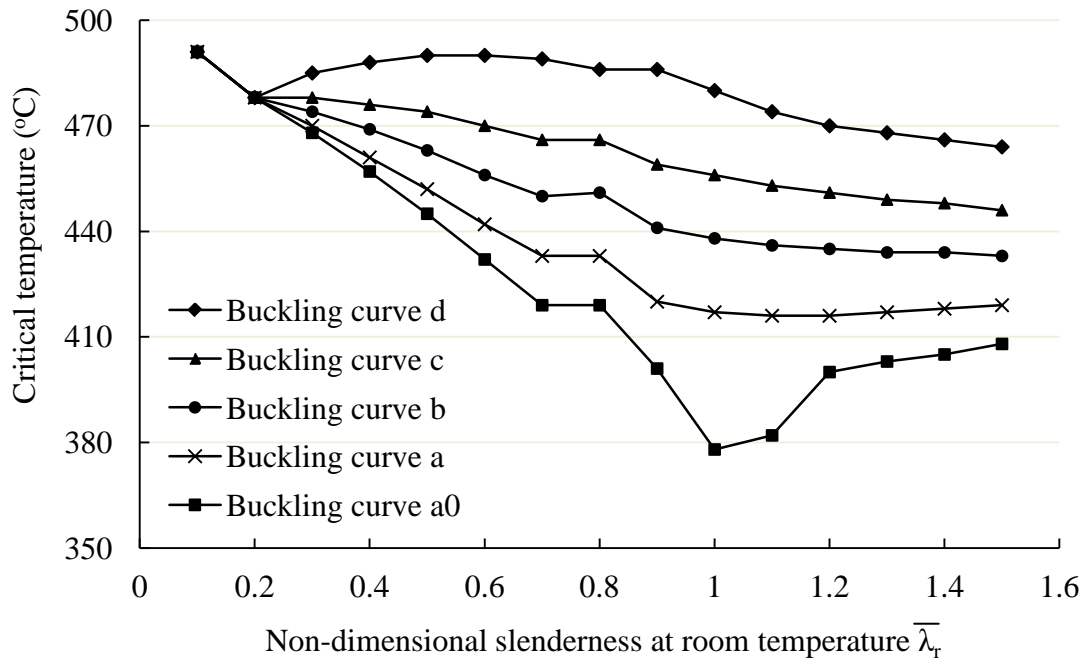
Figure 3.13: Critical temperatures of columns with HSS RQT701 based on different

buckling curves at room temperature

Chapter 4   Behavior of Ultra-High Strength Concrete after Heating

4.1 Overview

In this chapter, the spalling behavior of ultra-high strength concrete (UHSC) with additions of different fiber types is investigated. Then, the residual mechanical properties after heating, including strength and elastic modulus, are presented and compared based on different fiber dosages, heating rates and curing conditions. The residual strength and residual elastic modulus are also compared with normal strength concrete (NSC) and high strength concrete (HSC) in literature. Finally, the effective fiber type and fiber dosage in UHSC are recommended for prevention of spalling.

4.2 Effect of Types of Fibers on Prevention of Spalling

4.2.1   Test Specimens

Two types of fiber, steel fiber and polypropylene (PP) fiber, are taken into account to prevent the spalling of UHSC under high temperatures. The mechanisms of steel fiber and PP fiber to prevent spalling are different. The steel fiber can increase the tensile strength of concrete; hence the cracking can be delayed and limited. Whereas PP fiber will melt after the temperature reaches approximately $170^{o}C$; then the vapor pressure can be released through the voids left by the melted PP fiber.

The investigated UHSC is a Ducorit product of DENSIT company (www.densit.com). It is called Ducorit ® D4. It is made from a pre-blended mixture comprising cementitious material superplasticizer and fine bauxite aggregates with maximum sizes less than 4.75mm. The mixing proportions for plain UHSC are shown in Table

4.1. Four batches of UHSC with additions of fibers were investigated as shown in Table 4.2. The properties of steel fiber are shown in Table 4.3 and Figure 4.1; whereas Table 4.4 and Figure 4.2 for polypropylene fiber.

4.2.2   Test Procedure

Three cylinder specimens, 100mm diameter by 200mm height, were cast for each batch of UHSC mixture. After demoulding, the specimens were covered by plastic sheet and cured in lab air for 28 days. The relative humidity of lab air is approximately 85% and the room temperature is about 30°C.

After curing, the specimens were heated up in an electrical oven to a target temperature of 800°C with a heating rate of 5°C/min. The target temperature was maintained for 4 hours to reach a uniform temperature distribution inside the specimen. After that, the specimen was kept in the oven and cooled down naturally to room temperature.

During this heating/cooling process, the specimen was laterally covered by a steel casing in case the spalling would damage the oven.

4.2.3   Test Results

UHSC-P and UHSC-SP specimens were first heated. There was no spalling observed. Then the specimens of UHSC-S were heated. However, they spalled. The temperature inside the specimen was not recorded during heating. However the air temperature in oven was recorded and was approximately 490°C at spalling. The spalled specimens are shown in Figure 4.3. It is noticed that the UHSC with steel fiber although was

spalled, there was no debris blown away. The peripheral concrete was peeled off, but it was still attached to the core concrete by the steel fibers. The plain UHSC was not heated in case the spalled debris would damage the oven.

The residual compressive strengths were tested for all the unspalled specimens after cooling down. The residual strength and their reduction factors are shown in Table 4.5. It can be seen that the addition of steel fibers slightly increased the compressive strength under room temperature. The reason is due to the confinement effect of steel fibers which increased the radial and circumferential strengths of cylindrical concrete.

The UHSC with 1% of PP fibers or a combination of 0.5% steel and 0.5% PP fibers had lower strengths than the plain UHSC. The lower strength could be attributed to the effect of PP fibers on workability, poorer consolidation of the concrete. The difference in residual strengths of UHSC-P and UHSC-SP was approximately 7.5%. Their reduction factors show same difference.

From the test results, it can be found that the incorporation of steel fibers was not effective to prevent spalling of UHSC even with dosage as high as 1% by volume. PP fiber is effective in preventing spalling of UHSC with a dosage of 1% by volume. However, the addition of PP fiber reduced the compressive strength of UHSC due to poorer workability.

As recommended in EN 1992-1-2 (2004), more than $2kg/m^3$ (0.25% by volume) of monofilament propylene fibers should be included in high strength concrete mixtures to prevent spalling. As mentioned above, the 1% PP fiber addition could be too high to achieve good workability. Thus, it is necessary to further reduce the dosage of PP fibers and investigate the consequent effects.

4.3 Effect of Polypropylene Fibers on Prevention of Spalling

4.3.1 Test Materials and Procedure

Both UHSCs with additions of PP fiber and NSC C50 were investigated. The investigated PP fiber dosages were 0, 0.1%, 0.25% and 0.5%. Two heating rates were considered: 5^oC/min and 30^oC/min.

NSC C50 was prepared from ordinary Portland cement, sand, coarse aggregates with a maximum size of 10mm, and water. The mix proportions are shown in Table 4.6. There was no addition of PP fibers inside NSC C50.

The specimens were covered by plastic sheet and cured in air for 28 days. The target temperatures include room temperature (30^oC), 200^oC, 400^oC, 600^oC and 800^oC. The holding time was 4 hours after the target temperature was achieved. After that, the specimens naturally cooled down in oven.

No spalling was observed during heating for all specimens. Plain UHSC specimens were not heated after 400^oC in case the spalled debris would damage the oven. Compression tests were carried out at room temperature after cooling down to get the residual compressive strength and residual elastic modulus. The failure modes of UHSC mixtures subjected to different temperatures are shown in Figure 4.4. It was observed that the UHSC mixture without heating was crushed into pieces with very loud noise heard; whereas it had better ductility and lower noise after subject to high temperatures. Furthermore, the appearances of UHSC mixtures were different after heated to different temperatures due to the changes of microstructures.

4.3.2 Residual Strength

The residual compressive strengths of UHSC mixtures and NSC C50 are shown in Table 4.7. Due to the running out of the pre-blended mixture for UHSC, the batch of UHSC with addition of 0.1% PP fiber under heating rate of 30°C/min was cast using pre-blended mixture from the second shipment. It can be seen that the compressive strength at room temperature from the second shipment were higher than those from the first shipment.

Generally, the residual compressive strength decreases with increasing dosage of PP fiber. The reason is due to the fact that higher dosages of PP fiber will have a higher effect on the workability of the concrete mixtures.

Compared with strength at room temperature, the residual strength of UHSC slightly increased for temperature at 200°C, but decreased beyond 200°C. It is still not clear why there was an increase of in strength at 200°C. There are some hypotheses. Dias et al. (1990) attributed the increase to a rehydration of the paste due to the migration of the water in the pores. Khoury (1992) assumed that the silanol groups lose a portion of their bonds with water, which induces the creation of shorter, stronger siloxane elements (Si-O-Si) with potentially larger surface energies that contribute to the increase in strength. Tanyildizi and Coskun (2008) attributed this increase to the formation of tobermorite from the reaction between the unhydrated cement particles and the lime at high temperatures. The prevailing hypothesis is from Castillo and Durrani (1990) and Behnood and Ziari (2008). They explained that the increase of strength may be attributed to the increase in the forces between the gel particles (Van der Walls forces) due to the water removal and the consequent shrinkage.

The decrease in strength at 400°C, 600°C, and 800°C were related with the decomposition of hydration products such as calcium silicate hydrate (C-S-H) and

calcium hydroxide $Ca(OH)_2$, deterioration of aggregates, and cracking due to thermal incompatibility between the aggregate and cement paste which led to stress concentration.

Comparing plain UHSC with plain NSC C50 in Figure 4.5, it is found that the residual strength factors of UHSC were larger than those of C50. This is due to the fact that the bauxite aggregate in UHSC had better fire resistance than the siliceous aggregate used in C50. It is also observed at 200^oC that the residual strength of UHSC increased compared with the strength at room temperature while NSC C50 did not. This is due to the water removal. Water removal induces shrinkage of concrete meanwhile makes the microstructure of concrete more porous. Shrinkage will increase the Van der Walls forces between gel particles and thus increase the compressive strength of concrete. Whereas increasing porosity will decrease the compressive strength of concrete. NSC C50 has higher water content than UHSC. Hence the loss of strength from the increasing porosity overwhelms the benefit from shrinkage. As a result, the compressive strength of NSC C50 did not increase at 200^oC. It can be seen from Figure 4.5 that the difference of their residual factors was around 8% at 200^oC. However, the difference of 8% needs to be confirmed with range of test results for each type of concrete. This would be done in future work.

The effects of dosage of PP fiber on residual strength factor of UHSC mixtures are shown in Figure 4.6 and Figure 4.7. At the heating rate of $5^oC/min$, the residual strength factors of UHSC with 0.25% and 0.5% PP fiber at 400^oC and 600^oC are lower than those of UHSC with 0.1% PP fiber; a difference of around 18%. For other temperatures, they are very similar. At the heating rate of $30^oC/min$, the differences are not significant and the compressive strengths were similar.

The effects of heating rate on the residual strength factors of UHSC mixtures are shown in Figure 4.8~Figure 4.10. The trend seems to be that the residual strength at higher heating rate (30°C/min) reduced faster for a lower content of PP fiber (0.1%), whereas at a higher content of PP fiber (0.5%), the detrimental effect of a lower heating rate was more.

The residual strengths of UHSC with addition of 0.1% PP fibers are compared with those of concretes in the literature as shown in Figure 4.11. It can be seen that the residual strength of UHSC is reduced slower than other concretes in the literature. This is due to the bauxite aggregate in UHSC which has better fire resistance than the conventional siliceous or calcareous aggregates.

4.3.3   Residual Elastic Modulus

According to ASTM C469-02 (2002), the elastic modulus is the secant modulus between the stress equal to 40% of peak stress and the stress corresponding to a strain of 5×10^{-5}.

Generally, the residual elastic modulus decreases with increasing temperature as given in Table 4.8, there was no increase at 200°C. Comparing plain UHSC with plain NSC C50 in Figure 4.12, it can be seen that the residual factors for the elastic modulus of C50 are smaller than those of UHSC at 200°C and 400°C. The difference is 13% and 35% respectively.

The effects of dosage of PP fiber on the residual factors for the elastic modulus of UHSC mixtures are shown in Figure 4.13 and Figure 4.14. No clear difference was observed with regard to the effect of PP fiber dosage on the residual factors. This

indicates that the shrinkage of UHSC after water removal had minor effect on the elastic modulus since the primary factors are the type of aggregate and the presence of sustained stress during heating (Naus, 2006).

The effects of heating rate on the residual factors of elastic modulus of UHSC mixtures are shown in Figure 4.15 ~ Figure 4.17. It is found that the elastic modulus reduced faster under higher heating rates. And the difference between the residual factors at $5^{o}C$ and $30^{o}C$ increases with increasing PP fiber dosage.

The residual elastic moduli of UHSC with the addition of 0.1% PP fibers are compared with those of concretes in the literature as shown in Figure 4.18. It can be seen that the residual strength of UHSC reduced slower than the other concretes, except for concrete from Hertz (1984&1991) where the concrete strength is 150MPa.

4.4 Effect of Curing Condition

4.4.1   Test Material and Curing Conditions

The investigated material is UHSC with the addition of 0.1% PP fiber by volume. The specimens were cylinders with 100mm diameter and 200mm height. After casting, the specimens were cured under three conditions as follows.

1) **UHSC-D:** Bare specimens were cured in lab air with relative humidity (RH) of 85% and temperature of $30^{o}C$ for daytime and $25^{o}C$ for night (normal RH);

2) **UHSC-H:** Bare specimens were cured in the fog room with a constant RH of 100% and temperature of $28^{o}C$ (High RH);

3) **UHSC-S:** Specimens were sealed with aluminum foil and cured in dry lab air. It was prepared to reflect the curing condition when concrete is infilled in hollow steel tubes (Actual RH in concrete filled tubes).

After 28 days curing, the specimens were heated. The heating rate was 30°C/min. The heating and test procedure were same with those forementioned. There was no spalling observed during heating.

4.4.2   Test Results

The residual compressive strength and residual elastic modulus are shown in Table 4.9. It indicates that the compressive strength and elastic modulus of UHSC prepared using different curing conditions at room temperature were almost unaffected by the initial curing conditions. This might be due to the fact that UHSC is very dense and its permeability is low. Thus, little water was absorbed even when cured in the fog room. Furthermore there is an increase of strength under all curing conditions at 200°C. However, there was no increase in elastic modulus.

The residual factors of strength and elastic modulus are plotted in Figure 4.19~Figure 4.20. No clear difference was observed with regard to the effects of curing conditions on the reduction factors of residual strength and elastic modulus. This might be due to the fact that all water would be released as vapor when the specimens were subjected to high temperatures regardless of how much water contain there in. Thus, the residual mechanical properties would be similar for specimens from different curing conditions. Comparing the reduction factors between residual strength and residual elastic modulus as shown in Figure 4.21, it is found that the residual elastic modulus

reduced faster under all curing conditions. Especially at 400°C, the residual elastic modulus is reduced by 55%, but the residual compressive strength is reduced by 30%.

4.5 Summary

The spalling behavior and residual properties of ultra-high strength concrete (UHSC) were introduced in this chapter. The following conclusions can be drawn.

(1) Steel fiber was not effective in preventing spalling of UHSC even with a dosage was as high as 1% by volume. Polypropylene fibers at a dosage of 0.1% was found to be effective even when the temperature was as high as 800°C since the polypropylene fiber can melt and then leave voids for the release of vapor.

(2) Compressive strength of UHSC was affected by the dosage of PP fibers due to the detrimental effect on workability. However, the reduction factors for the residual strength were not affected by the fiber dosage after heating to 800°C.

(3) Residual strength of UHSC at a heating rate of 30°C/min reduced faster than that at 5°C/min when the PP fiber dosage was 0.1%. However, the heating rate of 5°C/min is more severe at fiber dosage of 0.5%.

(4) Residual strength of UHSC was reduced slower than other concretes in the literature including NSC and HSC.

(5) Elastic modulus of UHSC was affected by the dosage of PP fibers as workability was affected. However, the reduction factors for the residual elastic modulus were unaffected by the fiber dosage.

(6) Residual elastic modulus of UHSC was reduced faster under higher heating rate. The difference between the reduction factors at 5°C/min and 30°C/min increased with increasing PP fiber dosage.

(7) Residual elastic modulus of UHSC was reduced slower than other concretes from literature, except for concrete from Hertz's tests where the concrete compressive strength was 150MPa.

(8) Curing conditions had no effect on the reduction factors for residual strength and residual elastic modulus of UHSC.

(9) Residual elastic modulus was reduced faster than that for compressive strength under all curing conditions.

Table 4.1: Mixing proportions of plain UHSC

Water/D4	Water (*kg*)	D4 (*kg*)	Grount Volume (*liters*)
0.076	1.9	25	9.4

Table 4.2: Mixing proportions of UHSC with additions of fibers

Specimen	Steel Fiber		Polypropylene Fiber		Water (*kg*)	D4 (*kg*)	Grount Volume (*liters*)
	% in volume	Weight (*kg*)	% in volume	Weight (*kg*)			
UHSC	-	-	-	-	1.9	25	9.4
UHSC-S	1%	0.7379	-	-	1.88	24.75	9.4
UHSC-P	-	-	1%	0.0865	1.88	24.75	9.4
UHSC-SP	0.5%	0.369	0.5%	0.0432	1.88	24.75	9.4

Table 4.3: The properties of steel fiber

Code	Diameter (*mm*)	Length (*mm*)	Aspect Ratio	Density (*kg/m³*)	Tensile Strength (*MPa*)	Elastic Modulus (*GPa*)	Coating
SF13/80	0.16	13	80	7850	2300	200	Brass

Table 4.4: The properties of polypropylene fiber

Type	Diameter (*mm*)	Length (*mm*)	Density (*kg/m³*)	Tensile Strength (*MPa*)	Water Absorbency
Monofilament	0.03±0.005	13	910±0.01%	≥450MPa	No

Table 4.5: The residual strength of UHSC mixtures after 800°C

No.	Strengths (MPa)		Reduction factor
	Room temperature	After 800°C	
UHSC	166.6	Not heated	-
UHSC-S	170.1	Spalling (no strength was tested)	-
UHSC-P	144.1	33.8	0.235
UHSC-SP	155.8	39.8	0.255

Table 4.6: The mix proportions of NSC C50

Water/Cement	Water (kg/m^3)	Cement (kg/m^3)	Sand (kg/m^3)	Coarse Aggregate (kg/m^3)
0.5	225	450	625	1005

Table 4.7: Residual strengths (MPa) from different fiber dosage and heating rate

Temp (°C)	UHSC with no fiber	C50 with no fiber	UHSC with 0.1% fiber		UHSC with 0.25% fiber		UHSC with 0.5% fiber	
	5 °C/min	5 °C/min	5 °C/min	30 °C/min	5 °C/min	30 °C/min	5 °C/min	30 °C/min
30	163	46	161	183	151	151	147	147
200	171	44	171	184	164	159	153	149
400	128	35	126	128	101	105	97	95
600	-	19	74	80	59	60	52	55
800	-	9	41	28	36	31	34	31

Table 4.8: Residual elastic modulus (GPa) from different fiber dosage and heating rate

Temp. (^{0}C)	UHSC with no fiber	C50 with no fiber	UHSC with 0.1% fiber		UHSC with 0.25% fiber		UHSC with 0.5% fiber	
	5 ^{o}C/min	*5 ^{o}C/min*	*5 ^{o}C/min*	*30 ^{o}C/min*	*5 ^{o}C/min*	*30 ^{o}C/min*	*5 ^{o}C/min*	*30 ^{o}C/min*
30	60	27	61	65	54	54	53	53
200	58	22	56	61	51	47	52	43
400	32	10	28	30	24	22	24	20
600	-	3	22	17	18	15	18	12
800	-	1	21	9	20	12	19	10

Table 4.9: Residual strength and elastic modulus from different curing conditions

Temp. (^{o}C)	UHSC-D		UHSC-H		UHSC-S	
	f_{ck} (*MPa*)	E_c (*GPa*)	f_{ck} (*MPa*)	E_c (*GPa*)	f_{ck} (*MPa*)	E_c (*GPa*)
30	183	65	181	67	186	66
200	184	61	186	60	189	60
400	128	30	137	29	129	30
600	80	17	74	18	77	18
800	28	9	31	10	30	9

Figure 4.1: Steel fiber

Figure 4.2: Polypropylene fiber

Figure 4.3: Spalled UHSC specimens with steel fiber after taken out from oven

| Room temperature | 200 ^{0}C | 400 ^{0}C | 600 ^{0}C | 800 ^{0}C |
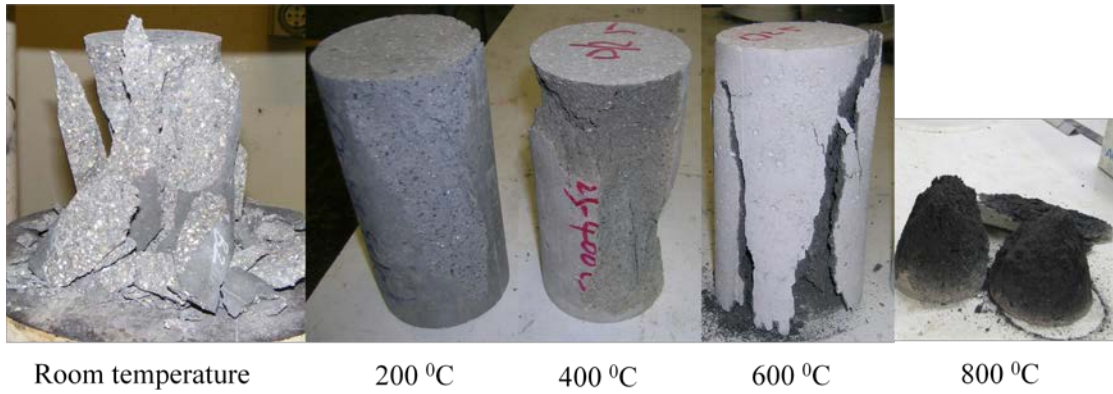
Figure 4.4: Failure modes after being subjected to the target temperatures and

compression
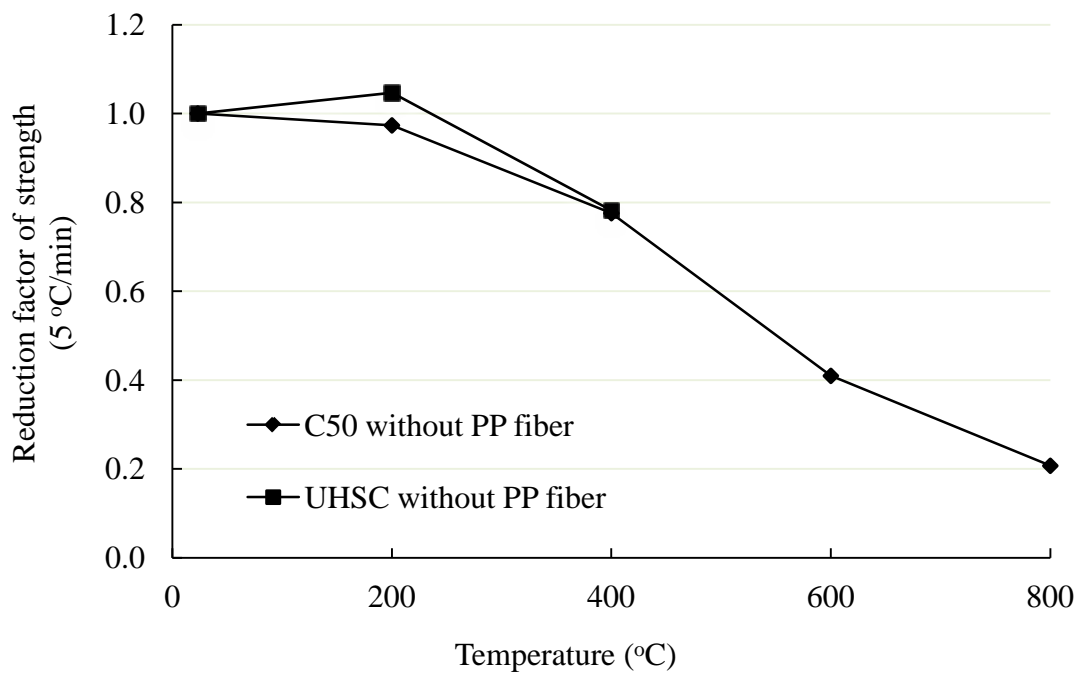
Figure 4.5: Comparison between reduction factors of residual strength of plain UHSC

and C50 without PP fiber
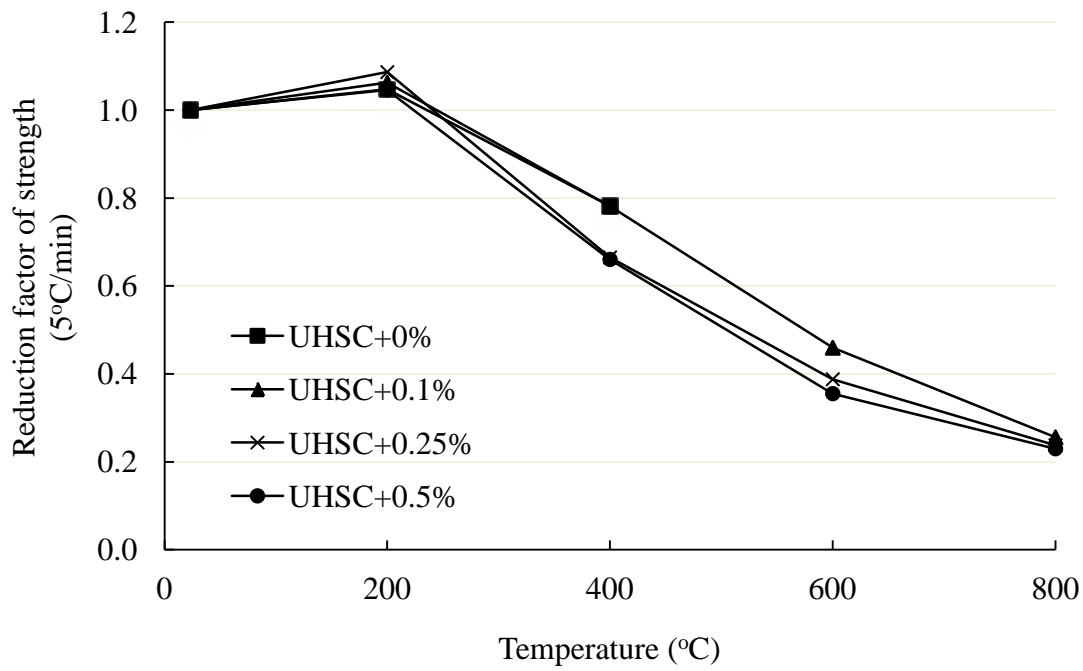
Figure 4.6: Effects of fiber dosage on reduction factors of residual strength of UHSC

mixtures-5°C/min
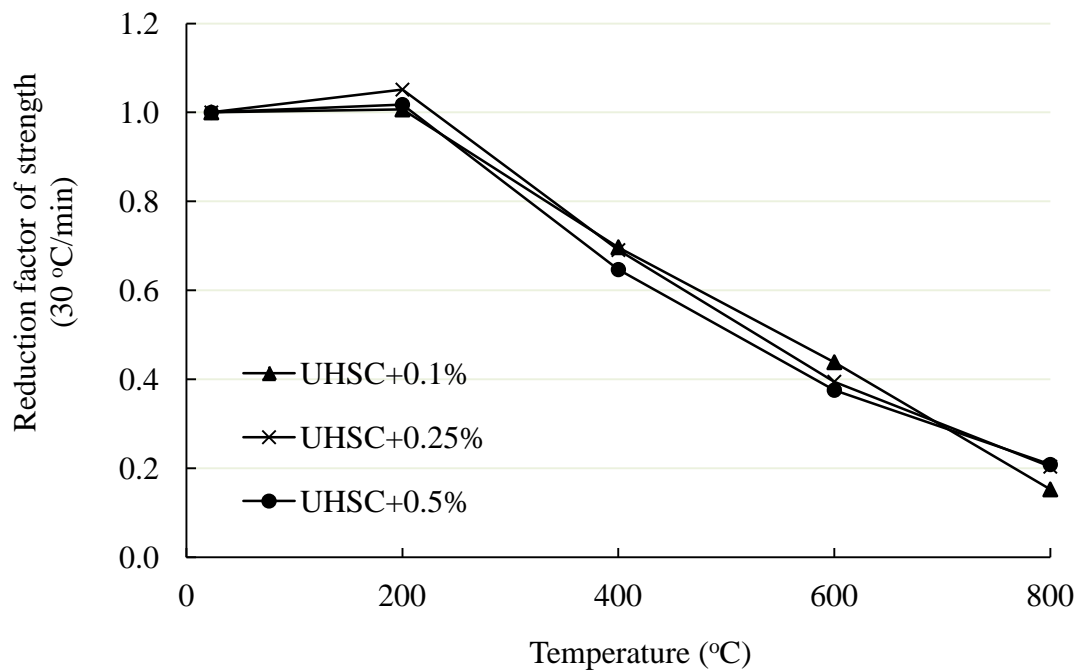
Figure 4.7: Effects of fiber dosage on reduction factors of residual strength of UHSC

mixtures-30°C/min
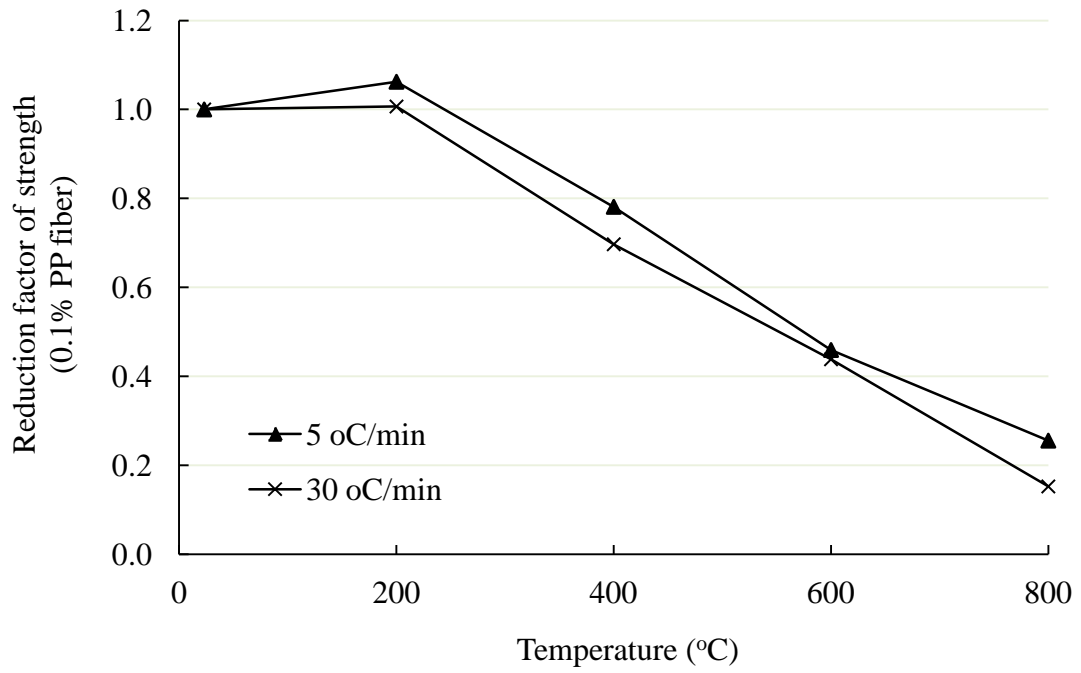
Figure 4.8: Effects of heating rate on reduction factors of residual strength of UHSC mixtures-0.1% PP fiber
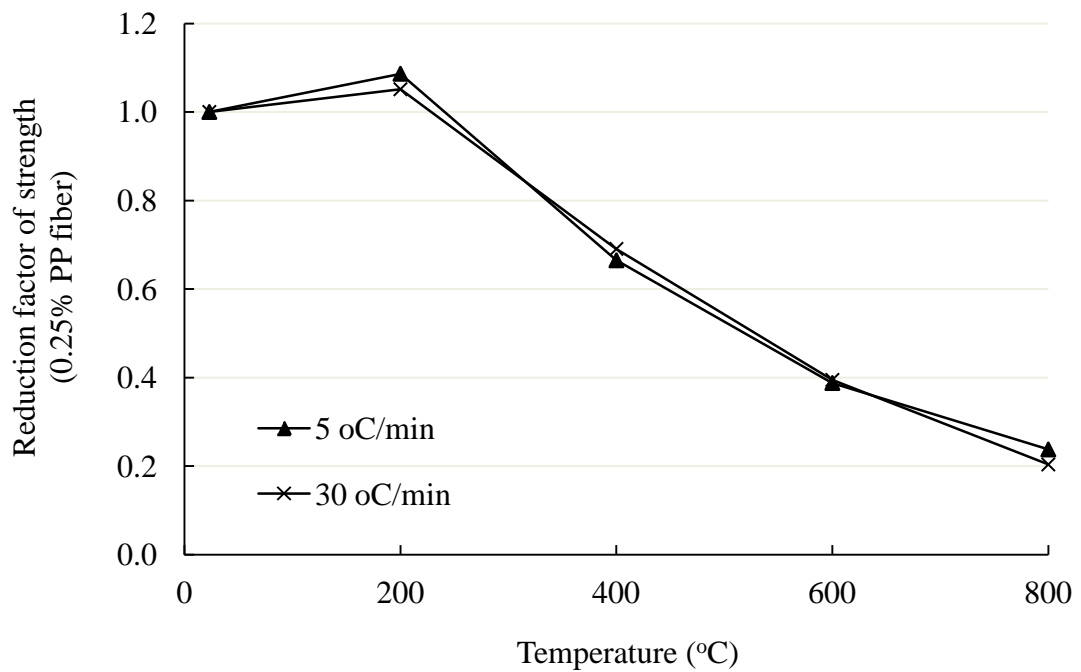
Figure 4.9: Effects of heating rate on reduction factors of residual strength of UHSC mixtures-0.25% PP fiber
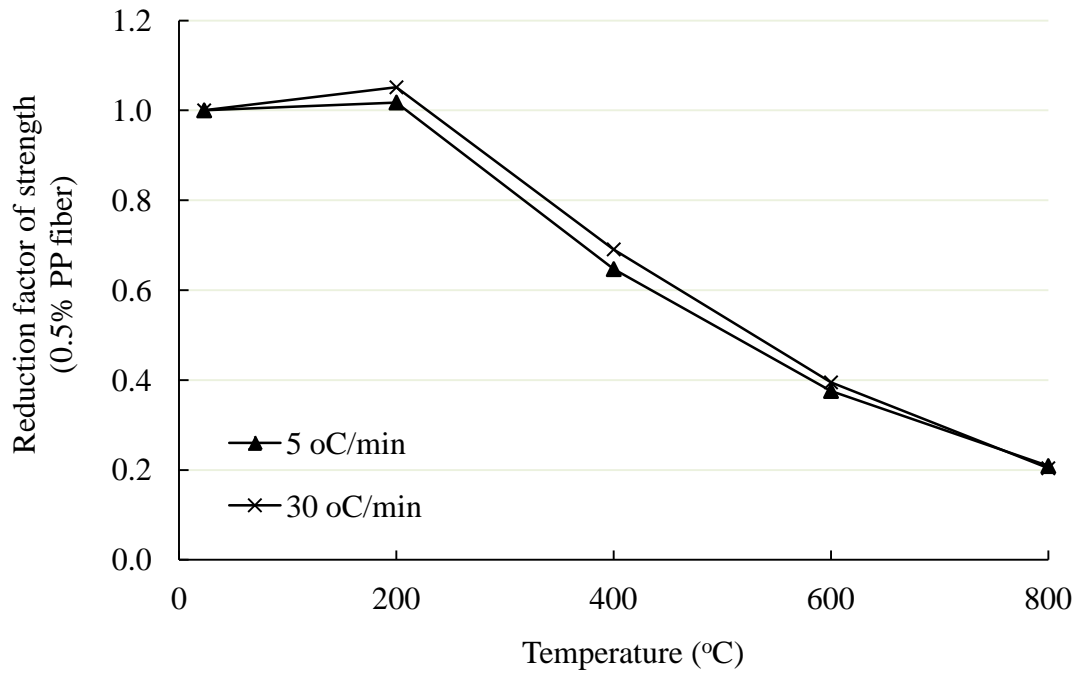
Figure 4.10: Effects of heating rate on reduction factors of residual strength of UHSC

mixtures-0.5% PP fiber
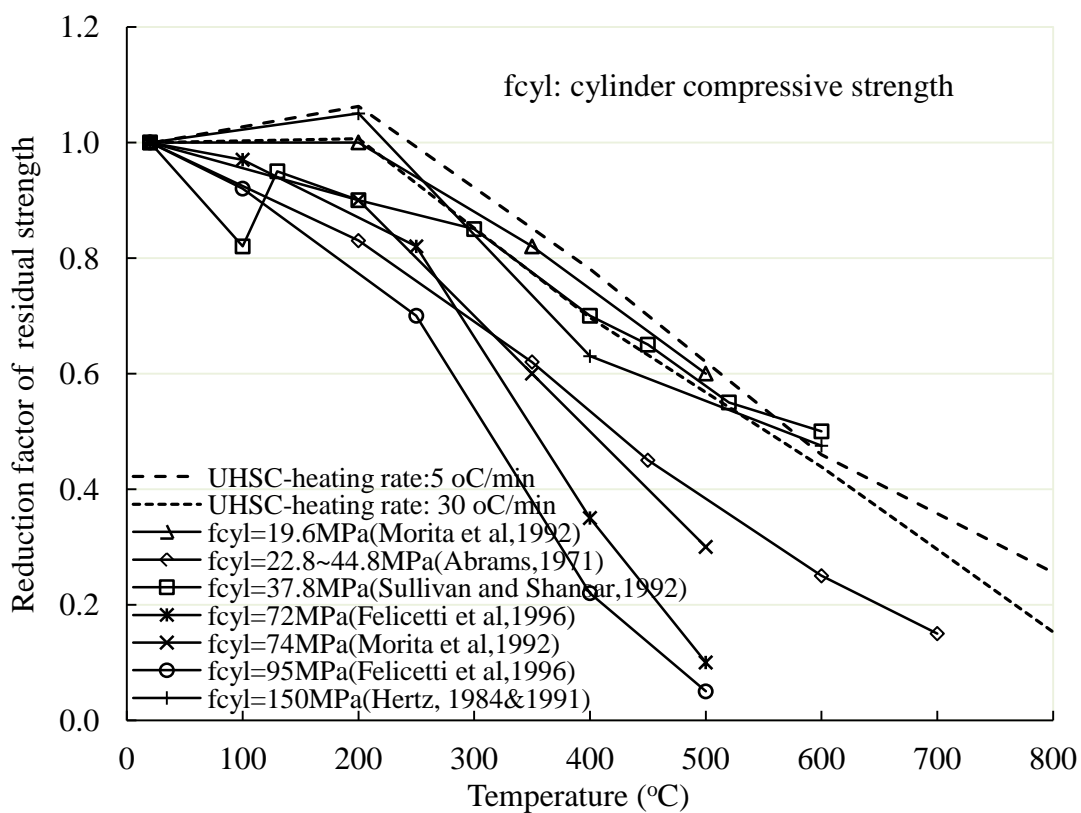
Figure 4.11: Comparison between reduction factors of residual strengths of UHSC

with addition of 0.1% PP fiber and concretes in literature
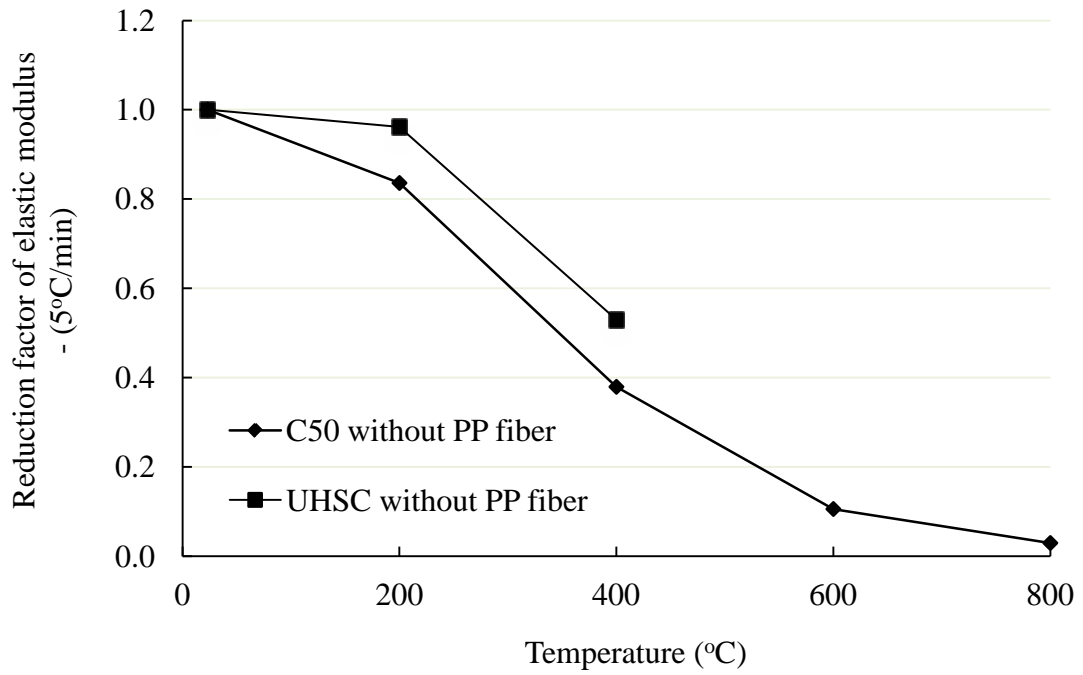
Figure 4.12: Comparison between reduction factors of residual elastic modulus of

plain UHSC and C50 without PP fiber
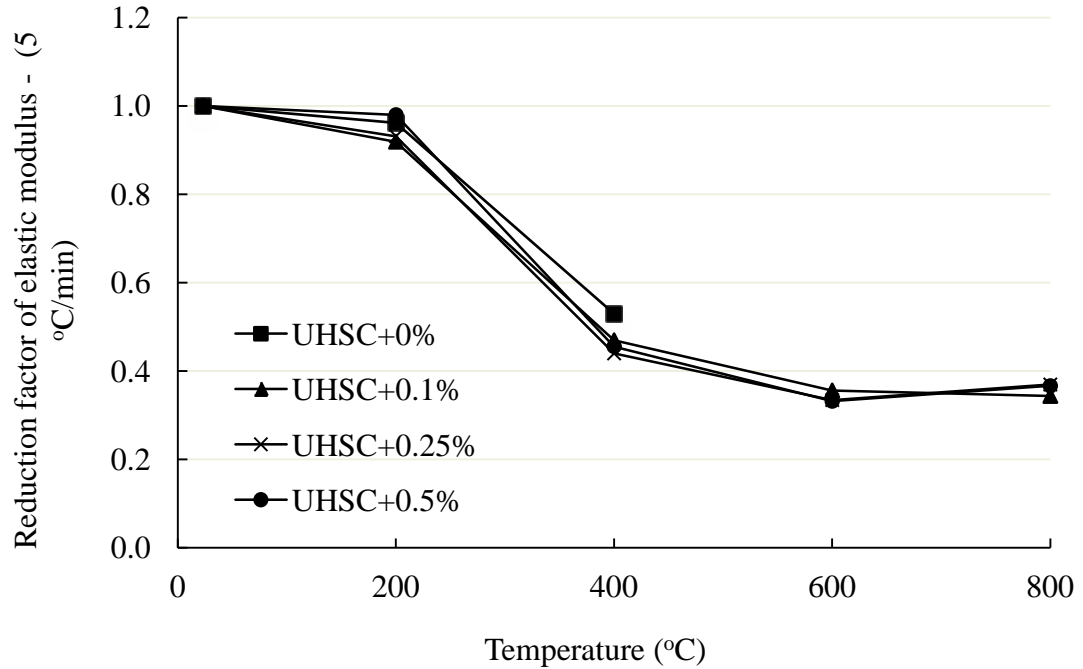
Figure 4.13: Effects of fiber dosage on residual elastic modulus factor of UHSC

mixture-5°C/min
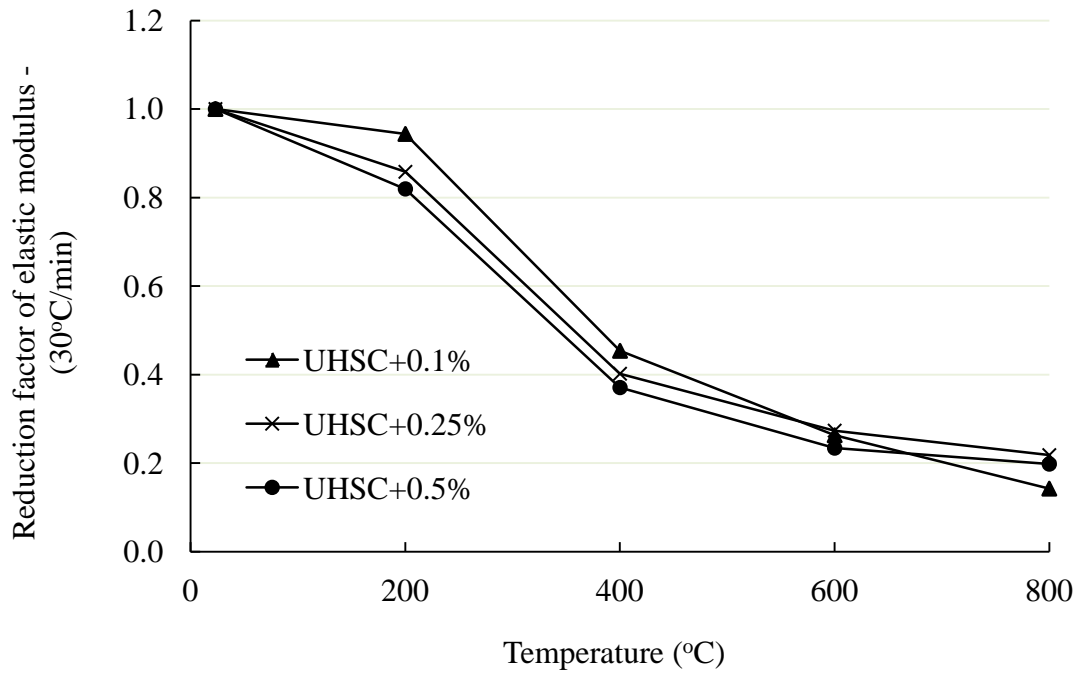
Figure 4.14: Effects of fiber dosage on residual elastic modulus factor of UHSC

mixture-30°C/min
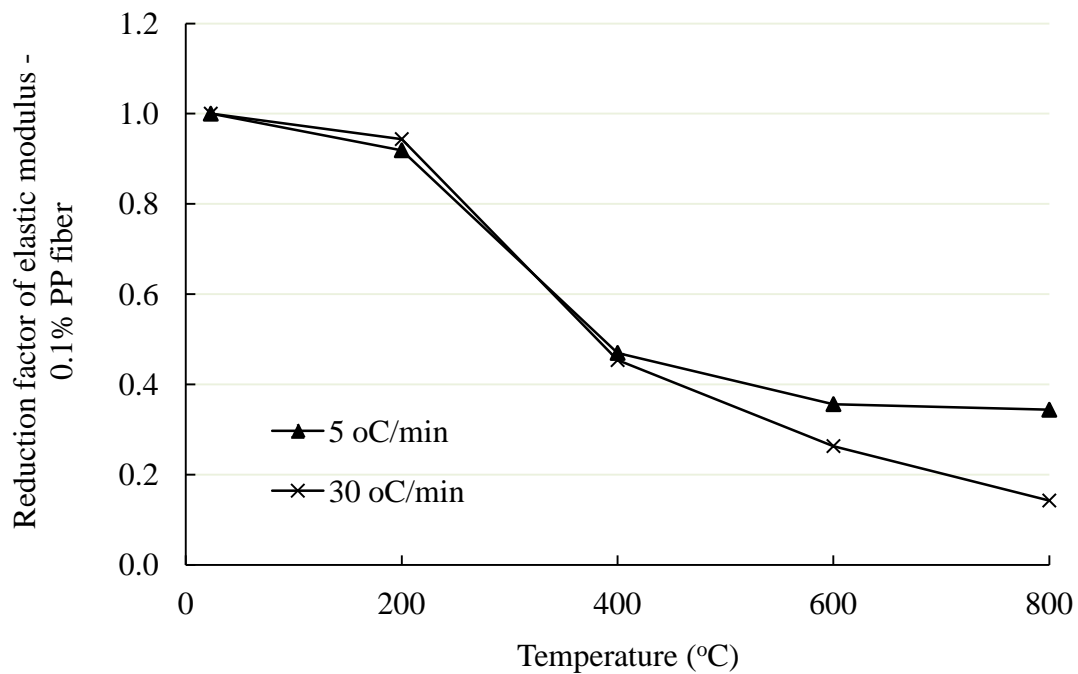
Figure 4.15: Effects of fiber dosage on residual elastic modulus factor of UHSC

mixture-0.1% PP fiber
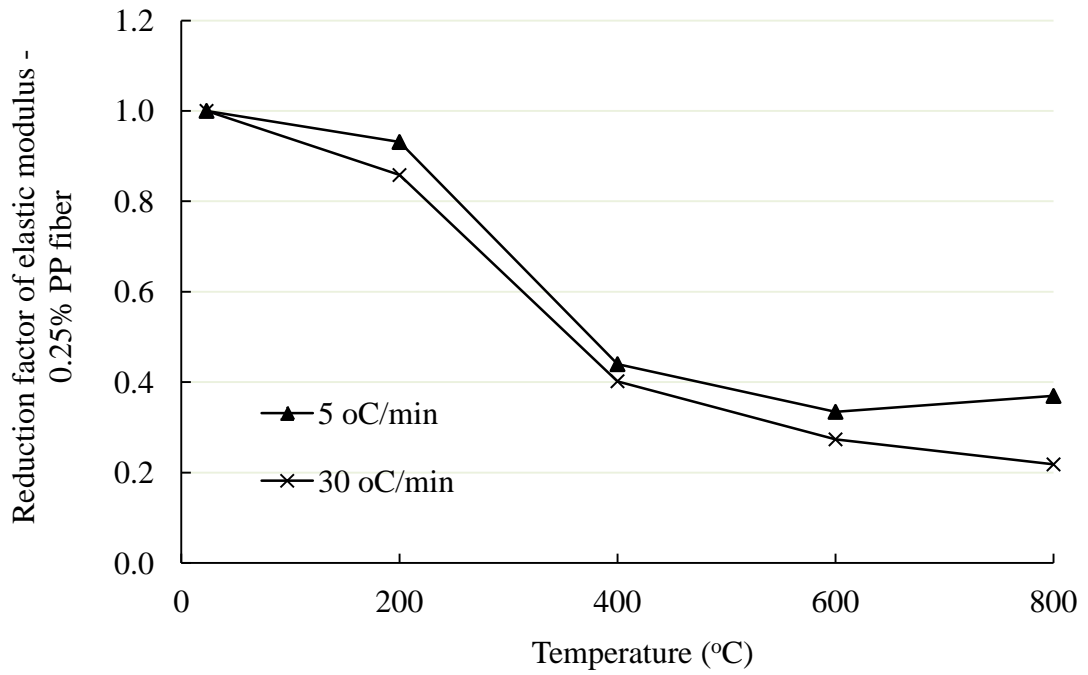
Figure 4.16: Effects of fiber dosage on residual elastic modulus factor of UHSC

mixture-0.25% PP fiber
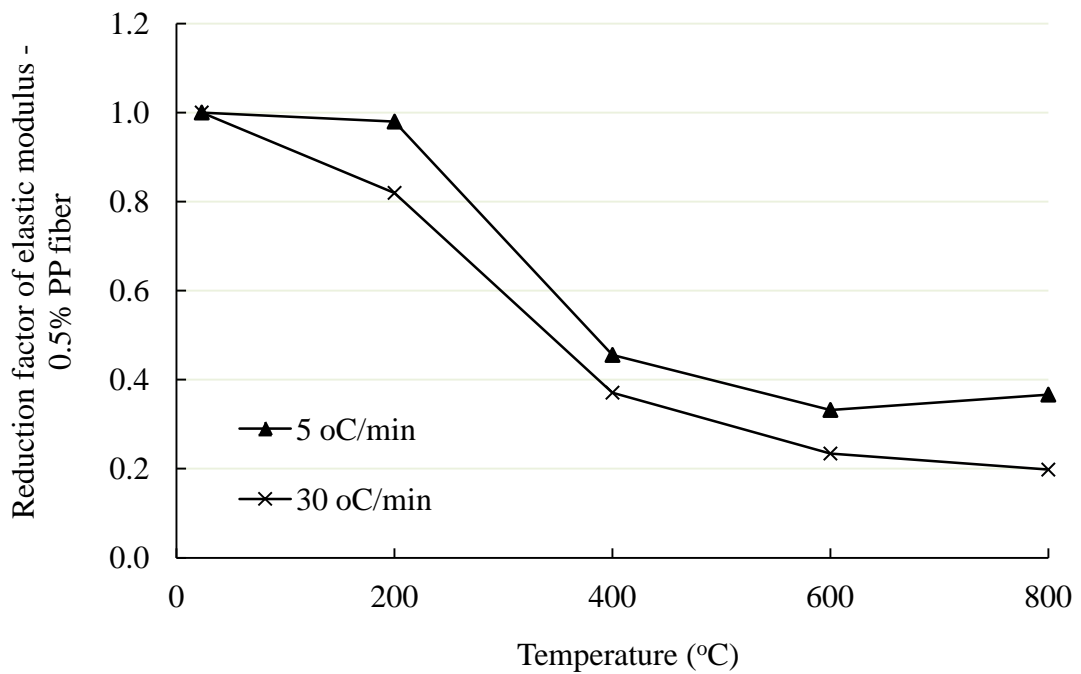
Figure 4.17: Effects of fiber dosage on residual elastic modulus factor of UHSC

mixture-0.5% PP fiber
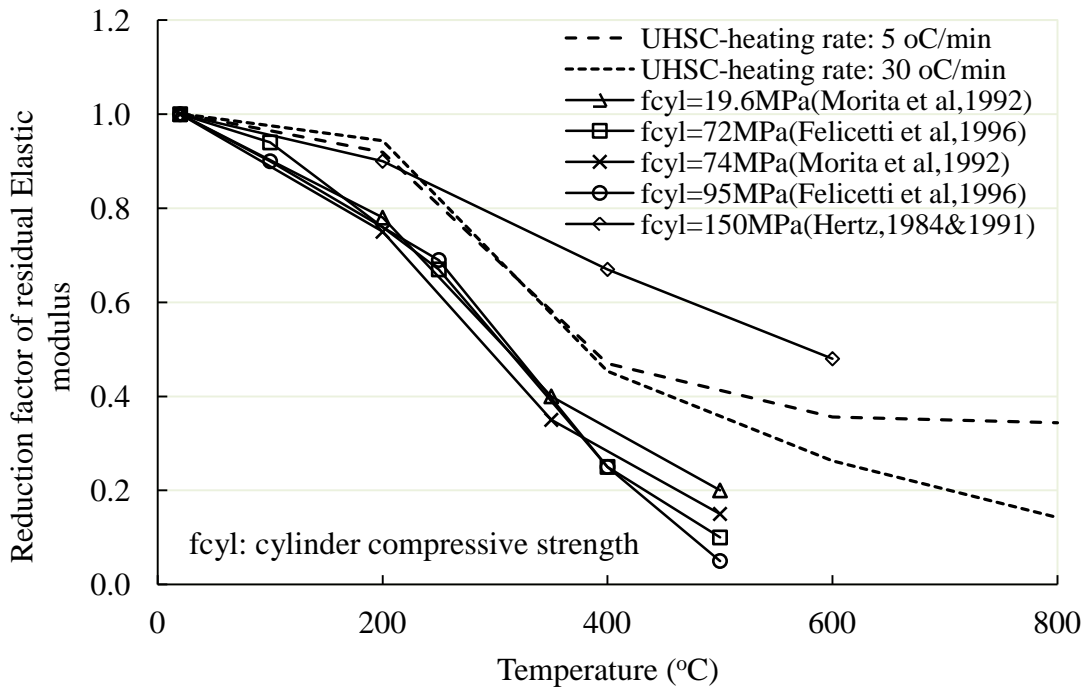
Figure 4.18: Comparison between reduction factors of residual elastic modulus of

UHSC with addition of 0.1% PP fiber and concretes in literature
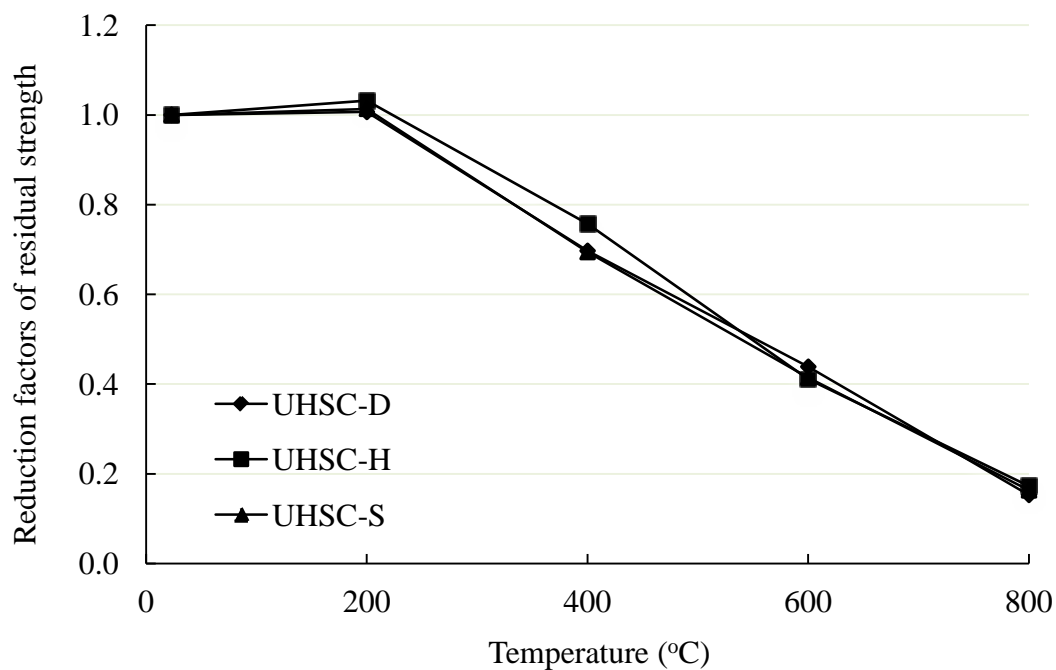
Figure 4.19: Effects of curing conditions on reduction factors of residual strength of
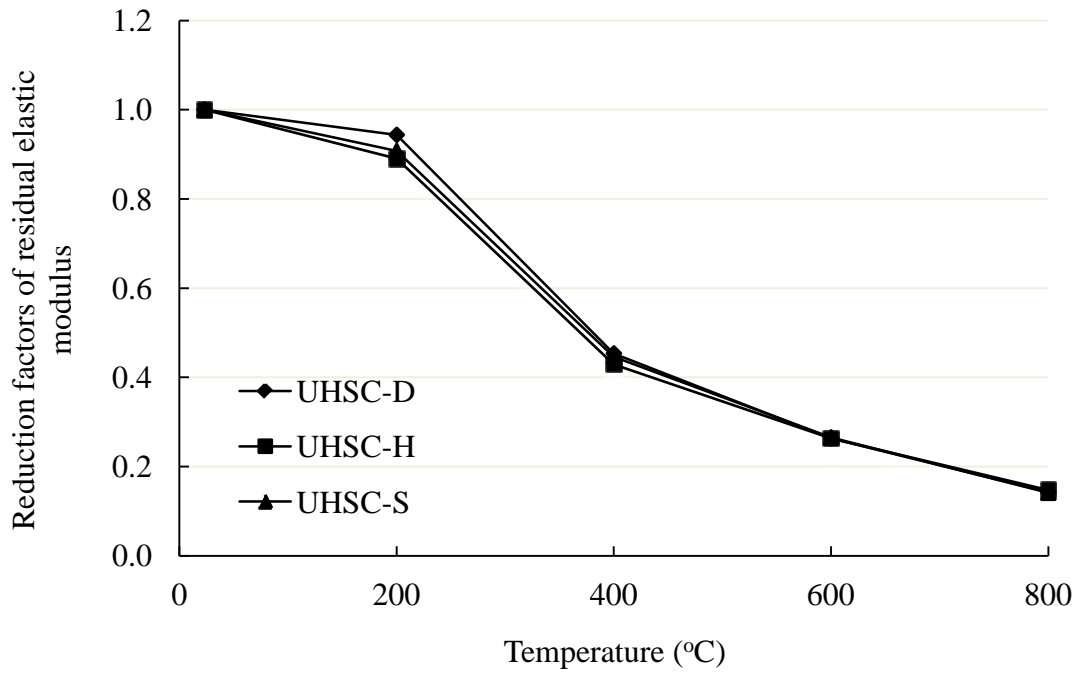
UHSC mixtures

Figure 4.20: Effects of curing conditions on reduction factors of residual elastic

modulus of UHSC mixtures
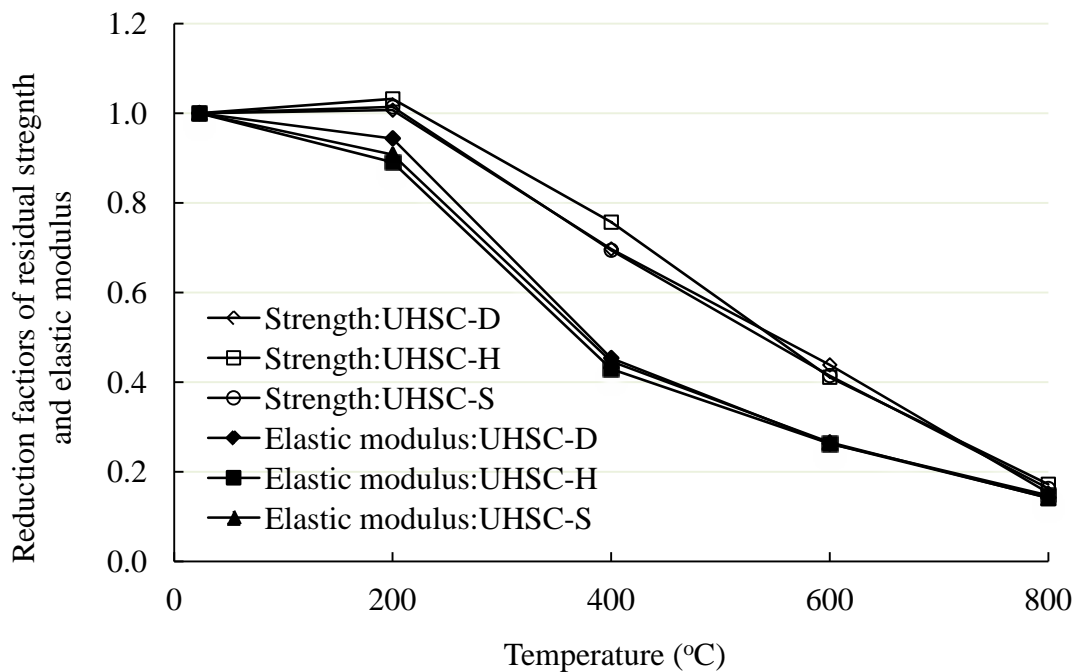
Figure 4.21: Comparison between reduction factors of residual strength and residual

elastic modulus under all curing conditions

Chapter 5 Behavior of Ultra-High Strength Concrete at Elevated Temperatures

5.1 Overview

This chapter introduces the experimental investigations on the mechanical properties of ultra-high strength concrete (UHSC) at elevated temperatures. The investigated parameters were only elastic modulus and cylindrical compressive strength, limited by the testing facilities. Axial compression tests were carried out at elevated temperatures. The test results were compared with those for normal strength concrete (NSC) and high strength concrete (HSC) as given in EN 1992-1-2 as well as HSC in the literature. These reduction factors for compressive strength and elastic modulus are proposed for fire resistant design in Chapter 7.

5.2 Compression Tests at Elevated Temperature

5.2.1 Test Specimens

The material of UHSC was the same as that introduced in Chapter 4. Cylinder specimens with diameter of 100mm by height of 200mm were cast. After demoulding, the specimens were covered by plastic sheet and cured in lab air. The relative humidity of lab air was around 85% and the temperature was about 30°C. Dosage of 0.1% polypropylene in volume was added into UHSC in case of spalling during heating. The diameters and heights of specimens were measured before testing.

5.2.2 Test Equipments

The compression tests were conducted on a servo-hydraulic testing machine, with a maximum 300mm stroke displacement and capacity of 1000ton.

The heat apparatus is a split-tube furnace with two-zone configuration and an optional side entry extensometer port. The furnace is constructed with S304 stainless steel shell and alumina insulation material. Heating elements are coils of Fe-Cr-Al alloy 0Cr27a17mo2. A type K thermocouple is mounted in the center of each heating zone. The external dimensions (diameter x height) are 700 x 600mm and internal heating dimensions (diameter x height) are 350 x 400mm. The furnace can heat up to a maximum temperature of 800°C.

Model 3548HI high temperature furnace extensometer was used to measure the relative deformation in gauge length. It is a strain gauged sensor, compatible with nearly any signal conditioning electronics designed for strain gauged transducers (Epsilon Technology Corp, 2000). The arms of the extensometer are alumina rods. It is specified for a gauge length of 50mm and the arms of extensometer can relatively travel 10mm under either tension or compression. Thus the maximum measurable strain is 20%. Water cooling is used to protect the extensometer and cool down the mounting block.

5.2.3 Test Setup

Since the loading head of compression machine could not be extended into the furnace to compress the specimen under high temperature, the cooling plate was fabricated with one end connected to the loading head and another end inside furnace applying load on to specimen. The cooling plate is a steel cylinder with water circulation paths drilled inside which is shown in Figure 5.1.

The test setup is schematically shown in Figure 5.2. The compression load was applied from the bottom of specimen. During heating, the water was circulating in the cooling plate. During loading, the specimen was covered by a steel casing in case the spalling of concrete at failure would damage the furnace as shown in Figure 5.4. Specimen without protection by steel casing is for reference as shown in Figure 5.3.

The rods of the extensometer were attached to the middle 1/4 height of the specimen. A vertical gap was cut in the steel casing so that the extensometer could be extended through the gap and attached to the surface of the specimen. For each target temperature, the extensometer was removed when the stress of concrete reached around 40% of the compressive strength of specimen. Otherwise, the spalling of concrete at failure would damage the extensometer. Hence, the full stress-strain curves could not be measured.

5.2.4   Test Method

The test method followed the recommendation of RILEM TC 200-HTC: mechanical concrete properties at high temperatures—modeling and applications, Part 2: Stress–strain relation (RILEM Technical Committee, 2007). Stressed and unstressed testing methods are available. In stressed testing, the specimen is pre-loaded before it is heated. Contrarily, unstressed testing is defined as specimens without pre-loading during the period of temperature exposure prior to testing. Unstressed testing was adopted in the current research.

Prior to testing, a small compressive stress referred to as "pre-load level", about 0.05MPa, was applied in the direction of the specimen's central axis, in order to maintain the specimen at the center of loading machine. Then, the specimen was

subjected to three load cycles between the pre-load level and 15% or between 5% and 15% of the reference strength, as shown in Figure 5.5. The holding time at 5% and 15% load levels was 60s.

After load cycling, the specimen was subjected to heating with a heating rate of 5°C/min. After the target temperature was achieved, it was held for 4 hours to ensure that the temperature was uniformly distributed inside both the furnace and the specimen. In addition to ambient temperature which is about 30°C, the target temperatures ranged between 100°C~800°C at increments of 100°C. For each target temperature, three specimens were tested.

After holding of the target temperature, the specimen was subjected to compression until failure. Displacement control was adopted during loading. The displacement rate was 0.4mm/min.

5.3 Test Results

5.3.1 Compressive Strength

Spalling was not observed during heating of all the specimens. The compressive strength of UHSC at room temperature was 166MPa which was averaged from 6 specimens. The reduction factors for compressive strength under high temperatures are shown in Figure 5.6. Overall, the strength decreased sharply as the temperature increased to 100°C. However with a further increase in temperature to 300°C, the strength was partly recovered. This will be explained later. Beyond 300°C, the strength decreased with increasing temperature. At 800°C, the strength was about 30% of that at room temperature.

The comparisons between the reduction factors for strength at elevated temperatures and residual strength after elevated temperatures are also shown in Figure 5.6. It can be seen that the residual strength was reduced faster than the strength when temperature was higher than 300°C. This might be attributed to two facts. One fact is that the residual strength was affected by the internal micro-cracking induced by differential thermal strain since the specimens naturally cooled down in furnace after heating. Another fact is that the calcium oxide (CaO) from the decomposition of hydration products $Ca(OH)_2$ absorbed water after cooling down from high temperatures. Then, it expanded and increased cracking inside the concrete. As a result, the residual compressive strength was lower (Li et al., 2006).

It is believed that the changes in the chemical composition of the cement paste are not noticeable around 100°C. Thus, the unusual deterioration of strength at 100°C might be due to either the expansion of the cement paste or to the change in porosity caused by evaporation of free water (Naus, 2006).

However, as mentioned in Chapter 4 for residual compressive strength after high temperatures, the recovery in strength at a temperature between 100°C and 300°C still remains unaccounted for. The prevailing attribute was the general stiffening of the cement gel, in other words, the increase in surface forces (Van der Walls forces) between gel particles due to the removal of water. The temperature at which water is removed and the strength begins to increase depends on the porosity of the concrete (Chen and Liu, 2004).

It is believed that the reasons for the decrease in strength beyond 300°C are similar to those for residual strength. Thus, it was attributed to the decomposition of hydration products such as C-S-H and $Ca(OH)_2$, deterioration of the aggregates, and cracking

due to thermal incompatibility between the aggregate and the cement paste which led to stress concentration.

The comparisons between the strength reduction factors of UHSC and NSC in EN 1992-1-2 are shown in Figure 5.7. It is supposed that the strength of UHSC would reduce faster than that of NSC. However, it can be seen that, beyond 200°C, the reduction factors of UHSC are similar with those of NSC with calcareous aggregate, but higher than those of NSC with siliceous aggregate. The reason could be due to the effect of aggregate type since the aggregate normally occupy 65% to 75% of the concrete volume. Bauxite aggregate is used in UHSC (Densit, 2008).

The effect of aggregate depends mainly on the thermal stability or integrity of aggregate at high temperatures (Naus, 2008). Commonly used aggregate materials are thermally stable up to 300°C~350°C. However for bauxite aggregates, it is normally used for refractory concrete thus can produce significant improvements in the heat resistance of concrete (Naus, 2008; Ouedraogo et al., 2011). That is why UHSC had comparable strength reduction factors with NSC. The comparison between strength reduction factors of UHSC and HSC in EN 1992-1-2 are shown in Figure 5.8. Obviously, the strength of UHSC was reduced slower than that of HSC.

The comparisons between the strength reduction factors of UHSC and HSC in the literature are shown in Figure 5.9. It can be seen that the unusual deterioration around 100°C and recovery of strength between 100°C~300°C were also captured in previous research. Overall, the strengths of UHSC at elevated temperatures were reduced slightly slower.

5.3.2 Elastic Modulus

Similar to residual elastic modulus as presented in Chapter 4, the elastic modulus at high temperature was taken as the secant modulus between the stress equal to 40% of peak stress and the stress corresponding to strain of 5×10^{-5} (ASTM C469-02, 2002). The elastic modulus of UHSC at room temperature was 61GPa which was averaged from 6 specimens. The reduction factors for elastic moduli at elevated temperatures are shown in Figure 5.10. Similar to strength, the unusual deterioration and recovery were also observed for elastic modulus.

A comparison of the reduction factors for elastic modulus and residual elastic modulus are also shown in Figure 5.10. For residual elastic modulus, there was no unusual deterioration and recovery at the temperature range of 100°C~200°C. The elastic modulus was reduced slightly slower than the residual elastic modulus at temperatures between 200°C~500°C, but faster beyond 500°C.

A comparison of the reduction factors for elastic modulus of UHSC and HSC as published in the literature are shown in Figure 5.11. Unusual deterioration and recovery were also observed in some research. Overall, the reduction factors for the elastic modulus of UHSC are close to the upper limit in the band enclosed by these reduction factors.

5.4 Summary

The test results of mechanical properties of UHSC at elevated temperatures, including cylindrical compressive strength and elastic modulus, are presented in this chapter. The findings from these tests are summarized as follows:

(1) There was no spalling observed during heating of all the specimens tested.

(2) For compressive strength of UHSC at elevated temperatures, an unusual deterioration was observed at a temperature of 100°C. However, it was partly recovered in the range of 100°C~300°C.

(3) Comparing strength with residual strength, strength was reduced slower than residual strength when the temperature was higher than 300°C.

(4) Strengths of UHSC at elevated temperatures were reduced slower than those of NSC and HSC as presented in EN 1992-1-2.

(5) Unusual deterioration around $100°$C and recovery of the strength between $100°$C~$300°$C were also observed in previous experimental studies. Strengths of UHSC at elevated temperatures are reduced slightly slower than HSC reported in previous research.

(6) For the elastic modulus of UHSC at elevated temperatures, an unusual deterioration and recovery were observed at the temperature range of 100°C~200°C.

(7) Comparing elastic modulus with residual elastic modulus of UHSC, the elastic modulus was reduced slightly slower than the residual elastic modulus at temperatures between $200°$C~$500°$C, but faster beyond $500°$C.

(8) Unusual deterioration and recovery of elastic modulus were also observed in previous experimental studies. Reduction factors for elastic modulus of UHSC are close to the upper limit among the reduction factors reported in previous research.
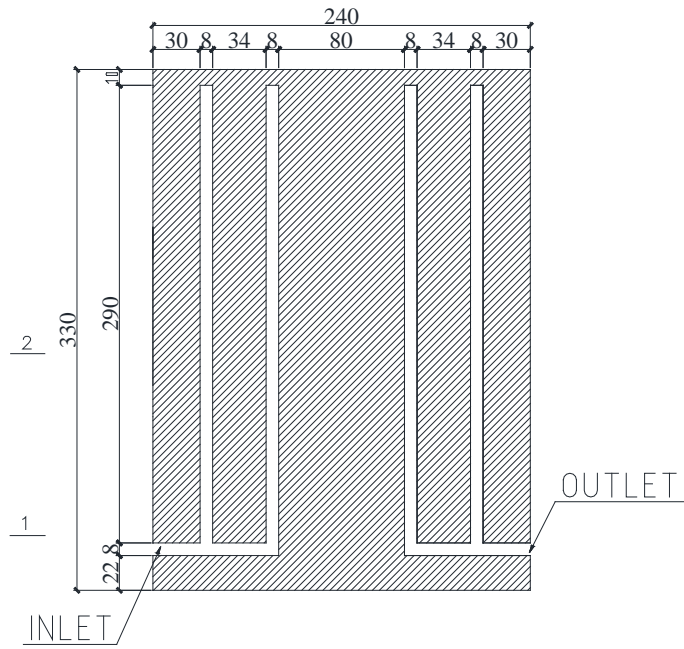
(a) Cut view
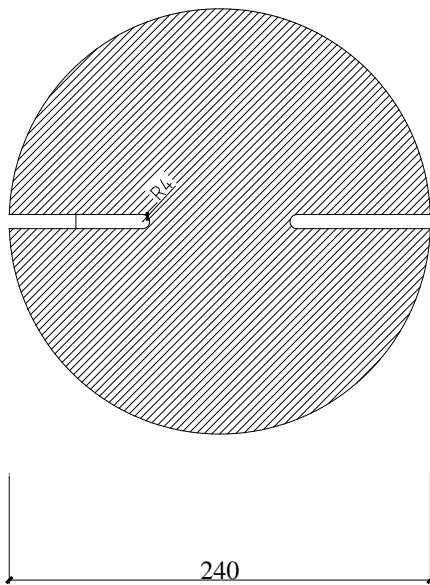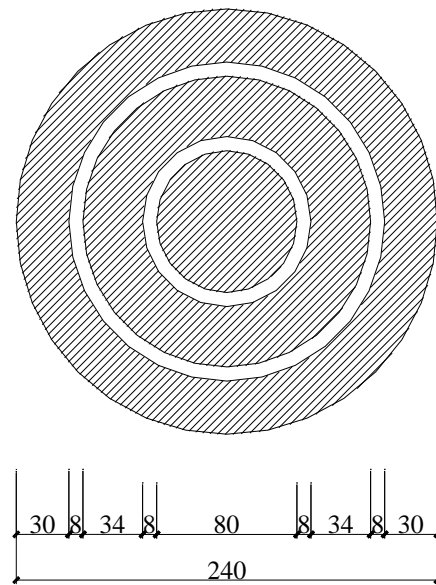
(b) Section view 1-1   (c) Section view 2-2

Figure 5.1: Details of cooling plate
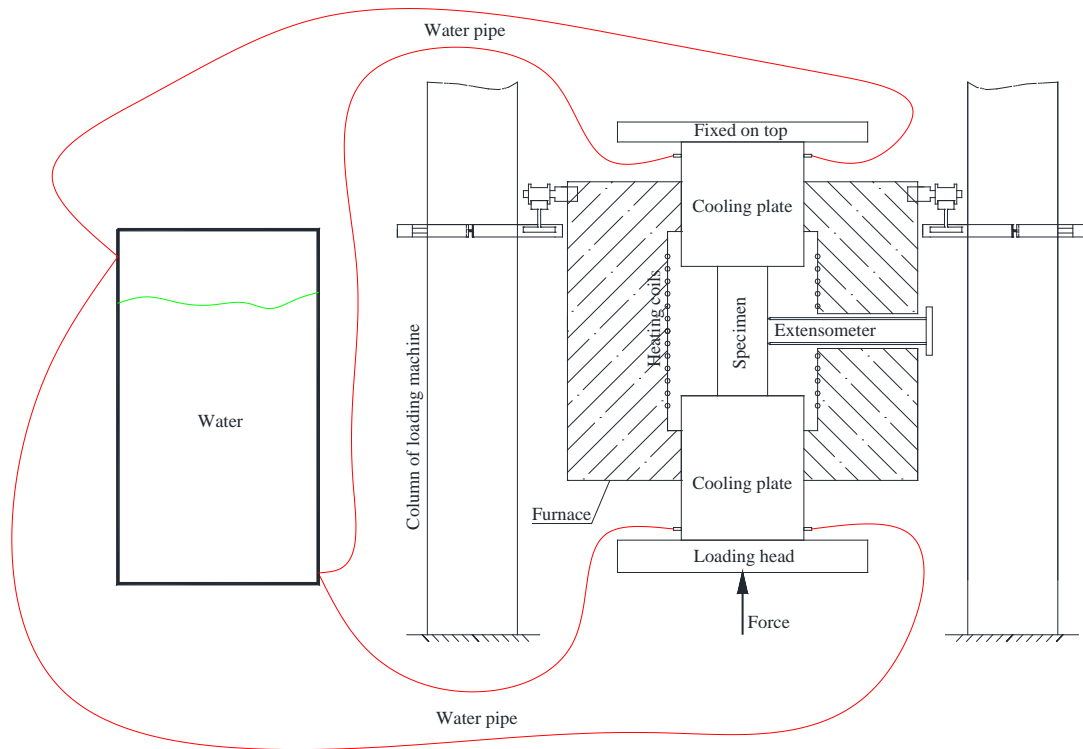
Figure 5.2: Test setup
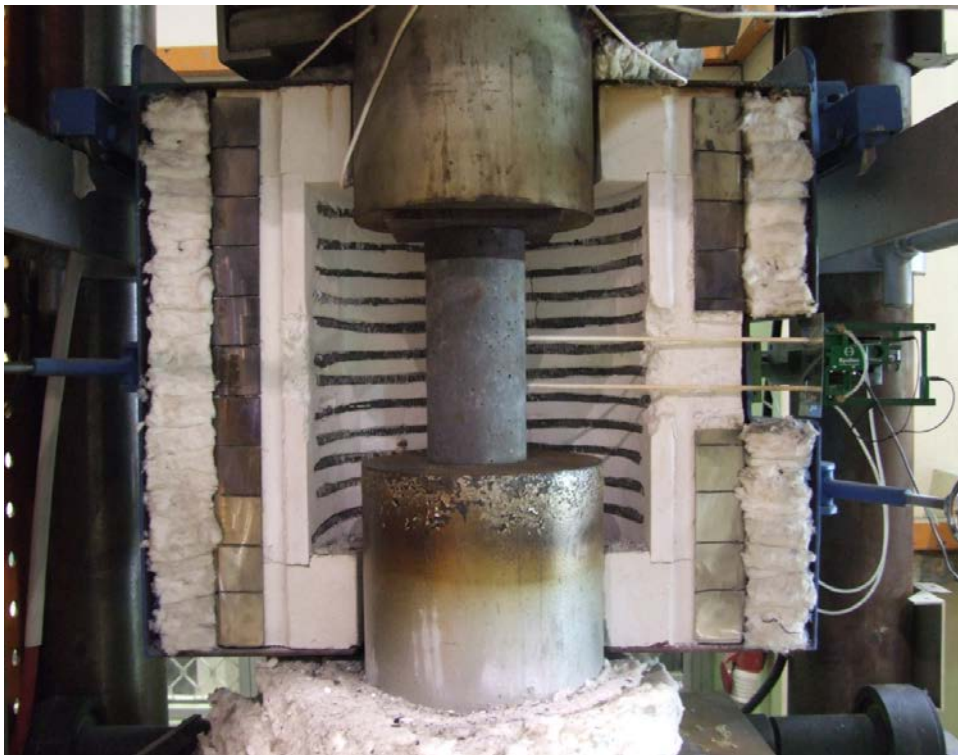
Figure 5.3: Specimen without protection by steel casing
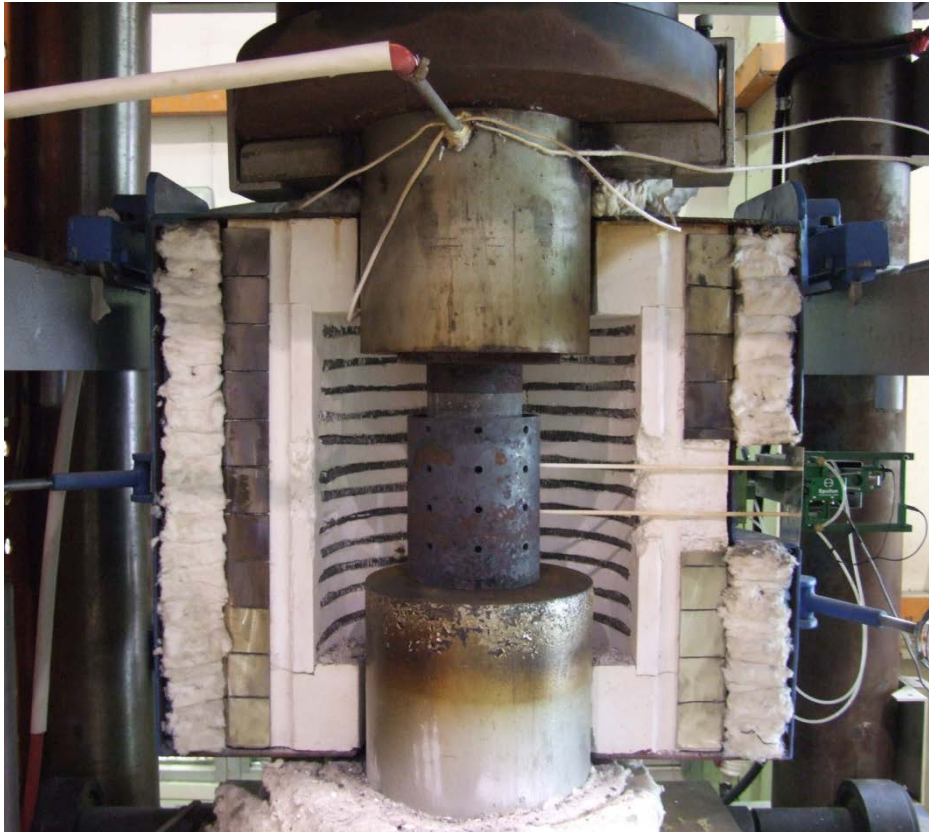
Figure 5.4: Specimen with protection by steel casing
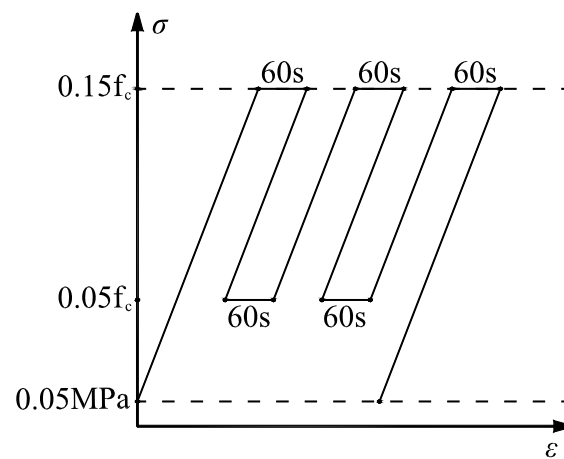
Figure 5.5: Schematic illustration of preloading cycles applied on the test specimens
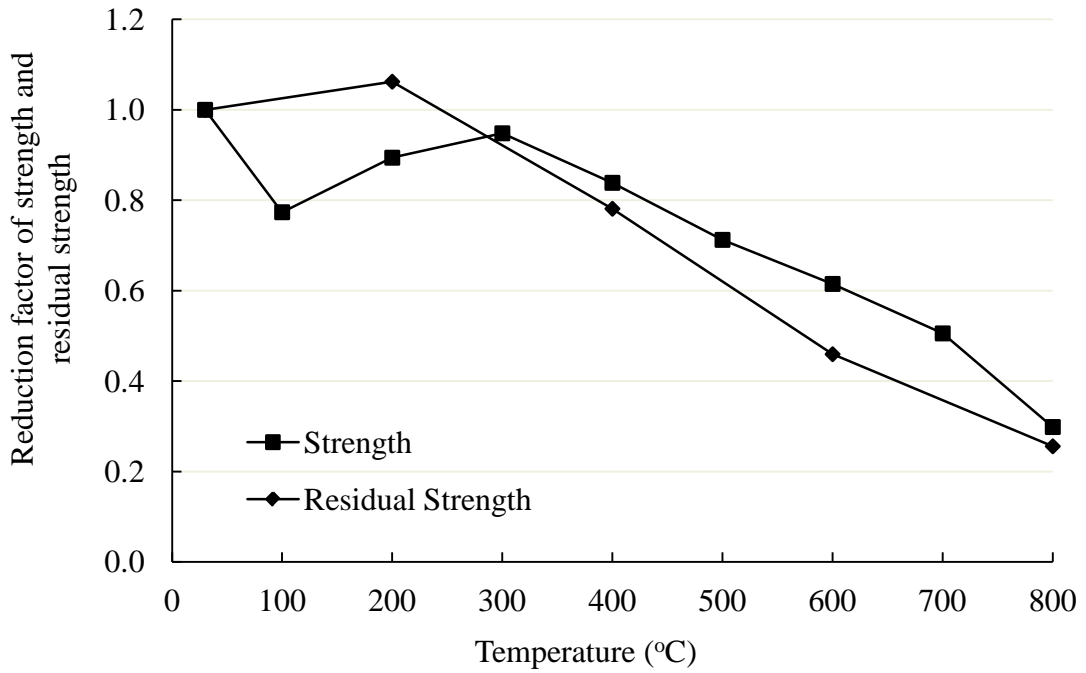
Figure 5.6: Comparison between reduction factors of strength and residual strength
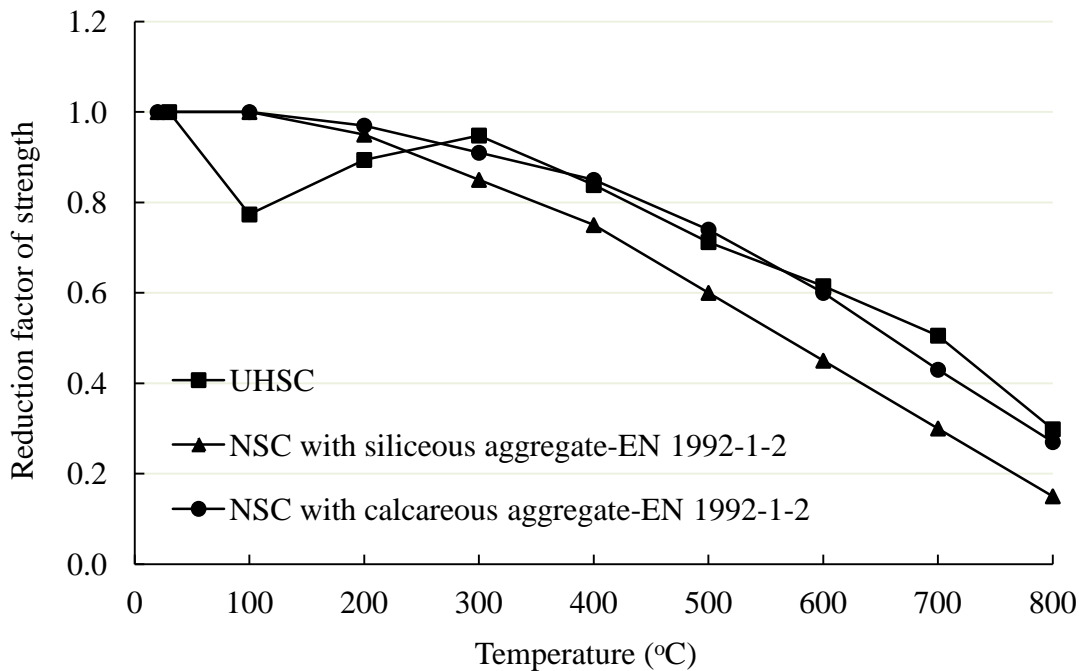
Figure 5.7: Comparison between strength reduction factors of UHSC and NSC as

given in EN 1992-1-2
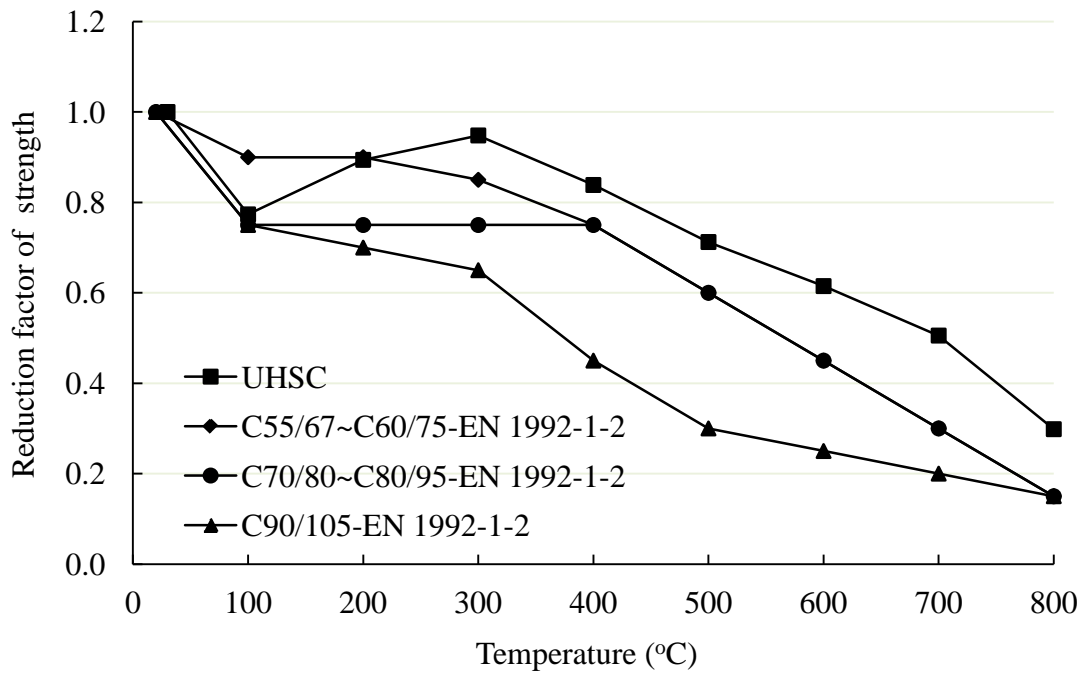
Figure 5.8: Comparison between strength reduction factors of UHSC and HSC as

given in EN 1992-1-2
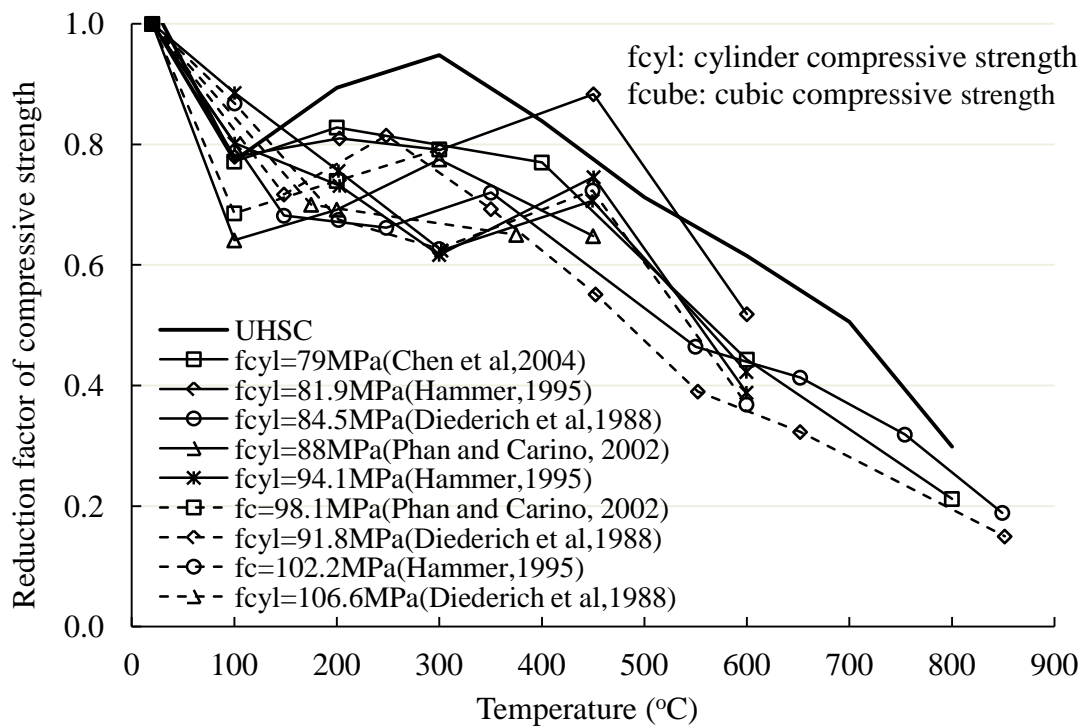
Figure 5.9: Comparison between strength reduction factors of UHSC and HSC with

results from previous researches
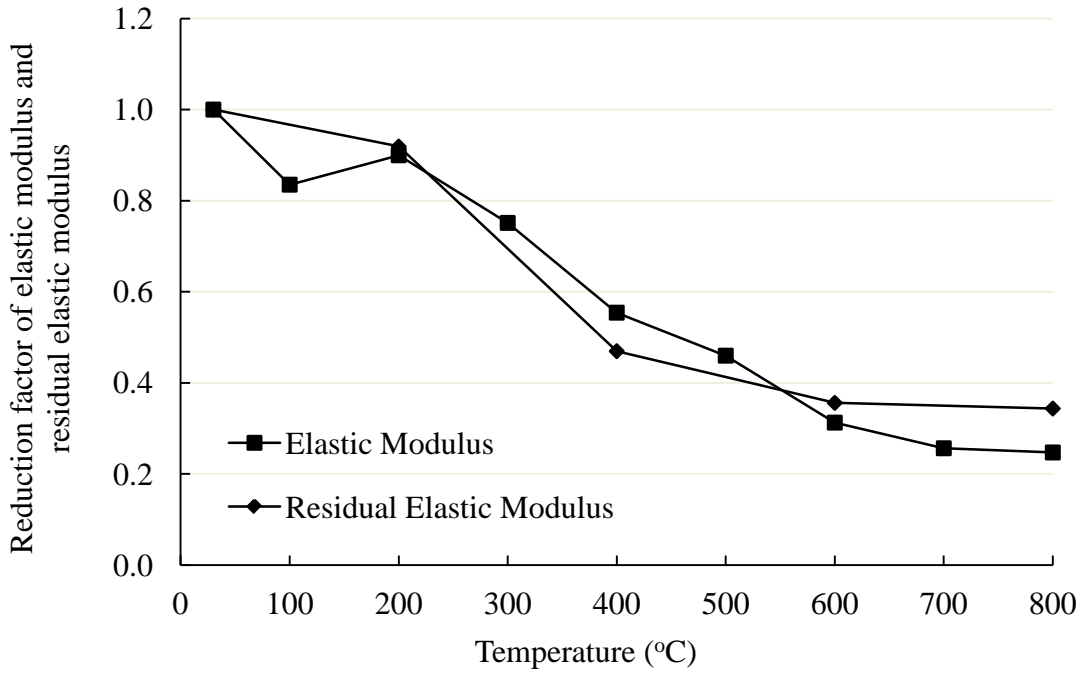
Figure 5.10: Comparison between reduction factors of elastic modulus and residual
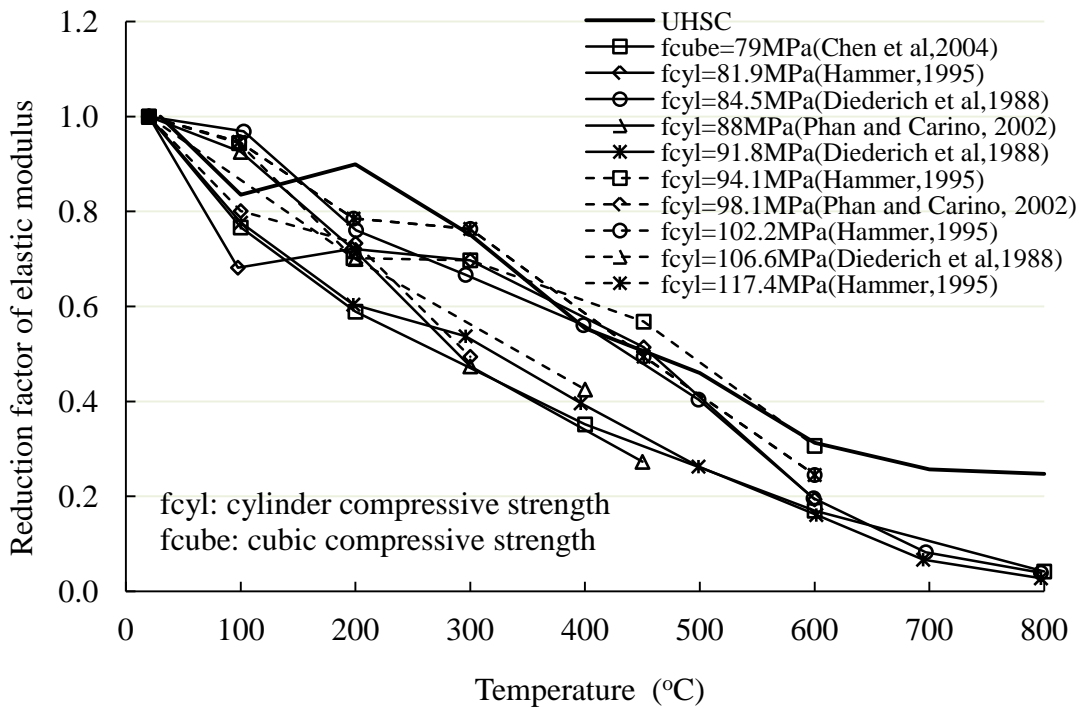
elastic modulus

Figure 5.11: Comparison between reduction factors of elastic modulus of UHSC and

HSC as given in previous researches

Chapter 6   Fire Tests on Ultra-High Strength Concrete Filled Steel Tubular Columns

6.1 Overview

In this chapter, the experimental studies based on standard fire tests on the behaviors of CFST columns with UHSC and HSS are presented. Both columns with single-tube and double-tube were tested. The test results, including temperature profiles of columns, axial deformations, fire resistance time, and failure modes are presented. In addition, the details of tested CFST columns, load level, boundary conditions, concrete casting method, steaming hole, fire protection material, thermocouples, test setup, instrumentation, test procedure and failure criteria are also described.

6.2 Details of Concrete Filled Steel Tubular Columns

6.2.1   Specimen Design

The details of CFST columns are shown in Figure 6.1 ~ Figure 6.4. The investigated parameters are the profiles of cross-section (circular and square), single-tube, double-tube, cross-sectional size, thickness of steel tube, strength of steel, load level, boundary condition, eccentricity of load and thickness of fire protection (FP) material. The hot-rolled steel S355 was used for all circular columns. All square column sections were pre-fabricated by welding four HSS plates at the corners, except for column LS-2-1 with hot-finished steel S355. The behavior of HSS at elevated temperatures has been discussed in Chapter 3. With regard to the welded sections, the back strip steel plate was used in the welding as shown in Figure 6.5. The backing

plate was S275 with a width of 37mm and thickness of 6mm. Continuous full length welds were used to fabricate the backing plates and box columns.

The column ends were welded with end plates by fillet welds. The interior height of the furnace for the fire tests was about 3.0 meter. In order to make sure the column is loaded and supported outside the furnace, all columns were designed to be 3.81 meter long including the thickness of end plates. In addition, the cross-sectional sizes of all columns were around 200mm~300mm. The size of column could not be larger because the strengths of the concrete and steel were high and the capacity of load machine was only about 600tons.

The column end was welded to an end plate with stiffeners to avoid local failure around the ends. Considering that there is no tension force under axial compression, eight Grade 8.8 M16 bolts were used, only for holding purpose to connect the end plates to supports for all columns.

The dimensions of columns, material properties, load eccentricities, boundary conditions, thickness of fire protection material, applied loads and the tested fire resistance time are shown in Table 6.1.

6.2.2   Design of Supports

Both fixed and pinned supports were used in the fire tests. In order to bring down the fabrication cost, the support was designed to be applicable for both fixed and pinned connections. The details of pinned support are shown in Figure 6.6. For fixed support, two fixers are attached to the support to restrain the rotation as shown in Figure 6.7. Regarding its strength, the fixed support was designed based on the maximum

moment resistance of tested CSFT columns, thus, it was a full-strength support. Regarding its stiffness, the fixed support can be classified as rigid according to EN 1993-1-8 (2005) since the two fixers are subjected to pure tension and compression in tests (moment from column is resisted by the force couple formed by the tension and compression forces in fixers). The fabricated supports are shown in Figure 6.8.

6.2.3   Concreting and Construction of Fire Protection Material

All columns were cast with UHSC which has been introduced in Chapter 4 and Chapter 5. The concrete was pumped in at the bottom of the columns using grouting pipes as shown in Figure 6.9. Before pumping, the inner surfaces of the tubes were wetted with water to make sure that the concrete can flow smoothly. During pumping, the top of the columns remained opened so that air could be compressed out. The pumping rate was slow that it took approximately 15 minutes to grout one column. The preparation of fresh concrete should be consistent with the pumping rate. Otherwise the concrete would harden and the pumping pipes would become clogged. After pumping, the concrete coming out from the top of the column was removed by toweling.

The fire protection material was a mixture of Portland cement, perlite, vermiculite and water. The fire protection material was applied by scraper after the columns had been primed. The fire protection material was applied when the columns were upright. Thus, the wet fire protection material sagged under gravity and there were some bulges on the surface after it hardened. These bulges were removed by grinding before measuring the thickness of the fire protection material applied. The thickness of the fire protection material was determined base on the average measurements

taken from 16 points which were uniformly located along the column height and four sides of the column. The CFST columns applied with fire protection material are shown in Figure 6.10.

6.2.4 Locations of Steaming Holes and Thermocouples

Eight circular steaming holes with diameter of 10mm were provided on each column to release the vapor inside the concrete during heating. The locations are shown in Figure 6.11. The steaming holes were temporarily sealed by bolts during casting of concrete to prevent leakage. The bolts were removed when the concrete has hardened.

Type K thermocouples were used for measuring the temperature inside the columns during testing. A thermocouple consists of two conductors of different materials that produce a voltage in the vicinity of the point where the two conductors are in contact. A change in the temperature at the junction of the two conductors is determined based on the voltage produced. The material of conductors of type K thermocouple is chromel which consists of 90% nickel and 10% chromium. Type K is the most common general purpose thermocouple with a sensitivity of 41μV/°C. It is applicable for temperature ranging between −200°C to +1250°C. There were three thermocouples installed in each column. The locations of the thermocouples are shown in Figure 6.12.

6.3 Test Setup and Procedure

6.3.1 Test Apparatus

The standard fire tests were conducted in the Civil Engineering Laboratory at South East University in China. Gas furnace, control unit, reaction frame, loading system and data acquisition system were provided for the fire tests.

A hydraulic jack with a capacity of 600tons was used to apply the axial load on the tested columns. The loading cell was located at the top of the column. In order to maintain the applied fire load, the fire load was manually adjusted to compensate for variations due to the axial deformations of the columns at elevating temperatures.

The interior space of the furnace is 3.0m x 3.0m x 3.0m. For illustration of fabrication of furnace, it is shown in Figure 6.13. The furnace is divided into two parts: fixed part and mobile part. The fixed part is insulated with fire-resistant bricks, whereas the mobile part is insulated with fire-resistant wool. There are 16 gas burners for heating and 12 thermocouples for monitoring the temperatures in the furnace. The gas volume of burners and gas pressure inside the furnace were recalibrated to ensure that the furnace temperature can achieve the standard ISO-834 temperature-time curve.

6.3.2   Test Setup

The column was first moved into position, and then bolted at both ends. The top and bottom 405mm height of the column were protected by fire-resistant wool so that the fire exposed length of the column was 3m. The supports were also protected by fire-resistant wool.

Due to the fact that the loading cell should not be rotated during testing, there was an anti-rotational steel plate installed in between the top support and the loading cell. When the plate was about to rotate in testing, the bolts on the four sides of the anti-

rotational plate can stop the rotations, but not the vertical translations. There were two pairs of bolts on each side of the anti-rotational plate. The test setup is shown in Figure 6.14.

The axial vertical displacement of the column during the fire test was measured by four LVDTs located at equal spacing around the loading cell, as shown in Figure 6.15. The readings of the LVDTs and temperatures from the thermocouples were automatically recorded by the data acquisition system.

6.3.3 Fire Exposure

The standard fire tests were conducted based on EN 1365-4 (1999). The columns were exposed to the standard ISO-834 fire with temperature-time relationship described as (EN 1991-1-2, 2002).

$$T_f = 20 + 345 \log_{10}^{(8t+1)} \tag{6.1}$$

T_f is the temperature inside the furnace in $^{\circ}$C; t is the heating time in minute.

6.3.4 Test Procedure and Failure Criteria

After the column was installed properly, it was loaded to the target load level. After the load level was stable, gas and air were sucked into the furnace and mixed properly. Then the standard ISO-834 fire started until the column failed. The column was heated on all faces. The relation between the vertical displacement of the column head and heating time was automatically recorded during the test. The test was terminated when the vertical displacement fulfills the following two criteria, whichever was earlier (ISO-834, 1999).

Vertical displacement: $0.01L_{ex}$,   [mm]

Velocity of vertical displacement: $0.003L_{ex}$,   [mm/min]

L_{ex} is the fire exposed height of column.

6.4 Test Data

6.4.1   Temperature Distribution

There were 3 thermocouples in each column when the concrete was cast. However, some were damaged during transportation of the columns. Thus, the temperatures at those locations were not recorded. For those thermocouples not damaged, the temperature readings were obtained. The measured curves of temperature versus fire exposure time are given in Figure 6.16.

LC-2-1 was the first column which was tested. However, due to manufacturing of the gas burners of the furnace, the furnace temperature could not reach the standard ISO-834 fire temperature. After the first test, the furnace was maintained and the furnace temperatures for the rest of the tests showed good agreement with standard ISO-834 fire temperature.

It is observed that the temperatures of the steel tube were higher than those of concrete. However, the temperature did not monotonically decrease from the steel tube to the concrete. This means that the distance between point 1 and 2 is same as that between point 2 and 3, but the temperature variations are not same. This is due to the fact that the conductivity of concrete does not vary linearly with temperature. With regard to the temperatures of the single-tube columns, the variations are larger

102

than those of double-tube columns. This is because the thickness of the concrete in single-tube columns is larger than that of double-tube columns.

For normal strength concrete with relative by high moisture content, there would be a stable stage of temperature reached in the concrete when the temperature is about 100°C. This is attributed to the phase change of water which is heated into vapor. During this phase change of water, most of the heat is absorbed by the water rather than consumed in elevating the temperature in the concrete. However, this stable stage of temperature was not observed for UHSC. This is due to the low water content on the UHSC.

It is noticed that some temperature measurements on the steel tube (point 3) were terminated before column failure, such as LC-2-1, LC-3-1, LSH-2-2, LSH-2-3, and LSH-2-5. This might be due to the fact that the sensitivity of the conductors of thermocouples at point 3 was affected by the turbulence of fire flame because point 3 was directly attached on the steel tube, nearest to the fire. That is also the reason why the temperature at point 3 fluctuated the most due to turbulence.

6.4.2   Failure Temperature of Outer Steel Tube

The temperatures of the steel tubes at failure of the tested CFST columns are given in Table 6.2. The failure temperature of the steel tubes in the CFST columns is different from the critical temperature of steel columns. This is because the critical temperature is only related with the load level of the steel columns according to EN 1993-1-2. In other words, two steel columns will fail at the same steel temperature as long as they have the same load levels, irrespective of the column size.

However, this is not true for the CFST columns since there is concrete infill in the tube. Temperature is not uniformly distributed in the concrete and the temperature distribution is related with the cross-sectional size of column. The failure temperature of the CFST columns depends not only on the load level but also the cross-sectional size. In other words, two CFST columns may not fail at the same steel temperature even they have the same load levels.

Two stub CFST columns are used to illustrate the effects of cross-sectional size and load level on the failure temperature, as shown in Figure 6.17. The stub columns are assumed as governed by cross-sectional failure for both ambient temperature situation and fire situation. The load level is same for the two stub columns. The external loads for the two stub columns in the fire situation can be formulated as:

$$N_1 = \mu \left(f_y A_s + f_c A_{c1} \right) \tag{6.2}$$

$$N_2 = \mu \left(f_y A_s + f_c A_{c1} + f_c A_{c2} \right) \tag{6.3}$$

$$N_2 - N_1 = \mu f_c A_{c2} \tag{6.4}$$

N_1 and N_2 are the external loads for column 1 and column 2. μ is the load level in fire situation. f_y and f_c are the yield strength and compressive strength of steel and concrete respectively. At failure under fire, the external load is equal to the cross-sectional capacity of the stub column, which are formulated as:

$$N_1 = \left(k_s^1 f_y \right) A_s + \left(k_{c1}^1 f_c \right) A_{c1} \tag{6.5}$$

$$N_2 = \left(k_s^2 f_y \right) A_s + \left(k_{c1}^2 f_c \right) A_{c1} + \left(k_{c2}^2 f_c \right) A_{c2} \tag{6.6}$$

k_s and k_c are the strength reduction factors of steel and concrete respectively at failure of column. The superscript "1" and "2" refer to column 1 and column 2 respectively. The subscript "c1" and "c2" respectively stands for concrete area 1 and concrete area 2. Assuming that the two stub columns have the same failure temperatures in their outer steel tubes, then $k_s^1 = k_s^2$ and following equation is obtained:

$$N_2 - N_1 = \left(k_{c1}^2 f_c\right) A_{c1} + \left(k_{c2}^2 f_c\right) A_{c2} - \left(k_{c1}^1 f_c\right) A_{c1} \qquad (6.7)$$

Assuming $A_{c1} = A_{c2}$ and equating Eqn.(6.4) and Eqn.(6.7) give:

$$k_{c1}^2 + k_{c2}^2 - k_{c1}^1 - \mu = 0 \qquad (6.8)$$

It is clear that k_{c1}^2 and k_{c2}^2 are larger than k_{c1}^1 since the temperatures of the concrete in column 2 are lower than that in column 1 when the outer tube temperatures are the same. The difference between k_{c1}^2, k_{c2}^2 and k_{c1}^1 are not constant and will change with the cross-sectional size of the column. Eqn. (6.8) can only be satisfied in very rare cases where μ is set to be ($k_{c1}^2 + k_{c2}^2 - k_{c1}^1$). Thus in most cases, two CFST columns would not fail at the same steel tube temperature even when they have the same load levels.

It should be noted that the non-dimensional slenderness ratio of columns at ambient temperature is not taken into account in derivation forementioned. It would become more complicated when the non-dimensional slenderness ratio is considered. As discussed in Chapter 3, the critical temperature of the steel column decreases with increasing non-dimensional slenderness ratio. The non-dimensional slenderness ratio would affect the failure temperature of the outer tube of the CFST column in a similar way. Overall, the concept of critical temperature is not applicable for CFST columns.

It can be seen in Table 6.2 that column LC-3-2 failed when the temperature of the outer steel tube reached 94°C. This is due to the high load level which was 0.88; and the fact that UHSC suffered large deteriorations in both strength and elastic modulus which was respectively reduced by 20% and 15% at around 100°C. These deteriorations have been discussed in Chapter 5.

6.4.3 Displacement-Time Relationship

The columns were axially loaded with or without eccentricities. The relations between vertical displacement and fire exposure time, as shown in Figure 6.18 ~ Figure 6.22, were recorded during testing. All tests were terminated when the vertical displacement exceeded 30mm which is 0.01times the fire exposed length of columns.

It was observed that, during the early stages of fire exposure, the steel tube resisted most of the load due to the thermal expansion of the steel tube under faster increasing temperatures. The magnitude of thermal expansion depends on the load level, load eccentricity, and the cross-sectional size of the column. It is clear that the higher the load level, the smaller the thermal expansion. The load eccentricity causes the column to bend laterally; thus the thermal expansion is converted into the lateral deflection of column rather than the vertical displacement. The influence of cross-sectional size on thermal expansion can be attributed to the temperature gradient from the outer tube to the inner concrete. The larger the cross-sectional size, the higher the temperature gradient. As a result, the thermal expansion of the concrete is much smaller than that of the outer tube. Thus, the thermal expansion of the outer tube is actually constrained by the inner concrete.

When the temperature of the steel tube reaches around $600^{\circ}C$, the thermal expansion terminated and a sudden contraction occurred due to the strength loss of steel. After which the concrete took over in resisting the load until the column failed. The duration between the sudden contraction and failure of the column depends on the load level, the thickness of fire protection material, and the cross-sectional size of the column. The lower the load level, the larger the capacity reserve of the concrete. As a result, longer fire exposure time is needed to consume the capacity reserve after the sudden contraction of concrete. The influences on this duration after contraction occurs are similar as for the thickness of fire protection material and the cross-sectional size since they affect the variations in temperature within the concrete, thus affecting the variation in the capacity reserve of the concrete. The duration between the sudden contraction and failure of column can be used to determine the ductility of columns under fire situations.

Comparisons among the circular columns from LC-2-2 to LC-2-6 are shown in Figure 6.18. LC-2-1 is not included in this comparison since the furnace temperature did not achieve the standard ISO-834 fire temperature. It shows that LC-2-5 exhibited the largest upward thermal expansion. This indicates that the lower load level induced larger thermal expansion. Load eccentricity also exerted effects on the thermal expansion. Displacement of LC-2-6 implied that there might be no thermal expansion if there is a load eccentricity. In terms of ductility, it can be seen that LC-2-5 exhibited a longer duration between the sudden contraction and failure of the column since it had the smallest load level. Compared with these circular columns, square columns showed the similar trends on the thermal expansion and the ductility as shown in Figure 6.20.

Comparisons among columns LC-3-1, LC-3-2, and LC-4-1 are shown in Figure 6.19. These columns were larger than other circular columns and were designed to investigate the size effect. It can be seen that there was almost no thermal expansion because of the larger cross-sectional sizes and load eccentricity. LC-3-1 and LC-4-1 exhibited longer duration between contraction and failure of the column, and thus better ductility than LC-3-2. The better ductility resulted from a lower load level.

A comparison among the double-tube columns are shown in Figure 6.21 and Figure 6.22 respectively for circular and square columns. It can be seen that LDC-2-3 and LDSH-2-3 exhibited smaller thermal expansions and poorer ductility compared to other columns since they were eccentrically loaded. With regard to the protected columns, it took a longer time to reach the peak thermal expansion since the increase in temperature was slower.

6.5 Test Observations

Based on the experimental findings in Chapter 4, 0.1% polypropylene fiber by volume was added into all the tested CFST columns when the concrete was cast. It was observed that no spalling occurred. The noise of crack was also not heard. However, the fire protection material spalled for most columns. The spalling process of the fire protection was not recorded since the columns in furnace could not be observed during testing.

The failed columns after tests are shown in Figure 6.23. Comparisons between the failure modes are shown in Figure 6.24, Figure 6.25 and Figure 6.26. LC-2-1, LC-2-2 and LC-2-3 were the first three columns tested. LC-2-2 and LC-2-3 were respectively designed to be "fixed-fixed" and "fixed-pinned" columns. However it can be seen that

LC-2-2 and LC-2-3 seemed to deform as "pinned-pinned" columns after testing. This was due to the rotation of the load cell. The rotation induced premature failure of LC-2-2 and LC-2-3 which will be discussed in Chapter 7. In order to restrain the rotation of the load cell, the four sides of the steel plate between the top support and the load cell was anchored with high strength bolts as shown in Figure 6.14. When the plate tends to rotate, these bolts pull it back. The bolts could not restrain the vertical movement of the load cell.

The failure observations on the cross sections of columns are shown in Figure 6.27. It can be seen that the concrete colours were different after being subjected to different fire exposure times. Specimen LC-2-3 was subject to a fire exposure time of 71 minutes. The temperature at the centre of the cross-section was 123°C. Thus, the concrete was gray colour. Specimen LC-2-4 was subject to a fire exposure time of 122 minutes. The temperature at the centre of the cross-section was 320°C. Hence, the concrete colour was black. The colour of the concrete was affected by its microstructural changes during heating. It was also found in Figure 6.27 that there were no cracks occurring on the cross sections. Slip between concrete and steel tube were also not observed.

6.5.1 Cross-Sectional Failure

It can be seen from Figure 6.23~Figure 6.26 that column LC-4-1, LSH-2-2 and LSH-2-3 failed by cross-sectional failure accompanied by local bulging on the outer tube. The local bulging might be caused by local buckling. However it is excluded from an analysis of the section classification of steel tubes under fire. The section

classification of steel hollow sections could be performed by the reduction factor of ε as given in the following equation (Lennon et al., 2007).

$$\varepsilon = \sqrt{\frac{k_{E,\theta}}{k_{f,\theta}}} \sqrt{\frac{235}{f_y}} \tag{6.9}$$

$k_{E,\theta}$ and $k_{f,\theta}$ are the reduction factors for elastic modulus and yield strengths of steel. For S355 steel, $k_{E,\theta}$ and $k_{f,\theta}$ are taken from EN 1993-1-2 (2005); whereas the reduction factors in Chapter 3 are adopted for HSS RQT 701. With regard to the section classification, the maximum width-to-thickness ratios for circular compression members are given by (EN 1993-1-1, 2005) as:

Class 1: $\qquad\qquad\qquad\qquad D_e / t_e \leq 50\varepsilon^2$ $\qquad\qquad\qquad$ (6.10)

Class 2: $\qquad\qquad\qquad\qquad D_e / t_e \leq 70\varepsilon^2$ $\qquad\qquad\qquad$ (6.11)

Class 3: $\qquad\qquad\qquad\qquad D_e / t_e \leq 90\varepsilon^2$ $\qquad\qquad\qquad$ (6.12)

For the section classification of square compression members, the maximum width-to-thickness ratios are given by (EN 1993-1-1, 2005):

Class 1: $\qquad\qquad\qquad\qquad c_e / t_e \leq 33\varepsilon$ $\qquad\qquad\qquad$ (6.13)

Class 2: $\qquad\qquad\qquad\qquad c_e / t_e \leq 38\varepsilon$ $\qquad\qquad\qquad$ (6.14)

Class 3: $\qquad\qquad\qquad\qquad c_e / t_e \leq 42\varepsilon$ $\qquad\qquad\qquad$ (6.15)

D_e is the external diameter of circular columns; c_e is the height of the web of square external tubes; and t_e the thickness of outer tubes. The sections are classified based on the failure temperatures of the outer tubes when the CFST columns failed.

The relation between the section classification and temperature are shown in Figure 6.28 and Figure 6.29 for circular tubes and square tubes respectively. The D/t or c/t limits at elevated temperatures are compared with the actual values of the outer tubes. It can be observed that the outer tubes of LC-4-1, LSH-2-2 and LSH-2-3 are at least Class 2 sections, and therefore they should not fail by local buckling. Thus, the failure modes for these three specimens as observed from the tests seemed to be cross-sectional failure.

Cross-sectional failure was reflected by the presence of concrete cracks. After the columns were tested, the steel tubes were removed by gas cutting. The concrete cracks of LSH-2-2 and LSH-2-3 are similar to those of LC-4-1 which are shown in Figure 6.30. It can be seen that longitudinal splitting occurred on the concrete. Columns failed by cross-sectional failure are governed by the axial compression. The longitudinal splitting was caused by the lateral expansion of concrete under this axial compression since the steel tube yielded at elevated temperatures and could not provide adequate lateral confinement of the concrete.

Cross-sectional failure was also reflected by the weld tearing failure which was observed for LSH-2-2 as shown in Figure 6.31. The weld tearing was caused by the concrete expansion force which was transverse to the welds. As a result, the welds were subjected to transverse tension at elevated temperatures. However, weld failure was not found in another welded box column LSH-2-3 which was also classified under cross sectional failure as shown in Figure 6.32. This might be due to the fact that the failure temperature of the outer tube of LSH-2-3 was 393$^{\mathrm{o}}$C as given in Table 6.2. It was lower than that of LSH-2-2 which was 466$^{\mathrm{o}}$C. Hence, the strength of welds of LSH-2-3 was reduced less than that of LSH2-2 and as a result less likely to be torn.

The weld failure of LSH-2-2 can be prevented by proper commencement of welding which requires preheating and matching electrodes. The weld was torn in a manner indicating premature failure under compression.

6.5.2   Flexural Buckling Failure

Except for LC-4-1, LSH-2-2 and LSH-2-3, the other columns failed by flexural buckling which was reflected by the concrete cracks and deformations of the inner tubes. The concrete cracks of LC-2-5 which represents columns failed by flexural buckling are shown in Figure 6.33. It can be seen that the transverse cracks were observed due to the flexural action which caused cracks to occur in the tension zone. The crushing of concrete was found in the compression zone.

The deformations of the inner tubes in double-skin columns are shown in Figure 6.34. It can be see that there are local inward bulges on both circular and square inner tubes. Similar to the outer tubes, sections of the inner tubes are classified as shown in Figure 6.35 and Figure 6.36. The sections are classified based on the failure temperatures, reached by the inner tubes when the columns failed. It can be seen that the inner tubes are Class 1 sections, therefore the local inward bulges were not induced by local buckling. The local inward bulges on inner tubes could be caused by the compression forces generated due to large flexural deformations.

6.6 Summary

Fire tests on CFST columns with UHSC and HSS are presented in this chapter. The test results included temperatures, axial deformations, fire resistance time, and failure modes. The main findings are drawn as follows.

112

(1) During the early stages of fire exposure, the steel tube resisted most of the loads and expanded upwards. When the temperature of the steel tube reached around $600^{o}C$, the expansion terminated and the concrete took over in resisting the loads until the column failed.

(2) Stable stage of temperature values in the concrete was not observed when the temperature of concrete reached about $100^{o}C$. This was due to the low content of water in UHSC.

(3) Concept of critical temperature is not applicable for CFST columns. Two CFST columns with different cross-sectional sizes would not fail at the same outer tube temperature even if they have the same load level. This is because the outer tube temperature is governed not only by the load level, but also the cross-sectional size and the non-dimensional slenderness ratio of the column.

(4) Magnitude of thermal expansion in CFST columns depends on the load level, load eccentricity, and the cross-sectional size of the column. The ductility of CFST columns under fire situations can be reflected by the time duration between sudden contraction and failure of column. The duration depends on the load level, the thickness of fire protection material, and the cross-sectional size of column.

(5) No spalling was observed for all the tested columns with addition of 0.1% polypropylene fiber in the UHSC. The fire protection material spalled on most of the columns because of large deformations.

(6) Most columns failed by flexural buckling except for three columns through cross-sectional failure. Transverse cracking of the concrete were observed for columns failing by flexural buckling due to flexural action. Longitudinal splitting of the

concrete was found on columns failing under cross-sectional failure due to the lateral expansion of the concrete under compression. Local inward bulges on inner the tubes were found due to the compression forces induced by flexural deformations.

(7) No cracking and slip were observed respectively on the cross sections and between the concrete and the steel tubes. Weld tearing failure was found in one column attributed to the workmanship of welding.

Table 6.1: Details of CFST and CFDST column specimens for fire tests

Specimen	Sizes D(mm) x t(mm)	f_y (MPa)/ E_s (GPa)	f_c (MPa)	FP (mm)	BC.	Ecc. (mm)	$N_{f,20}$ (kN)	$N_{f,fire}$ (kN)
LC-2-1	219.1x16	432/204	163	0.0	F-F	0	8210	2900
LC-2-2			161	5.9	F-F	0	8093	5131
LC-2-3			165	9.5	F-P	0	7421	5131
LC-2-4			168	6.4	P-P	0	5363	3178
LC-2-5			164	8.1	P-P	0	5338	2489
LC-2-6			163	7.8	P-P	50	2922	2443
LC-3-1	273x16	422/203	181	6.8	P-P	0	9442	5037
LC-3-2			181	8.3	P-P	50	5714	5037
LC-4-1	273x10	418/201	180	8.6	P-P	0	7964	4434
LSH-2-1	200x12	785/211	163	0.0	F-F	0	10845	3735
LSH-2-2			174	8.0	F-F	0	11243	5261
LSH-2-3			173	11.5	F-P	0	9668	5504
LSH-2-4			170	9.1	P-P	0	6279	5039
LSH-2-5			166	8.8	P-P	0	6262	3144
LSH-2-6			166	9.5	P-P	50	4072	3207
LS-2-1	200x12.5	499/206	166	7.9	P-P	0	5841	4047
LDC-2-1	219.1x16 114.3x6.3	432/203 468/183	165	0.0	F-F	0	7334	2428
LDC-2-2			163	8.2	P-P	0	4578	2736
LDC-2-3			165	7.9	P-P	50	2902	2736
LDSH-2-1	200x12 100x8	785/211 825/202	170	0.0	F-F	0	11103	3715
LDSH-2-2			172	9.2	P-P	0	5877	2942
LDSH-2-3			165	9.0	P-P	50	4010	3109

Notes:

1,

LC   LSH   LDC   LDSH
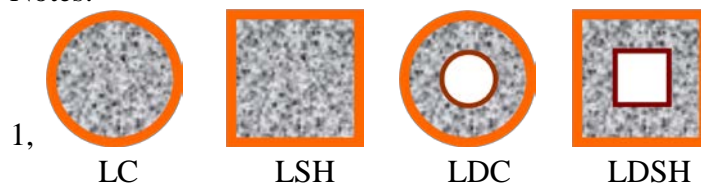
2, "FP" is fire protection material; "Ecc." is eccentricity of load; "BC." is boundary condition;

3, "$N_{f,20}$" is axial load capacity under ambient temperature based on EN 1994-1-1. "$N_{f,fire}$" is the applied axial load in fire test.

Table 6.2: Failure temperatures on steel tubes and failure modes

Specimen	Sizes D(mm) x t(mm)	Critical temperature (^{o}C)		T_t (min.)	Load level	Failure mode
		Outer tube	Inner tube			
LC-2-1	219.1x16	748	-	96	0.35	B
LC-2-2		410	-	84	0.63	B
LC-2-3		269	-	71	0.69	B
LC-2-4		540	-	122	0.59	B
LC-2-5		618	-	175	0.47	B
LC-2-6		116	-	24	0.84	B
LC-3-1	273x16	589	-	192	0.53	B
LC-3-2		94	-	18	0.88	B
LC-4-1	273x10	560	-	175	0.56	C
LSH-2-1	200x12	717	-	42	0.34	B
LSH-2-2		466	-	118	0.47	C
LSH-2-3		393	-	135	0.57	C
LSH-2-4		469	-	104	0.80	B
LSH-2-5		654	-	156	0.50	B
LSH-2-6		339	-	70	0.79	B
LS-2-1	200x12.5	336	-	79	0.69	B
LDC-2-1	219.1x16 114.3x6.3	781	413	59	0.33	B
LDC-2-2		518	325	134	0.60	B
LDC-2-3		143	101	25	0.94	B
LDSH-2-1	200x12 100x8	734	278	47	0.33	B
LDSH-2-2		521	350	150	0.50	B
LDSH-2-3		283	224	76	0.78	B

Notes:

1, "B" stands for flexural buckling failure

2, "C" stands for cross-sectional failure

3, "T_t" is the tested maximum fire resistance time
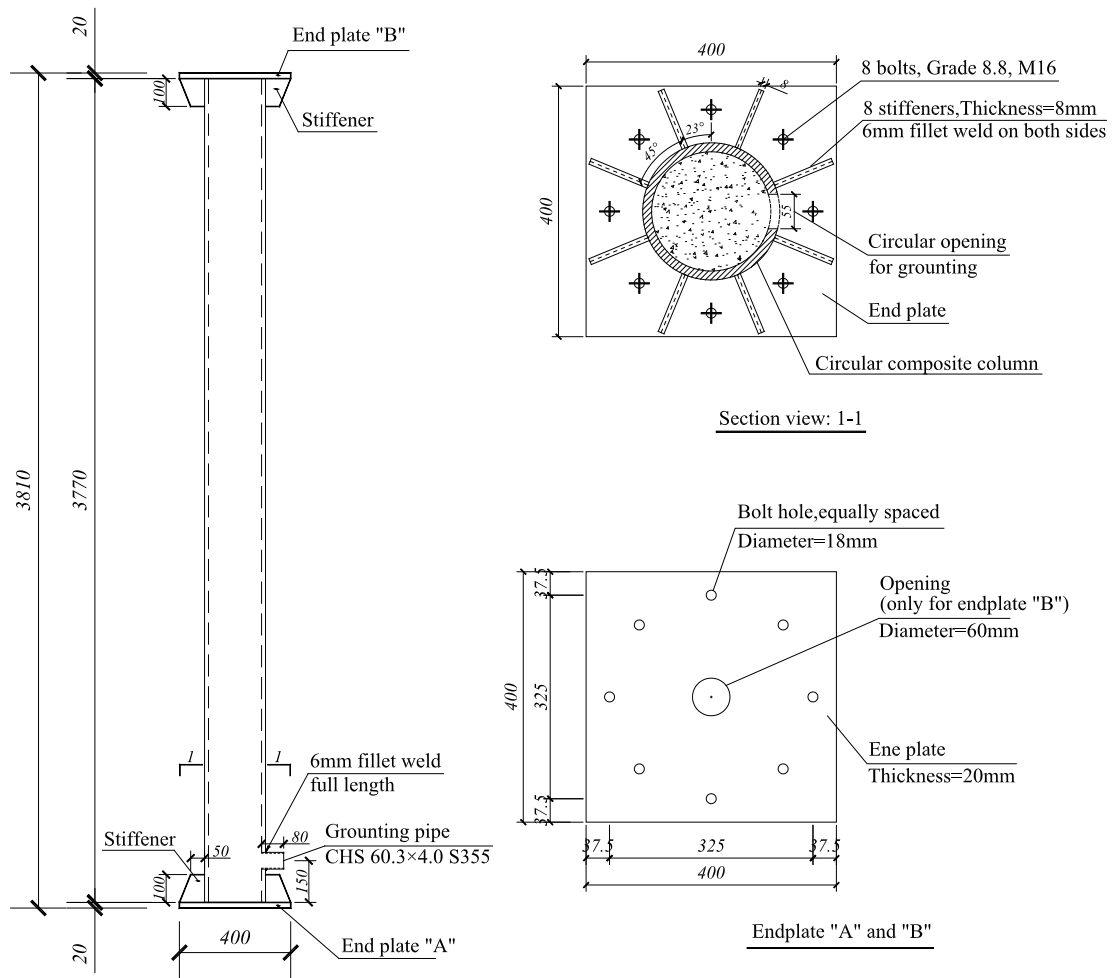
4, Load level= $N_{f,fire} / N_{f,20}$

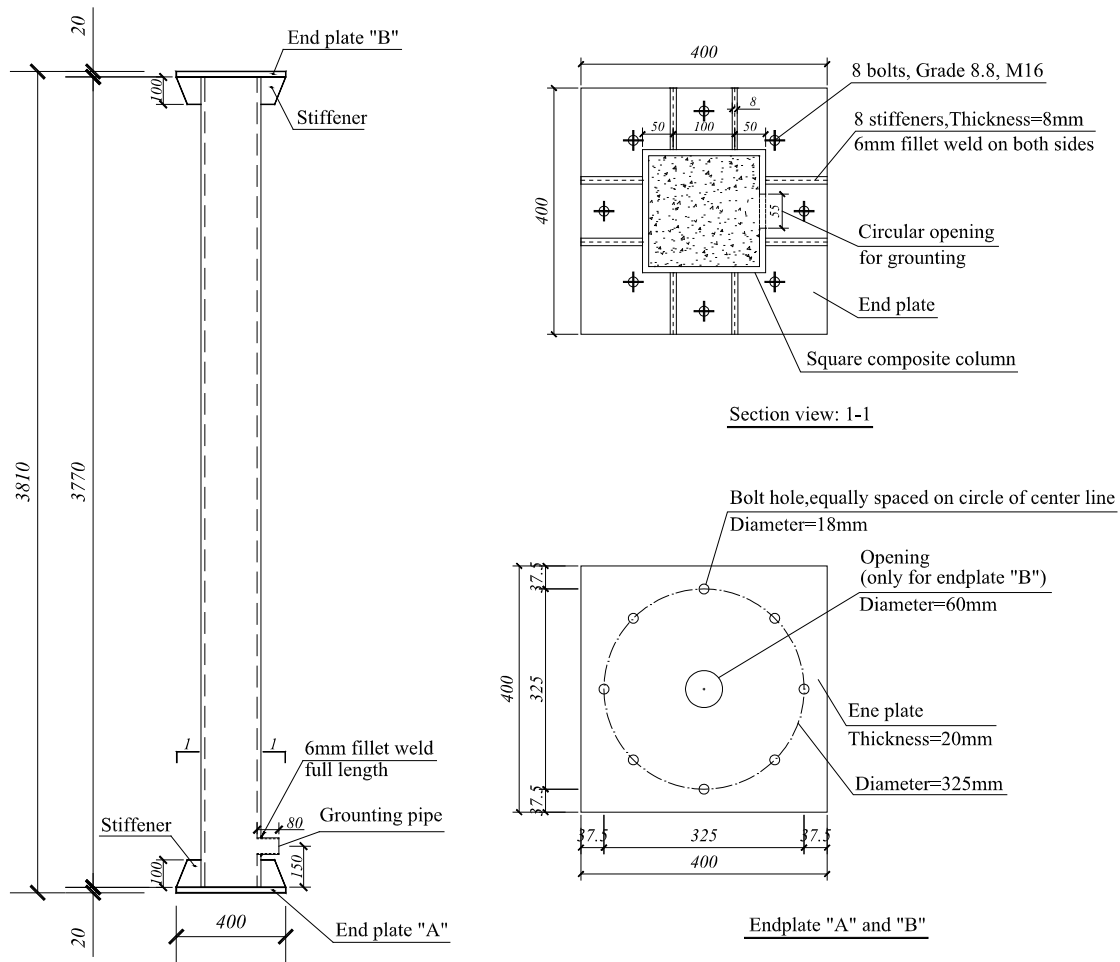Figure 6.1: Dimensions of circular CFST columns

Figure 6.2: Dimensions of square CFST columns
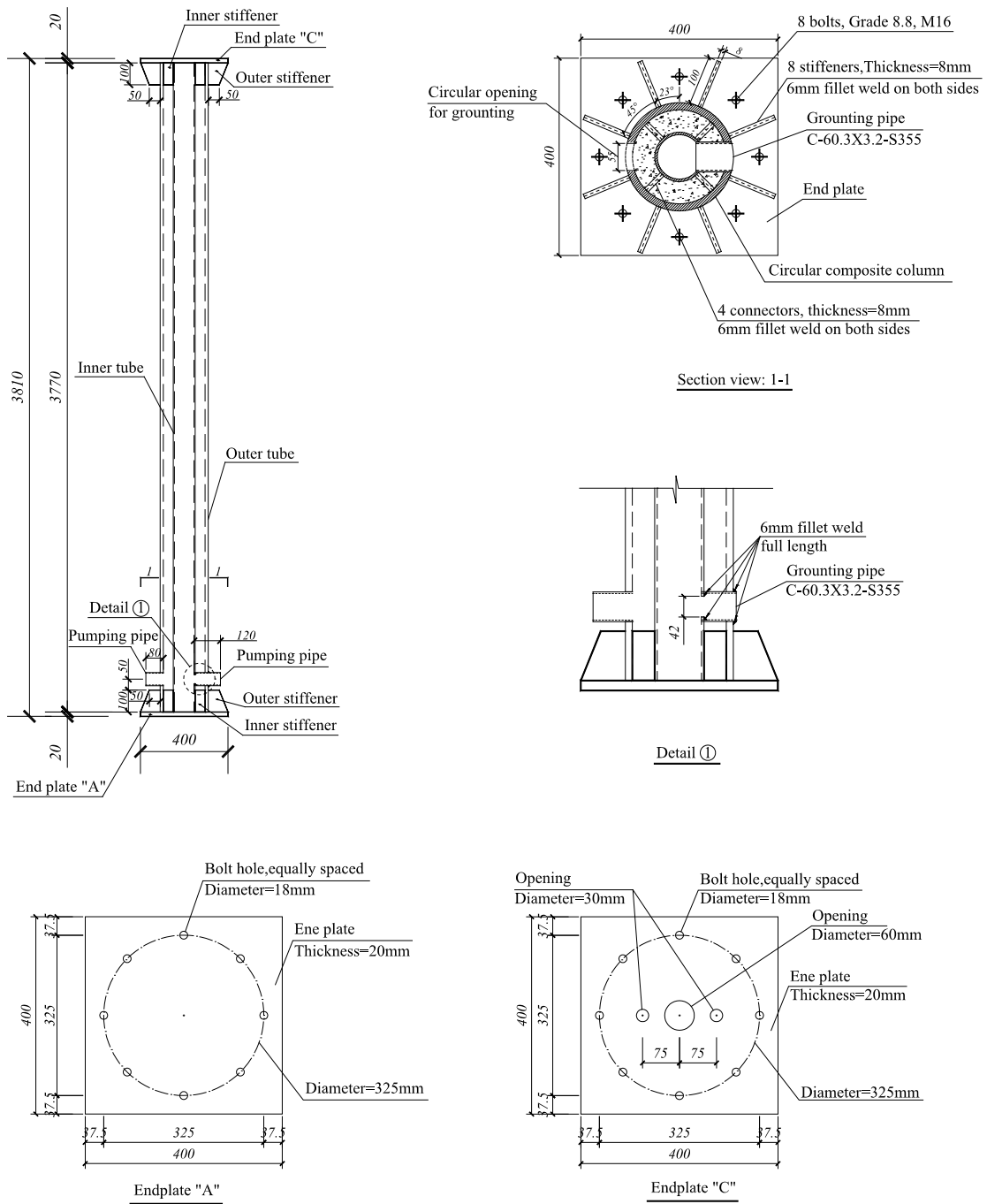
Figure 6.3: Dimensions of circular CFDST columns
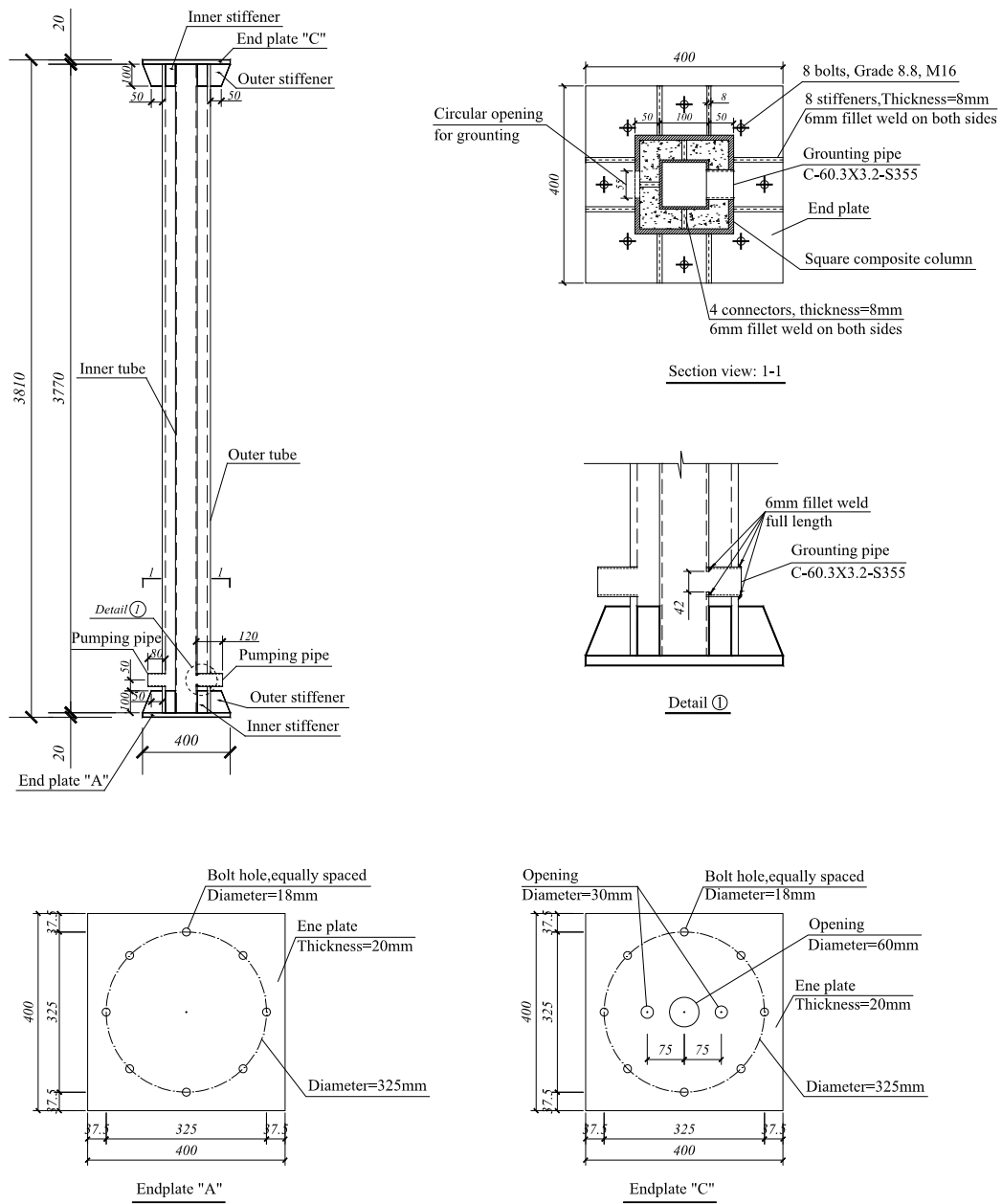
Figure 6.4: Dimensions of square CFDST columns

(a) Single-tube   (b) Double-tube
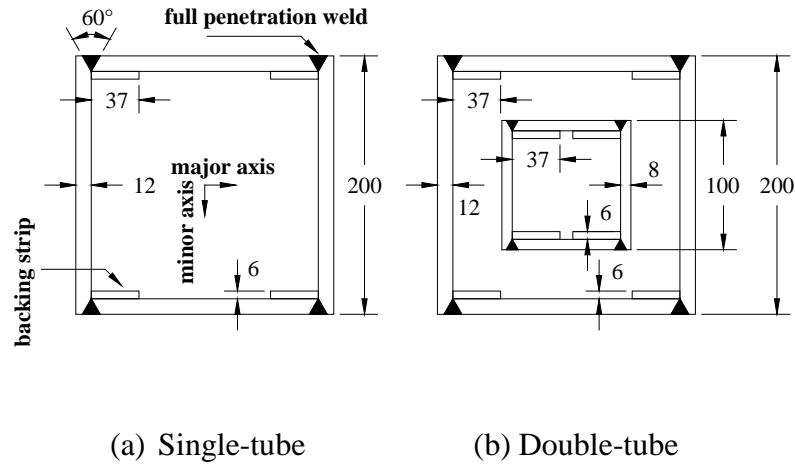
Figure 6.5: Welding details of boxed columns
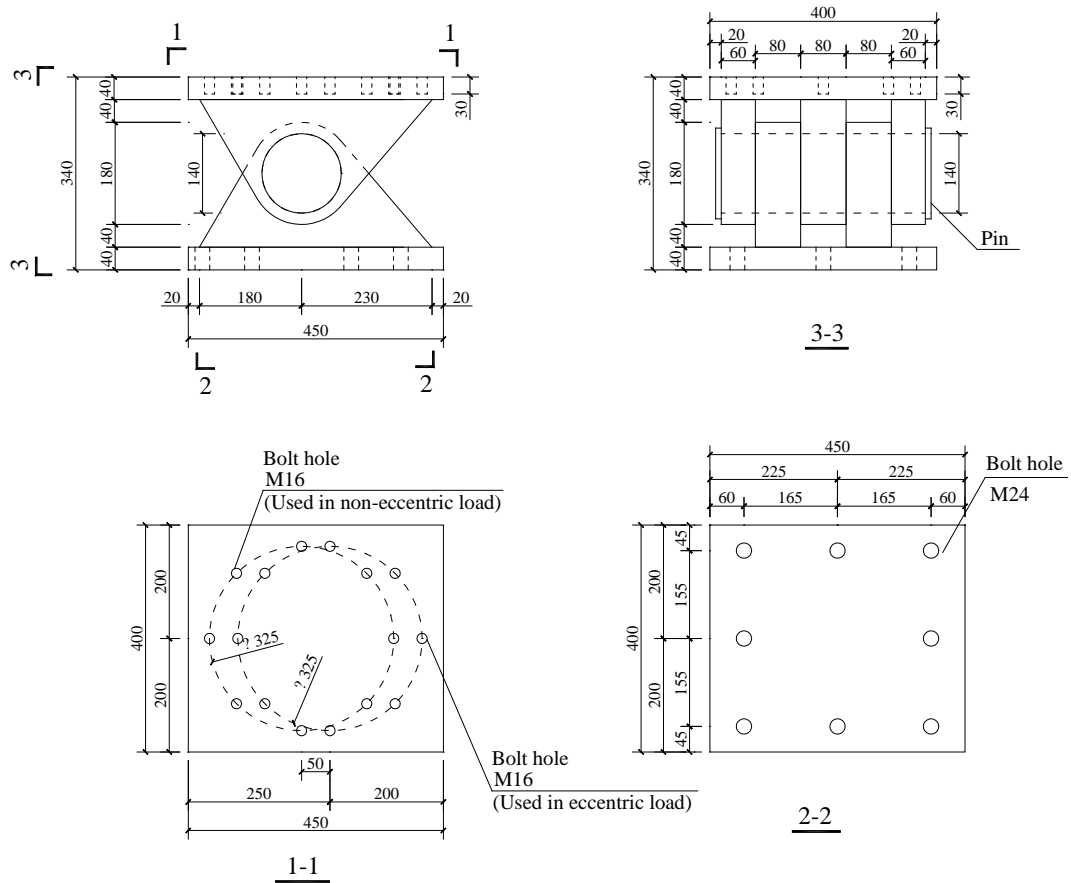
1,All bolts are Grade 8.8.
2,All steel are Grade Q345.
  (Chinese steel)

Figure 6.6: Pinned support allowing free rotation
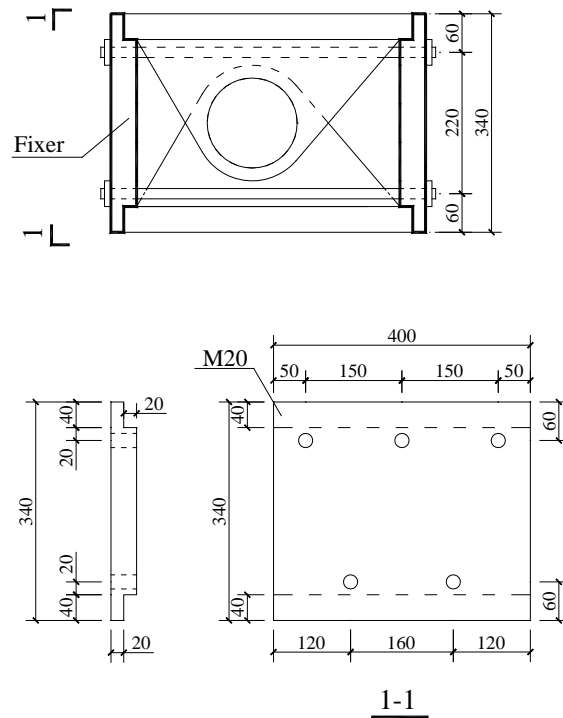
Figure 6.7: fixed support with fixer plate to prevent rotation

        (a) Pinned   (b) fixed

Figure 6.8: Supports in fire test

Steel frame to
ensure columns
upright

Grouting pipe
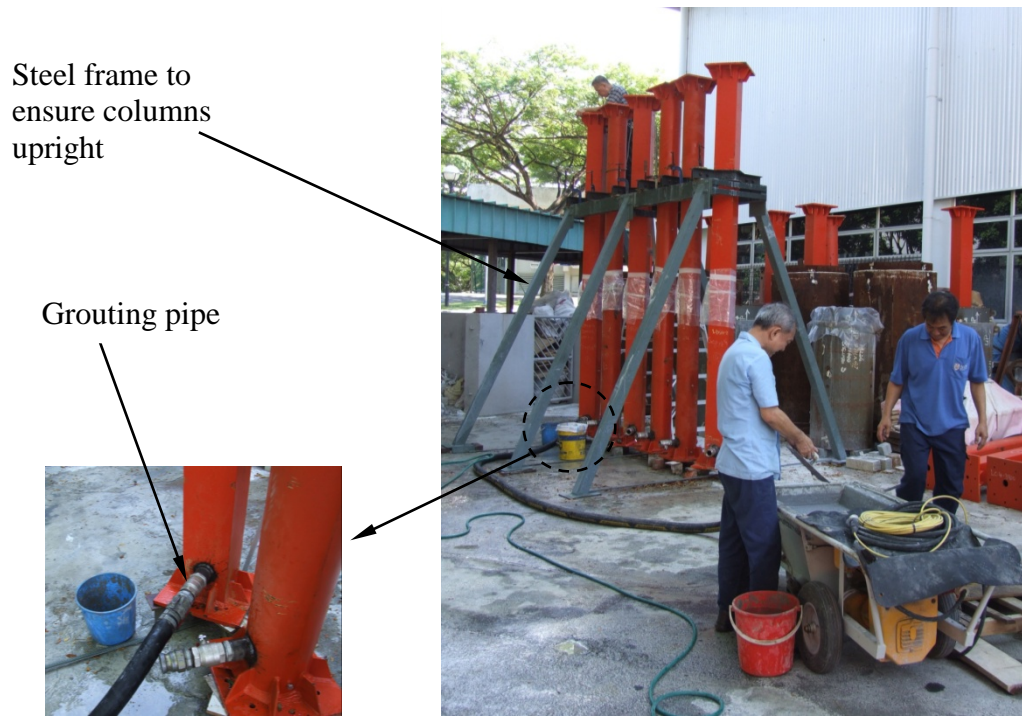
Figure 6.9: Casting of concrete

Thermocouple

Figure 6.10: CFST columns applied with fire protection material
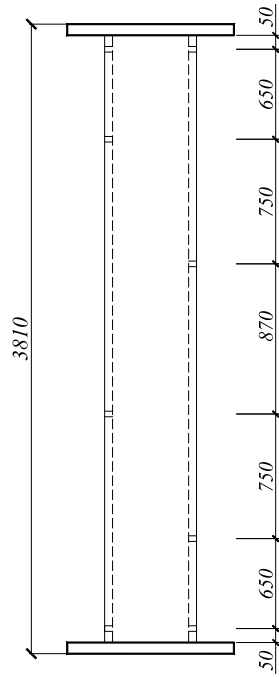
Figure 6.11: Locations of steaming holes
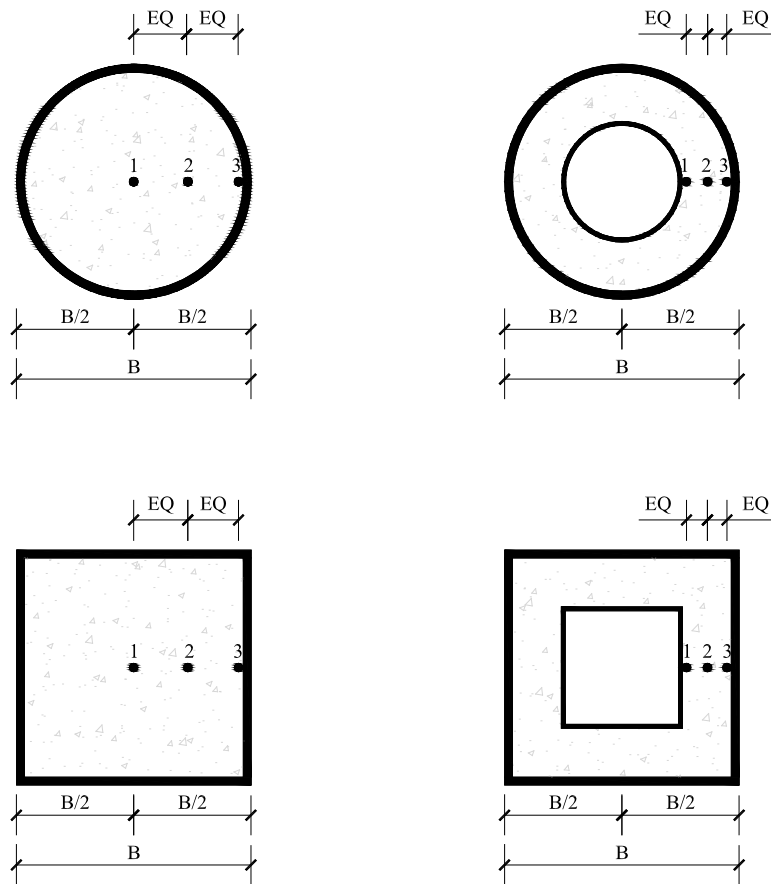
Figure 6.12: Locations of thermocouples

Constructed with bricks

Inside fixed part

Constructed with wool

Inside mobile part
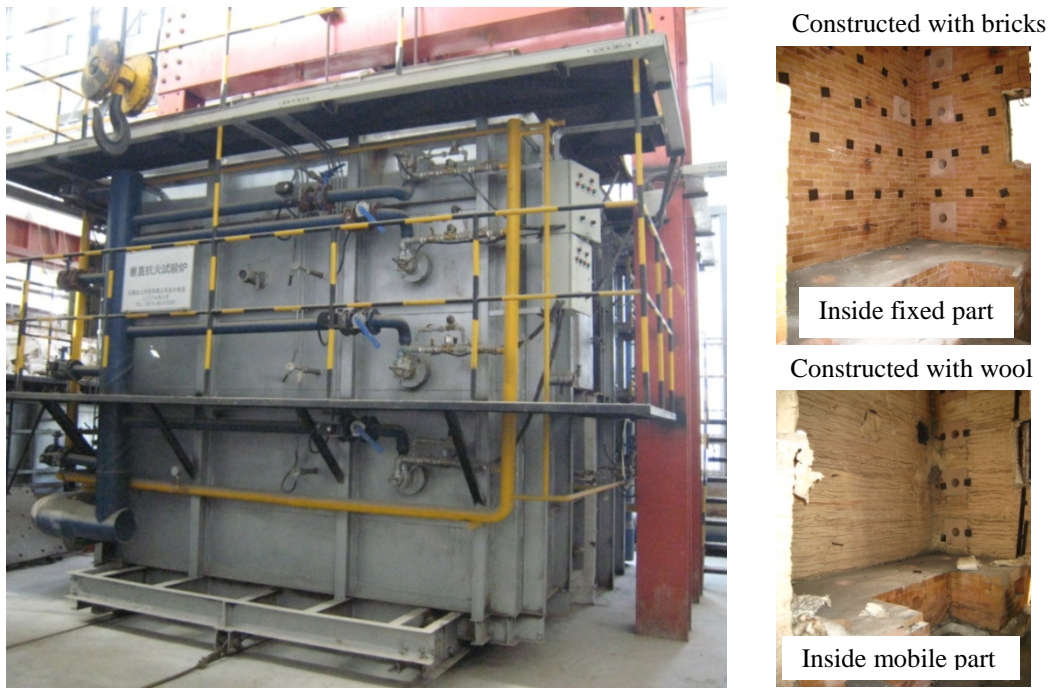
Figure 6.13: Furnace for standard fire test

Applied load

Anti-rotational plate

Loading cell

Box beam of test rig

Support

End plate

340

405

3810

3000

405

340

Furnace

Tested column

Base plate
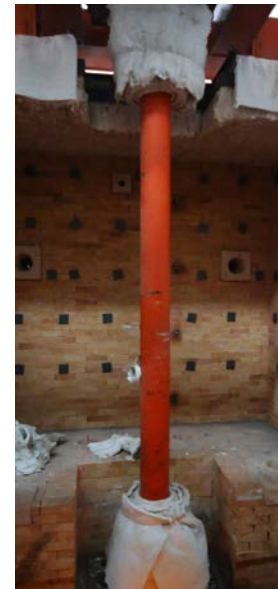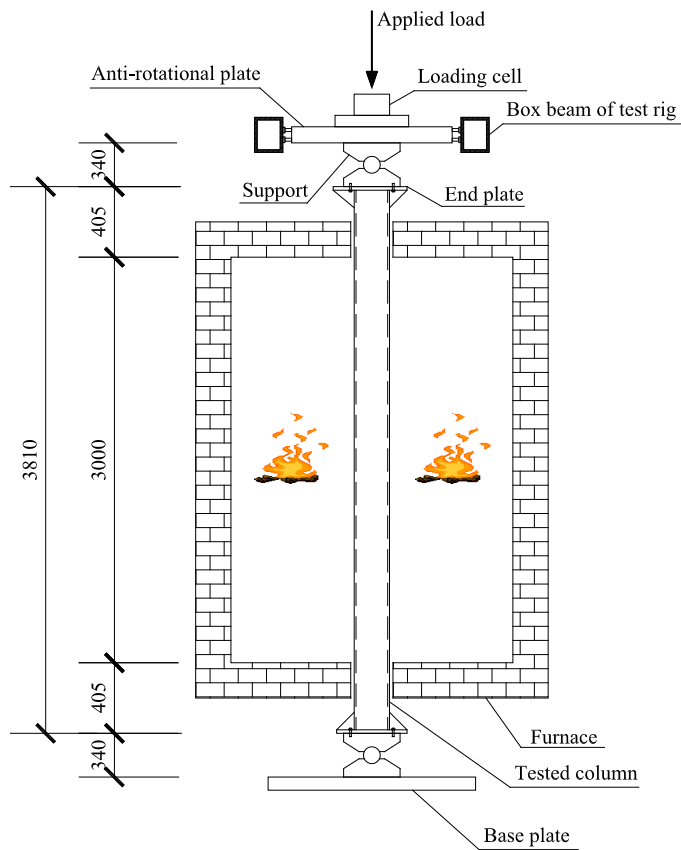
Figure 6.14: Test setup
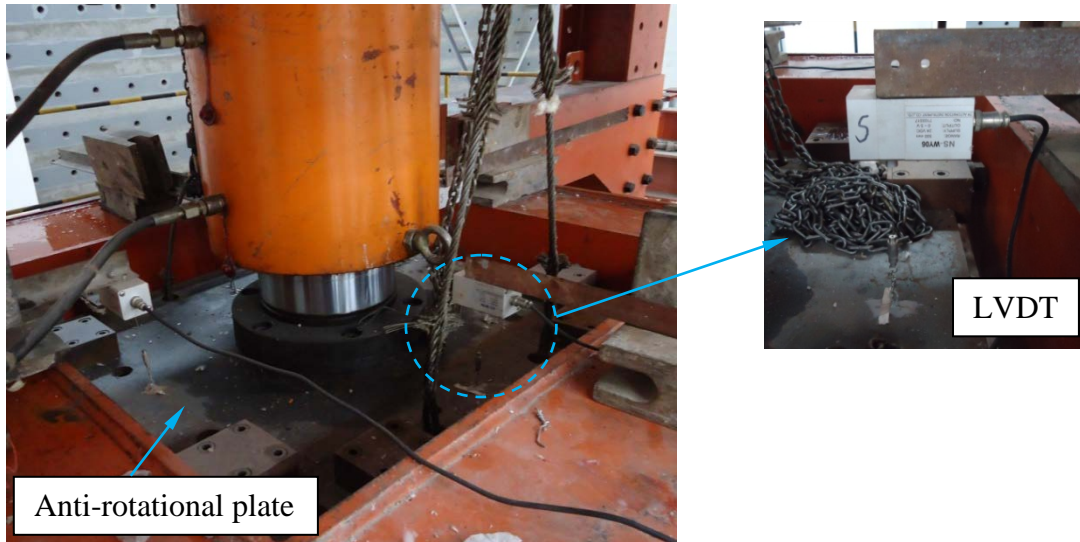
Figure 6.15: Measurements of axial displacements of columns
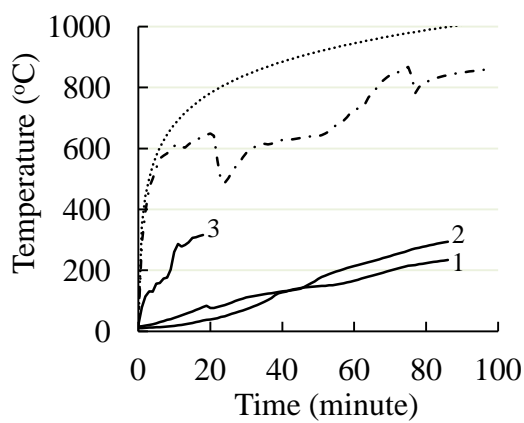
(a) LC-2-1
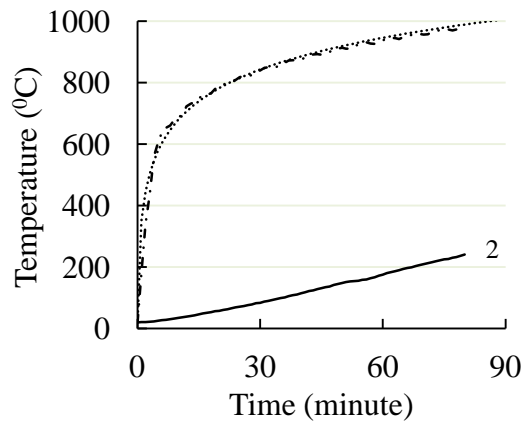
(b) LC-2-2
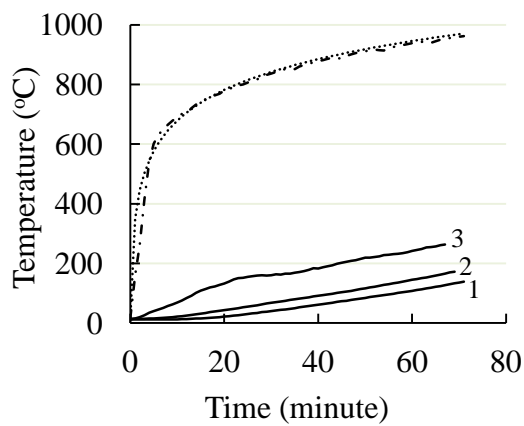
(c) LC-2-3
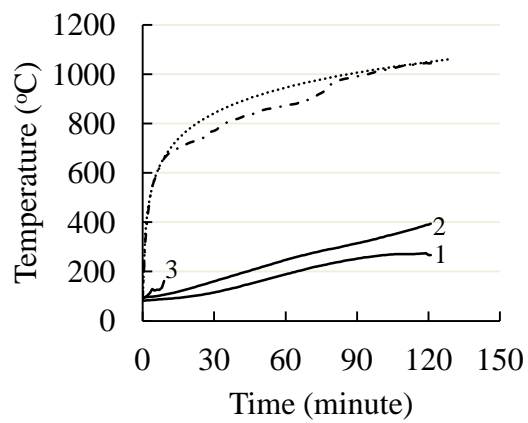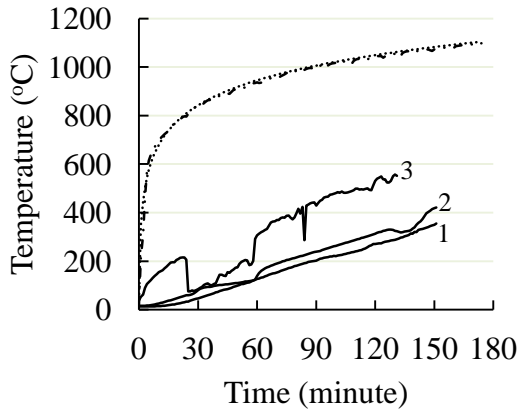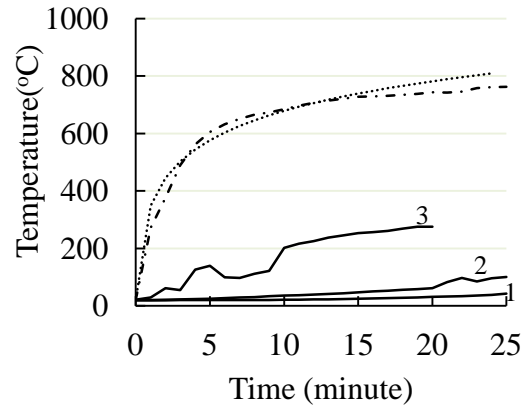
(d) LC-2-4

(e) LC-2-5

(f) LC-2-6

(g) LC-3-1

(h) LC-3-2

(i) LC-4-1

(j) LDC-2-1

(k) LDC-2-2

(l) LDC-2-3

(m) LSH-2-1

(n) LSH-2-2

(o) LSH-2-3

(p) LSH-2-4

(q) LSH-2-5   (r) LSH-2-6

(s) LDSH-2-1   (t) LDSH-2-2

(u) LDSH-2-3   (v) LS-2-1

·············· ISO 834 fire   – – – Furnace temperature
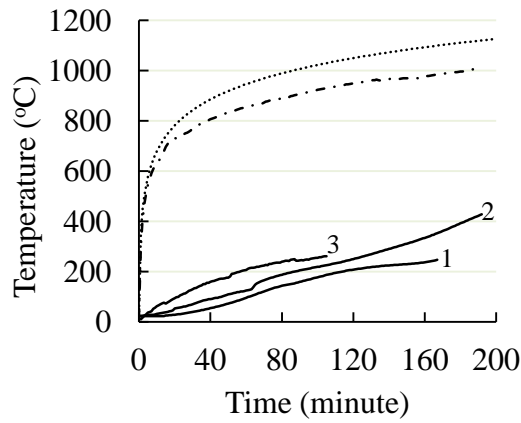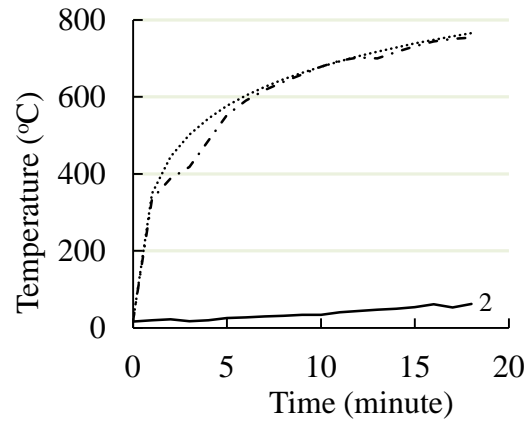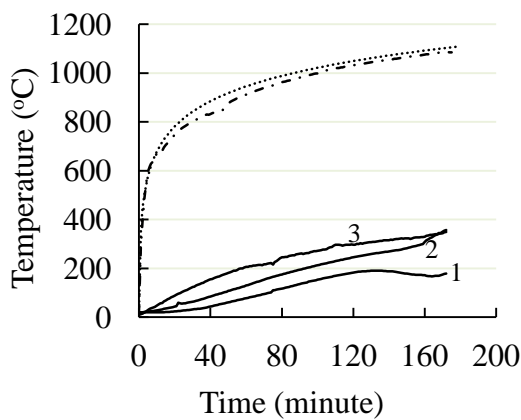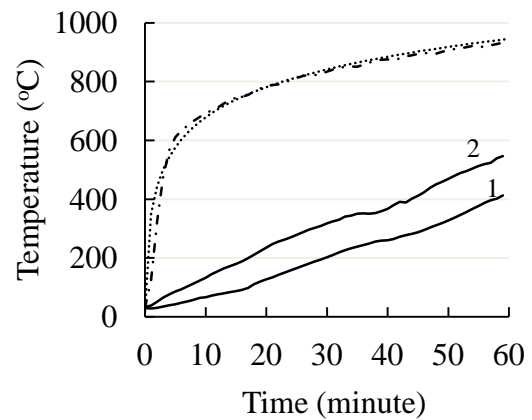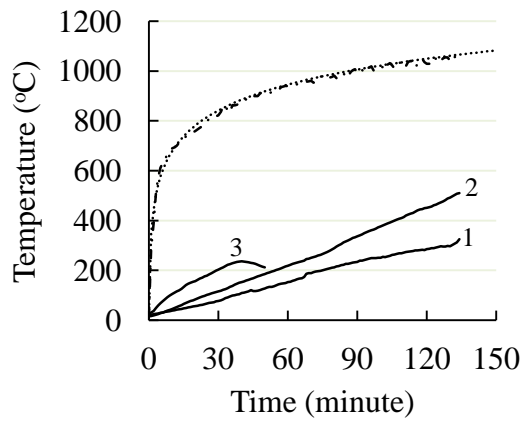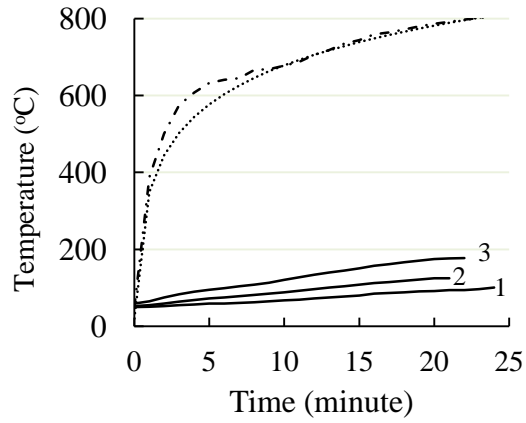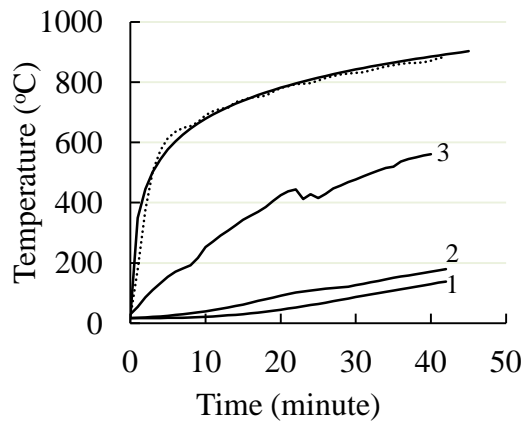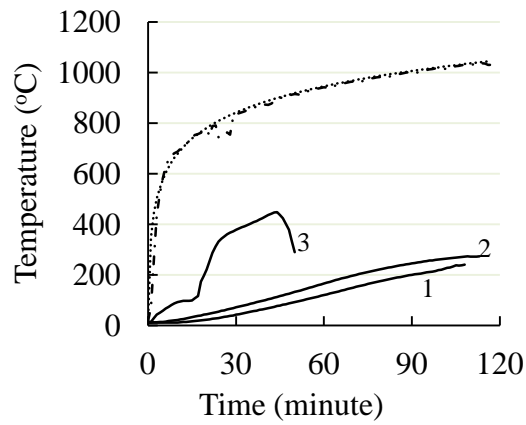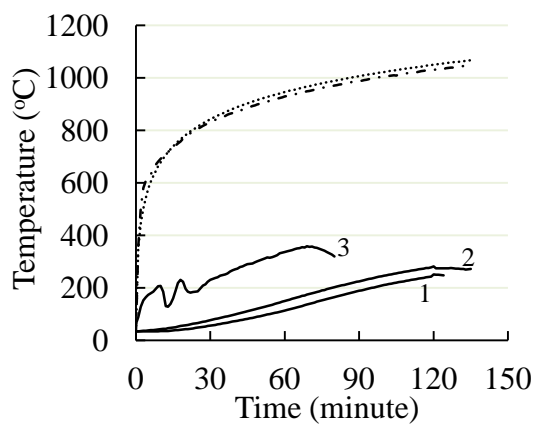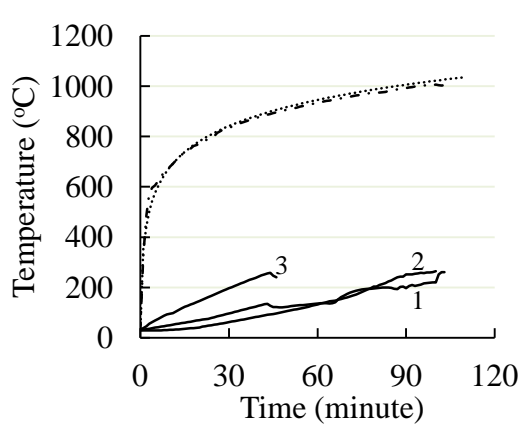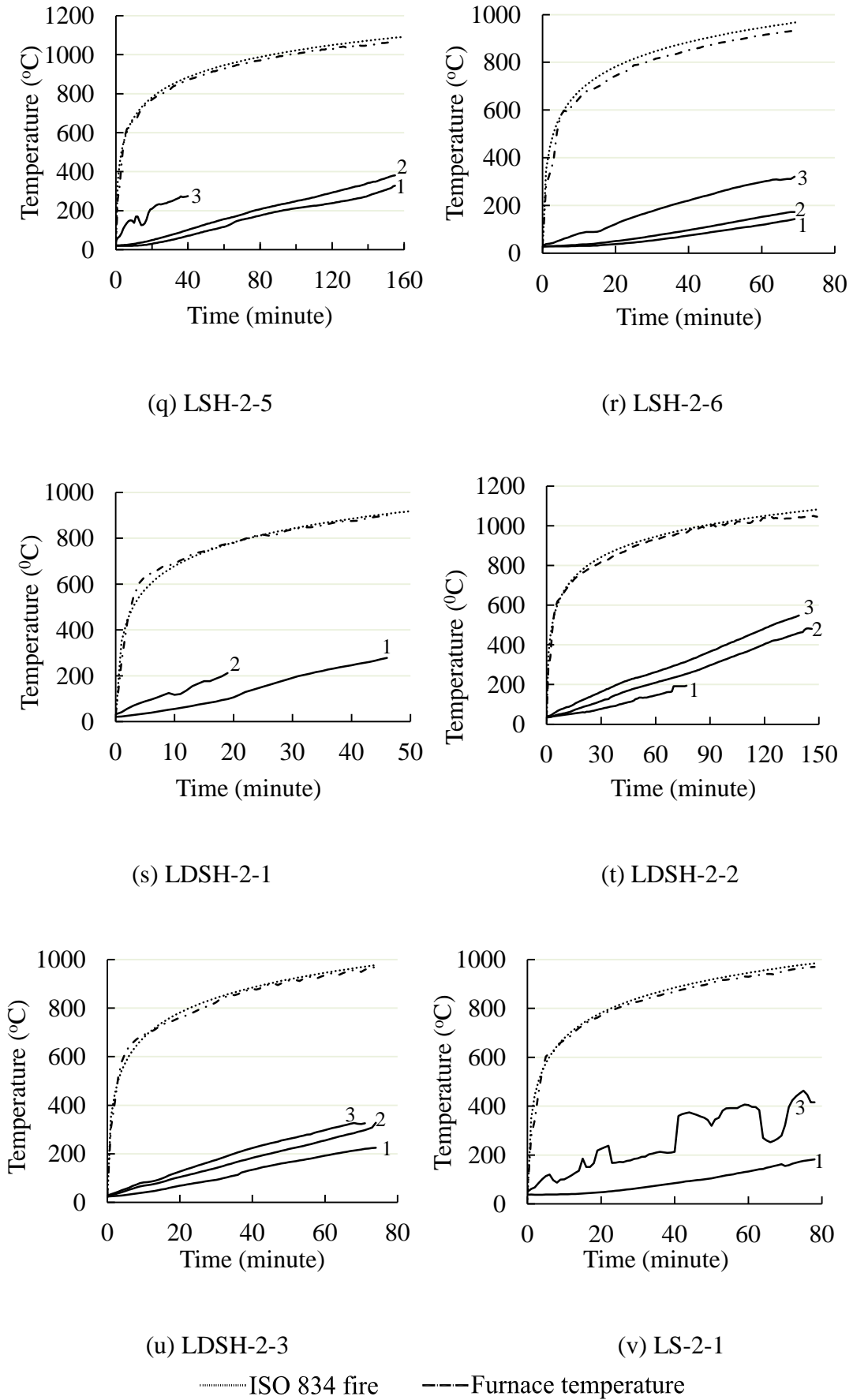
Figure 6.16: Measured temperatures in tested columns
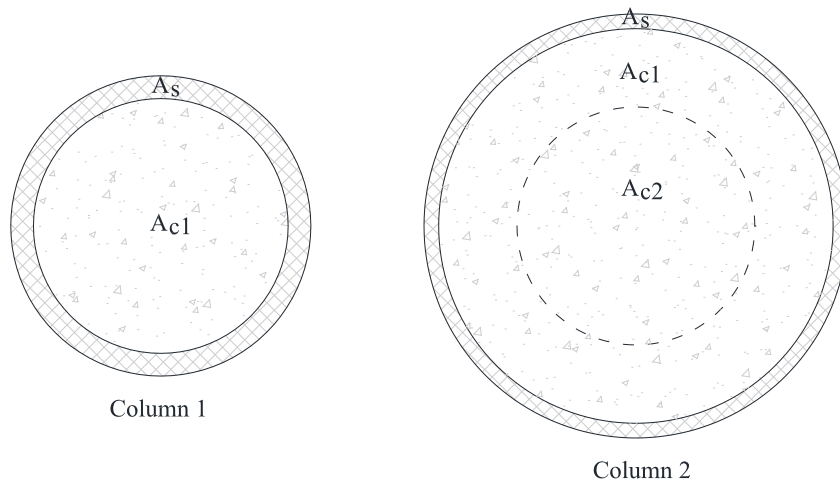
Figure 6.17: Stub composite columns to illustrate the effects of cross-sectional size

and load level on the failure temperature of outer tube
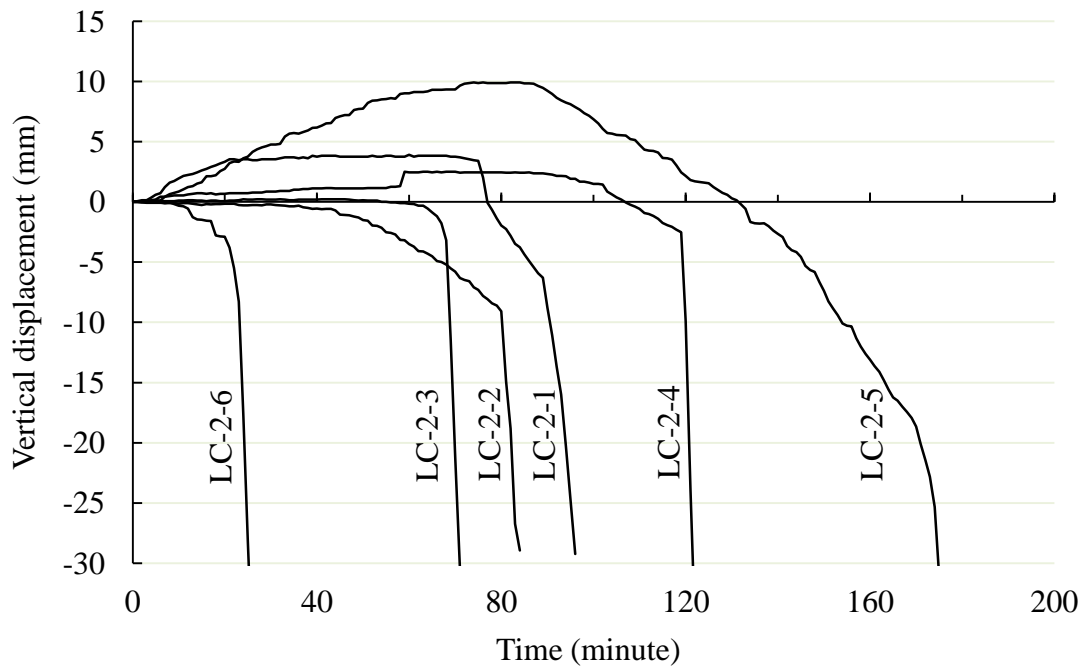
Figure 6.18: Curves of vertical displacements versus fire exposure time of column

LC-2-1 ~ LC-2-6
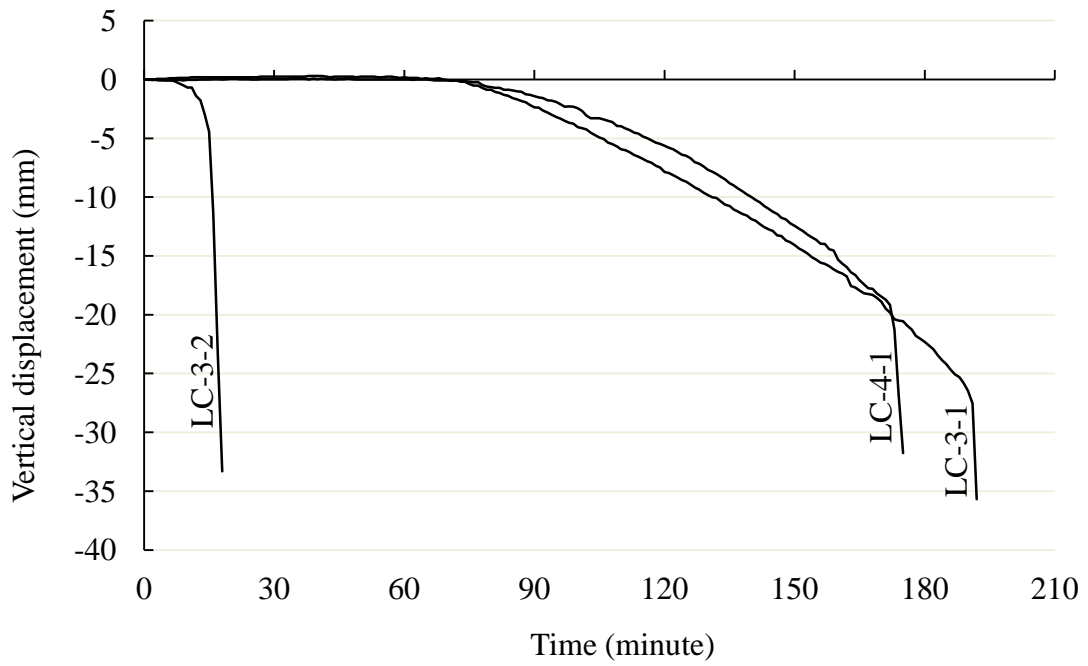
Figure 6.19: Curves of vertical displacements versus fire exposure time of column

LC-3-1, LC-3-2, and LC-4-1
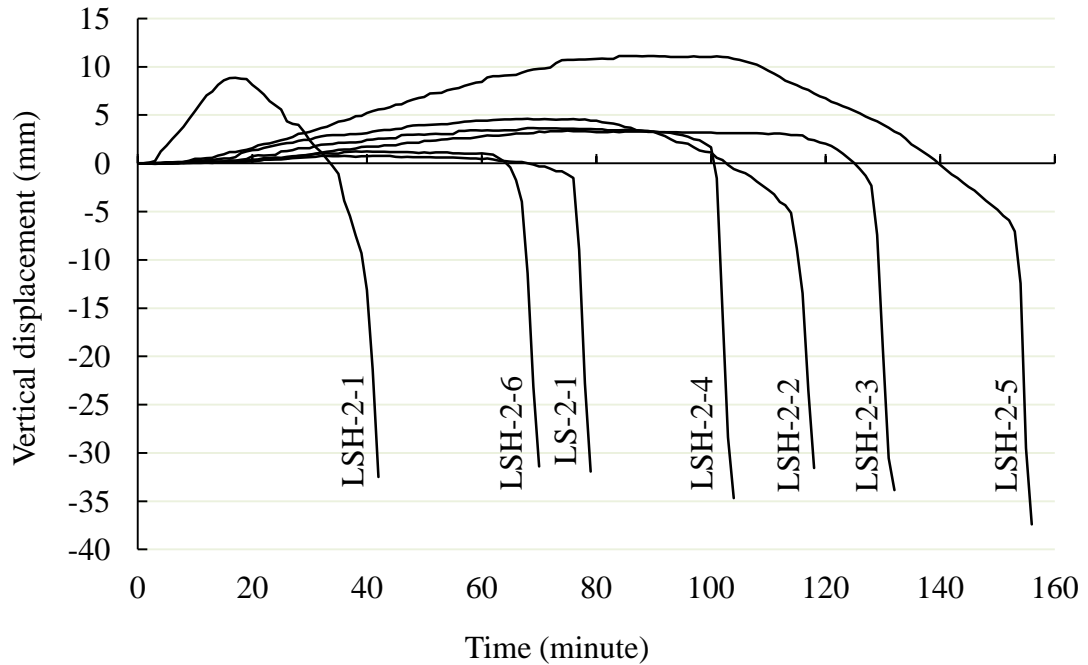
Figure 6.20: Curves of vertical displacements versus fire exposure time of column

LSH-2-1 ~ LSH-2-6 and LS-2-1
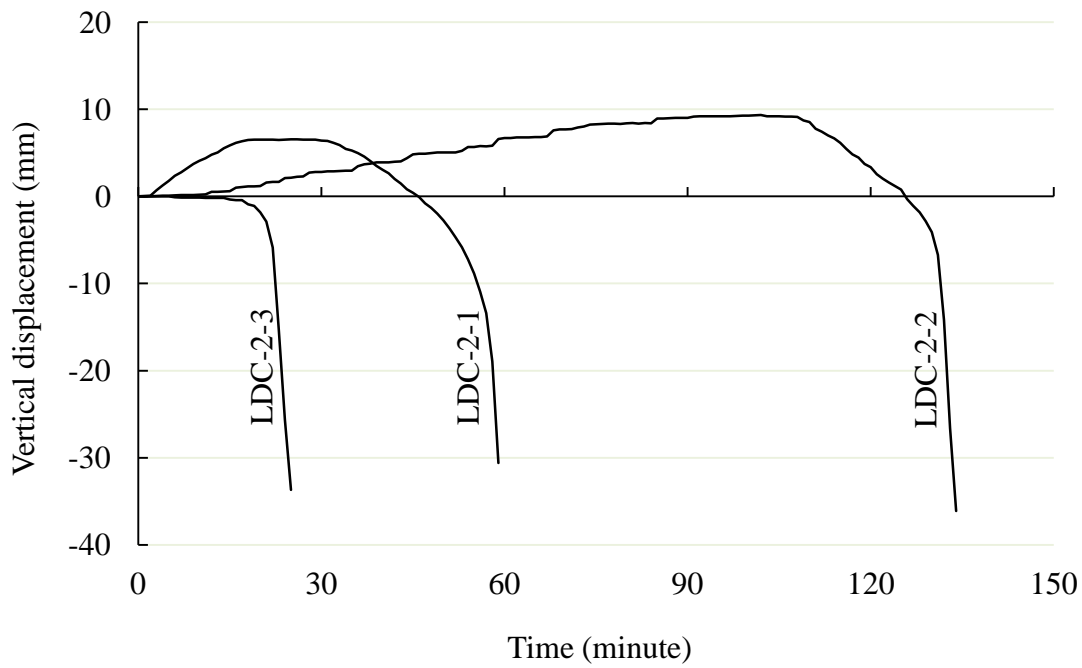
Figure 6.21: Curves of vertical displacements versus fire exposure time of column

LDC-2-1, LDC-2-2 and LDC-2-3
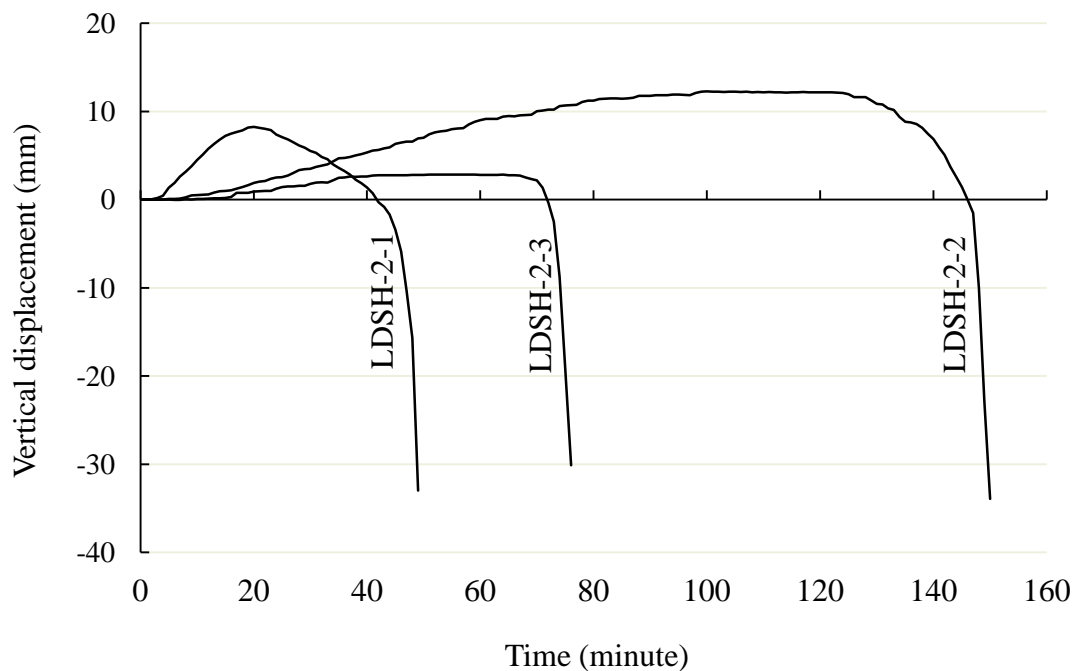
Figure 6.22: Curves of vertical displacements versus fire exposure time of column

LDSH-2-1, LDSH-2-2 and LDSH-2-3

(a) LC-2-1

(b) LC-2-2

(c) LC-2-3

(c) LC-2-4

(e) LC-2-5

(f) LC-2-6

(g) LC-3-1

(h) LC-3-2

(i) LC-4-1

(j) LSH-2-1

(k) LSH-2-2

(l) LSH-2-3

(m) LSH-2-4

(n) LSH-2-5

(o) LSH-2-6

(p) LS-2-1

(q) LDC-2-1

(r) LDC-2-2

(s) LDC-2-3

(t) LDSH-2-1

(u) LDSH-2-2   (v) LDSH-2-3

Figure 6.23: Failure modes of tested CFST columns

Figure 6.24: Comparions between failure modes of circualr single-tube columns

LSH-2-1   LSH-2-2   LSH-2-3   LSH-2-4   LSH-2-5   LSH-2-6   LS-2-1
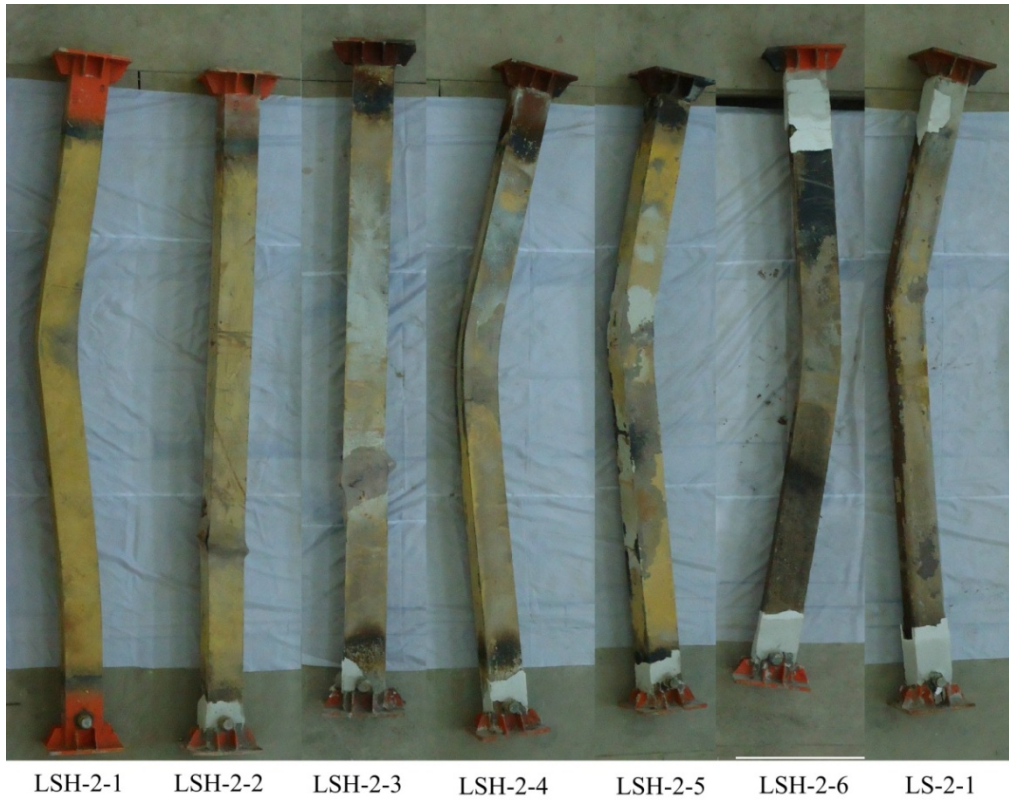
Figure 6.25: Comparions between failure modes of square single-tube columns

LDC-2-1   LDC-2-2   LDC-2-3   LDSH-2-1   LDSH-2-2   LDSH-2-3

Figure 6.26: Comparions between failure modes of double-skin columns

139
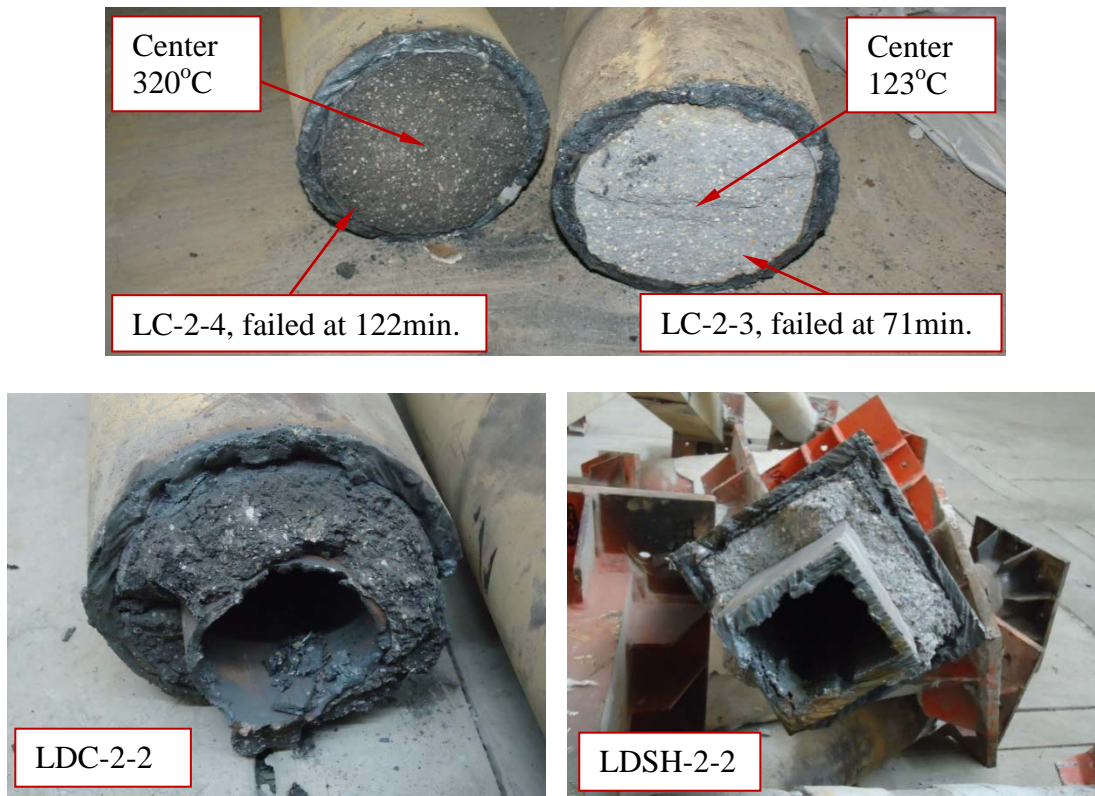
Figure 6.27: Faliure observations at cross sections
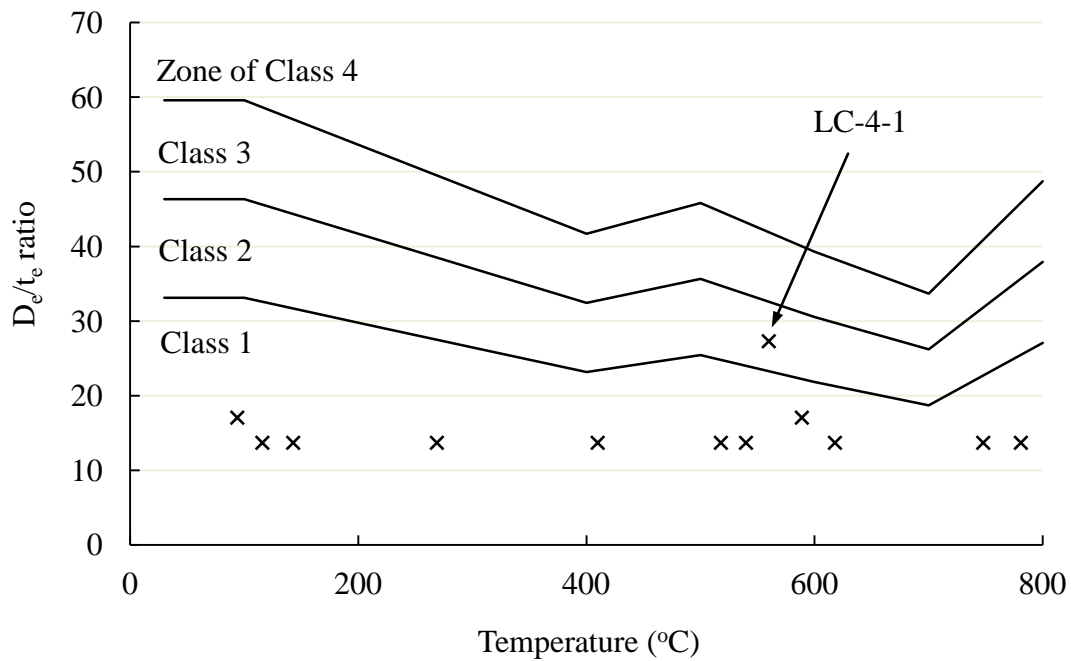
Figure 6.28: Relation of section classification and temperature for circular external

tubes with S355 steel
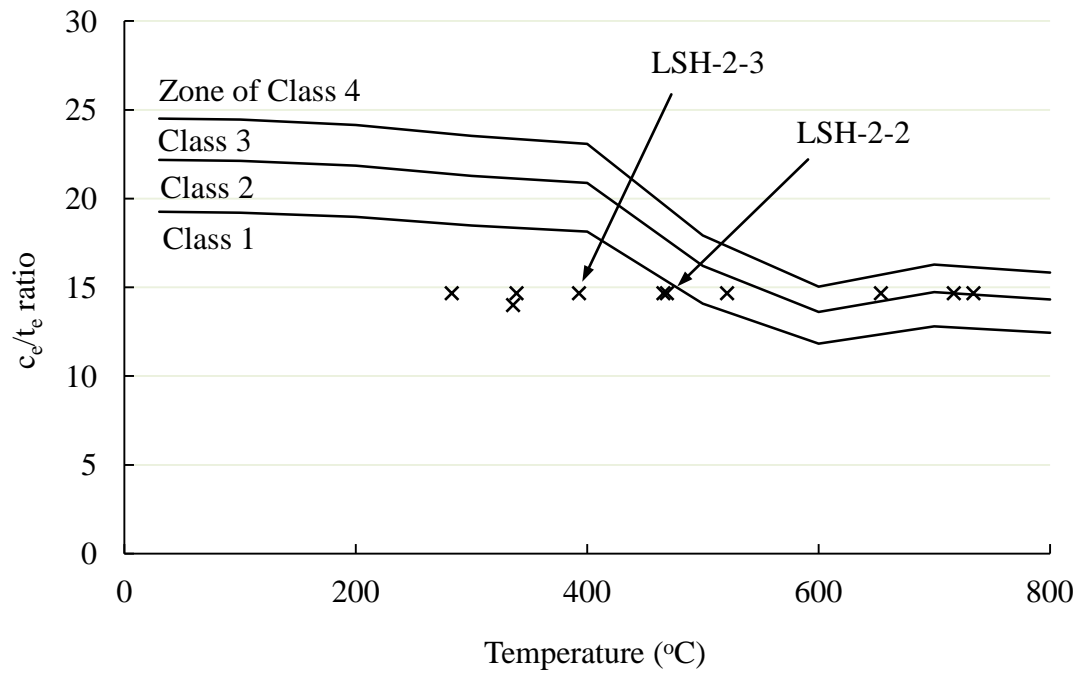
Figure 6.29: Relation of section classification and temperature for square external

tubes with S690 steel
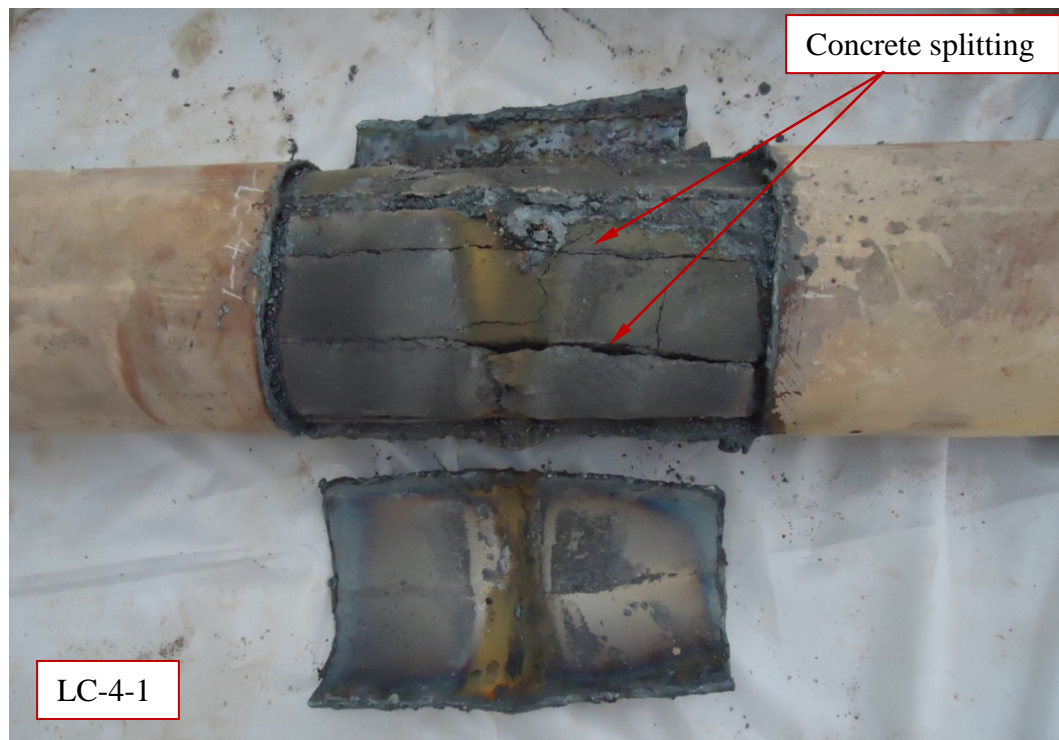
Figure 6.30: Longitudinal splitting of concrete by cross-sectional failure
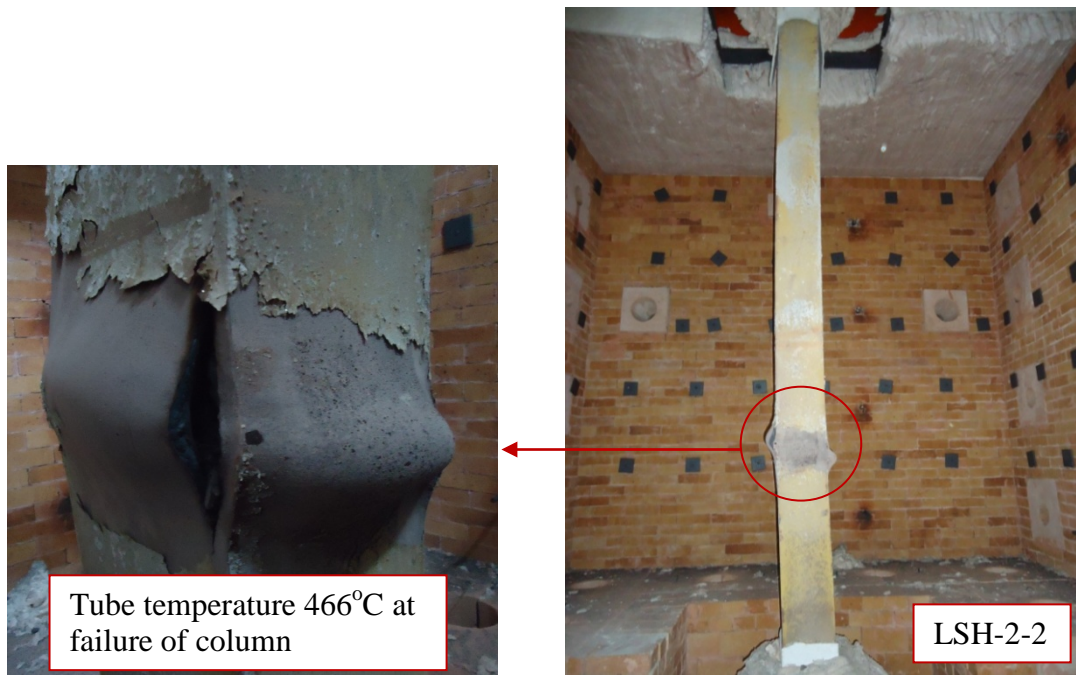
Figure 6.31: Weld tearing of welded box section
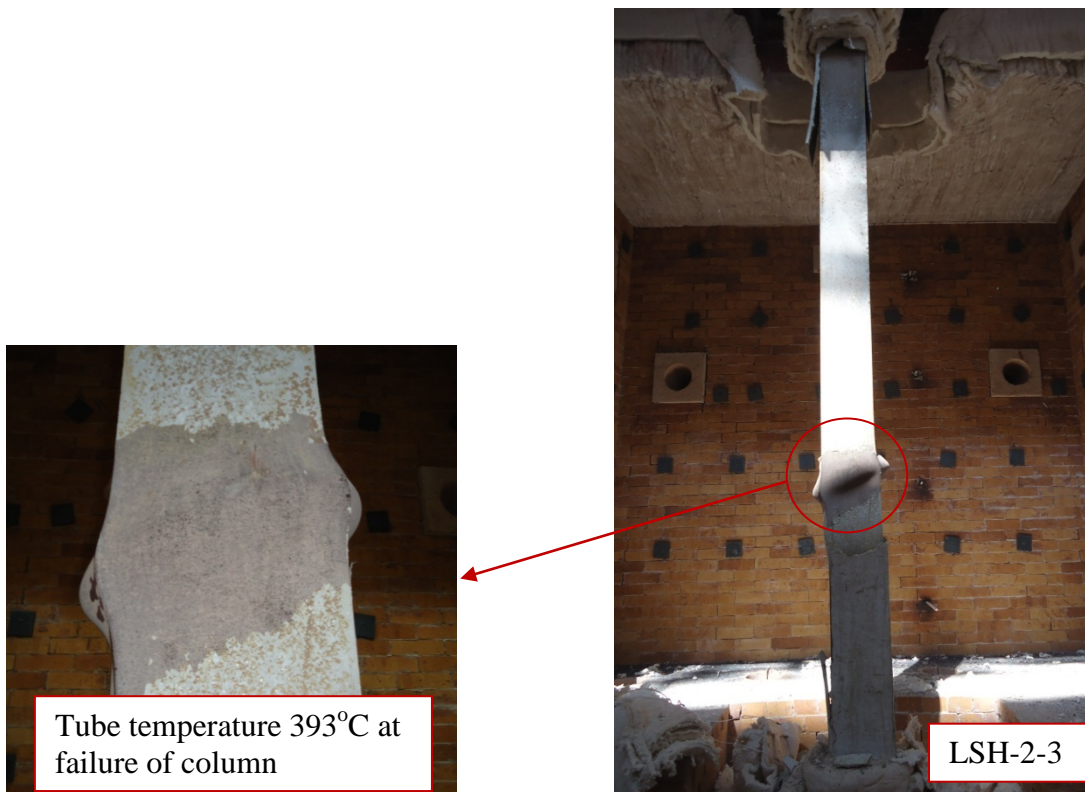
Figure 6.32: Intact welding of welded box section
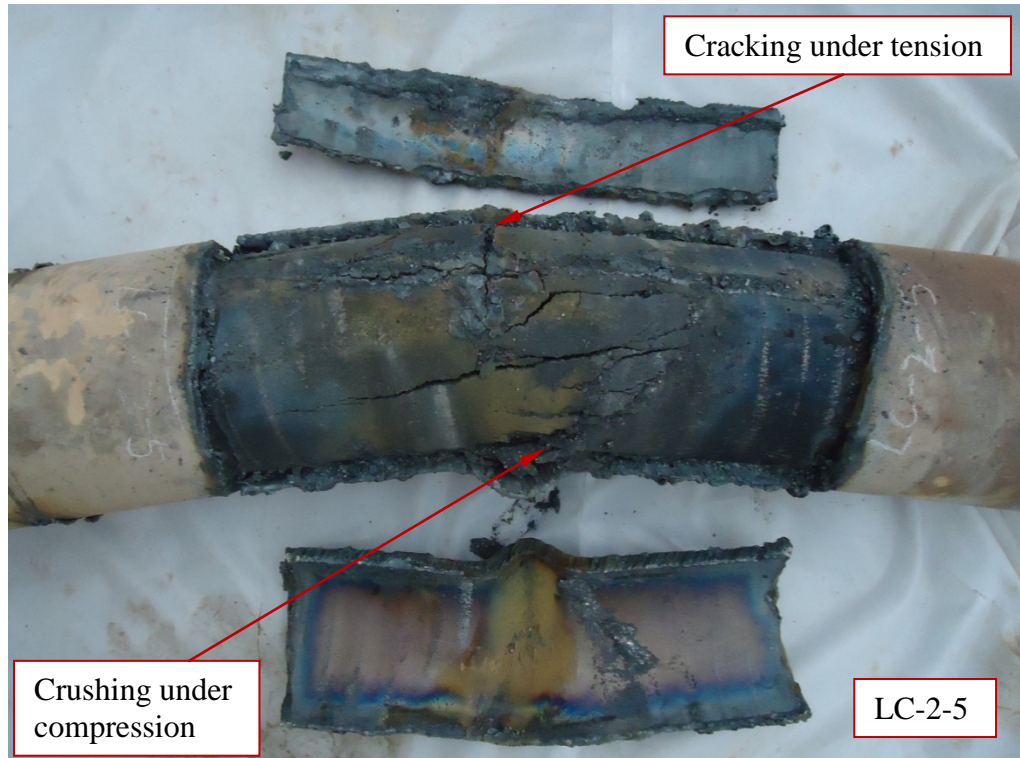
Figure 6.33: Transversal cracking of concrete by flexural buckling failure

(a) Circular double-skin column LDC-2-2

(b) Square double-skin column LSDH-2-2

Figure 6.34: Local bulge of inner tube
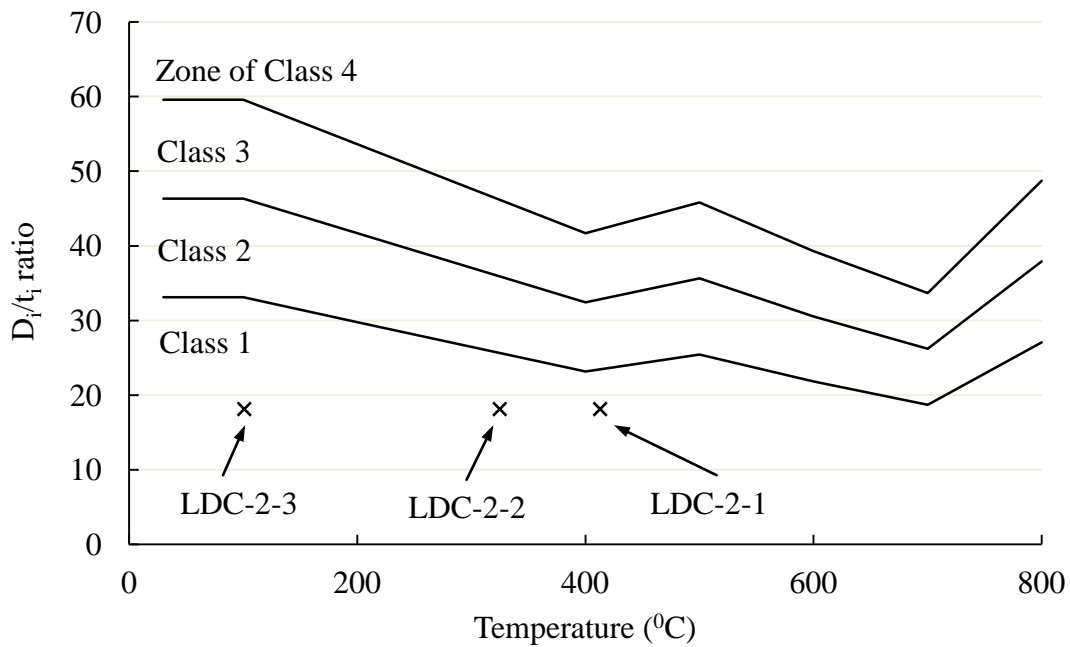
Figure 6.35: Relation of section classification and temperature for circular inner tubes

with S355 steel
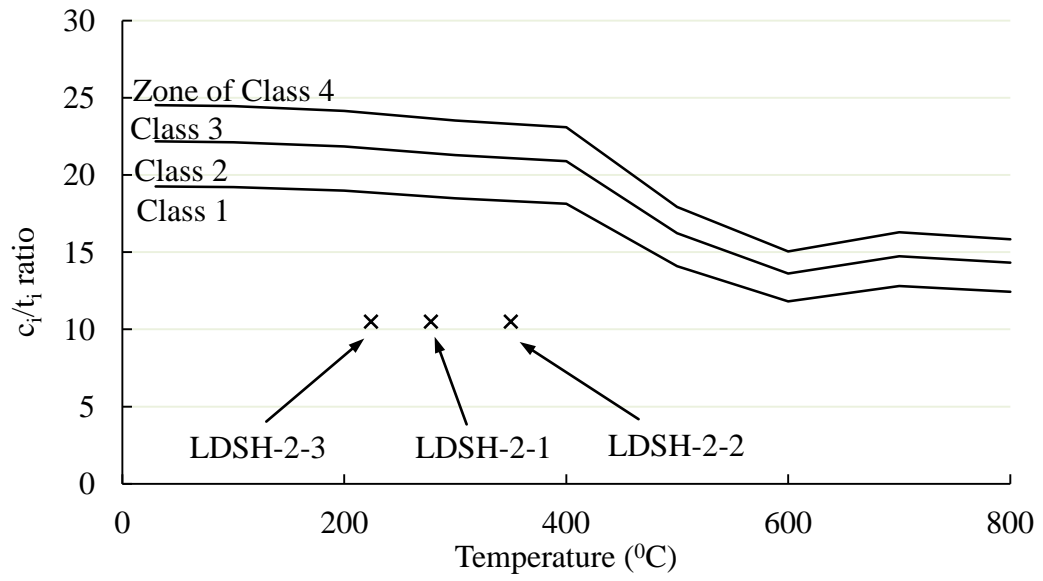
Figure 6.36: Relation of section classification and temperature for square inner tubes

with S690 steel

Chapter 7 Fire Resistant Design of Concrete Filled Steel Tubular Columns

7.1 Overview

This chapter presents the methodologies for the fire resistant design of CFST columns. The design is based on the existing simple calculation model (SCM) as given in EN 1994-1-2 and the proposed M-N interaction model (MNIM). SCM and MNIM are implemented in the numerical software MATLAB. By using SCM and MNIM, the temperature profiles of columns are calculated based on the finite difference method (FDM), whereas the effective length of a column under fire testing is derived based on the 4th-order differential equation of the lateral displacement of the column. FDM, SCM and MNIM are validated by the fire tests on the UHSC filled steel tubes in Chapter 6 and the test data of normal strength materials in the literature. The parametric analyses on effects of strengths of steel and concrete on the fire resistance time are carried out based on the validated MNIM.

7.2 Heat Transfer Analysis by Finite Difference Method

7.2.1 Basics of Heat Transfer

Heat transfer focuses on a study of the transition of thermal energy from a hotter object to a cooler object due to temperature difference. There are three ways of heat transfer which are heat conduction, heat convection and heat radiation. Heat conduction is the transfer of heat energy by the direct contact between particles of the material. Heat convection is the transfer of heat energy when nearby liquids or gases

pass through a solid surface. Heat radiation is the transfer of heat energy by electromagnetic waves.

In order to get the temperature field of any object, the partial differential equation (PDE) of heat transfer can be used. The PDE can be derived according to the law of Fourier's and the law of conservation of energy as shown below (Tao, 2006).

$$\rho c \frac{\partial T}{\partial t} = \frac{\partial}{\partial x}\left(\lambda \frac{\partial T}{\partial x}\right) + \frac{\partial}{\partial y}\left(\lambda \frac{\partial T}{\partial y}\right) + \frac{\partial}{\partial z}\left(\lambda \frac{\partial T}{\partial z}\right) \qquad (7.1)$$

The λ, ρ, c are the thermal conductivity, density and specific heat respectively. For steady-state heat transfer problems, the term $\rho c \dfrac{\partial T}{\partial t}$ is equal to zero.

7.2.2   Finite Difference Method

Integration techniques are needed to solve the heat transfer equation (7.1). In structures with simple geometries and boundary conditions, the analytical solutions can be obtained. However, in most cases, it is difficult to obtain the analytical solutions. Hence, approximate solutions are needed. In recent decades, numerical methods are widely used with the rapid development of computer techniques such as finite element method (FEM), finite difference method (FDM) and boundary element method (BEM) and so on. Comparisons between FEM, FDM and BEM indicate that the principle of FDM is relatively simple and easily understood. It provides a powerful and efficient technique for the solution of heat transfer problems.

There are two ways of introducing FDM (Harmathy, 1993). The former consists of replacing the space and time derivatives in the equations of heat condition by finite difference quotients. This method is favored by mathematicians who are interested not

only in problem solving, but also in such questions as truncation error and convergence. Engineers usually prefer to formulate the finite difference procedure by writing energy conservation equations for each volumetric element, assuming that for a short time period, quasi-steady-state conditions prevail.

To clarify the basics of FDM, consider the PDE of heat transfer of a 2-dimensional problem which is shown in following equation.

$$\frac{\partial^2 T}{\partial x^2} + \frac{\partial^2 T}{\partial y^2} = \frac{\rho c}{\lambda} \frac{\partial T}{\partial t} \tag{7.2}$$

Domain discretization of the analyzed object is the first step. The discretization for a 2-dimensional heat transfer problem is shown in Figure 7.1. The domain is discretized into many small areas by the gridlines. The intersection point of two gridlines is a node. The distance between two adjacent nodes is step length, denoted by Δx or Δy. Each node is at the center of an area (hatched area) which is enclosed by the perpendicular lines from the midway of two nodes, this area is representative of an element or control volume of node (m, n, i). Symbol i means the ith time step.

Assuming that the temperatures at nodes (m, n, i), (m+1, n, i), (m-1, n, i), (m, n+1, i) and (m, n-1, i) are denoted by $T^i_{m,n}$, $T^i_{m+1,n}$, $T^i_{m-1,n}$, $T^i_{m,n+1}$ and $T^i_{m,n-1}$ respectively, expanding $T^i_{m,n-1}$ and $T^i_{m,n+1}$ by Taylor series at node (m, n, i) gives:

$$T^i_{m,n-1} = T^i_{m,n} + \Delta x \frac{\partial T^i_{m,n}}{\partial x} + \frac{(\Delta x)^2}{2!} \frac{\partial^2 T^i_{m,n}}{\partial x^2} + O\left((\Delta x)^2\right) \tag{7.3}$$

$$T^i_{m,n+1} = T^i_{m,n} - \Delta x \frac{\partial T^i_{m,n}}{\partial x} + \frac{(\Delta x)^2}{2!} \frac{\partial^2 T^i_{m,n}}{\partial x^2} + O\left((\Delta x)^2\right) \tag{7.4}$$

Adding above equations gives:

$$T_{m,n-1}^{i} + T_{m,n+1}^{i} = 2T_{m,n}^{i} + \left(\Delta x\right)^{2} \frac{\partial^{2} T_{m,n}^{i}}{\partial x^{2}} + O\left(\left(\Delta x\right)^{2}\right) \tag{7.5}$$

After rearranging, it gives:

$$\frac{\partial^{2} T_{m,n}^{i}}{\partial x^{2}} = \frac{T_{m,n-1}^{i} - 2T_{m,n}^{i} + T_{m,n+1}^{i}}{\left(\Delta x\right)^{2}} + O\left(\left(\Delta x\right)^{2}\right) \tag{7.6}$$

If the truncation error $O\left(\left(\Delta x\right)^{2}\right)$ can be ignored without convergence problems being

caused, the second partial differential $\frac{\partial^{2} T_{m,n}^{i}}{\partial x^{2}}$ and $\frac{\partial^{2} T_{m,n}^{i}}{\partial y^{2}}$ can be well approximated as

follows:

$$\frac{\partial^{2} T_{m,n}^{i}}{\partial x^{2}} = \frac{T_{m,n-1}^{i} - 2T_{m,n}^{i} + T_{m,n+1}^{i}}{\left(\Delta x\right)^{2}} \tag{7.7}$$

$$\frac{\partial^{2} T_{m,n}^{i}}{\partial y^{2}} = \frac{T_{m-1,n}^{i} - 2T_{m,n}^{i} + T_{m+1,n}^{i}}{\left(\Delta y\right)^{2}} \tag{7.8}$$

Thus, the second partial differential terms on the left-hand side of Eqn.(7.2) are

approximated by finite difference expressions shown in Eqn.(7.7) and Eqn.(7.8). With

regard to the first partial differential term on the right-hand side of Eqn. (7.2), it also

can be converted into a finite difference expression. Three types of finite difference

expressions can be used: forward difference, central difference and backward

difference which are separately discussed as follows.

Forward difference: expanding $T_{m,n}^{i+1}$ about node (m,n,i) by Taylor series and ignoring

the truncation error gives:

$$\frac{\partial T_{m,n}^{i}}{\partial t} = \frac{T_{m,n}^{i+1} - T_{m,n}^{i}}{\Delta t} \tag{7.9}$$

Backward difference: expanding $T_{m,n}^{i-1}$ about node (m,n,i) by Taylor series and ignoring the truncation error give:

$$\frac{\partial T_{m,n}^{i}}{\partial t} = \frac{T_{m,n}^{i} - T_{m,n}^{i-1}}{\Delta t} \tag{7.10}$$

Central difference: adding Eqn. (7.9) and Eqn. (7.10) gives:

$$\frac{\partial T_{m,n}^{i}}{\partial t} = \frac{T_{m,n}^{i+1} - T_{m,n}^{i-1}}{2\Delta t} \tag{7.11}$$

It can be found by comparing the three different expressions that a special starting procedure is needed for the backward difference and central difference methods. That is because $T_{m,n}^{-1}$ is needed when $T_{m,n}^{0}$ is calculated. It is not convenient to get $T_{m,n}^{-1}$.

Hence, the forward difference method is preferred in approximating the term $\frac{\rho c}{\lambda} \frac{\partial T}{\partial t}$.

Substituting equations Eqn. (7.7), Eqn. (7.8) and Eqn. (7.9) into Eqn. (7.2) gives:

$$\frac{T_{m,n-1}^{i} - 2T_{m,n}^{i} + T_{m,n+1}^{i}}{(\Delta x)^{2}} + \frac{T_{m-1,n}^{i} - 2T_{m,n}^{i} + T_{m+1,n}^{i}}{(\Delta y)^{2}} = \frac{\rho c}{\lambda} \frac{T_{m,n}^{i+1} - T_{m,n}^{i}}{\Delta t} \tag{7.12}$$

If $\Delta x = \Delta y = \Delta L$ and $\alpha = \lambda/\rho c$, then above equation can be rearranged as follows:

$$T_{m,n}^{i+1} = \frac{\alpha \Delta t}{(\Delta L)^{2}} \left(T_{m+1,n}^{i} + T_{m-1,n}^{i} + T_{m,n+1}^{i} + T_{m,n-1}^{i} \right) + \left(1 - \frac{4\alpha \Delta t}{(\Delta L)^{2}} \right) T_{m,n}^{i} \tag{7.13}$$

It is noted that α is changed with temperature $T_{m,n}^{i}$. The temperature at an internal node (m, n, i+1) can be calculated from the temperatures at nearby nodes at the *i*th

time step explicitly. This method is known as the explicit forward time central space difference method. In order to ensure that the temperature $T_{m,n}^{i+1}$ is higher than $T_{m,n}^{i}$ during the heating up process or lower during the cooling down process, the stability requirement as given in following equation should be satisfied (Bayazitoglu and Ozisik, 1988).

$$1 - \frac{4\alpha\Delta t}{(\Delta L)^2} \geq 0 \tag{7.14}$$

Eqn. (7.13) could also be derived by the energy balance method (EBM). According to the law of energy conservation, the heat energy flowing into node (m,n,i) from neighboring nodes (m+1,n,i), (m-1,n,i), (m,n+1,i) and (m,n-1,i) should be equal to the energy consumed by the temperature increase of node (m, n, i). It is formulated as:

$$\lambda \frac{T_{m-1,n}^{i} - T_{m,n}^{i}}{\Delta y}\Delta x + \lambda \frac{T_{m+1,n}^{i} - T_{m,n}^{i}}{\Delta y}\Delta x + \lambda \frac{T_{m,n-1}^{i} - T_{m,n}^{i}}{\Delta x}\Delta y + \lambda \frac{T_{m,n+1}^{i} - T_{m,n}^{i}}{\Delta x}\Delta y = \rho c \Delta x \Delta y \frac{T_{m,n}^{i+1} - T_{m,n}^{i}}{\Delta t} \tag{7.15}$$

The left-hand side of equation (7-15) is representative of the heat energy flowing into node (m, n, i); whereas it is the heat energy consumed by the temperature increase of node (m, n, i) on the right hand side of equation (7-15). After rearranging, equation (7-15) becomes Eqn. (7.13).

The energy balance method is convenient and efficient for the temperature calculations of edge nodes such as node (1, 1) and node (m, 1) as shown in Figure 7.1, or nodes at the interface of different materials. The calculation for node (1, 1) and (m, 1) can be formulated by energy balance as shown in following equations.

Node (1, 1):

$$T_{1,1}^{i+1} = \frac{2\alpha\Delta t}{(\Delta L)^2}\left(T_{1,2}^i + T_{2,1}^i\right) + \left(1 - \frac{4\alpha\Delta t}{(\Delta L)^2} - \frac{4\alpha\beta\Delta t}{\Delta L}\right)T_{1,1}^i + \frac{4\alpha\beta\Delta t}{\Delta L}T_f^i \qquad (7.16)$$

Stability requirement for Node (1, 1):

$$1 - \frac{4\alpha\Delta t}{(\Delta L)^2} - \frac{2\alpha\beta\Delta t}{\Delta L} \geq 0 \qquad (7.17)$$

Node (m, 1):

$$T_{m,1}^{i+1} = \frac{\alpha\Delta t}{(\Delta L)^2}\left(2T_{m,2}^i + T_{m+1,1}^i + T_{m-1,1}^i\right) + \left(1 - \frac{4\alpha\Delta t}{(\Delta L)^2} - \frac{2\alpha\beta\Delta t}{\Delta L}\right)T_{m,1}^i + \frac{2\alpha\beta\Delta t}{\Delta L}T_f^i \qquad (7.18)$$

Stability requirement for Node (m, 1):

$$1 - \frac{4\alpha\Delta t}{(\Delta L)^2} - \frac{2\alpha\beta\Delta t}{\Delta L} \geq 0 \qquad (7.19)$$

T_f^i is the temperature of the external heat source, such as fire, at the ith time step. Assuming $\Delta x = \Delta y = \Delta L$, $\alpha = (\lambda/\rho c)$, and $\beta = (h/\lambda)$, h is the sum of coefficients of heat convection h_e and heat radiation h_r. In the current research, the convection coefficient h_e is taken as 25W/m$^2\cdot$K for exposure under the standard ISO-834 fire (EN 1991-1-2, 2002). The radiation coefficient is calculated as:

$$h_r = \Phi \cdot \varepsilon_m \cdot \varepsilon_f \cdot \sigma\left[\left(T_f + 273\right)^2 + \left(T + 273\right)^2\right]\left(T_f + T + 546\right) \qquad (7.20)$$

Φ is the configuration factor which is taken as 1.0 by ignoring the position and shadow effects. ε_m is the surface emissivity where it is taken as 0.7 and 0.8 respectively for unprotected and protected steel member. ε_f is the emissivity of the fire which is generally taken as 1.0. σ is the Stephan Boltzmann constant which is equal to

5.67×10^{-8} W/m²K⁴. T_f the effective radiation temperature of the fire environment and T is the surface temperature of the member.

7.2.3 Temperature Calculations of Circular CFST and CFDST Columns

Due to uniformity along the column height and symmetry of cross sections, the temperatures of circular CFST and CFDST columns can be calculated using a 1-D partial difference equation as given by:

$$\rho c \frac{\partial T}{\partial t} = \lambda \left(\frac{\partial^2 T}{\partial r^2} + \frac{1}{r} \frac{\partial T}{\partial r} \right) \tag{7.21}$$

The discretizations of cross-sections of circular CFST and CFDST columns are given in Figure 7.2 and Figure 7.3. The symbols d_c, d_s (d_{si} or d_{so}), d_p are respectively the element length of the concrete, the steel tube (inner tube or outer tube) and the fire protection material; whereas n_c, n_p are the element numbers of concrete and fire protection material respectively. Due to its high conductivity, the steel tube is meshed into one element. According to the energy balance method, the temperature calculation for the inner node, for example node (m, i) in the concrete, in the form of finite difference can be given as:

$$T_m^{i+1} = T_m^i + \frac{d_t}{p_c A_m} \left[\lambda_c^{\left(\frac{T_{m-1}^i + T_m^i}{2} \right)} \frac{T_{m-1}^i - T_m^i}{d_c} l_{m1} + \lambda_c^{\left(\frac{T_{m+1}^i + T_m^i}{2} \right)} \frac{T_{m+1}^i - T_m^i}{d_c} l_{m2} \right] \tag{7.22}$$

$$l_{m1} = (m - 1.5) d_c; l_{m2} = (m - 0.5) d_c; A_m = \frac{1}{2} \left(l_{m2}^2 - l_{m1}^2 \right)$$

Where p_c is the specific heat capacity which is the product of specific heat and density, subscript "c" stands for concrete. $\lambda_c^{\left(\frac{T_{m-1}^i+T_m^i}{2}\right)}$ means that λ_c is the function of $\frac{T_{m-1}^i+T_m^i}{2}$. The rest could be deduced by analogy.

Thus, the temperature T_m^{i+1} at node (m) and (i+1)th time step can be explicitly calculated. It is noted that the thermal conductivity λ_c changes with temperature. As the heat energy, flowing from node (m-1) into node (m), passes through elements with different temperatures, the thermal conductivity is thus calculated based on the averaged temperatures at element (m-1) and element (m) (Croft and Lilley, 1977).

Similarly, the temperature for the center node (1) of CFST column is calculated as:

$$T_1^{i+1} = T_1^i + \frac{d_t}{p_c d_c^2} \lambda_c^{\left(\frac{T_2^i+T_1^i}{2}\right)} \left(T_2^i - T_1^i\right) \tag{7.23}$$

With regard to the temperature calculation of node (1) of CFDST column, the effect of air in the inner tube is not taken into account. This means that the inner surface of inner tube is assumed to be insulated. The temperature calculation is shown as follows.

$$T_1^{i+1} = T_1^i + \frac{d_t l_{21}}{d_{si} p_s A_{21}} \lambda_s^{\left(\frac{T_1^i+T_2^i}{2}\right)} \left(T_2^i - T_1^i\right) \tag{7.24}$$

Where r_i is the inner radius of inner steel tube; $l_{21} = r_i + d_{si}/2$; $A_{21} = \frac{1}{2}\left(l_{21}^2 - r_i^2\right)$

The thermal resistance is not taken into account at the interface between concrete and steel tube. Thus, there is no heat energy loss at interface. The temperature of the nodes

at the interface in CFST and CFDST columns can be calculated as given in the following two equations.

CFST column:

$$T_{nc+1}^{i+1} = T_{nc+1}^{i} + \frac{d_t}{p_c A_c + p_s A_s}\left[\lambda_c^{\left(\frac{T_{nc}^{i}+T_{nc+1}^{i}}{2}\right)}\frac{T_{nc}^{i}-T_{nc+1}^{i}}{d_c}l_c + \lambda_s^{\left(\frac{T_{nc+2}^{i}+T_{nc+1}^{i}}{2}\right)}\frac{T_{nc+2}^{i}-T_{nc+1}^{i}}{d_s}l_s\right] \quad (7.25)$$

where $\begin{cases} l_c = (n_c - 0.5)d_c \\ l_{cs} = n_c \cdot d_c \\ l_s = n_c \cdot d_c + 0.5d_s \end{cases}$ $\begin{cases} A_c = \frac{1}{2}\left[l_{cs}^2 - l_c^2\right] \\ A_s = \frac{1}{2}\left[l_s^2 - l_{cs}^2\right] \end{cases}$

CFDST column:

$$T_{nc+2}^{i+1} = T_{nc+2}^{i} + \frac{d_t}{p_c A_c + p_s A_s}\left[\lambda_c^{\left(\frac{T_{nc+1}^{i}+T_{nc+2}^{i}}{2}\right)}\frac{T_{nc+1}^{i}-T_{nc+2}^{i}}{d_c}l_c + \lambda_s^{\left(\frac{T_{nc+3}^{i}+T_{nc+2}^{i}}{2}\right)}\frac{T_{nc+3}^{i}-T_{nc+2}^{i}}{d_{so}}l_s\right] \quad (7.26)$$

where $\begin{cases} l_c = r_i + d_{si} + (nc - 0.5)d_c \\ l_{cs} = r_i + d_{si} + nc \cdot d_c \\ l_s = r_i + d_{si} + nc \cdot d_c + 0.5d_{so} \\ A_c = \frac{1}{2}\left[l_{cs}^2 - l_c^2\right]; A_s = \frac{1}{2}\left[l_s^2 - l_{cs}^2\right] \end{cases}$

The temperature of the nodes at the perimeter which is exposed to fire can be calculated as given in the following two equations.

CFST column: (7.27)

$$T_{nc+np+2}^{i+1} = T_{nc+np+2}^{i} + \frac{dt}{p_p A_{ep}}\left[\lambda_p^{\left(\frac{T_{nc+np+1}^{i}+T_{nc+np+2}^{i}}{2}\right)}\frac{T_{nc+np+1}^{i}-T_{nc+np+2}^{i}}{d_p}l_{p1} + h\left(T_f^{i}-T_{nc+np+2}^{i}\right)l_{p2}\right]$$

$l_{p1} = D_e/2 + (n_p - 0.5)d_p$; $l_{p2} = D_e/2 + n_p \cdot d_p$; $A_{ep} = \frac{1}{2}\left(l_{p2}^2 - l_{p1}^2\right)$

D_e is the outer diameter of the column.

CFDST column:

$$T_{nc+np+3}^{i+1} = T_{nc+np+3}^{i} + \frac{d_t}{p_p A_{ep}} \left[\lambda_p^{\left(\frac{T_{nc+np+2}^{i} + T_{nc+np+3}^{i}}{2} \right)} \frac{T_{nc+np+2}^{i} - T_{nc+np+3}^{i}}{d_p} l_{p1} + h \left(T_f^{i} - T_{nc+np+3}^{i} \right) l_{p2} \right] \quad (7.28)$$

where $l_{p1} = D_e/2 + (np - 0.5)d_p ; l_{p2} = D_e/2 + np \cdot d_p ; A_{ep} = \frac{1}{2} \left(l_{p2}^2 - l_{p1}^2 \right)$

7.2.4 Temperatures of Square CFST and CFDST Columns

The discretizations of square CFST and CFDST columns are shown respectively in Figure 7.4 and Figure 7.5. The temperatures of square CFST and CFDST columns can be calculated using a 2-D partial difference equation as given in Eqn. (6.2). The temperature calculations at some critical nodes are given herein. The temperature at the rest of the nodes can be similarly calculated.

The temperature at the corner node of the cross-section is calculated as given by:

$$T_{1,1}^{i+1} = T_{1,1}^{i} + \frac{2d_t}{p_p d_p^2} \left[\lambda_p^{\left(\frac{T_{1,2}^{i} + T_{1,1}^{i}}{2} \right)} \left(T_{1,2}^{i} - T_{1,1}^{i} \right) + \lambda_p^{\left(\frac{T_{2,1}^{i} + T_{1,1}^{i}}{2} \right)} \left(T_{2,1}^{i} - T_{1,1}^{i} \right) + 2hd_p \left(T_f - T_{1,1}^{i} \right) \right] \quad (7.29)$$

The temperature calculation for the nodes at the interface between the fire protection material and steel or between the steel and concrete in the CFST column are shown in Eqn.(7.30) (m=np+1, n=np+1). The temperature can be obtained similarly for CFDST columns.

$$T_{m,n}^{i+1} = T_{m,n}^{i} + \frac{2d_t}{d_s\left(p_p d_p + p_s d_s\right) + p_p d_p\left(d_p + d_s\right)} \begin{bmatrix} \lambda_p^{\left(\frac{T_{m,n-1}^{i}+T_{m,n}^{i}}{2}\right)}\dfrac{\left(d_p+d_s\right)\left(T_{m,n-1}^{i}-T_{m,n}^{i}\right)}{d_p} + \\[2ex] \dfrac{\lambda_p^{\left(\frac{T_{m,n+1}^{i}+T_{m,n}^{i}}{2}\right)}d_p + \lambda_s^{\left(\frac{T_{m,n+1}^{i}+T_{m,n}^{i}}{2}\right)}d_s}{d_s}\left(T_{m,n+1}^{i}-T_{m,n}^{i}\right)+ \\[2ex] \lambda_p^{\left(\frac{T_{m-1,n}^{i}+T_{m,n}^{i}}{2}\right)}\dfrac{\left(d_p+d_s\right)\left(T_{m-1,n}^{i}-T_{m,n}^{i}\right)}{d_p} + \\[2ex] \dfrac{\lambda_p^{\left(\frac{T_{m+1,n}^{i}+T_{m,n}^{i}}{2}\right)}d_p + \lambda_s^{\left(\frac{T_{m+1,n}^{i}+T_{m,n}^{i}}{2}\right)}d_s}{d_s}\left(T_{m+1,n}^{i}-T_{m,n}^{i}\right) \end{bmatrix}$$

(7.30)

The temperature of the inner tube in the double-skin square column is calculated as given in Eqn.(7.31) (m=np+nco+nci+3, n=np+nco+3).

$$T_{m,n}^{i+1} = T_{m,n}^{i} + \frac{d_t}{p_s d_{si} d_{ci}} \begin{bmatrix} \dfrac{d_{si}}{d_{ci}}\left(\lambda_s^{\frac{T_{m-1,n}^{i}+T_{m,n}^{i}}{2}}\left(T_{m-1,n}^{i}-T_{m,n}^{i}\right)+\lambda_s^{\frac{T_{m+1,n}^{i}+T_{m,n}^{i}}{2}}\left(T_{m+1,n}^{i}-T_{m,n}^{i}\right)\right) \\[2ex] +\lambda_s^{\frac{T_{m,n-1}^{i}+T_{m,n}^{i}}{2}}\dfrac{2d_{ci}\left(T_{m,n-1}^{i}-T_{m,n}^{i}\right)}{d_{si}} \end{bmatrix}$$ (7.31)

7.3 Simple Calculation Model

In the simple calculation method (SCM) as given in EN 1994-1-2, the design resistance of the CFST column under axial compression is calculated as:

$$N_{fi,Rd} = \chi N_{fi,pl,Rd} \tag{7.32}$$

where χ is the reduction coefficient which depends on the buckling curve "*c*" as stipulated in EN 1994-1-2 (2005). $N_{fi,pl,Rd}$ is the design value of the plastic resistance to axial compression in a fire situation. Assuming the cross section of a CFST or

CFDST column is divided into various parts, and they are denoted "*a*" for the steel profile and "*c*" for the concrete, then the design value for the plastic resistance to axial compression in a fire situation is given by:

$$N_{fi,pl,Rd} = \sum_{j} \left(\frac{A_{a,\theta} f_{ay,\theta}}{\gamma_{M,fi,a}} + \frac{A_{c,\theta} f_{c,\theta}}{\gamma_{M,fi,c}} \right) \tag{7.33}$$

where $A_{a,\theta}$ or $A_{c,\theta}$ is the area of steel or concrete element of the cross-section to which is attributed a certain temperature θ. j is the number of elements in the discretized cross-section. In order to calculate the reduction coefficient χ, the relative slenderness under a fire situation is needed and given by:

$$\overline{\lambda}_{\theta} = \sqrt{N_{fi,pl,R} \Big/ N_{fi,cr}} \tag{7.34}$$

where $N_{fi,pl,R}$ is the characteristic value of the plastic resistance to axial compression, and $N_{fi,cr}$ is the Euler buckling load in a fire situation which is given as:

$$N_{fi,cr} = \frac{\pi^2 (EI)_{fi,eff}}{l_{\theta}} \tag{7.35}$$

where l_θ is the buckling length of column in the fire situation, the effective flexural stiffness under fire is calculated as:

$$(EI)_{fi,eff} = \sum_{j} \left(\varphi_{a,\theta} E_{a,\theta} I_{a,\theta} \right) + \sum_{k} \left(\varphi_{c,\theta} E_{c,\theta} I_{c,\theta} \right) \tag{7.36}$$

where $I_{a,\theta}$ and $I_{c,\theta}$ are second moment of area of the steel and concrete of the cross-section for bending around the weak or strong axis. $E_{a,\theta}$ is the elastic modulus of steel. $E_{c,\theta}$ is the characteristic value for the secant modulus of concrete in the fire situation,

given by $f_{c,\theta}$ divided by strain corresponding to $f_{c,\theta}$. $\varphi_{a,\theta}$ and $\varphi_{c,\theta}$ are the reduction coefficients respectively for the steel and concrete, depending on the effect of thermal stresses. $\varphi_{c,\theta}$ is recommended as 0.8 for concrete. $\varphi_{a,\theta}$ is related with the shape of the cross-section and the fire resistance time of columns. It is proposed that design calculations should use a constant value of $\varphi_{a,\theta}$=1.0 (Wang, 2002). The proposed simplification is reasonable because:

(1)   The factors of $\varphi_{c,\theta}$ and $\varphi_{a,\theta}$ are empirical and are only obtained for the standard fire condition and may not be more widely applied under actual fire exposures;

(2)   Inaccuracy in mechanical properties of the steel and concrete at elevated temperatures overwhelms that caused by inaccuracies in $\varphi_{c,\theta}$ and $\varphi_{a,\theta}$ factors;

(3)   The proposed simplification is consistent with the approach under ambient temperature conditions.

Finally, the reduction coefficient χ is calculated as:

$$\chi = \frac{1}{\Phi + \sqrt{\Phi^2 - \bar{\lambda}_\theta^2}}$$
(7.37)

where

$$\Phi = 0.5\left[1 + 0.49\left(\bar{\lambda}_\theta - 0.2\right) + \bar{\lambda}_\theta^2\right]$$
(7.38)

The reduction factors for the mechanical properties of steel and concrete at elevated temperatures, recommended in EN 1992-1-2 (2004) and EN 1993-1-2 (2005), are given Table 7.1.

7.4 M-N Interaction Model

The M-N interaction model is used to evaluate the fire resistance of CFST columns, including UHSC and HSS, with combined bending moment and axial force. The M-N interaction curves of the CFST columns constrict with increasing fire exposure time. The interaction curves of a composite column cross-section are assumed to be polygonal diagrams as shown in Figure 7.6. The selected points on the curves are derived based on plastic analysis. The following assumptions were made for the application of the M-N interaction model in the current research.

(1)   The cross-section of the steel tube is at least compact.

(2)   The tensile strength of concrete is ignored.

(3)   There is no slip between the steel tube and concrete.

(4)   The cross-section remains plane.

(5)   The shear deformation is ignored.

(6)   The creep and shrinkage of concrete are ignored.

In Figure 7.6, $N_{\mathrm{fi,pm,Rd}}$ is the plastic resistance of the concrete in the whole cross-section in a fire situation. $M_{\mathrm{fi,pl,Rd}}$ and $M_{\mathrm{fi,max,Rd}}$ are the plastic moment resistances of the composite section in a fire situation. $N_{\mathrm{fi,pl,Rd}}$, $N_{\mathrm{fi,pm,Rd}}$, $M_{\mathrm{fi,pl,Rd}}$ and $M_{\mathrm{fi,max,Rd}}$ can be calculated based on the plastic stress block diagrams as illustrated in Figure 7.6. The confinement effect of concrete under fire is not taken into account for slender columns. However, the second-order effect is considered due to the large deformation under fire. The second-order effect is allowed for by multiplying the greatest first-order design moment by a factor of k_{fi} which is calculated as follows.

$$k_{fi} = \frac{\beta}{1 - N_{fi,Ed}/N_{fi,cr}}, \geq 1.0 \tag{7.39}$$

$N_{fi,Ed}$ is the applied load under fire and $N_{fi,cr}$ is the elastic critical load calculated from Eqn.(6.35). β is the equivalent moment factor which is related to the distribution of the first-order bending moment within the column length. It should be noted that there are two first-order bending moments for columns with an eccentric axial load. One is induced by the eccentricity of the load and the other is caused by initial geometric imperfections of column. For first-order bending moment from eccentricity, β is taken as 1.1. For first-order moment from imperfection, β is equal to 1.0. The member initial geometric imperfection is taken as $L/150$ which corresponds to buckling curve "c" as recommended in the simple calculation model of EN 1994-1-2 (2005). The imperfection is considered only in the plane in which failure is expected to occur. For symmetrical sections, imperfection is only applied in one direction. For combined compression and moment, the following condition should be satisfied for the stability check within the column length.

$$\frac{M_{fi,Ed}}{\mu_{fi,d} M_{fi,pl,Rd}} \leq \alpha_{fi,M} \tag{7.40}$$

$M_{fi,Ed}$ is the greatest of the end moments and the maximum bending moment within the column length, including imperfections and second order effects. $\mu_{fi,d}$ is the moment utilization factor in a fire situation. $\mu_{fi,d}$ greater than 1.0 is used where the bending moment depends directly on the action of the axial force, for example where the moment results from an eccentricity of the axial load.

In the ambient design situation according to EN 1994-1-1, the coefficient $\alpha_{fi,M}$ is generally taken as 0.9 for steel grades between S235 and S355 inclusive and for steel

grades S420 and S460 as 0.8. The value $\alpha_{fi,M}$ is taken into account in case of premature crushing of the concrete before the steel yields. The higher the steel grade, the more likely the concrete will be crushed prematurely. However, in the present fire design methods, the premature crushing of concrete is not considered. The reason is attributed to two facts. Firstly, concrete, even high strength concrete, generally loses its strength and shows better ductility under fire than when under ambient temperature. Concrete is more ductile at elevated temperatures, it is less prone to be crushed before steel yields. Secondly, the steel tube is softened and loses its capacity to prevent the lateral expansion of concrete under fire. As a result, the concrete is more prone to be laterally split rather than crushed. Hence, the coefficient $\alpha_{fi,M}$ is taken as 1.0 in the present fire resistance calculations.

7.5 Effective Length of Column in Fire Test

Generally in standard fire tests, the column is tested with part of the column length exposed to fire and the top and bottom parts unexposed to fire. With regard to the calculation of fire resistance time for the column in the fire test by using SCM or MNIM, the effective buckling length is required. Nowadays in research and design codes, the effective length is empirically determined. Lie and Chabot (1990) and Mao and Kodur (2011) proposed that the effective length in standard fire tests is taken as 2/3 times the column length exposed to fire for columns with "fixed-fixed" ends. For columns with pinned-pinned ends, the effective length is taken as the column length exposed to fire. These assumptions do not consider the effects of the column lengths which are not exposed to fire. Hence, the proposed effective length is rather arbitrary.

The effective length of a column in a standard fire test is governed by the types of end supports, column length unexposed to fire, and the stiffness ratio between the exposed part and the unexposed part during heating. It can be derived by solving the 4th-order differential equation (FODE) of the lateral displacement of column under fire. The derivations of the effective lengths of columns with pinned-pinned, pinned-fixed, fixed-fixed ends are respectively given in Section 7.5.1, Section 7.5.2 and Section 7.5.3. In the derivations, the temperature profiles are assumed to be uniformly distributed along the exposed column length. The temperature of the unexposed parts is taken as the same as that under ambient temperature.

7.5.1 Column Pinned at Both Ends

The FODEs of the lateral displacement of a column with pinned-pinned ends under axial load is given in Eqn. (7.41) and Eqn. (7.42). The definitions of the variables involved can be referred to Figure 7.7. Half length of the column is investigated due to symmetry.

$$w_1''' + k_1^2 w_1'' = 0 \quad k_1^2 = \frac{P}{(EI)_1} \quad x = [-L_1, 0] \tag{7.41}$$

$$w_2''' + k_2^2 w_2'' = 0 \quad k_2^2 = \frac{P}{(EI)_2} \quad x = [0, L_2] \tag{7.42}$$

The general solutions for above equations are:

$$w_1(x) = A_1 \cos k_1 x + B_1 \sin k_1 x + C_1 x + D_1 \quad x = [-L_1, 0] \tag{7.43}$$

$$w_2(x) = A_2 \cos k_2 x + B_2 \sin k_2 x + C_2 x + D_2 \quad x = [0, L_2] \tag{7.44}$$

The first, second and third differential of $w_1(x)$ and $w_2(x)$ can be calclated as:

163

$$\begin{cases} w'_1(x) = -A_1 k_1 \sin k_1 x + B_1 k_1 \cos k_1 x + C_1 \\ w''_1(x) = -A_1 k_1^2 \cos k_1 x - B_1 k_1^2 \sin k_1 x \\ w'''_1(x) = A_1 k_1^3 \sin k_1 x - B_1 k_1^3 \cos k_1 x \\ w'_2(x) = -A_2 k_2 \sin k_2 x + B_2 k_2 \cos k_2 x + C_2 \\ w''_2(x) = -A_2 k_2^2 \cos k_2 x - B_2 k_2^2 \sin k_2 x \\ w'''_2(x) = A_2 k_2^3 \sin k_2 x - B_2 k_2^3 \cos k_2 x \end{cases} \qquad (7.45)$$

The boundary conditions are needed to determine the coefficients in the genernal solutions. The boudary conditions are shown as follows.

At x=-L_1:

$$\begin{cases} w_1(-L_1) = 0 \\ M_1(-L_1) = 0 \end{cases} \qquad (7.46)$$

At x=L_2:

$$\begin{cases} w'_2(L_2) = 0 \\ V(L_2) = 0 \end{cases} \qquad (7.47)$$

At x=0:

$$\begin{cases} w_1(0) = w_2(0) \\ w'_1(0) = w'_2(0) \\ V_1(0) = V_2(0) \\ M_1(0) = M_2(0) \end{cases} \qquad (7.48)$$

Substituting the above boundary conditions into Eqn. (7.43) ~ Eqn. (7.45) and rearranging give:

$$\begin{cases} A_1 \cos k_1 L_1 - B_1 \sin k_1 L_1 = 0 \\ A_1 k_2 \sin k_2 L_2 - B_1 k_1 \cos k_2 L_2 = 0 \end{cases} \tag{7.49}$$

In order to get a non-zero solution for the above set of equations, the determinant as shown in the following equation shoud be equal to zero.

$$\begin{vmatrix} \cos k_1 L_1 & -\sin k_1 L_1 \\ k_2 \sin k_2 L_2 & -k_1 \cos k_2 L_2 \end{vmatrix} = 0 \tag{7.50}$$

Solving the above determinant gives:

$$\sqrt{m_P} \tan\left(\frac{n_P}{\sqrt{m_P}} kL\right) \tan(kL) = 1 \tag{7.51}$$

The effective length is calculated by solving the transcendental equation as shown in Eqn. (7.51). It is difficult to find this solution by hand-calculations since iterative methods such as the Newton method or bisection method are involved (Wang et al., 2004). In this study, commercial software MATLAB is used. Assuming kL has been solved from Eqn. (7.51). Then the coefficient for the effective length of column with pinned-pinned ends, relative to column length exposed to fire, is calculated as:

$$\mu_{P-P} = \frac{L_{eff}}{L_{ex}} = \frac{1}{2}\frac{\pi}{kL} \tag{7.52}$$

7.5.2   Column Fixed at Both Ends

The calculation diagram for column with fixed-fixed ends is shown in Figure 7.8. Half column is investigated due to symmetry. The FODEs of lateral displacement and

general solutions are the same as those of a column with "pinned-pinned" ends. The boundary conditions are different which are given in the following four equations.

At $x = -L_1$:

$$\begin{cases} w_1(-L_1) = 0 \\ w_1'(-L_1) = 0 \end{cases}$$ (7.53)

At $x = L_2$:

$$\begin{cases} V(L_2) = 0 \\ w_2'(L_2) = 0 \end{cases}$$ (7.54)

At $x = 0$:

$$\begin{cases} w_1(0) = w_2(0) \\ w_1'(0) = w_2'(0) \\ V_1(0) = V_2(0) \\ M_1(0) = M_2(0) \end{cases}$$ (7.55)

Substituting the above boundary conditions into Eqn. (7.43) ~ Eqn. (7.45) and rearranging give:

$$\begin{cases} A_1 \sin k_1 L_1 - B_1 \cos k_1 L_1 - D_1 = 0 \\ A_1 \cos k_1 L_1 + B_1 \sin k_1 L_1 = 0 \\ A_1 k_1 \cos k_2 L_2 - B_1 k_2 \sin k_2 L_2 = 0 \end{cases}$$ (7.56)

Solving the determinant from the above set of equations gives:

$$\sqrt{m_F} \tan(kL) + \tan\left(\frac{n_F}{\sqrt{m_F}} kL\right) = 0 \qquad (7.57)$$

Thus, the coefficient of effective length of column with fixed-fixed ends, relative to the column length exposed to fire, can be calculated as:

$$\mu_{F-F} = \frac{L_{eff}}{L_{ex}} = \frac{1}{2} \frac{\pi}{kL} \qquad (7.58)$$

7.5.3 Column Fixed at One End and Pinned at another End

The calculation diagram for a column with fixed-pinned ends is shown in Figure 7.9. Whole length of the column is investigated. The FODEs of lateral displacement is given as follows.

$$w_1^{''} + k_1^2 w_1 = 0 \quad k_1^2 = \frac{P}{(EI)_1} \qquad x = [0, L_1] \qquad (7.59)$$

$$w_2^{''} + k_2^2 w_2 = 0 \quad k_2^2 = \frac{P}{(EI)_2} \qquad x = [L_1, L_1 + L_2] \qquad (7.60)$$

$$w_3^{''} + k_3^2 w_3 = 0 \quad k_3^2 = \frac{P}{(EI)_3} \qquad x = [L_1 + L_2, L_1 + L_2 + L_3] \qquad (7.61)$$

The general solutions for above equations are:

$$w_1(x) = A_1 \sin k_1 x + B_1 \cos k_1 x + C_1 x + D_1 \qquad x = [0, L_1] \qquad (7.62)$$

$$w_2(x) = A_2 \sin k_2 x + B_2 \cos k_2 x + C_2 x + D_2 \qquad x = [L_1, L_1 + L_2] \qquad (7.63)$$

$$w_3(x) = A_3 \sin k_3 x + B_3 \cos k_3 x + C_3 x + D_3 \qquad x = [L_1 + L_2, L_1 + L_2 + L_3] \qquad (7.64)$$

The first, second and third differential of $w_1(x)$, $w_2(x)$ and $w_3(x)$ can be calclated similarly to those of a column with pinned-pinned ends.

The boundary conditions are given as follows:

At x=0:

$$\begin{cases} w_1(0) = 0 \\ M_1(0) = 0 \end{cases} \tag{7.65}$$

At x=L$_a$:

$$\begin{cases} w_3(L_a) = 0 \\ w'_3(L_a) = 0 \end{cases} \tag{7.66}$$

At x=L$_1$:

$$\begin{cases} w_1(L_1) - w_2(L_1) = 0 \\ w'_1(L_1) - w'_2(L_1) = 0 \\ V_1(L_1) - V_2(L_1) = 0 \\ M_1(L_1) - M_2(L_1) = 0 \end{cases} \tag{7.67}$$

At x=L$_{12}$:

$$\begin{cases} w_2(L_{12}) - w_3(L_{12}) = 0 \\ w'_2(L_{12}) - w'_3(L_{12}) = 0 \\ V_2(L_{12}) - V_3(L_{12}) = 0 \\ M_2(L_{12}) - M_3(L_{12}) = 0 \end{cases} \tag{7.68}$$

Substituting the boundary conditions into the general solutions and the first, second and third differential of $w_1(x)$, $w_2(x)$ and $w_3(x)$ give set of equations as follows:

$$
\begin{cases}
A_3 \sin k_3 L_a + B_3 \cos k_3 L_a + C_3 L_a + D_3 = 0 \\
A_3 k_3 \cos k_3 L_a - B_3 k_3 \sin k_3 L_a + C_3 = 0 \\
A_1 \sin k_1 L_1 - A_2 \sin k_2 L_1 - B_2 \cos k_2 L_1 - D_2 = 0 \\
A_2 \sin k_2 L_{12} - A_3 \sin k_3 L_{12} - B_3 \cos k_2 L_{12} - D_3 = 0 \\
A_1 k_1 \cos k_1 x - A_2 k_2 \cos k_2 x + B_2 k_2 \sin k_2 x = 0 \\
A_2 k_2 \cos k_2 L_{12} - A_3 k_3 \cos k_3 L_{12} + B_3 k_3 \sin k_3 L_{12} = 0 \\
A_1 \sin k_1 L_1 - A_2 \sin k_2 L_1 - B_2 \cos k_2 L_1 = 0 \\
A_2 \sin k_2 L_{12} - A_3 \sin k_3 L_{12} + B_2 \cos k_2 L_{12} - B_3 \cos k_3 L_{12} = 0
\end{cases}
\tag{7.69}
$$

In order to get the coefficient for the effective length, the following determinant from the above set of equations should be solved.

$$
\begin{vmatrix}
0 & \sin\left((1+n_1)kL\right) & P1 & 0 & P2 \\
\cos\left(\dfrac{n_1}{\sqrt{m_{FP}}}kL\right) & -\sqrt{m_{FP}}\cos(n_1 kL) & 0 & \sqrt{m_{FP}}\sin(n_1 kL) & 0 \\
0 & \sqrt{m_{FP}}\cos\left((1+n_1)kL\right) & -\cos\left(\dfrac{1+n_1}{\sqrt{m_{FP}}}kL\right) & 0 & \sin\left(\dfrac{1+n_1}{\sqrt{m_{FP}}}kL\right) \\
\sin\left(\dfrac{n_1}{\sqrt{m_{FP}}}kL\right) & -\sin(n_1 kL) & 0 & -\cos(n_1 kL) & 0 \\
0 & \sin\left((1+n_1)kL\right) & -\sin\left(\dfrac{1+n_1}{\sqrt{m_{FP}}}kL\right) & \cos\left((1+n_1)kL\right) & -\cos\left(\dfrac{1+n_1}{\sqrt{m_{FP}}}kL\right)
\end{vmatrix} = 0
$$

$$\tag{7.70}$$

where

$$\begin{cases} P1 = \sin\left(\dfrac{1+n_1+n_2}{\sqrt{m_{FP}}}kL\right) - \sin\left(\dfrac{1+n_1}{\sqrt{m_{FP}}}kL\right) - \dfrac{1+n_1+n_2}{\sqrt{m_{FP}}}kL\cos\left(\dfrac{1+n_1+n_2}{\sqrt{m_{FP}}}kL\right) \\[3mm] P2 = \cos\left(\dfrac{1+n_1+n_2}{\sqrt{m_{FP}}}kL\right) - \cos\left((1+n_1)kL\right) + \dfrac{1+n_1+n_2}{\sqrt{m_{FP}}}kL\sin\left(\dfrac{1+n_1+n_2}{\sqrt{m_{FP}}}kL\right) \end{cases}$$

(7.71)

Thus, the coefficient for the effective length of a column with fixed-pinned ends, relative to the column length exposed to fire, can be calculated as:

$$\mu_{F-P} = {L_{eff}}\Big/{L_{ex}} = \frac{\pi}{kL}$$

(7.72)

7.5.4   Comparisons

In the author's fire tests on CFST and CFDST columns, the overall column length was 3.81m. The height of the support at each end was 340mm. The exposed length to fire was 3m. The unexposed length at pinned end is a summation of the half height of support and half height of the unexposed part of the column. The unexposed length at the fixed end is only the half height of the unexposed part of the column. Overall, the ratios between unexposed length and exposed length, corresponding to the different end types, are given as follows.

$$\begin{bmatrix} n_P = 0.383 \\ n_F = 0.270 \\ n_1 = 0.192 \\ n_2 = 0.135 \end{bmatrix}$$

(7.73)

Substituting these ratios into the formulae for calculations of the effective lengths give the coefficients of effective lengths as shown in Figure 7.10. It should be noted that these coefficients are referrenced to the exposed length of column which was 3m in

the author's tests. It can be seen that the effective length decreases gradually with increasing m which represents deterioration of the stiffness of the exposed column length $(EI)_2$.

For the pinned-pinned column, the coefficient of effective length approaches 1.36. It indicates that the effective length approaches the full length of the column, including all exposed length and unexposed lengths. It also shows the non-conservative assumption by Lie and Chabot (1990) and Mao and Kodur (2011) where the effective length was only equal to the length of the exposed part of the column.

For the fixed-fixed column, the coefficient of the effective length approaches 0.5. It implies that the effective length is only half the exposed part. It is smaller than that from the assumption of Lie and Chabot (1990) and Mao and Kodur (2011) where the effective length was 2/3times the exposed part of the column.

For the fixed-pinned column, the coefficient of effective length is about 10% less than the average coefficients for the pinned-pinned and the fixed-fixed columns.

The length of the unexposed part of the column would be different in different researchers' fire tests. For the convenience of calculating the effective length of the column in a fire test, the coefficients of effective length, based on different ratios between unexposed length and exposed length, are given in charts as shown in Figure 7.11, Figure 7.12 and Figure 7.13. These ratios are mostly used in fire tests nowadays.

For verification of the proposed charts, it can be checked that, when m is equal to 1, the effective lengths are equal to those at room temperature. It can also be observed that the effective lengths approach 50%~60% of the exposed length of the column with increasing m for fixed-fixed columns. For pinned-pinned columns, the effective

lengths are not sensitive to increasing *m* and not much different from the whole column length including both the exposed and unexposed lengths.

7.6 Thermal Properties of Materials at High Temperatures

7.6.1 Steel

The thermal properties of steel, both NSS and HSS, at high temperatures were referred to EN 1993-1-2 (2005). They are given as follows.

Thermal conductivity:

$$\begin{cases} \lambda_a = 54 - 3.33 \times 10^{-2}\theta_a \quad W/m \cdot K & 20^o C < \theta < 800^o C \\ \lambda_a = 27.3 \quad W/m \cdot K & 800^o C \leq \theta \leq 1200^o C \end{cases} \tag{7.74}$$

Specific heat: $\tag{7.75}$

$$\begin{cases} c_a = 425 + 7.73 \times 10^{-1}\theta_a - 1.69 \times 10^{-3}\theta_a^2 + 2.22 \times 10^{-6}\theta_a^3 \quad J/kg \cdot K & 20^o C \leq \theta < 600^o C \\ c_a = 666 + \dfrac{13002}{738 - \theta_a} \quad J/kg \cdot K & 600^o C \leq \theta < 735^o C \\ c_a = 545 + \dfrac{17820}{\theta_a - 731} \quad J/k \cdot K & 735^o C \leq \theta < 900^o C \\ c_a = 650 \quad J/kg \cdot K & 900^o C \leq \theta \leq 1200^o C \end{cases}$$

The density of steel is 7850kg/m^3. It is assumed not to change with temperature.

7.6.2 Concrete

The thermal properties of concrete at high temperatures were referred to EN 1992-1-2 (2004). The lower limit of thermal conductivity is used for NSC; whereas the upper

limit is used for HSC and UHSC. For NSC and HSC, the moisture content is assumed to be 3%, whilst it is ignored for UHSC.

Lower limit of thermal conductivity:

$$\lambda_c = 1.36 - 0.136(\theta/100) + 0.0057(\theta/100)^2 \quad W/m \cdot K \quad 20^o C \le \theta \le 1200^o C \qquad (7.76)$$

Upper limit of thermal conductivity:

$$\lambda_c = 2 - 0.2451(\theta/100) + 0.0107(\theta/100)^2 \quad W/m \cdot K \quad 20^o C \le \theta \le 1200^o C \qquad (7.77)$$

Specific heat:

$$\begin{cases} c_c = 900 \quad J/kg \cdot K & 20^o C \le \theta \le 100^o C \\ c_c = 900 + (\theta - 100) \quad J/kg \cdot K & 100^o C < \theta \le 200^o C \\ c_c = 1000 + (\theta - 200)/2 \quad J/kg \cdot K & 200^o C < \theta \le 400^o C \\ c_c = 1100 \quad J/kg \cdot K & 400^o C < \theta \le 1200^o C \end{cases} \qquad (7.78)$$

Density:

$$\begin{cases} \rho_c(\theta) = \rho_c(20^o C) & 20^o C \le \theta \le 115^o C \\ \rho_c(\theta) = \rho_c(20^o C) \cdot [1 - 0.02(\theta - 115)/85] & 115^o C < \theta \le 200^o C \\ \rho_c(\theta) = \rho_c(20^o C) \cdot [0.98 - 0.03(\theta - 200)/200] & 200^o C < \theta \le 400^o C \\ \rho_c(\theta) = \rho_c(20^o C) \cdot [0.95 - 0.07(\theta - 400)/800] & 400^o C < \theta \le 1200^o C \end{cases} \qquad (7.79)$$

7.6.3 Fire Protection Material

In the author's fire tests, the fire protection material was a mixture of Portland cement (40%), perlite (25%), vermiculite (20%) and water (15%) by weight. The thermal

properties are assumed not to change with temperature. As provided by the supplier, the thermal conductivity is 0.116$W/m\cdot K$, specific heat is 1010$J/kg\cdot K$, and the density is 305kg/m^3. It is believed that these thermal properties are obtained through tests by the material supplier. Furthermore, these thermal properties have been validated by abundant numerical analyses from Han's researches (2004).

7.7 Validation of Proposed Methods

7.7.1 Validation with 66 Tests from the Literature

Besides the author's tests, the fire tests from Lie and Chabot (1992) and Romero et al. (2011) are used to validate FDM, SCM and MNIM for steel tubes infilled with NSC and HSC. There are in total 66 specimens.

In Lie and Chabot's tests (1992), the specimens were filled with both siliceous and calcareous aggregate concrete. The concrete strength varied from 23.8MPa to 58.3MPa. All the columns were tested with both ends fixed except for C-16 where both ends were simply supported and a load eccentricity of 34mm was applied. The column length was 3810mm and the exposed length to fire was 3200mm. Since the detailing of supports was not found in literature, the support height is ignored in the calculations. It should be noted that ignorance of the height of support will not affect the calculations for fixed-fixed columns. Overall, the ratio between the unexposed part and exposed part, as defined in Eqn. (6.73), is 0.27 for both pinned-pinned and fixed-fixed columns. The actual furnace temperatures during heating were given in their published paper. Hence, the calculations were done based on the actual furnace temperatures.

In Romero's tests (2011), the concrete strength varied from 28.55MPa to 71.14MPa. The type of aggregate was calcareous. The column length was 3180mm and the exposed length to fire was 2970mm. All columns were fixed at one end and simply supported at another end except for one column with both ends simply supported. The details of the support were given in their published paper. Overall, for pinned-pinned columns, the ratio between the unexposed and the exposed part is 0.121; for pinned-fixed columns, the ratio is 0.061 at the pinned end and 0.027 at the fixed end. The realistic furnace temperatures during heating were not provided in the published paper. Instead, the standard ISO-834 fire curve was used.

The details of CFST columns in Lie and Romero's tests are given in Table 7.2.

7.7.2   Validation of Finite Difference Method

The thermal properties of the concrete, steel and fire protection material presented in Section 7.6 are used to calculate the temperature profiles of CFST columns. The measured temperature profiles of the columns in Lie's tests were provided in their published paper. However, the temperature profiles were not given in Romero's tests. Thus, for validation of FDM, only Lie's and the author's tests are used.

The calculated and measured temperatures are plotted in Figure 7.14 and Figure 7.15 respectively for Lie's and the author's tests. The comparisons between measured and calculated temperatures show reasonable agreements, except for columns C-26, LC-2-6, LDC-2-3, and LC-3-2.

C-26 was taken from Lie's tests. According to the published paper (Lie and Chabot, 1992), the starting temperature of the furnace was around 130°C rather than ambient

temperature. This seems to indicate that the temperature inside furnace was not uniform. The non-uniform temperature might be attributed to the fact that the air and gas had not been properly mixed before it was ignited. As a result, the temperature of the thermocouple on furnace wall was higher than that around column. That is why the inner concrete temperature (point 5) was much lower than the furnace temperature at the starting of fire. However, after the temperature inside furnace became uniform after around 20 minutes, the measured concrete temperature at point 5 reached the calculated temperature.

LC-2-6, LDC-2-3 and LC-3-2 were taken from the author's tests. It is noticed that the fire resistance time of the three columns was around 25 minutes. The disagreement between the measured and calculated temperatures might be due to the unstable temperature distribution inside the furnace at the initial stages of heating.

Overall, the comparisons show that the thermal properties recommended in EN 1992-1-2 and EN 1993-1-2 are applicable respectively for UHSC and HSS.

7.7.3   Validation of SCM and MNIM

The mechanical properties in Table 7.1 are used for NSS, NSC and HSC; whereas those presented in Chapter 3 and Chapter 5 are respectively adopted for HSS and UHSC. The calculated fire resistance times are shown in Table 7.2 and Table 7.3. The standard deviation and average value are calculated based on the ratio between the calculated and experimental fire resistance time. It can be seen in Lie and Romero's tests that MNIM shows less scattered and are more conservative than SCM in terms of standard deviation and average value. But in the author's tests, MNIM presents

slightly higher average value but were less scattered than the SCM values. This could be related with the boundary conditions which are discussed below.

It is noted that the calculated values by SCM are generally higher than those by MNIM with regard to fixed-fixed columns. However in terms of pinned-pinned columns, the calculations by SCM are smaller. The calculations from SCM seem to be not consistent. The difference between SCM and MNIM is mainly due to the consideration of the second-order effect. For SCM, the second-order effect is taken into account by selecting a reasonable buckling curve. However, the buckling curve is normally summarised from thousands of columns subject to ambient temperature tests. The buckling curve does not take into account the deteriorated elastic moduli of steel and concrete under fire. As a result, the realistic lateral deformation of the column under fire is not captured. In terms of MNIM, the second-order effect is considered by multiplying the greatest first-order bending moment by a factor. This amplification factor takes into account the moment distribution within the column length and the deteriorated Euler buckling load of the column under fire. Thus, the MNIM is expected to give a more reasonable consideration of the second-order effect.

In the author's tests, the calculated fire resistance time from both SCM and MNIM are much higher than the experimental values for two columns which are labelled as LC-2-2 and LC-2-3. The reason is related to the boundary conditions. LC-2-2 and LC-2-3 were the second and third columns in the author's tests. At that time, the loading head had not been fully restrained by the anti-rotational plate as shown in Figure 6.15. Thus, the fixed end support could not be taken as rigid, and these two columns were failed prematurally.

For better illustration, the calculated and measured fire resistance time are plotted in Figure 7.16 and Figure 7.17 in terms of SCM and MNIM for all test results. The comparisons show that 61% of the calculations by MNIM are smaller than the test values, whereas only 45% in terms of SCM. For MNIM, the standard deviation and average value based on the ratio between calculated and experimental values are 0.218 and 0.985. For SCM, they are 0.246 and 1.077 respectively. Thus, MNIM shows more conservative and less scattered calculated values of the fire resistance time than SCM.

The validation indicates that MNIM can be proposed to design CFST columns under combined axial load and bending moment under fire. It is also applicable for fire resistant design of CFST columns with UHSC and HSS and thus can be extended to EN 1994-1-2 where only SCM is recommended.

For reference, the M-N interaction curves from four typical CFST columns in the author's tests are shown in Figure 7.18, Figure 7.19, Figure 7.20 and Figure 7.21. It is noted that the capacities of the bending moment and axial load are not monolithically reduced with fire temperature. They are improved after being exposed to the fire for some time, but finally reduced. This is due to the fact that the compressive strength and elastic modulus of UHSC recovered part of their deteriorations at the temperature range of $100^{o}C \sim 300^{o}C$. This phenomenon was discussed in Chapter 5. The applied axial load remains the same but the external bending moment increases with increasing temperature due to second-order effects. The column failed when the applied external loads exceeded the capacities of bending moment and axial force.

7.8 Parametric Analysis

7.8.1 Introduction

Han (2004) and Lu et al. (2010b) have done comprehensive parametric investigations on the fire performance of CFST columns with single-tube or double-tube based on the finite element method (FEM). The parameters included perimeter of section, size ratio of section, steel contribution ratio, slenderness ratio, eccentricity, yield strength of steel, compressive strength of concrete and thickness of fire protection. These investigations showed that the size ratio of section, steel contribution ratio, strengths of steel and concrete and eccentricity had little effect, but the perimeter of section, slenderness ratio and thickness of fire protection exhibited significant influences.

In this section, parametric analysis on the fire resistance time of CFST columns with UHSC and HSS is presented based on the validated MNIM. This analysis will only focus on the effects of strengths of steel and concrete since the other parameters have been investigated by Han and Lu. The specimens for parametric analysis are shown in Table 7.4 and Table 7.5. All the columns have a height of 3m and are pinned-pinned ends. The exposed length to fire is also 3m which is thus the effective length of column. The thickness of the fire protection material is 10mm for all columns. Eccentricity of load is not considered. The load level is 0.65 which is recommended in EN 1994-1-2 (2005). The thermal and mechanical properties are the same as those used in validations. Standard ISO-834 fire curve is used. Small and large cross-sections are investigated which are:

	Small cross-sections	Large cross-sections
Circular:	C219.1x16	C600x30

Double-Circular:	C219.1x16/C114.3x6.3	C600x30/C300x15
Square:	S200x12	S600x30
Double-Square:	DS200x12/DS100x8	DS600x30/DS300x15

Section factor is defined herein as the ratio between the exposed surface area and the volume of the CFST column. It is used to measure the rate of temperature increase in a column. The higher the section factor, the faster the section heats up. For CFST column with a uniform cross-sectional profile within its length, the section factor can be calculated as the ratio between the perimeter and the area of cross-section. The section factors for the investigated columns are given in Table 7.4 and Table 7.5.

7.8.2 Effects of Concrete Strength

The effect of strength of concrete is plotted in Figure 7.22. It can be seen that the effect of concrete strength on the fire resistance time of CFST columns is minor, except that the fire resistance time of columns with UHSC is slightly larger than that of columns with NSC and HSC. This is because the strength and elastic modulus of UHSC are reduced slower than those of NSC and HSC at high temperatures, which has been discussed in Chapter 5. The difference between the fire resistance time of columns with UHSC and columns with NSC and HSC is in the range of 2.4%~16.9%.

7.8.3 Effects of Steel Strength

The effect of strength of steel is plotted in Figure 7.23. Generally, the fire resistance time decreases with increasing yield strength of steel. The effect of steel strength is minor for CFST columns with steel grade from S275 to S460. However, the fire resistance time of columns with HSS is much smaller than that of columns with NSS.

This is attributed to the fact that the yield strength and elastic modulus of HSS are reduced much faster than those of NSS at high temperatures, especially when the temperature exceeds the tempering temperature of HSS. This has been discussed in Chapter 3. The difference between the fire resistance time of columns with HSS and columns with NSS is in the range of 11.3%~25.7%.

7.8.4   Comparisons between Circular and Square Columns

In terms of single-tube columns, the fire resistance time of circular columns is larger than that of square columns for small cross-sections. This is because the section factors of circular columns are smaller than those of square columns. As a result, circular columns exhibit slower heating up.

Herein the concept of unit fire resistance time per section factor (UFRT) is introduced as $T_{fr} \cdot \left(H_p / A \right)$. T_{fr} is the fire resistance time with unit of minute; whereas H_p/A is the section factor with unit of m^{-1}. H_p and A are the perimeter and cross-sectional area. Assuming the ratio between UFRTs of circular and square columns is formulated as:

$$k_{fs} = \frac{\left(T_{fr} \cdot \left(H_p / A \right) \right)_{circular}}{\left(T_{fr} \cdot \left(H_p / A \right) \right)_{square}} \tag{7.80}$$

The ratios K_{fs} for small cross-section single-tube columns are shown in Figure 7.24. It can be seen that the UFRTs are almost the same for circular and square columns. This indicates that the circular and square CFST columns would have comparable fire resistance time if their section factors are equal. This is justified by columns with large cross-sections.

In terms of double-tube columns, the ratios K_{fs} for CFST columns with small cross-sections are shown in Figure 7.25. It can be seen that the UFRTs of circular columns are slightly larger than those of square columns. This implies that the circular columns would exhibit better fire performance than the square columns even they have equal section factors. This is also the case for columns with large cross-sections.

7.8.5 Comparisons between Columns with Single-Tube and Double-Tube

It is obtained from Figure 7.22 and Figure 7.23 that, in terms of small cross-sections, single-tube columns exhibit longer fire resistance time than double-tube columns. However, when it comes to large cross-sections, double-tube columns exhibit longer fire resistance time than single-tube columns, except for square double-tube columns with various steel grades. Thus, it is difficult to determine superiority between single-tube columns and double-tube columns under fire situations. This is because there is a trade-off between the loss from the section factor and the benefit from having an inner tube. Comparing with single-tube columns, the double-tube columns have larger section factors, thus faster heating up. On other hand, the double-tube columns have smaller non-dimensional slenderness ratio which is shown in Eqn. (7.34). This is because the non-dimensional slenderness ratio is in first-order direct proportion to the diameter of the inner tube but in second-order inverse proportion to the diameter of inner tube. The non-dimensional slenderness ratio decreases with increasing diameter of the inner tube (for single-tube column, the diameter of inner tube can be takes as zero). As a result, the buckling resistance is improved.

7.9 Summary

This chapter presents the fire resistance design methods for CFST columns under standard fires. The first method is the simple calculation model (SCM) in EN 1994-1-2. This method is not applicable to UHSC and HSS when the bending moment is involved. The second method is M-N interaction model (MNIM) which is proposed to design CFST columns subject to combined bending moment and axial force, and it can be extended to CFST columns with UHSC and HSS.

In using SCM and MNIM, the first step is to calculate the temperature profiles of the columns under fire. There is no method recommended for the temperature calculation in Eurocodes. In this chapter, the finite difference method (FDM) is adopted and implemented in commercial software MATLAB. The FDM is validated by comparing the calculated temperatures with the measured temperatures from tests by Lie and Chabot (1992) and the author. The comparisons show reasonable agreement except for some columns which have been discussed.

In order to predict the fire resistance time by SCM and MNIM, the effective length of partially heated column specimens has been derived based on the 4th-order differential equation of lateral displacement of a column in a standard fire test. The effective length is related to the boundary conditions of the column and the length ratio between the fire exposed and unexposed parts of column when subjected to fire. In the author's tests, there are columns with pinned-pinned ends, fixed-fixed ends and fixed-pinned ends. For columns with pinned-pinned ends, the effective length approaches the full length of the column including both the exposed and unexposed parts as the fire exposure time increases. For columns with fixed-fixed ends, the effective length approaches half the length of the exposed part of the column. For

columns with fixed-pinned ends, the effective length is about 10% less than the average effective length of the pinned-pinned and fixed-fixed columns. The derived effective lengths are compared with those by the empirical method. The comparisons show that the empirical method under-predicts the effective length of pinned-pinned columns, but over-predicts the effective length of fixed-fixed columns. For the application of the derived effective lengths of columns under fire tests, design charts are made based on the different length ratios between the unexposed and the exposed parts.

Both SCM and MNIM are validated by tests in literature and the author's tests. The comparisons show that MNIM exhibits more conservative and less scattered calculated values than SCM. Strength predictions by SCM are generally higher than those by MNIM for fixed-fixed columns, but smaller for pinned-pinned columns. This is because MNIM considers the direct second-order effect of column under fire and it is more suitable for columns with a higher slenderness ratio. It is proposed that MNIM to be used to design CFST columns with UHSC and HSS, and it can be included in EN 1994-1-2.

Parametric analyses on fire resistance time of CFST columns have been done based on the validated MNIM. It focuses on the effects of strengths of steel and concrete. It shows that the fire resistance time of columns with UHSC is slightly higher than that of columns with NSC and HSC. This is because the strength and elastic modulus of UHSC are reduced slower than those of NSC and HSC at high temperatures. The fire resistance time of columns with HSS is smaller than that of columns with NSS. This is attributed to the fact that the yield strength and elastic modulus of HSS are reduced much faster than those of NSS at high temperatures

Circular and square CFST columns may have the same fire resistance time in terms of equal section factors and single-tube if other parameters such as load level, effective length etc remain the same. For columns with double-tube, circular columns have slightly longer fire resistance time than square columns even when they have equal section factors.

It is difficult to determine the superiority between single-tube columns and double-tube columns under fire situations. There is a trade-off between the loss arising from section factor and the benefit from having inner tube. Larger section factor makes the double-tube columns exhibit shorter fire resistance time. However, the double-tube columns have smaller non-dimensional slenderness ratio which results in higher buckling capacity and thus longer fire resistance time.

Table 7.1: Reduction factors of mechanical properties of steel and concrete at elevated temperature given in EN 1992-1-2 and EN 1993-1-2

Temp. (^{o}C)	Steel		Concrete					
	Elastic modulus $E_{a,\theta}$	Yield strength $f_{ay,\theta}$	Peak Strain $\varepsilon_{c1,\theta}$	Compressive Strength, $f_{c,\theta}$				
				<C55		C55~C60	C70~C80	C90
				siliceous	calcareous			
20	1	1	0.0025	1	1	1	1	1
100	1	1	0.004	1	1	0.95	0.75	0.75
200	0.9	1	0.0055	0.95	0.97	0.9	0.75	0.7
300	0.8	1	0.007	0.85	0.91	0.85	0.75	0.65
400	0.7	1	0.01	0.75	0.85	0.75	0.75	0.45
500	0.6	0.78	0.015	0.6	0.74	0.6	0.6	0.3
600	0.31	0.47	0.025	0.45	0.6	0.45	0.45	0.25
700	0.13	0.23	0.025	0.3	0.43	0.3	0.3	0.2
800	0.09	0.11	0.025	0.15	0.27	0.15	0.15	0.15
900	0.0675	0.06	0.025	0.08	0.15	0.08	0.08	0.08
1000	0.045	0.04	0.025	0.04	0.06	0.04	0.04	0.04

Notes: $\varepsilon_{c1,\theta}$ is the strain of concrete corresponding to $f_{c,\theta}$;

Table 7.2: Details of columns in Lie and Chabot (1992) and Romero's (2011) tests and comparison of test and predicted results

Specimen	Sizes D(mm)x t(mm)	f_y (MPa)	f_c (MPa)	BC.	F_{ap} (kN)	Fire resistance time (minute)				
						Test (T_t)	SCM		MNIM	
							T_{fr}	T_{fr}/T_t	T_{fr}	T_{fr}/T_t
C-02	141.3x6.55	350	33.1	F-F	110	55	80	1.45	65	1.18
C-04	141.3x6.55	350	31	F-F	131	57	68	1.19	57	1.00
C-05	168.3x4.78	350	32.7	F-F	150	76	101	1.33	83	1.09
C-06	168.3x4.78	350	32.7	P-P	150	60	30	0.50	29	0.48
C-08	168.3x4.78	350	35.5	F-F	218	56	66	1.18	53	0.95
C-09	168.3x6.35	350	35.4	F-F	150	81	91	1.12	78	0.96
C-11	219.1x4.78	350	31	F-F.	492	80	68	0.85	53	0.66
C-13	219.1x4.78	350	32.3	F-F	384	102	98	0.96	81	0.79
C-16*	219.1x8.18	350	31.9	P-P	525	33	-	-	28	0.85
C-17	219.1x8.18	350	31.7	F-F	525	82	79	0.96	64	0.78
C-20	273.1x5.56	350	28.6	F-F	574	112	122	1.09	103	0.92
C-21	273.1x5.56	350	29	F-F	525	133	135	1.02	119	0.89
C-22	273.1x5.56	350	27.2	F-F	1000	70	58	0.83	50	0.71
C-23	273.1x12.7	350	27.4	F-F	525	143	145	1.01	130	0.91
C-25	323.9x6.35	350	27.6	F-F	699	145	190	1.31	171	1.18
C-26	323.9x6.35	350	24.3	F-F	1050	93	99	1.06	83	0.89
C-28	355.6x6.35	350	23.8	F-F	1050	111	139	1.25	116	1.05
C-29	355.6x12.7	350	25.4	F-F	1050	170	167	0.98	141	0.83
C-31	141.3x6.55	350	30.2	F-F	80	82	112	1.37	90	1.10
C-32	141.3x6.55	350	34.8	F-F	143	64	74	1.16	56	0.88
C-34	219.1x4.78	350	35.4	F-F	500	111	111	1.00	88	0.79
C-35	219.1x4.78	350	42.7	F-F	560	108	101	0.94	83	0.77
C-40	273.1x6.35	350	46.5	F-F	1050	106	114	1.08	97	0.92
C-41	273.1x6.35	350	50.7	F-F	1050	76	98	1.29	83	1.09
C-42	273.1x6.35	350	55.4	F-F	1050	90	111	1.23	96	1.07
C-44	273.1x6.35	350	38.7	F-F	715	178	167	0.94	149	0.84
C-45	273.1x6.35	350	38.2	F-F	712	144	155	1.08	138	0.96
C-50	323.9x6.35	300	42.4	F-F	820	234	245	1.05	236	1.01
C-51	323.9x6.35	300	47.5	F-F	1180	114	162	1.42	150	1.32
C-53	355.6x6.35	300	42.4	F-F	1335	149	188	1.26	172	1.15
C-55	355.6x12.7	300	40.7	F-F	965	274	278	1.01	265	0.97
C-57	406.4x6.35	300	44	F-F	1400	294	280	0.95	277	0.94
C-59	406.4x12.7	300	37.4	F-F	1900	125	184	1.47	160	1.28
C-60	406.4x12.7	300	45.1	F-F	1900	152	228	1.50	208	1.37
C30-0-40	159x6	337.8	30.10	P-P	338	18	20	1.11	20	1.11
C30-0-20	159x6	337.8	35.75	F-P	198	42	44	1.05	39	0.93
C30-0-40	159x6	337.8	28.55	F-P	396	25	24	0.96	23	0.92
C30-0-60	159x6	337.8	34.05	F-P	594	14	19	1.36	19	1.36
C80-0-20	159x6	341.4	71.14	F-P	335	38	35	0.92	32	0.84
SQ-01	152.4x6.35	350	58.3	F-F	376	66	50	0.76	42	0.64
SQ-02	152.4x6.35	350	46.5	F-F	286	86	91	1.06	70	0.81
SQ-07	177.8x6.35	350	57	F-F	549	80	71	0.89	67	0.84
SQ-17	254x6.35	350	58.3	F-F	1096	62	109	1.76	92	1.48
SQ-20	254x6.35	350	46.5	F-F	931	97	117	1.21	99	1.02
							Standard deviation	0.229		0.204
							Average	1.114		0.967

Notes:

1, "*" load eccentricity=34mm;

2, "C" circular column; "S" square column;

3; "f_y" yield strength of steel; "f_c" cylindrical compressive strength of concrete; "BC." Boundary condition; "F_{ap}" applied load in fire test; "T_t" tested fire resistant time; "T_{fr}" predicted fire resistant time;

Table 7.3: Comparisons between Author's tested with calculated fire resistance time

Specimen	Tested fire resistance time T_t (min.)	Calculated fire resistance time T_{fr} (min.)			
		SCM		MNIM	
		Time T_{fr}	Ratio T_{fr}/T_t	Time T_{fr}	Ratio T_{fr}/T_t
LC-2-1	96	90.0	0.94	76	0.79
LC-2-2	84	119	1.42	106	1.26
LC-2-3	71	129	1.82	132	1.86
LC-2-4	122	97	0.80	110	0.90
LC-2-5	175	149	0.85	158	0.90
LC-2-6	24	-	-	27	1.13
LC-3-1	192	164	0.85	180	0.94
LC-3-2	18	-	-	15	0.83
LC-4-1	175	162	0.93	176	1.01
LDC-2-1	59	53	0.90	53	0.90
LDC-2-2	134	129	0.96	144	1.07
LDC-2-3	25	-	-	27	1.08
LSH-2-1	42	33	0.79	32	0.76
LSH-2-2	118	141	1.19	140	1.19
LSH-2-3	135	142	1.05	152	1.13
LSH-2-4	104	85	0.82	96	0.92
LSH-2-5	156	118	0.76	127	0.81
LSH-2-6	70	-	-	66	0.94
LS-2-1	79	73	0.92	105	1.33
LDSH-2-1	47	44	0.94	36	0.77
LDSH-2-2	150	120	0.80	130	0.87
LDSH-2-3	76	-	-	82	1.08
Standard deviation			0.271		0.246
Average			0.984		1.021

Table 7.4: Specimens designed for parametric analysis-circular columns

Specimen	Sizes D(mm)x t(mm)	f_y (MPa)	f_c (MPa)	$N_{f,20}$ (kN)	$N_{f,fire}$ (kN)	Section Factor (m^{-1})	T_{fr} (mins.)
C1	219.1x16	785	30	6936	4508	18.26	120
C2			55	7333	4766		121
C3			70	7562	4915		125
C4			90	7851	5103		121
C5			160	8835	5743		128
C6		275	160	6071	3946		149
C7		355		6602	4291		147
C8		460		7243	4708		146
C9	600x30	785	30	48049	31232	6.67	240
C10			55	53493	34770		246
C11			70	56750	36888		255
C12			90	61070	39696		244
C13			160	76161	49505		277
C14		275	160	50498	32824		373
C15		355		54572	35472		351
C16		460		59890	38929		336
DC1	219.1x16 114.3x6.3	785	30	7735	5028	23.27	113
DC2			55	7976	5184		114
DC3			70	8119	5277		116
DC4			90	8298	5394		113
DC5			160	8949	5817		120
DC6		275	160	5354	3480		148
DC7		355		6055	3936		145
DC8		460		6899	4484		142
DC9	600x30 300x15	785	30	56057	36437	8.36	254
DC10			55	59813	38878		259
DC11			70	62063	40341		275
DC12			90	65050	42283		261
DC13			160	75526	49092		297
DC14		275	160	43261	28120		384
DC15		355		48398	31459		370
DC16		460		55096	35812		357

Notes:

1, "C" single tube circular column; "DC" double tube circular column;

2, "$N_{f,20}$" axial buckling capacity at room temperature; "$N_{f,fire}$" applied load in fire;

Table 7.5: Specimens designed for parametric analysis-square columns

Specimen	Sizes D(mm)x t(mm)	f_y (MPa)	f_c (MPa)	$N_{f,20}$ (kN)	$N_{f,fire}$ (kN)	Section Factor (m^{-1})	T_{fr} (mins.)
S1	200x12	785	30	6535	4248	20	110
S2			55	7029	4569		110
S3			70	7315	4755		113
S4			90	7676	4989		109
S5			160	8902	5786		119
S6		275	160	6302	4096		140
S7		355		6782	4408		139
S8		460		7371	4791		138
S9	600x30	785	30	61731	40125	6.67	240
S10			55	68762	44695		246
S11			70	72970	47431		255
S12			90	78557	51062		245
S13			160	98090	63759		275
S14		275	160	64852	42154		364
S15		355		70115	45575		345
S16		460		76993	50045		330
DS1	200x12 100x8	785	30	7788	5062	24.28	104
DS2			55	8101	5266		104
DS3			70	8286	5386		106
DS4			90	8519	5537		103
DS5			160	9361	6085		110
DS6		275	160	5784	3760		126
DS7		355		6465	4202		125
DS8		460		7293	4740		124
DS9	600x30 300x15	785	30	72073	46847	8.36	249
DS10			55	76926	50002		252
DS11			70	79834	51892		263
DS12			90	83697	54403		252
DS13			160	97244	63209		279
DS14		275	160	55508	36080		349
DS15		355		62133	40386		339
DS16		460		70783	46009		323

Notes:

1, "S" single tube square column; "DS" double tube square column;
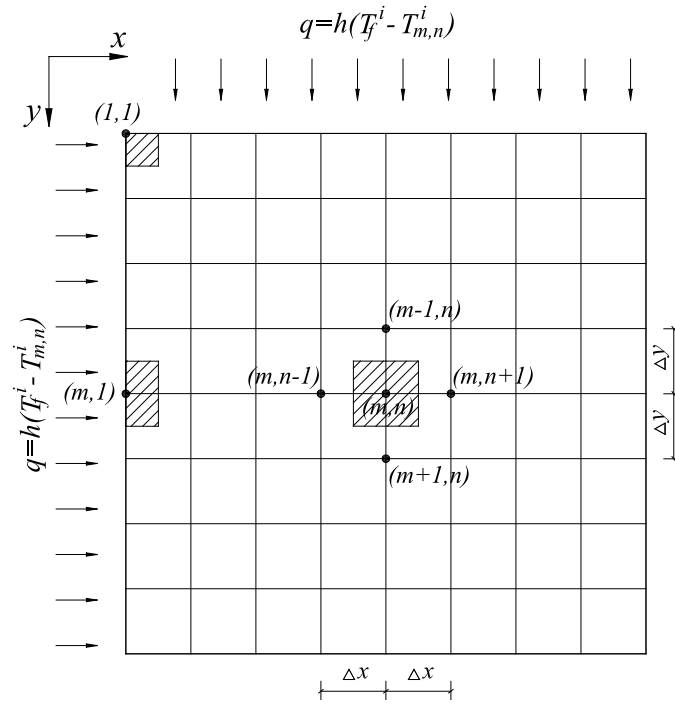
Figure 7.1: Discretization of 2-D heat transfer
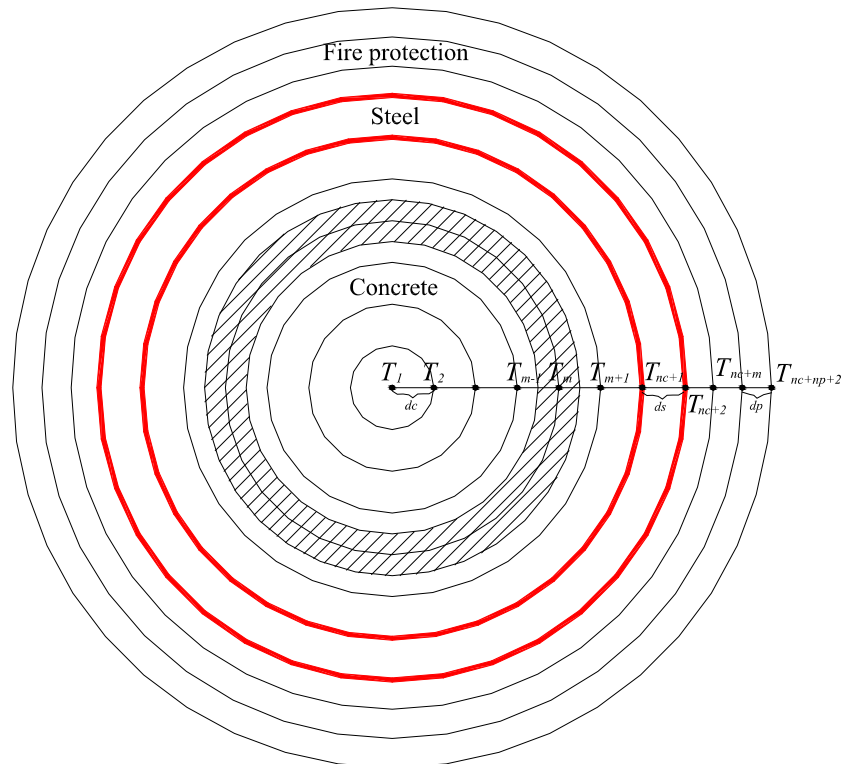
Figure 7.2: Discretization of circular CFST column
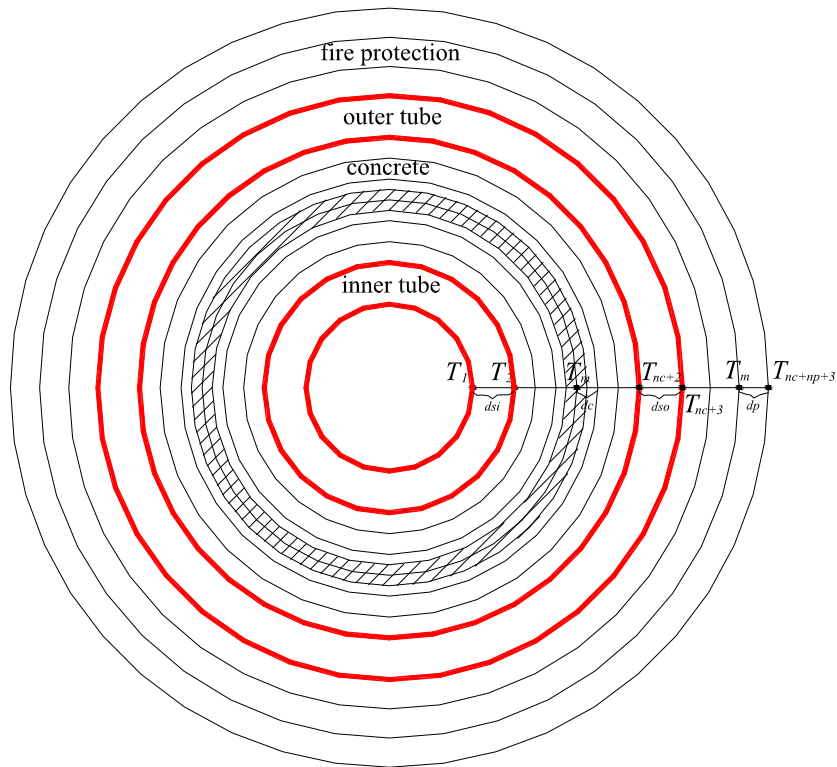
Figure 7.3: Discretization of circular CFDST column
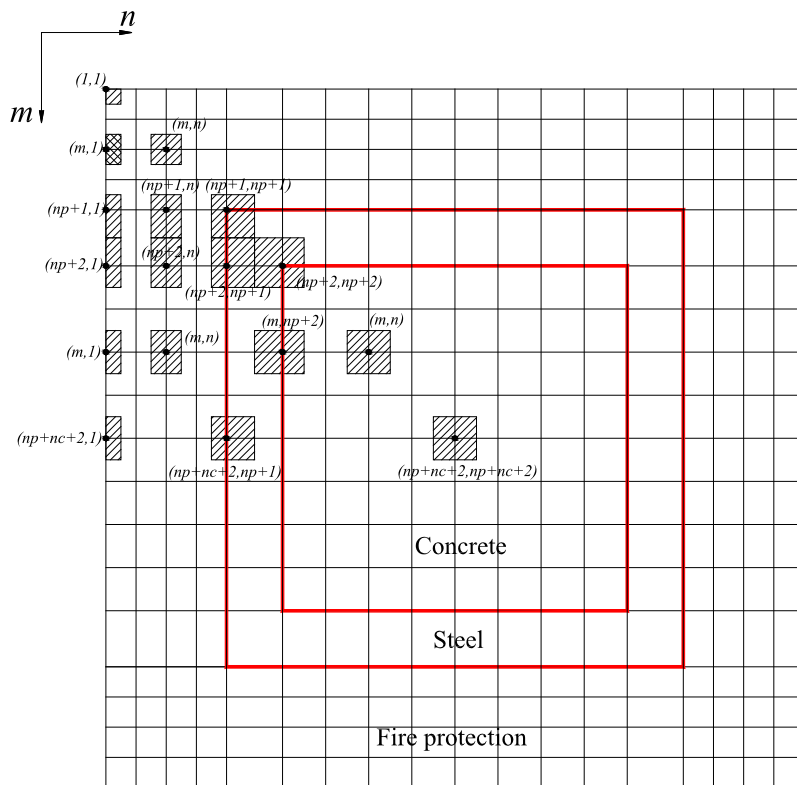
Figure 7.4: Discretization of square CFST column
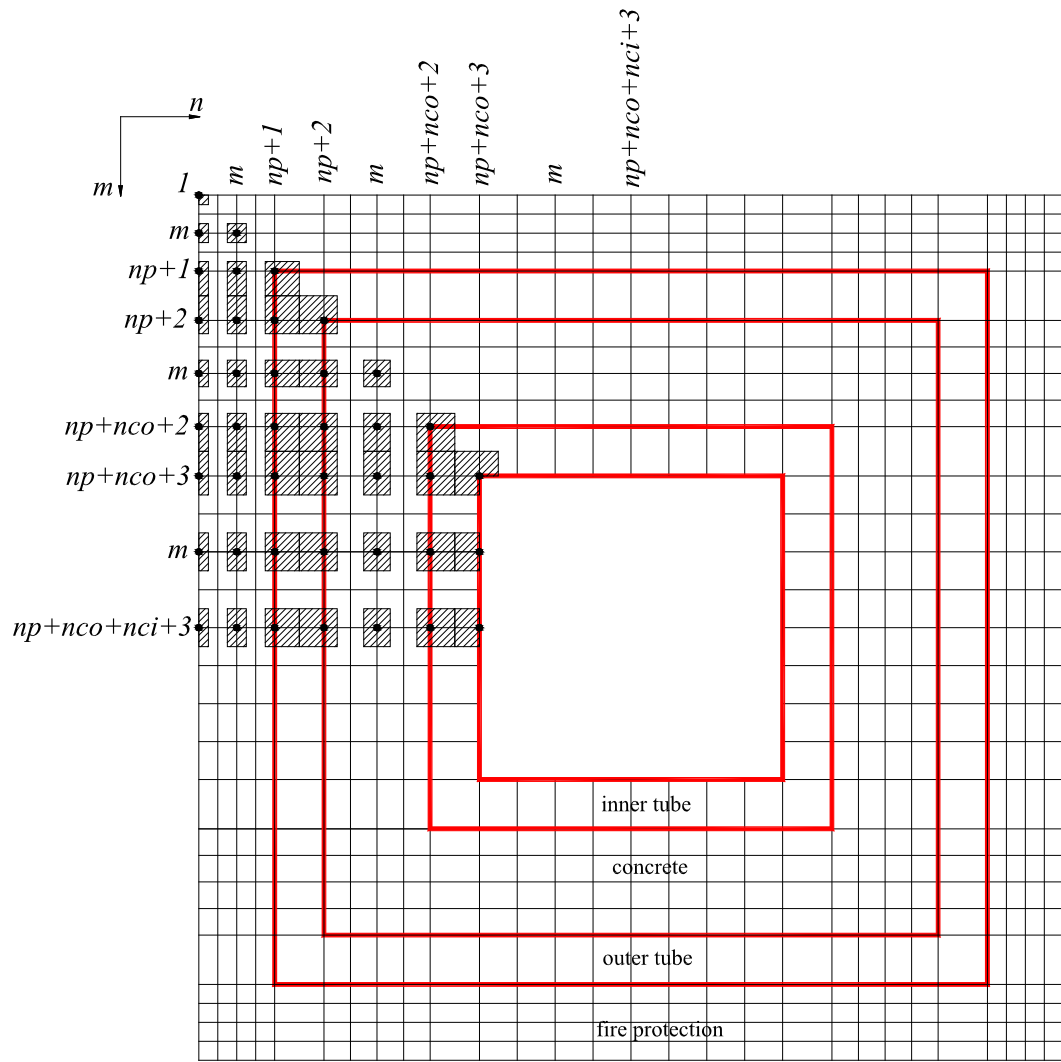
Figure 7.5: Discretization of square CFDST column
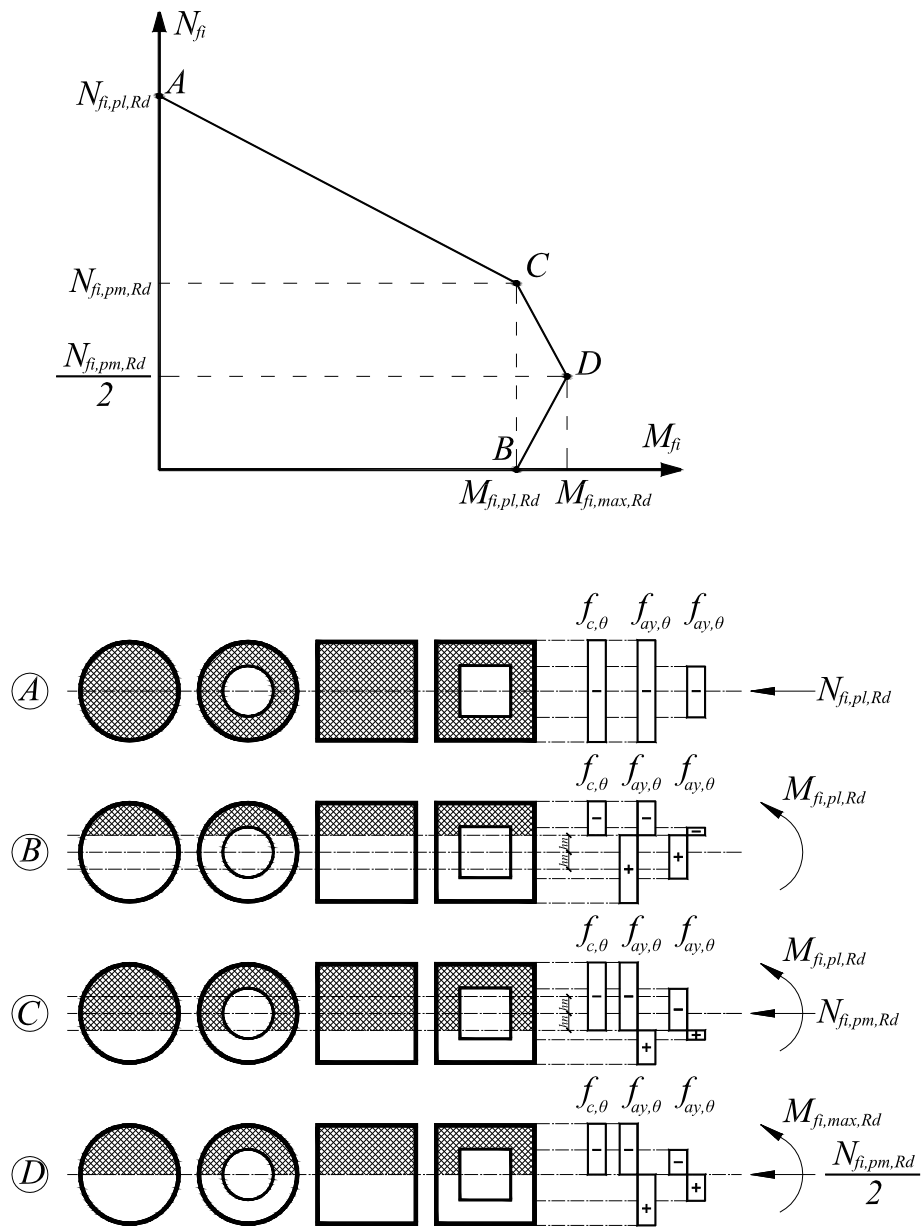
Figure 7.6: M-N interaction curve and corresponding stress distributions in fire

situation
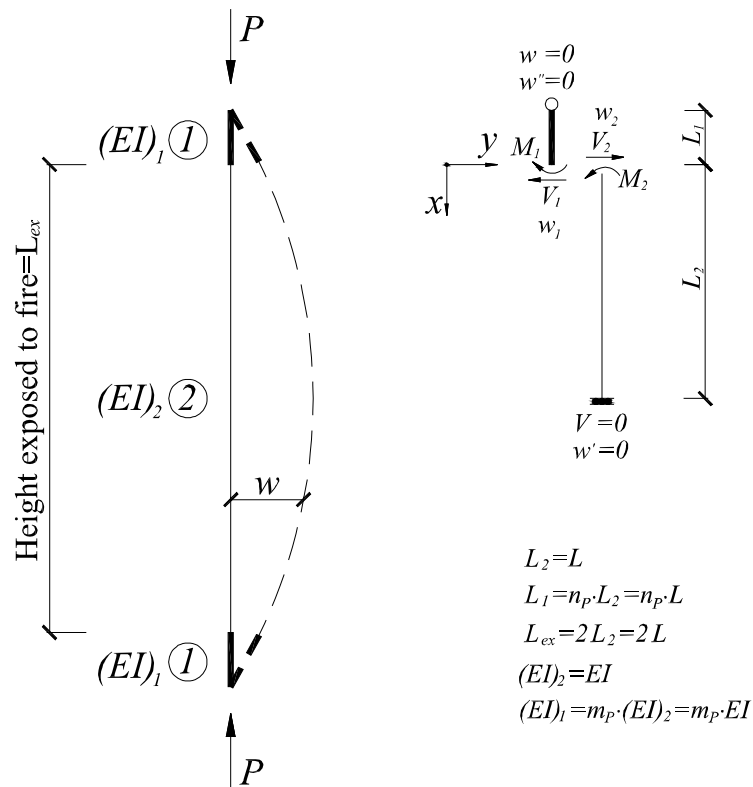
Figure 7.7: Diagram for calculation of effective length of pinned-pinned column
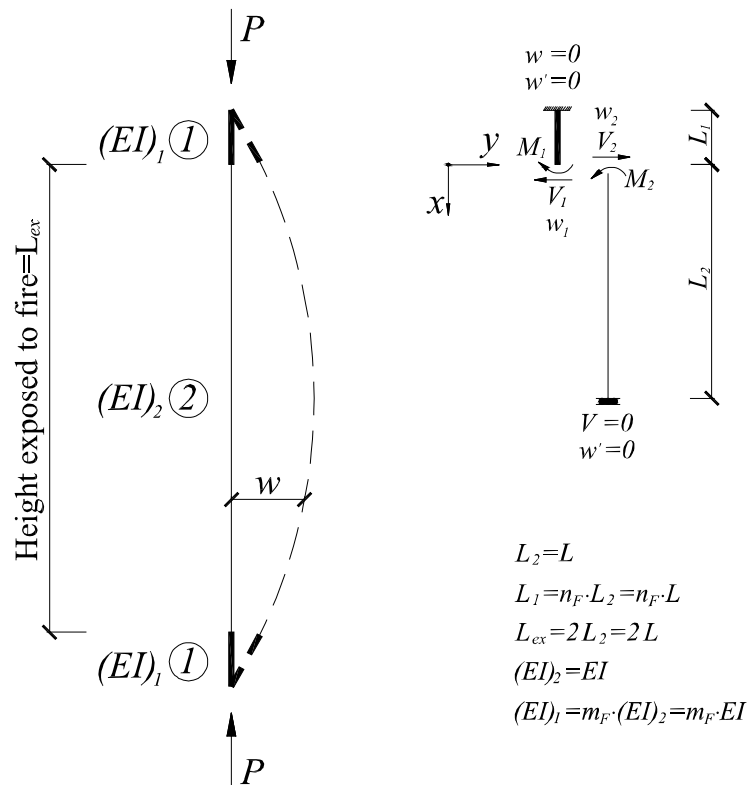
Figure 7.8: Diagram for calculation of effective length of fixed-fixed column

$L_2=L$
$L_1=n_1L_2=n_1L$
$L_3=n_2L_2=n_2L$
$L_{12}=L_1+L_2=(1+n_1)L$
$L_a=L_1+L_2+L_3=(1+n_1+n_2)L$
$(EI)_2=EI$
$(EI)_1=m_{FP}\cdot(EI)_2=m_{FP}\cdot EI$
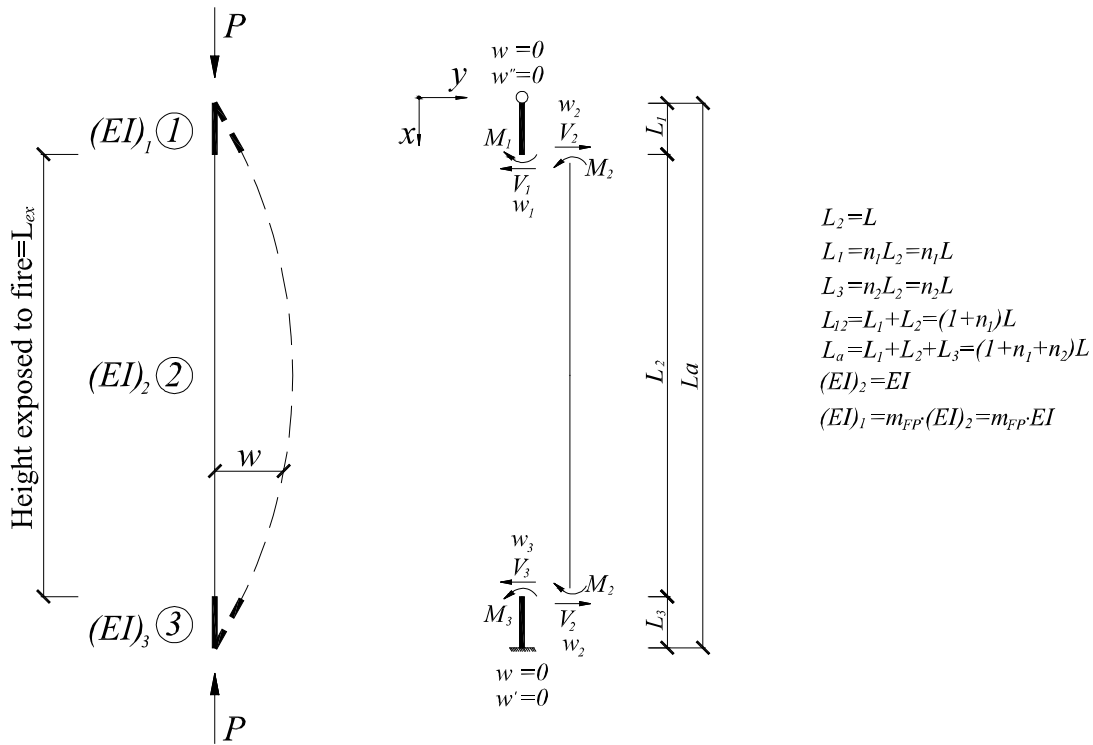
Figure 7.9: Diagram for calculation of effective length of fixed-pinned column
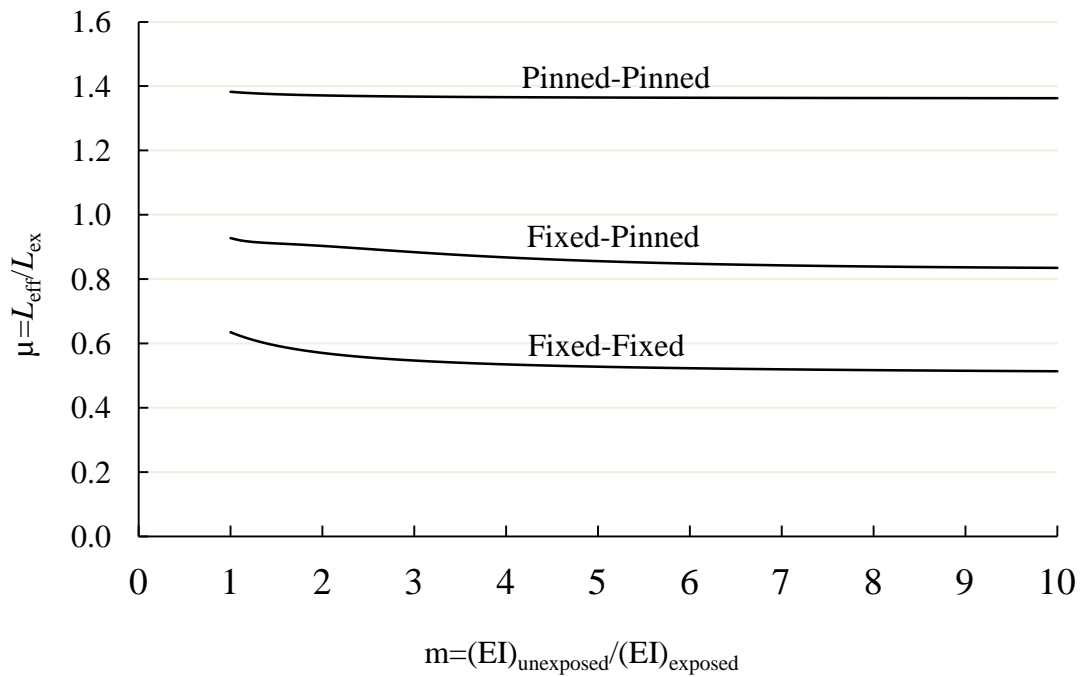
Figure 7.10: Coefficients of effective lengths of columns in author's fire tests
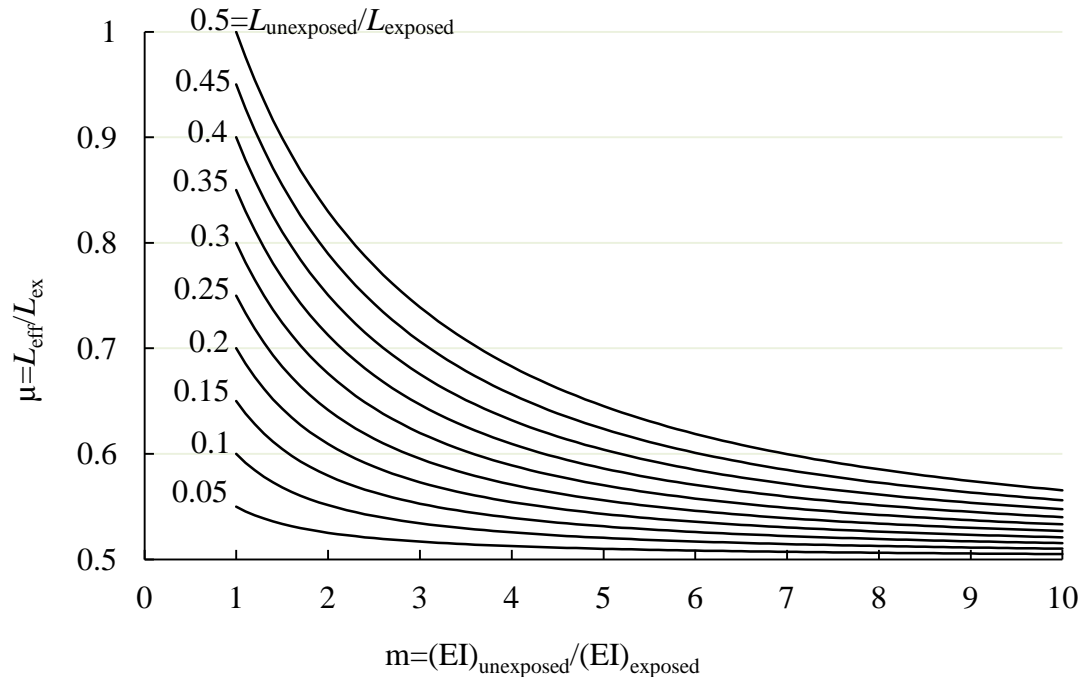
Figure 7.11: Coefficients of effective lengths of fixed-fixed columns under fire
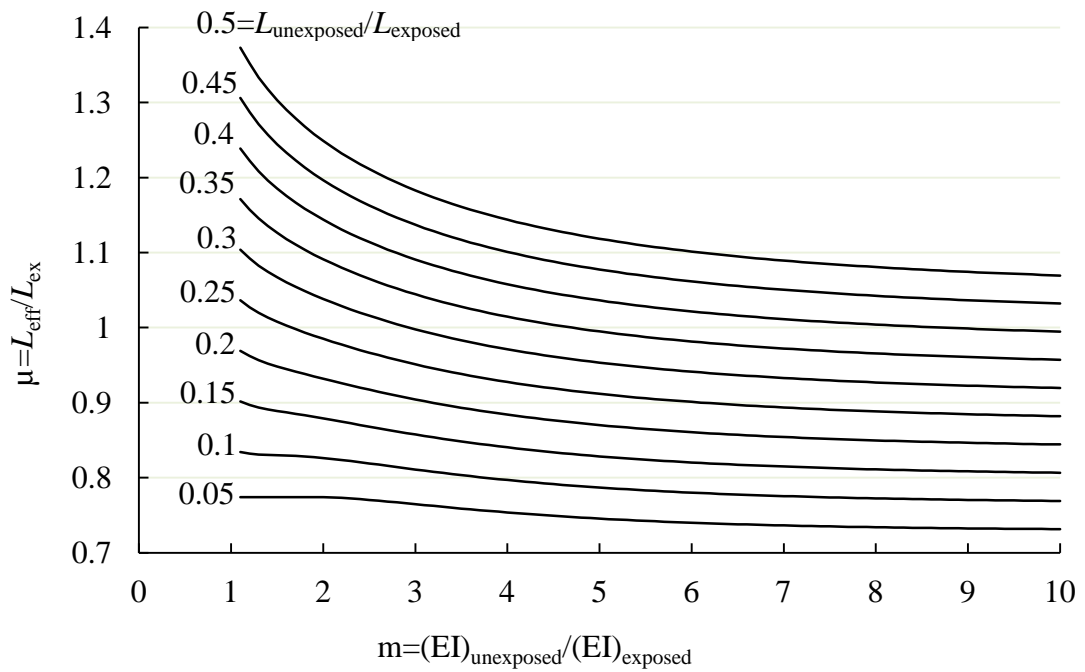
Figure 7.12: Coefficients of effective lengths of fixed-pinned columns under fire
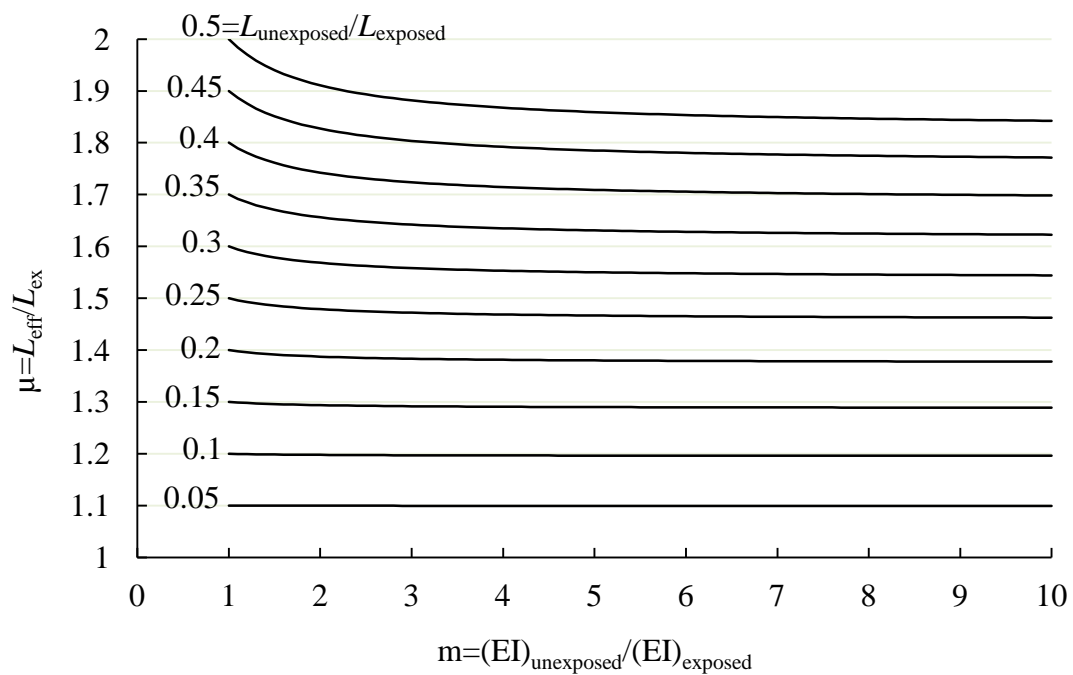
Figure 7.13: Coefficients of effective lengths of pinned-pinned columns under fire
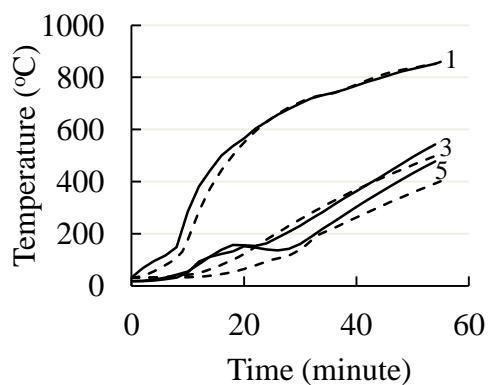
(a)C-02
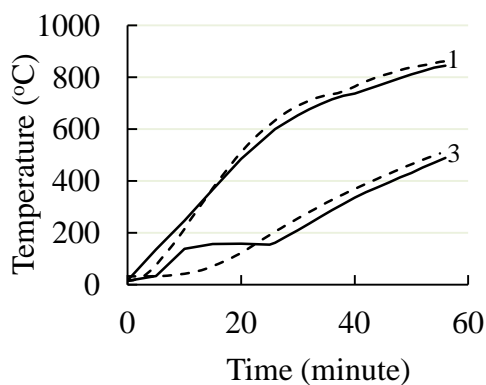
(b)C-04
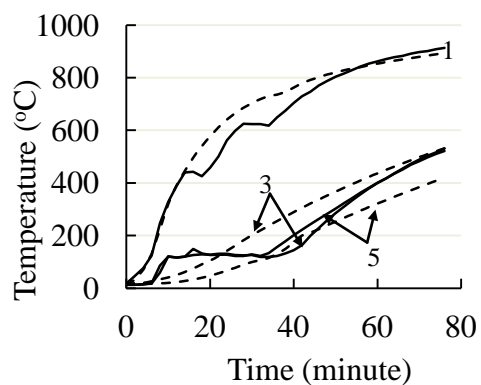
(a)C-05
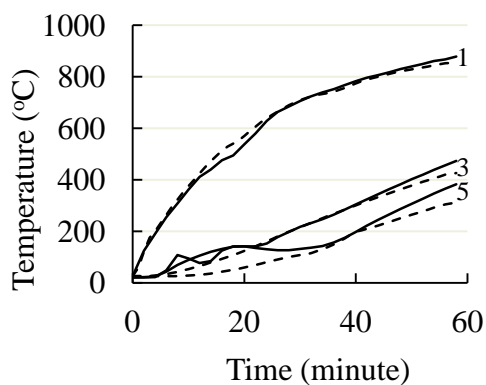
(b)C-06
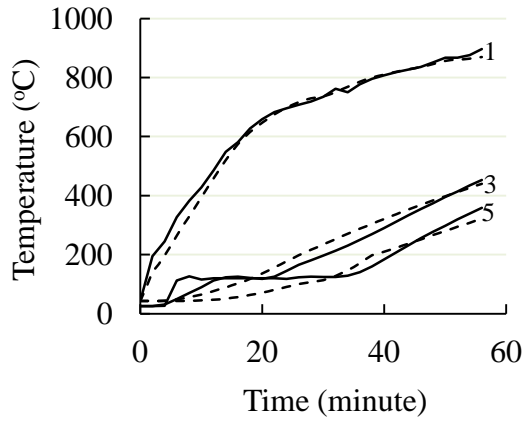
(e)C-08
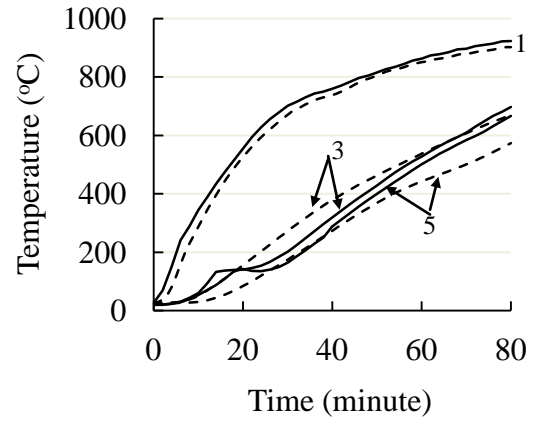
(f)C-09
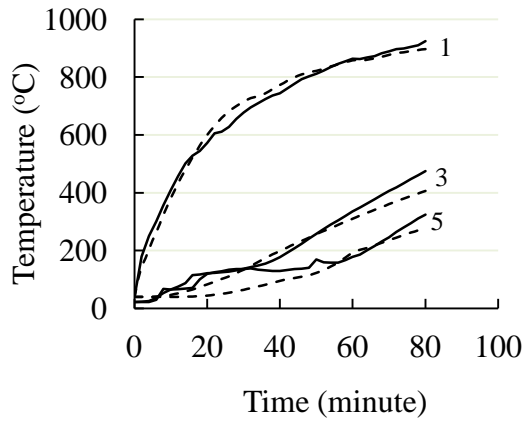
(g)C-11
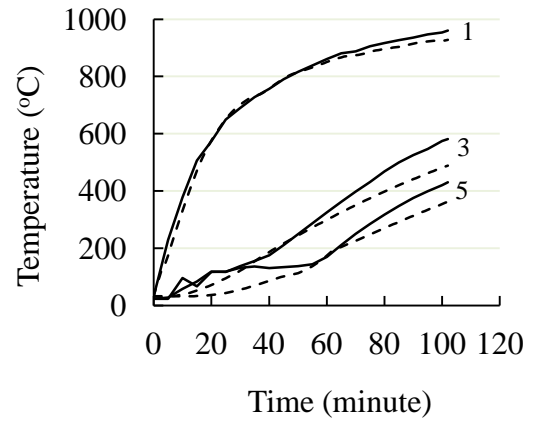
(h)C-13
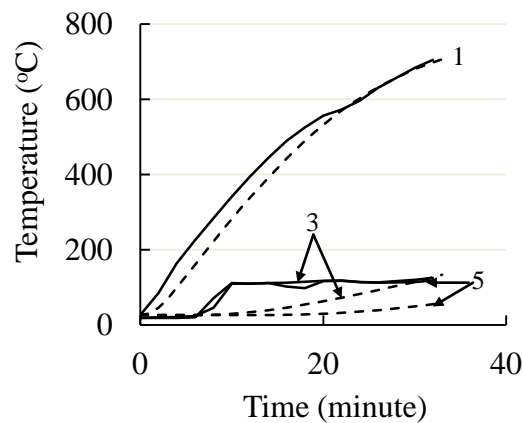
(i)C-16
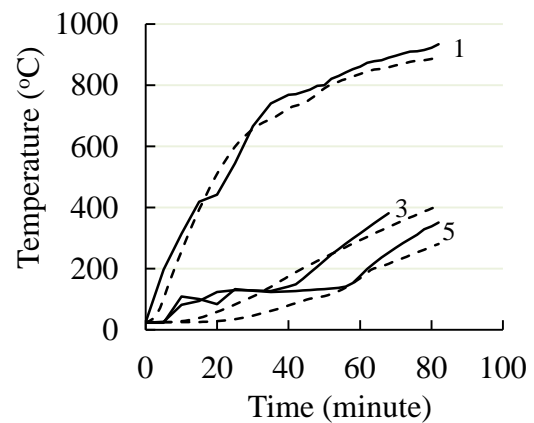
(j)C-17
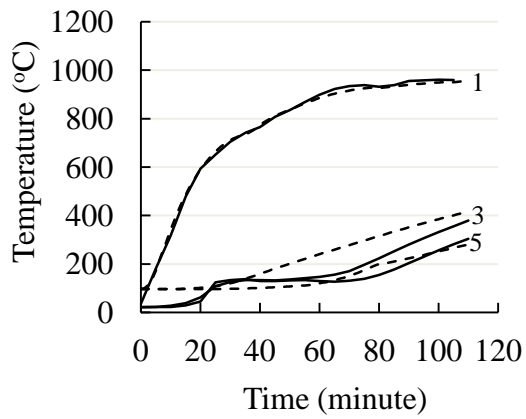
(k)C-20
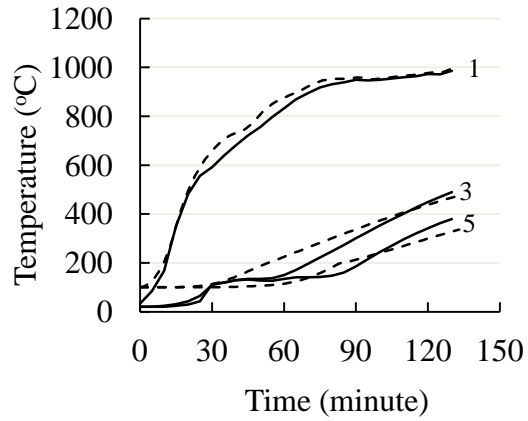
(l)C-21
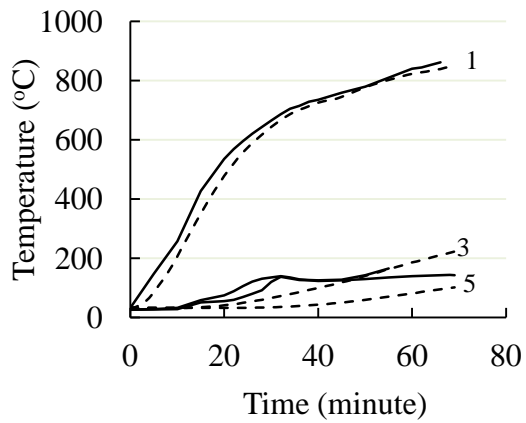
(m)C-22
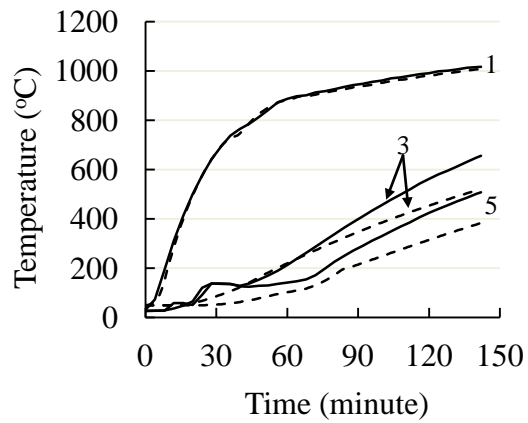
(n)C-23
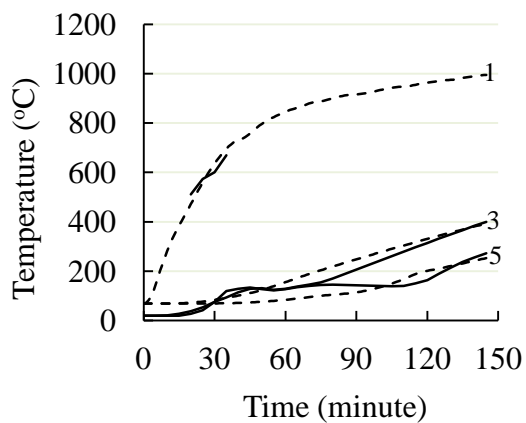
(o)C-25
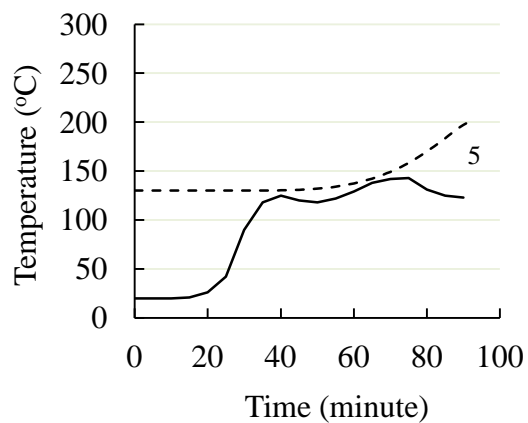
(p)C-26
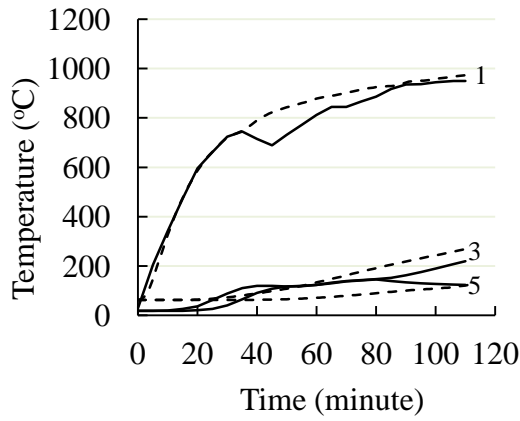
(q)C-28
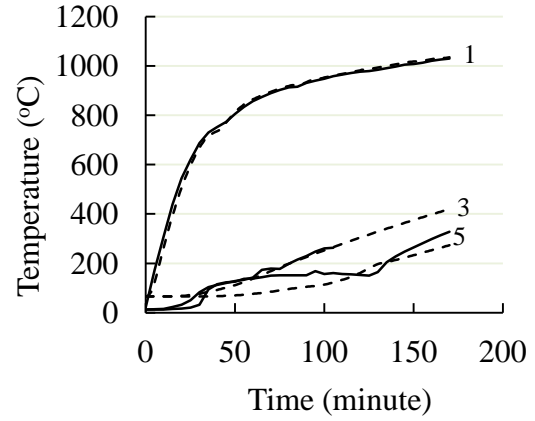
(r)C-29
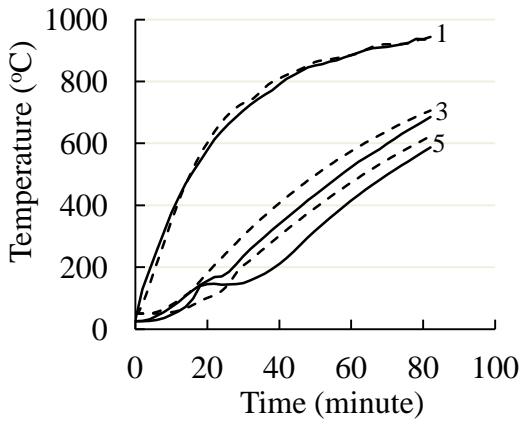
(s)C-31
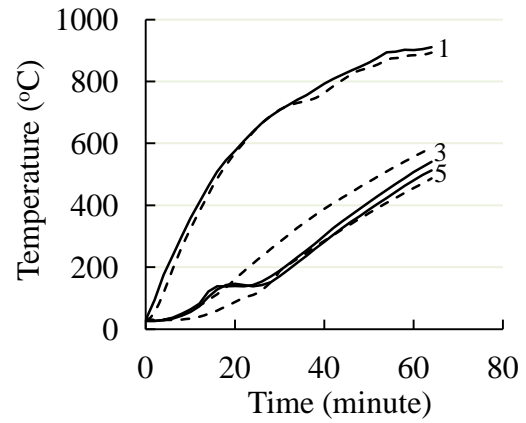
(t)C-32
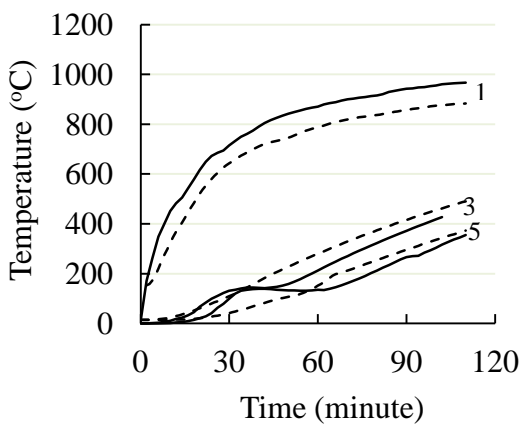
(u)C-34
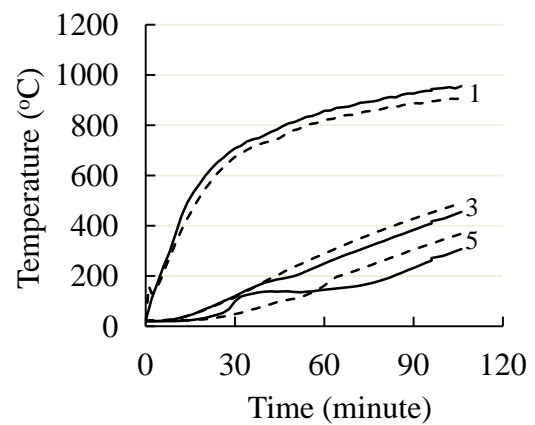
(v)C-35
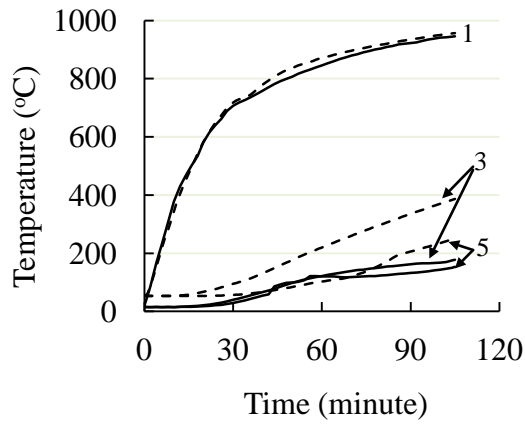
(w)C-40
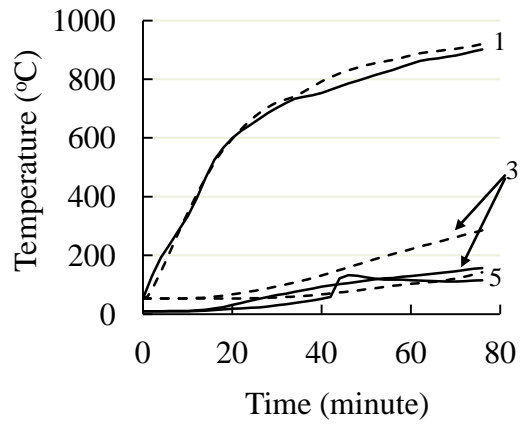
(x)C-41
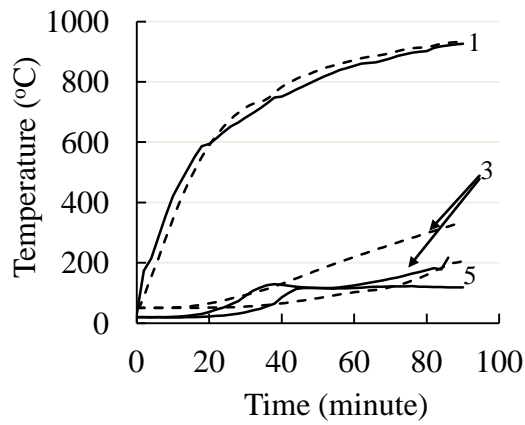
(y)C-42
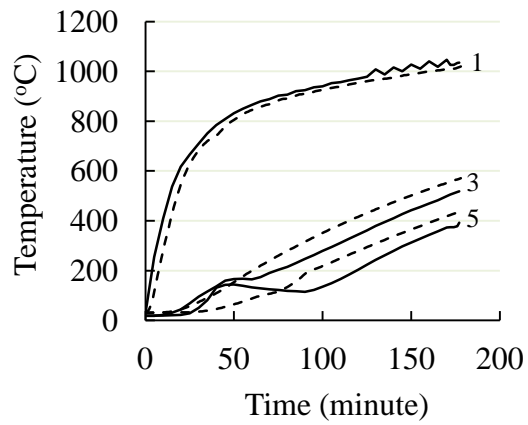
(z)C-44
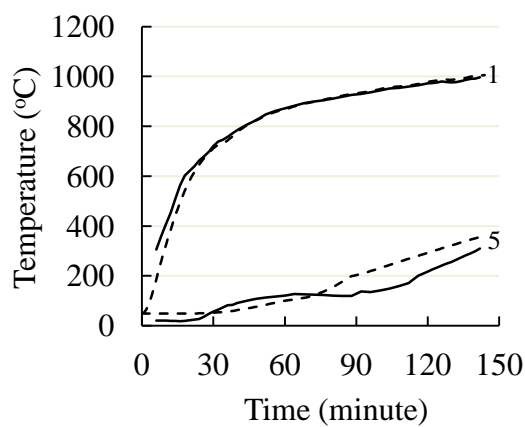
(aa)C-45
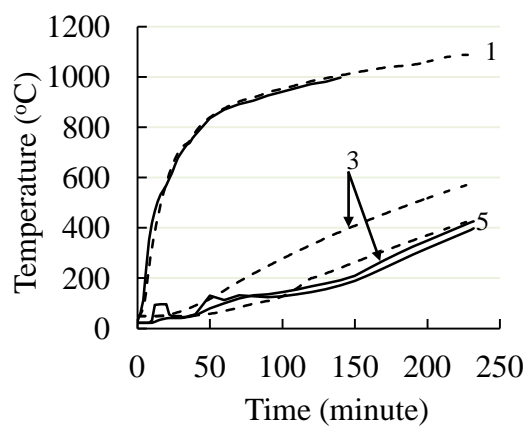
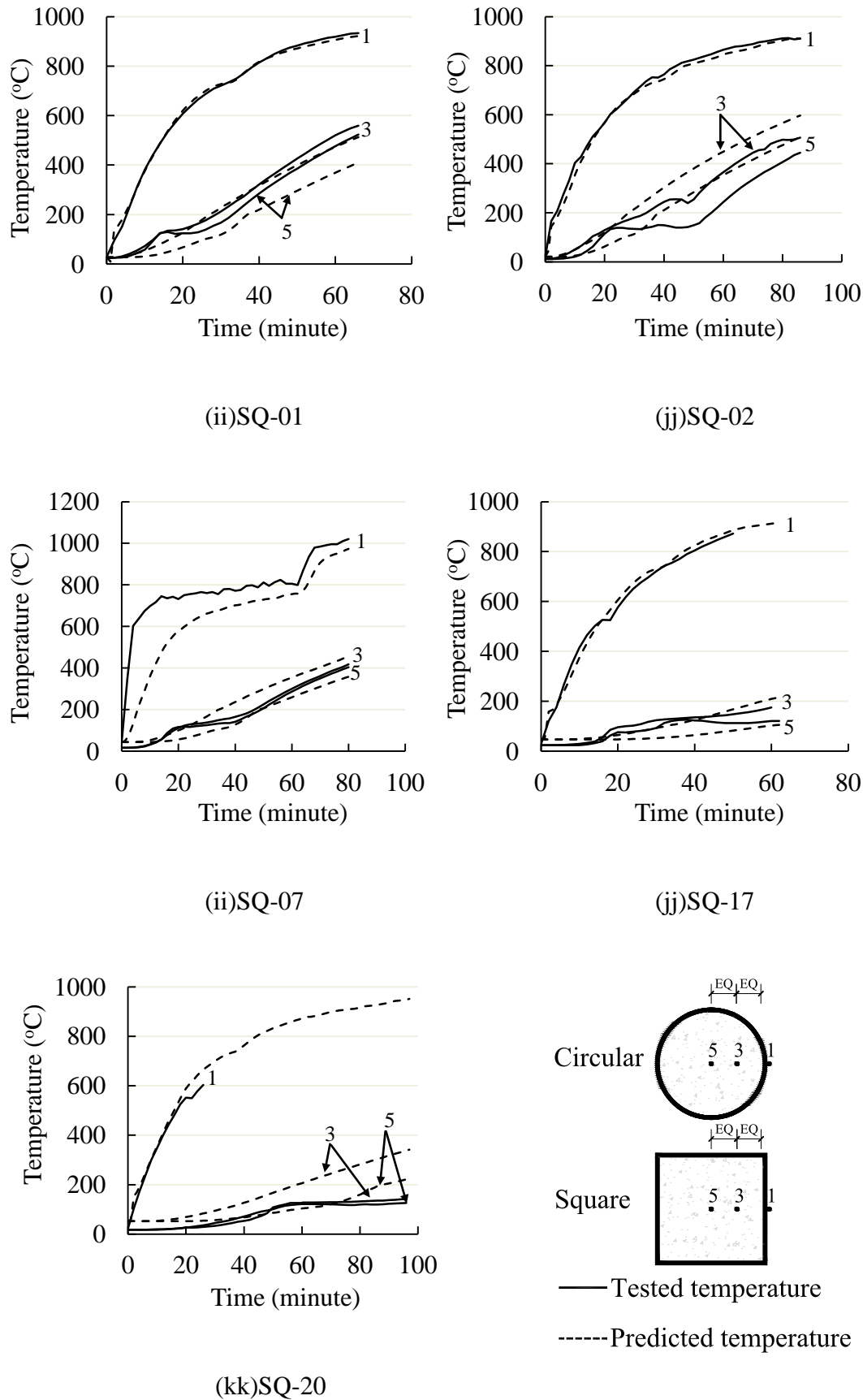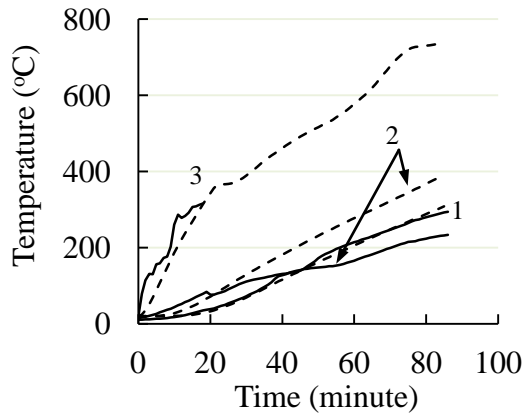(bb)C-50
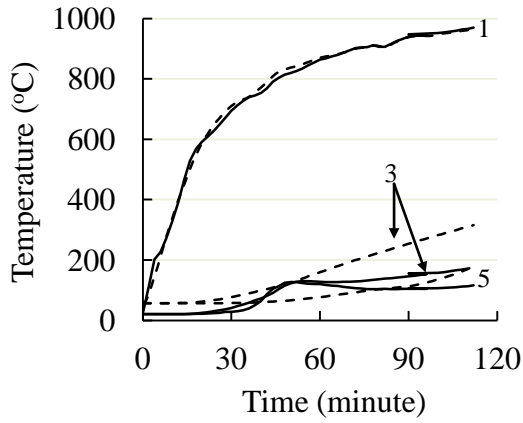
(cc)C-51
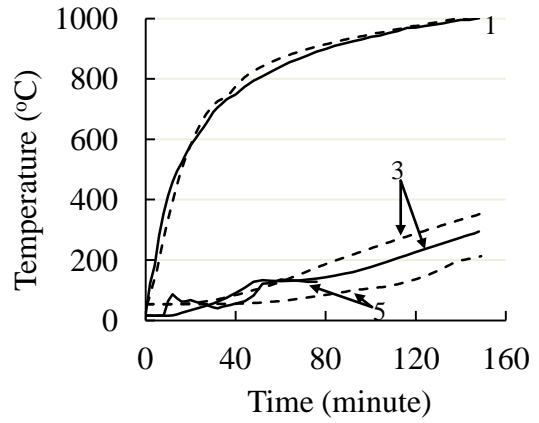
(dd)C-53

(ee)C-55

(ff)C-57

(gg)C-59

(hh)C-60
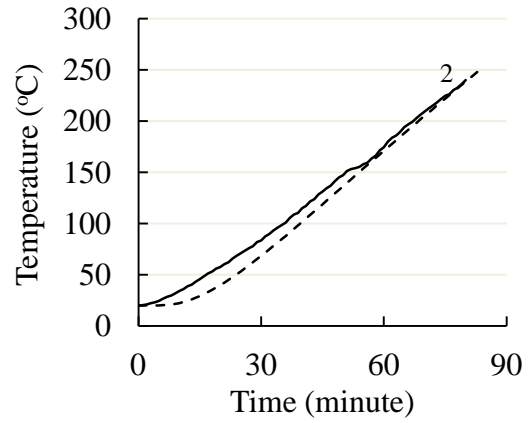
(ii)SQ-01

(jj)SQ-02
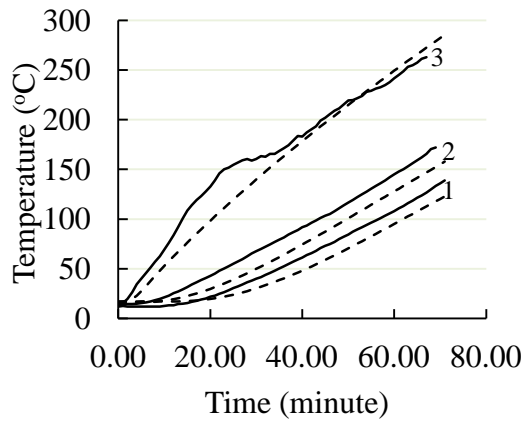
(ii)SQ-07

(jj)SQ-17
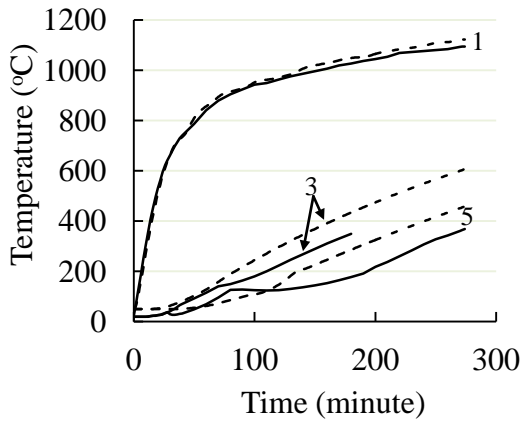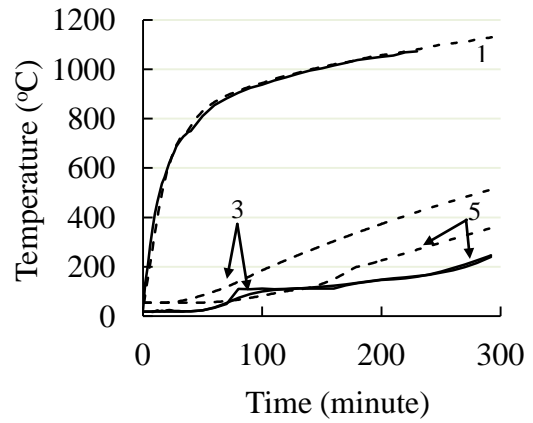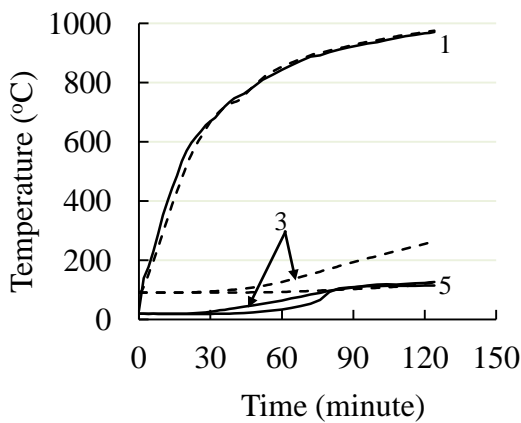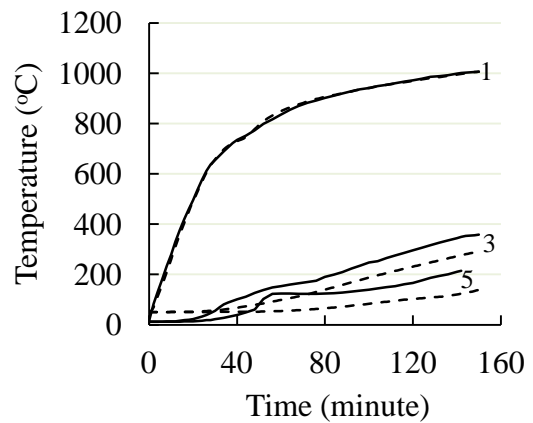
(kk)SQ-20
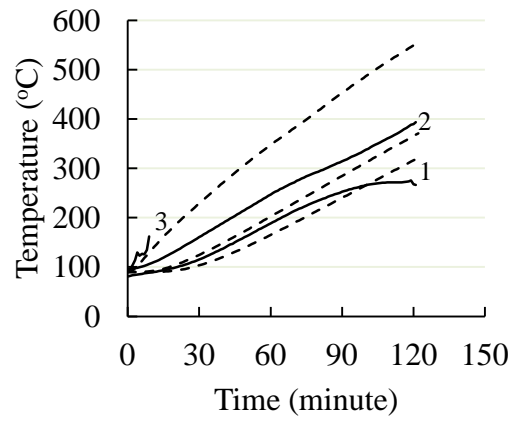
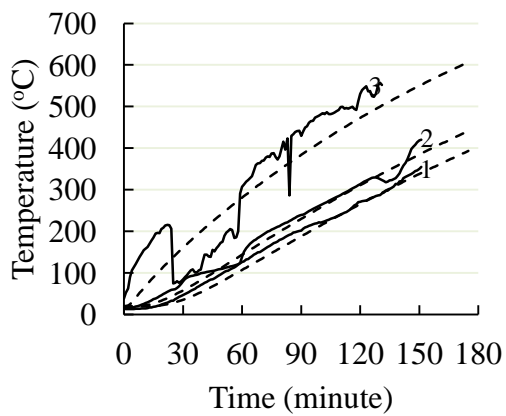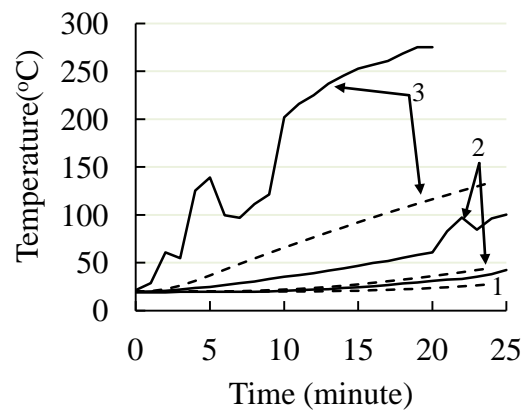Figure 7.14: Comparison between calculated and measured temperatures in Lie's tests

(a) LC-2-1

(b) LC-2-2
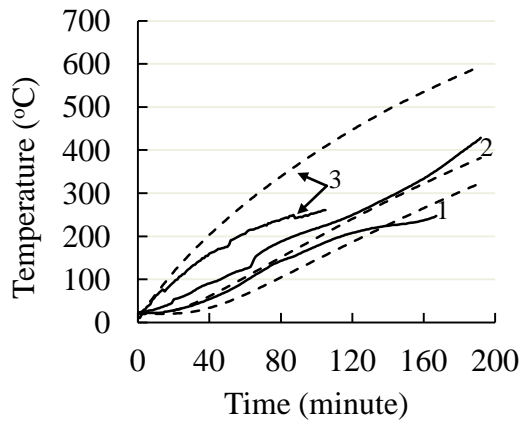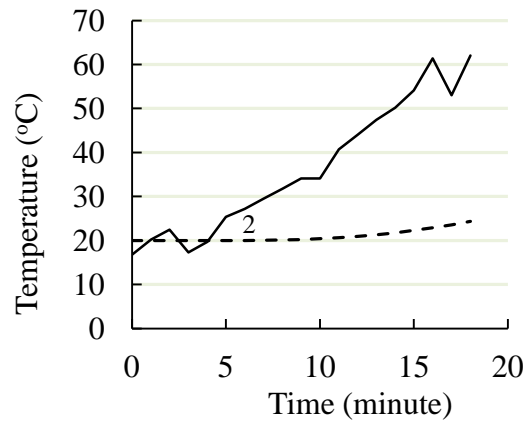
(c) LC-2-3
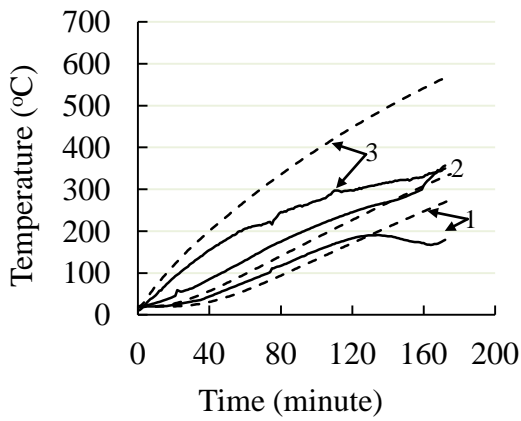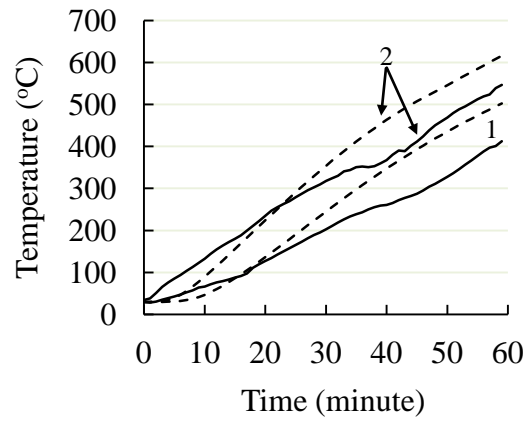
(d) LC-2-4

(e) LC-2-5

(f) LC-2-6

(g) LC-3-1

(h) LC-3-2

(i) LC-4-1

(j) LDC-2-1
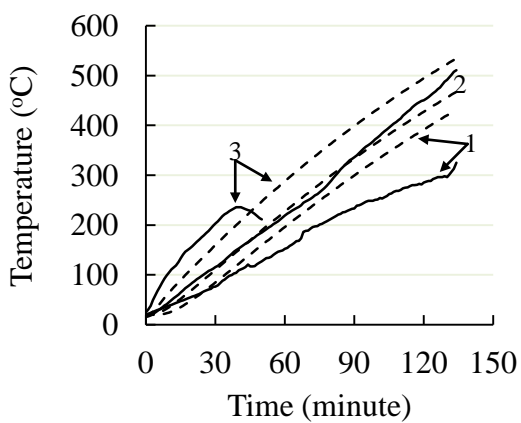
(k) LDC-2-2
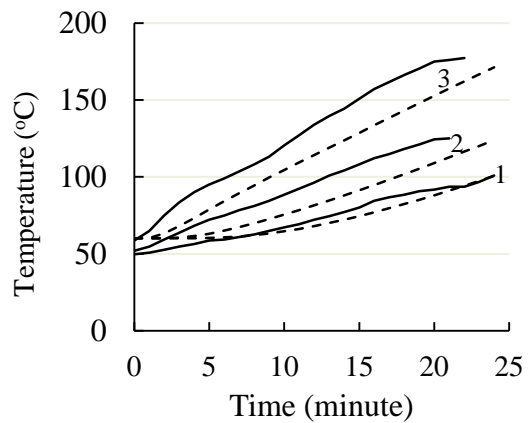
(l) LDC-2-3
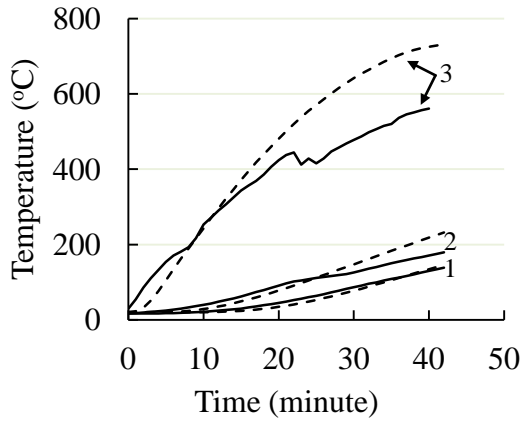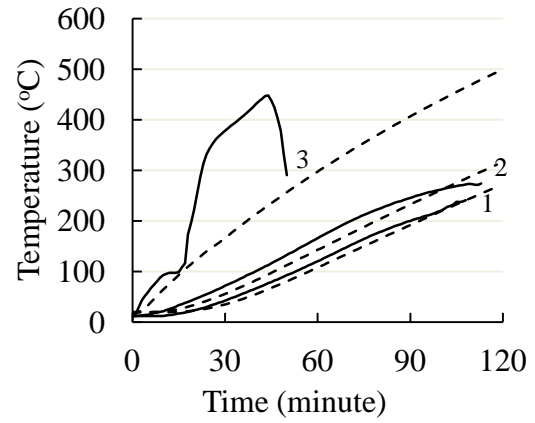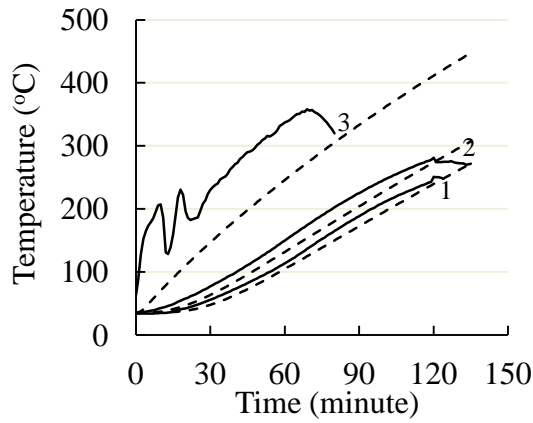
(m) LSH-2-1
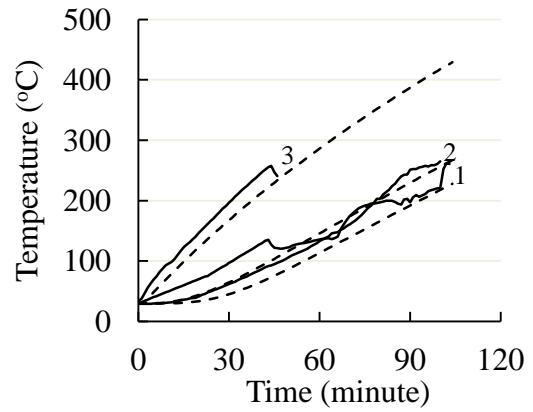
(n) LSH-2-2

(o) LSH-2-3

(p) LSH-2-4
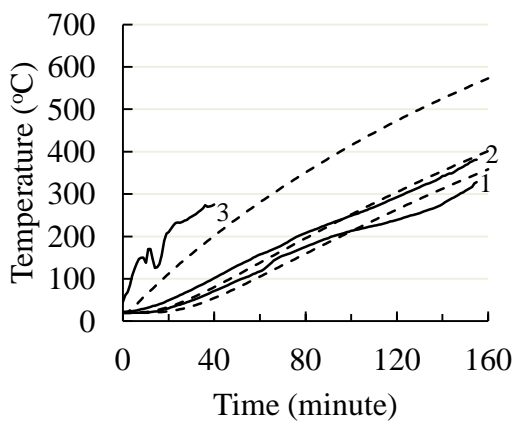
(q) LSH-2-5
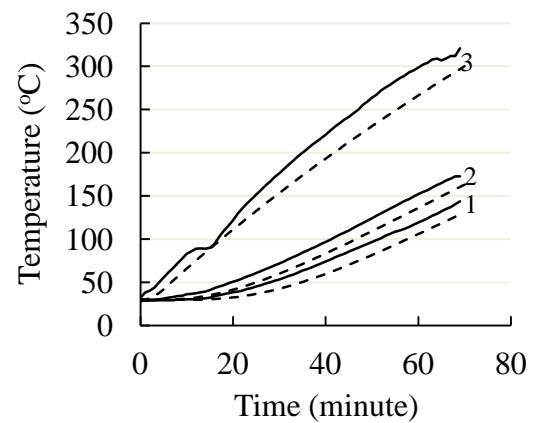
(r) LSH-2-6
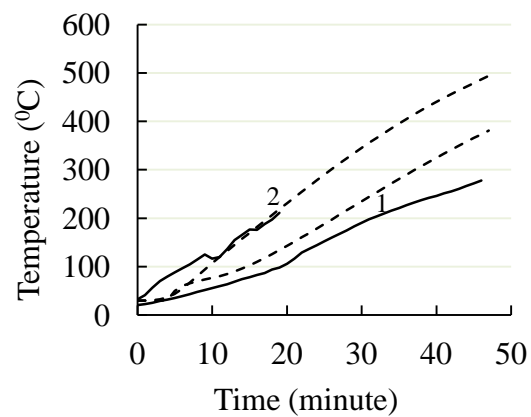
(s) LDSH-2-1
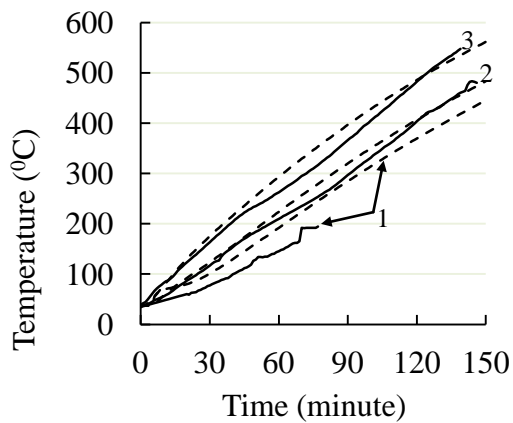
(t) LDSH-2-2
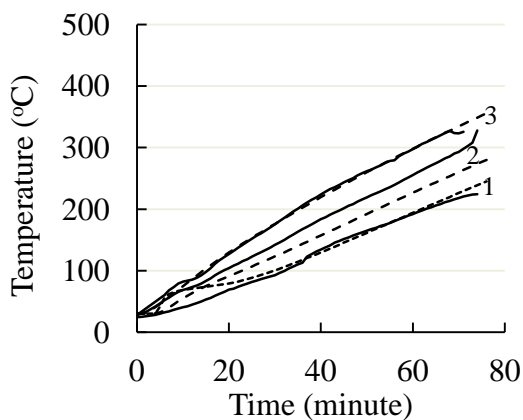
(u) LDSH-2-3
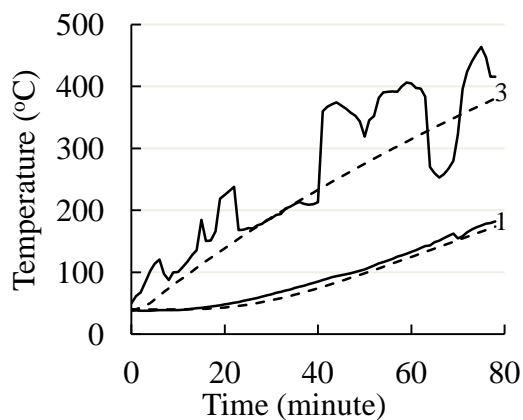
(v) LS-2-1

——Tested temperature

------Predicted temperature
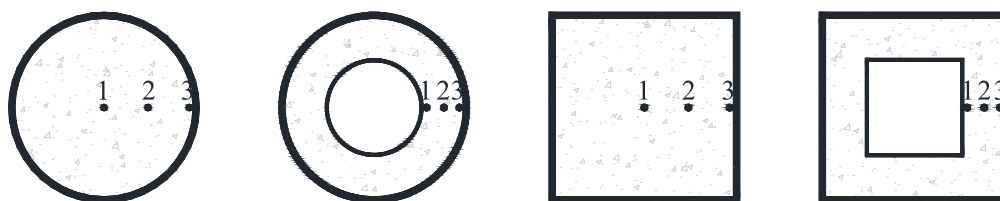
Figure 7.15: Comparison between measured and calculated temperatures in author's

tests
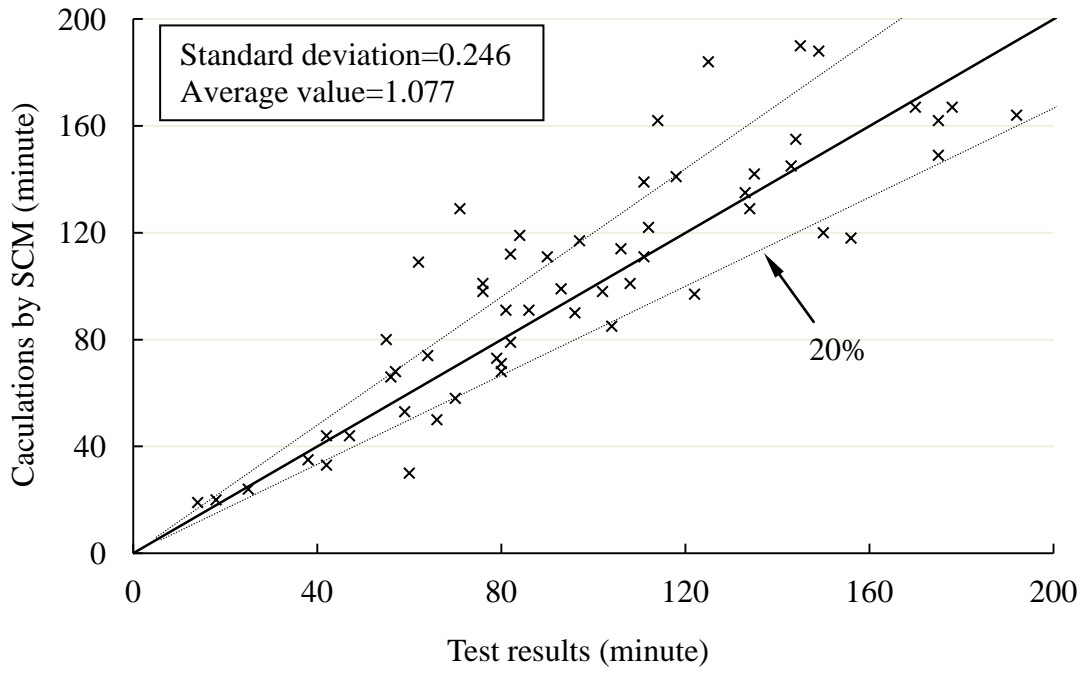
Figure 7.16: Comparisons between tested and calculated fire resistance time based on

SCM
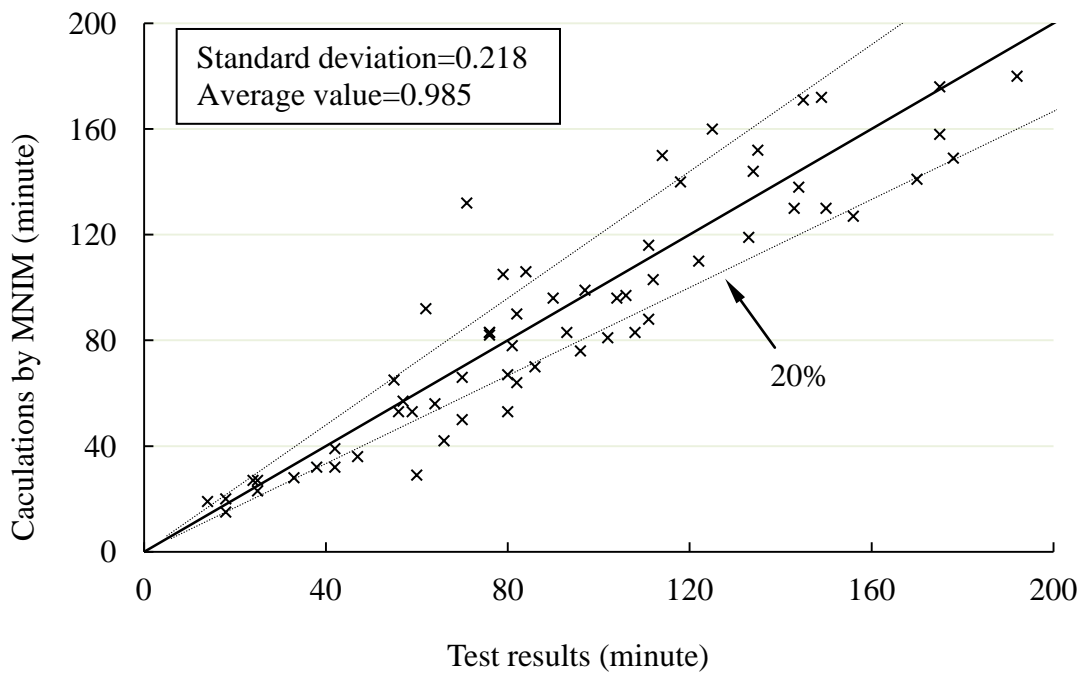
Figure 7.17: Comparisons between tested and calculated fire resistance time based on

MNIM

209
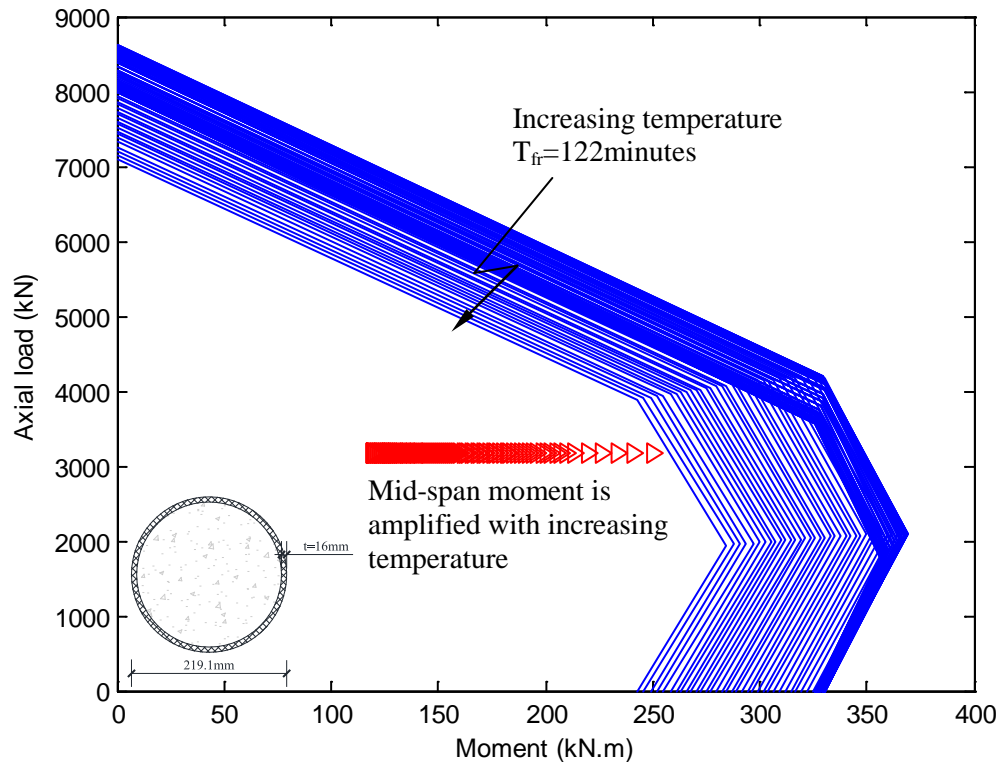
Figure 7.18: M-N curves of column LC-2-4 under fire
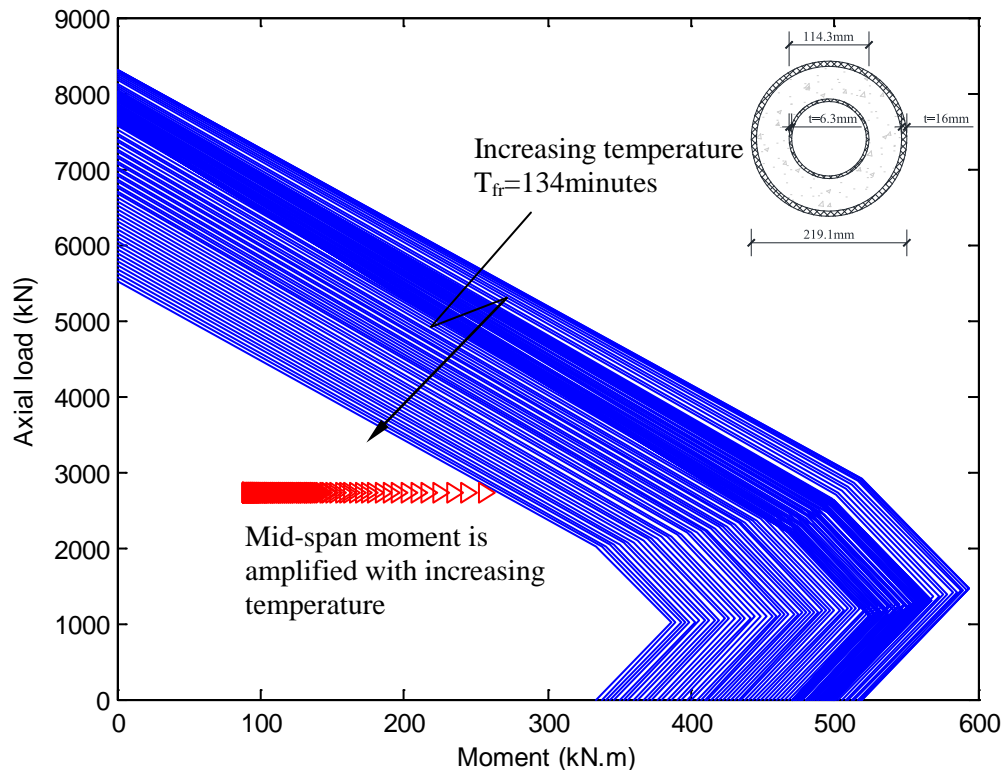
Figure 7.19: M-N curves of column LDC-2-2 under fire
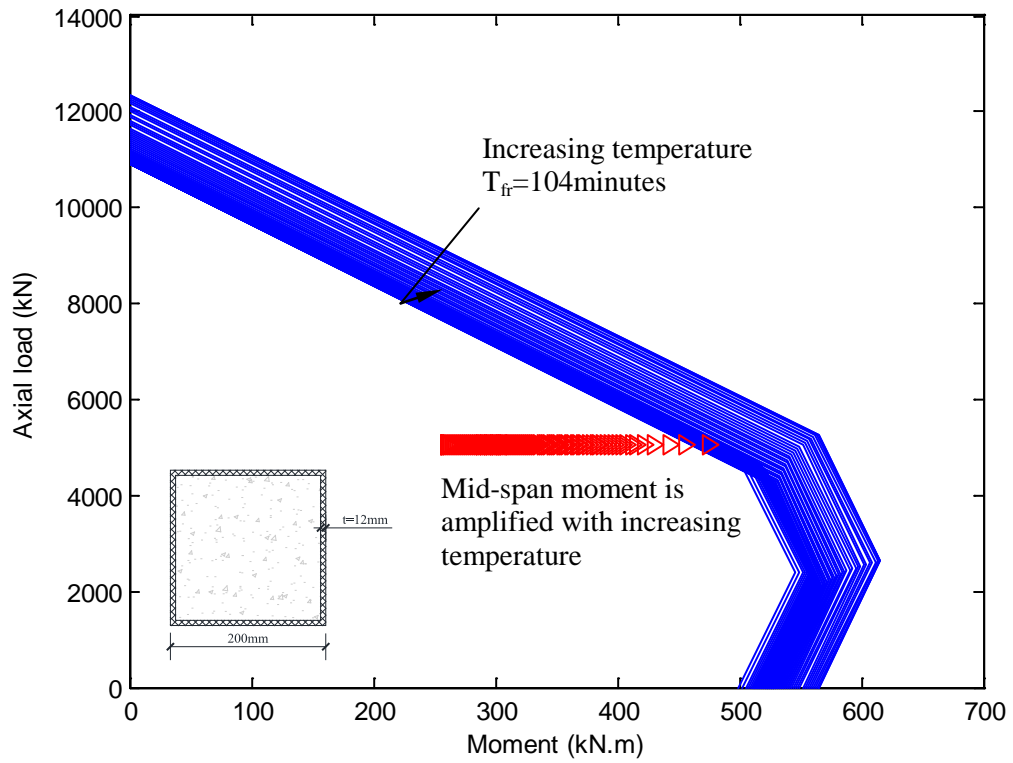
Figure 7.20: M-N curves of column LSH-2-4 under fire
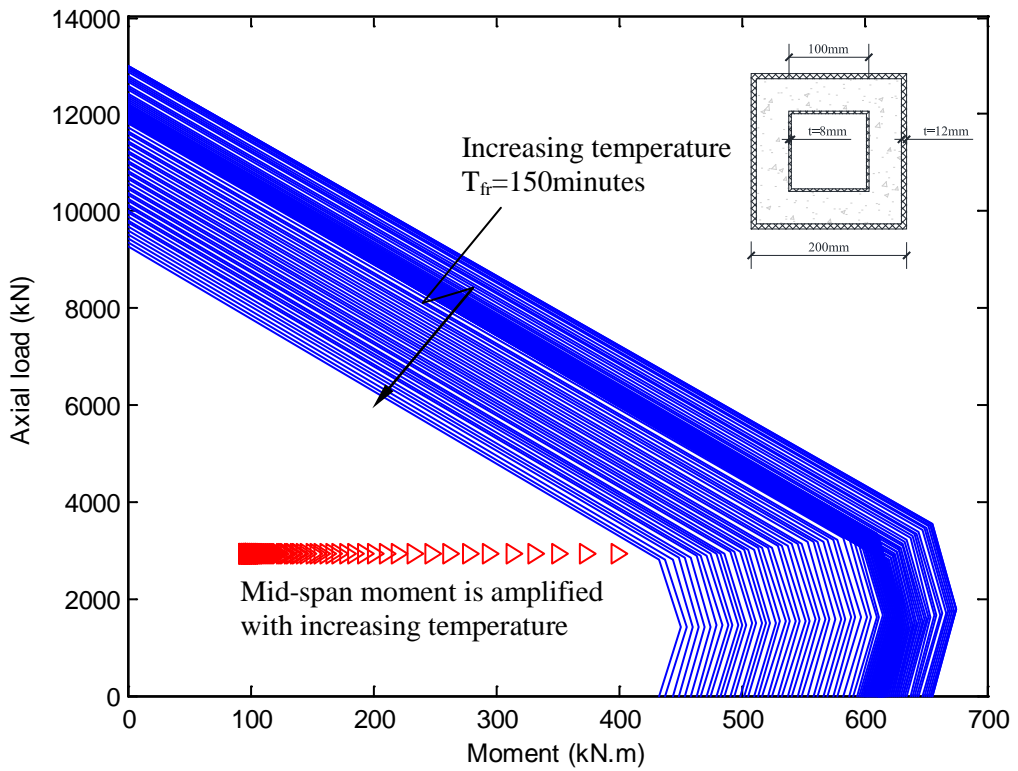
Figure 7.21: M-N curves of column LDSH-2-2 under fire
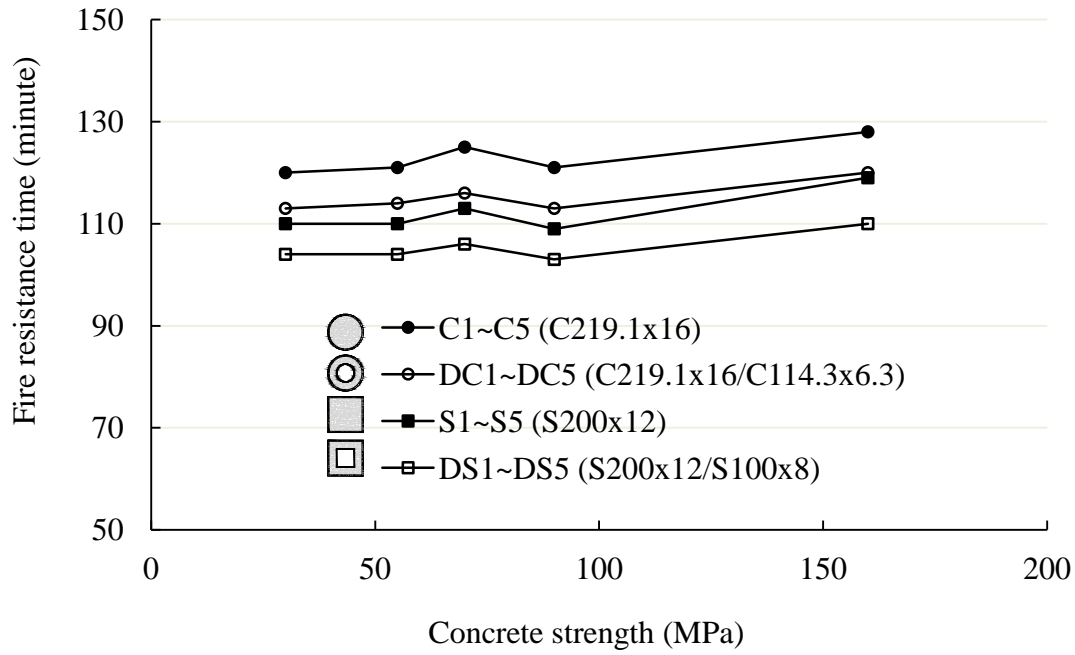
(a) Small cross-section
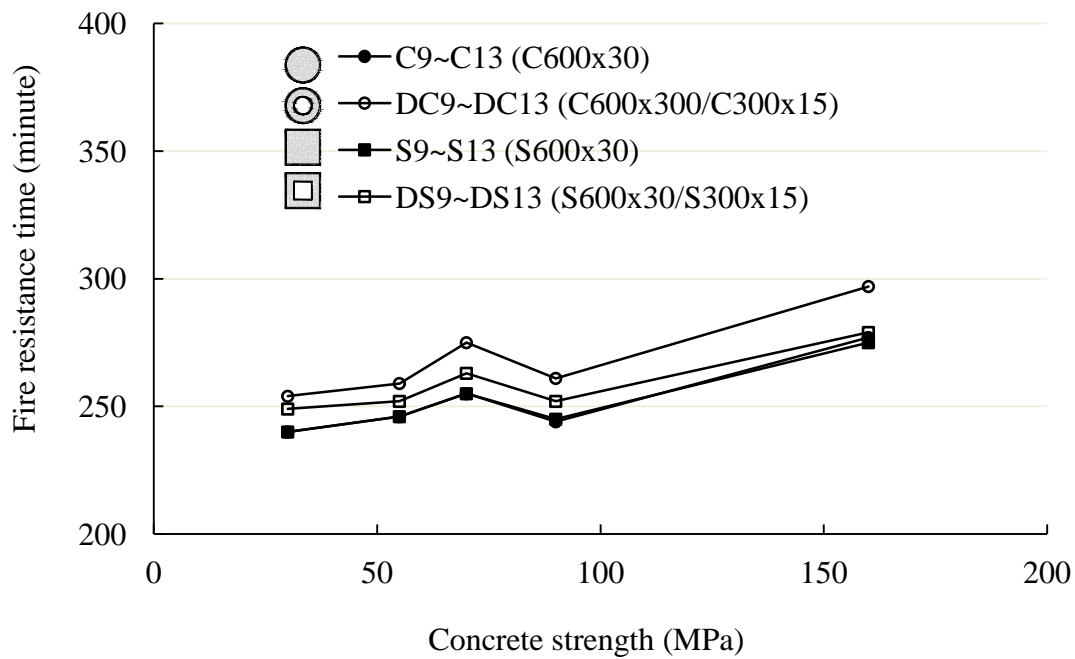
(b) Large cross-section

Figure 7.22: Effect of strength of concrete
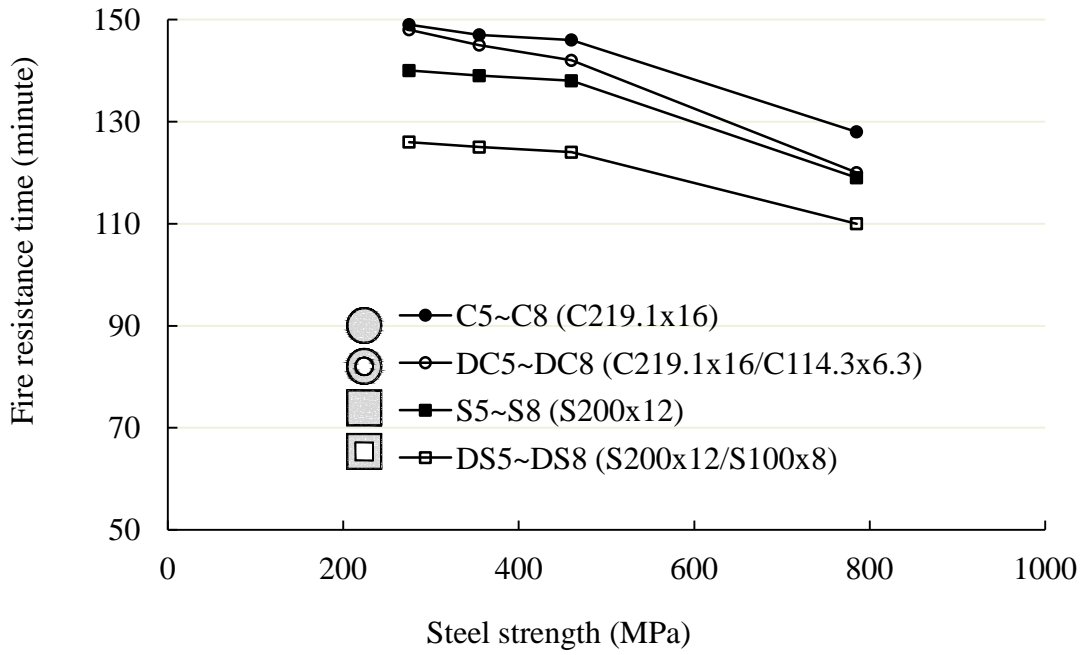
(a) Small cross-section
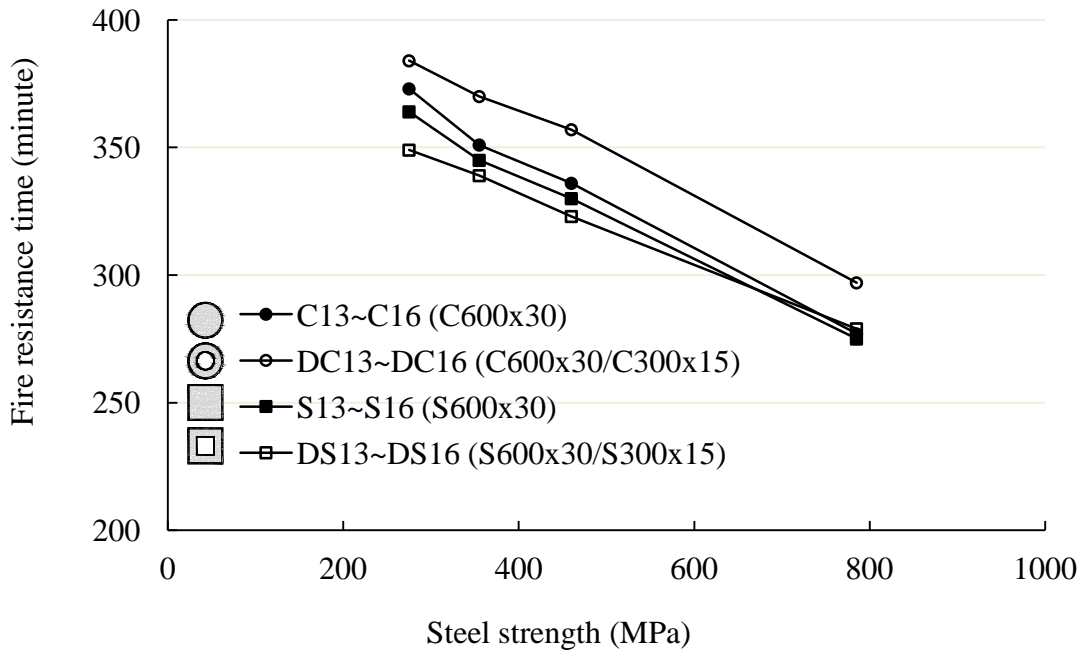
(b) Large cross-section

Figure 7.23: Effect of strength of steel
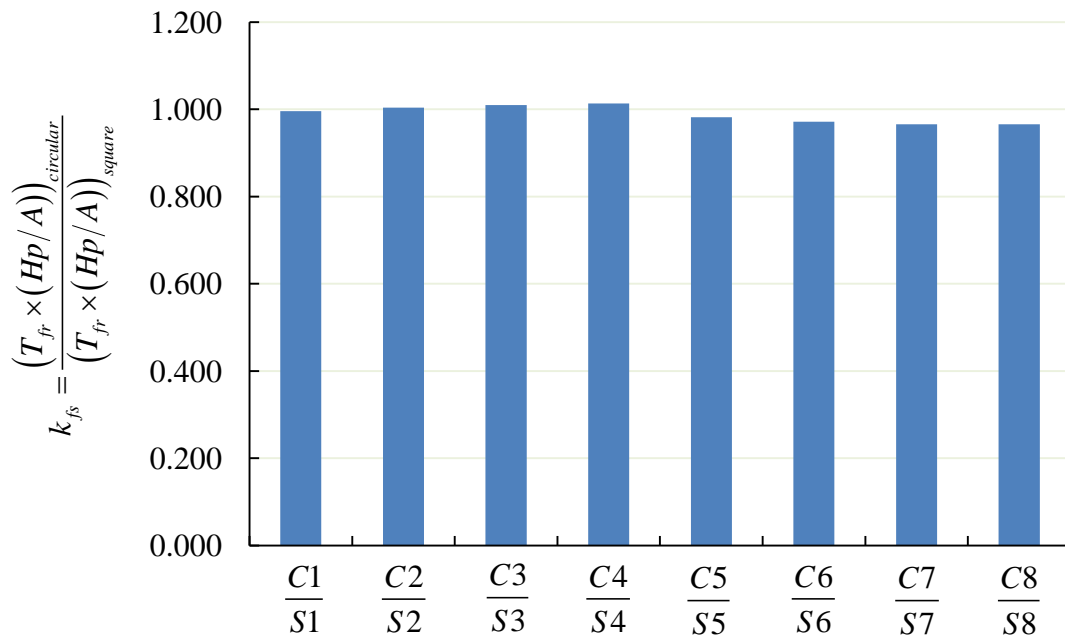
Figure 7.24: Ratio of fire resistance time per section factor between circular and

square columns with single-tube
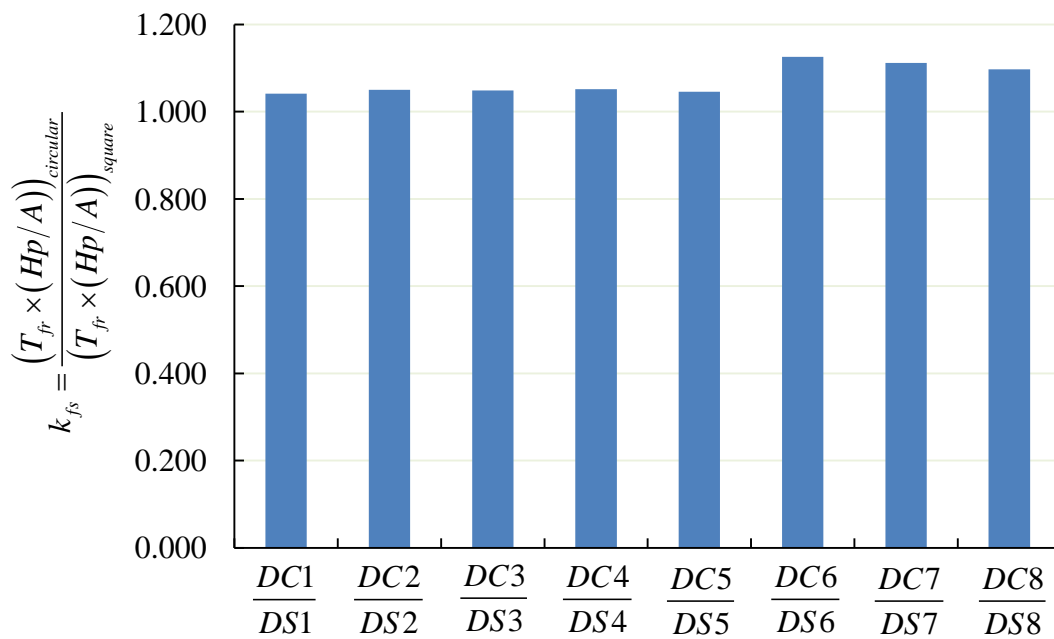
Figure 7.25: Ratio of fire resistance time per section factor between circular and

square columns with double-tube

Chapter 8   Conclusions and Recommendations

8.1 Review of Competed Research Work

This thesis presented extensive experimental and analytical investigations on the fire resistance of concrete filled steel tubular (CFST) columns with ultra-high strength concrete (UHSC) and high strength steel (HSS) materials. UHSC and HSS are proposed for the construction of high-rise buildings and other structures because of their architectural and economical advantages relative to normal strength materials. This research aims to extend the design code to the application of UHSC and HSS for column construction in high-rise buildings.

In Chapter 3, the temperature dependent mechanical properties of HSS, such as thermal elongation, elastic modulus, effective yield strength, critical temperature, and stress-strain curves were presented based on the experimental results. The tensile test was carried out based on standard coupon tests. A total of 73 specimens were tested by adopting both steady-heating and transient-heating methods. The effect of thermal creep was captured in the transient-heating test. Based on the tested mechanical properties, the critical temperature of columns with HSS was investigated. The temperature dependent mechanical properties and critical temperature of HSS were compared with those of NSS.

In Chapter 4, spalling behavior and residual properties of UHSC after elevated temperatures were introduced. The effects of types of fiber, dosages of polypropylene fibers, heating rates, and curing conditions were experimentally investigated. Steel fibers and polypropylene fibers were chosen. The dosages of polypropylene fibers were 0%, 0.1%, 0.25%, and 0.5% by volume. Heating rates were taken as 5$^\text{o}$C/min

216

and 30°C/min. Three curing conditions were bare specimens cured in air, bare specimens cured in fog room, and aluminum foil sealed specimens cured in air.

In Chapter 5, experimental investigations were carried out to determine the temperature dependent compressive strength and elastic modulus of UHSC. Stress-strain curves were not obtained due to the limit actions of the testing facilities. Unstressed testing method was adopted and a total of 27 specimens after heating to the target temperature were tested under compression. The compressive strength and elastic modulus of UHSC were obtained and compared with those of NSC and HSC.

In Chapter 6, fire performance of CFST columns with UHSC and HSS were investigated. Full-scale fire tests were carried out based on the standard ISO-834 fire. A total of 22 columns were tested, including both single-tube columns and double-tube concrete infilled sections. All columns were 3.81m height with 3m length exposed to the fire. The experimental investigation focused on varying the thickness of fire protection material, cross-sectional size, boundary condition, load level, and eccentricity of load. The testing observations included temperature profiles of columns, axial load- deformation relationship, fire resistance time, and failure modes.

In Chapter 7, simple calculation model (SCM) in EN 1994-1-2 and proposed M-N interaction model (MNIM) were used to predict the fire resistance of CFST columns. The predicted results were compared with the present tests and test results with normal strength materials in the literature. By using SCM and MNIM, the thermal properties of the steel and concrete were taken from EN 1993-1-2 and EN 1992-1-2 respectively. The mechanical properties of NSS, NSC and HSC were adopted from EN 1993-1-2 and EN 1992-1-2. As for HSS and UHSC, the test results from Chapter 3 and Chapter 5 were used. The temperature profiles of CFST columns were

217

calculated based on the finite difference method. And the effective length of columns in fire tests was derived based on the 4th-order differential equation of lateral displacement. The proposed MNIM was used to perform the parametric analyses which focused on the effects of the strengths of steel and concrete.

8.2 Conclusions

Within the scope of the experimental and analytical investigations reported in this thesis on fire resistance of CFST columns with UHSC and HSS, the following major conclusions can be drawn:

(1) Thermal creep significantly affected the elastic modulus of HSS when the temperature is higher than one third of its melting point. Compared with elastic modulus from steady-state tests, the elastic modulus from transient-state tests is reduced by 45%~65% beyond a temperature of 400°C. However, the effect is not significant on effective yield strengths of HSS which are similar for both steady-state and transient-state tests. Overall, the transient-heating test is recommended to investigate the mechanical properties of HSS at elevated temperatures since it takes into account the realistic load conditions and can capture the effects of thermal creep.

(2) Relative thermal elongations of HSS are smaller than those of NSS given in EN 1993-1-2. The difference is in the range of 2%~30%. This implies that the thermal expansion of HSS is smaller than NSS at elevated temperatures.

(3) Although the elastic modulus and effective yield strengths of HSS are reduced faster than NSS at elevated temperatures, the steel columns made from HSS may

not fail faster than NSS columns under fire situations. The fire resistance time of a steel column is determined based on the critical temperature. In EN 1993-1-2, the critical temperature is determined based on the regressed reduction factors of effective yield strength which may result in a higher critical temperature and an unsafe calculated fire resistance time. It is recommended that the non-dimensional slenderness ratio of a column at room temperature should be considered when calculating the critical temperature. The critical temperature will decrease with increasing non-dimensional slenderness ratio. Shorter HSS columns (with non-dimensional slenderness ratio < 0.8) will fail faster, but slender HSS columns (with non-dimensional slenderness ratio > 0.8) will fail slower as compared to columns with NSS.

(4) New tests were carried in Chapter 4 and Chapter 5 and test data has been made available on the mechanical properties and spalling behavior of UHSC at elevated temperatures. The experimental investigation on spalling behavior shows that it is necessary to add polypropylene fibers into UHSC to prevent spalling at elevated temperatures. The proposed effective dosage of polypropylene fibers is 0.1% by volume rather than at least 2kg/m^3 (0.25% by volume) as recommended in EN 1992-1-2. Experimental evidence also shows that polypropylene fibers with a dosage of 0.1% by volume would not affect the workability of UHSC and the compressive strength and elastic modulus at room temperature. However, the residual compressive strength and residual elastic modulus of UHSC after heating are affected by the dosage of polypropylene fibers and heating rate but was not affected by the curing conditions of concrete specimens.

(5)   Finite difference model has been developed to calculate the temperature profiles of columns in a fire. The predicted results are compared with the measured results from fire tests. The comparison shows reasonable agreements between the calculated and measured temperatures. The validation also shows that it is acceptable to take the thermal properties of UHSC and HSS as those from NSS, NSC and HSC given in EN 1993-1-2 and EN 1992-1-2.

(6)   Analytical model has been developed to calculate the effective length of column in a fire test. It is recommended that the effective length of partially heated columns should consider the unheated length and the heated length of column. Generally, the effective length approaches 0.5~0.6 times the fire exposed length of a fixed-fixed column with increasing heating time. Whereas for pinned-pinned column, the effective length is not sensitive to the heating time and could be taken as the overall column length including both heated and unheated parts.

(7)   Based on the proposed M-N interaction model (MNIM), parametric analyses indicate that CFST columns infilled with UHSC can be used in terms of their comparable fire resistance time with CFST columns with NSC or HSC. However, attention should be paid when using HSS in CFST columns since a thicker layer of fire resistance time is lower than that of CFST columns with NSS. Thus more fire protection material is needed. In terms of single-tube columns, it is equivalent to use circular and square columns if they have same section factors. In terms of double-tube columns, it is advisable to use circular columns due to higher fire resistance time if the section factor remains the same.

(8)   The superiority of single-tube columns over double-tube columns or vice versa under fire is not clear. It is suggested to consider the balance between section

factor and non-dimensional slenderness ratio for double-tube columns which exhibit shorter fire resistance time due to larger section factors but longer fire resistance time due to smaller non-dimensional slenderness ratio.

(9) Existing simple calculation model (SCM) in EN 1994-1-2 and proposed M-N interaction model (MNIM) are validated using the present fire tests and experimental results with normal strength materials available in the literature. The ratios between calculated and measured fire resistance time are mostly within 20%. The comparison between the two methods with tests shows that MNIM is a better method since it considers directly the second-order effects within the column and it is suitable for columns subject to combined moment and axial load. Thus, it is recommended to use MNIM for the design of CFST columns with either normal strength materials or high strength materials.

In terms of fire behavior, CFST columns with UHSC and HSS are suitable for use as the load bearing systems in high-rise buildings. CFST columns infilled with UHSC can exhibit fire resistance comparable to CFST columns with NSC or HSC. Hence, similar fire protection measures could be provided. Attention is needed if CFST columns with HSS are used since approximately 20% more fire protection is required vis-a-vis CFST columns with NSS. The proposed M-N interaction model is applicable for columns subjected to combined bending moment and axial load, and can be used to design the CFST columns with UHSC and HSS in fire situations.

8.3 Recommendations to Future Work

The followings are some ideas for further studies to attain better insights into the fire performance of CFST columns:

(1)   The thermal properties such as conductivity, specific heat capacity of UHSC and HSS were not physically tested. If the actual thermal properties are used, the calculations on temperature profiles of columns would be more accurate.

(2)   More tests for steel columns with HSS are required in order to determine its buckling curve at ambient temperature. As a result, the critical temperature of HSS column can be calculated. Since there is no research in literature reporting the fire resistance of single steel columns with HSS, it is necessary to provide more test data for this type of column.

(3)   There is also no research in literature reporting the fire resistance of reinforced UHSC columns. The spalling behavior and ductility under compression under fire for RC columns needs to be investigated.

(4)   Current research focuses mainly on the slender columns. Stub columns may have different fire performance due to the confinement effect from steel tube. In addition, the moment in the present columns are directly induced from the eccentricity of axial load, it does not fully exhibit the full range of behaviors of beam-columns in which the moment can be induced by lateral load acting on the column. Hence, in order to improve and establish further design guide for CFST columns with UHSC and HSS under fire, additional investigations on stub columns and beam-columns should be conducted.

(5)   In the current study, ultra-high strength concrete was used in CFST columns. But UHSC is about 20% heavier than NSC. In some applications where the self-weight is of concern, lightweight concrete could be used to increase the structural efficiency. The fire performance of lightweight concrete and CFST columns with lightweight concrete needs to be investigated.

References

Abrams M.S. (1971). Compressive strength of concrete at temperatures to 1600F. American Concrete Institute SP25, Temperature and Concrete, Detroit, Mechigan.

Access Steel. (2006). Buckling factors at elevated temperature, SD008a-EN-EU.

American Society of Civil Engineers (ASCE) & Society of Fire Protection Engineers (SFPE). (2000). Standard calculation methods for structural fire protection, No. ASCE/SFPE 29- 99, New York, NY.

ANSI/AISC 360-05. (2005). Specification for structural steel buildings. American Institute of Steel Construction, INC. March 9.

ASM Handbook Committee. (2000). Mechanical Testing and Evaluation, Volume 8.

ASTM C 469-02. (2002). Standard test method for static modulus of elasticity and Poisson's ratio of concrete in compression.

ASTM E 8M-04. (2004). Standard test methods for tension testing of metallic materials.

ASTM E 21-09. (2009). Standard test methods for elevated temperature tension tests of metallic materials.

Bayazitoglu Y, Ozisik M.N. (1988). Elements of heat transfer. Mcgraw-Hill International Editions: Mechanical Engineering Series.

Behnood A, Ziari H. (2008). Effects of silica fume addition and water to cement ratio on the properties of high-strength concrete after exposure to high temperatures. Cement & Concrete Composites, 30:106-112.

Bhadeshia H.K.D.H, Honeycombe R.W.K. (2006). Steels-microstructure and properties, third edition. Elsevier Ltd.

Binner C.R, Wilkie C.B, Miller P. (1949). Heat testing of high density concrete. Supplement, declassified report HKF-1, U.S. Atomic Energy Commission, June.

224

Bisalloy Steels. (2006). Technical Manual of BISPLATE, Rev 2, September.

British Standard. (2003). Structural use of steelwork in building - Part 8: code of practice for fire resistant design, BS 5950-8.

Callister D.W. (2007). Materials science and engineering: an introduction-7th edition. John Wiley & Sons, Inc.

Castillo C, Durrani A.J. (1990). Effect of transient high temperature on high strength concrete. ACI Materials Journal, 87:47-53.

Chen B., Liu J.Y. (2004). Residual strength of hybrid-fiber-reinforced high-strength concrete after exposure to high temperatures. Cement and Concrete Research, 34: 1065-1069.

Chen J, Young B., Uy B. (2006). Behavior of high strength structural steel at elevated temperatures. Journal of Structural Engineering, Vol.132, No.12: 1948-1954.

Chen J, Young B. (2007). Experimental investigation of cold-formed steel material at elevated temperatures. Thin-Walled Structures 45: 96-110.

Cheng F.P, Kodur V. K. R, Wang T.C. (2004). Stress-strain curves for high strength concrete at elevated temperatures. Journal of Materials in Civil Engineering, 16:84-90.

Colin B. (2000). Effective lengths of concrete-filled steel square hollow sections in fire. Proceedings of the Institution of Civil Engineers: Structures and Buildings, 140(2): 169-178, May.

Contro R, Poggi C, Cazzani A. (1988). Numerical analysis of fire effects on beam structures. Engineering Composite. 5:53-58.

Corradi L, Poggi C, Setti P. (1990). Interaction domains for steel beam columns in fire conditions. Journal of construction steel research, 17:217-235.

Corus Construction & Industrial. (2006). RQT Fabrication Guide.

Croft D.R, Lilley D.G. (1977). Heat transfer calculations using finite difference equations. Applied Science Publishers LTD, London.

References

Dolzhenkov I.E. (1971). The nature of blue brittleness of steel. Metal Science and Heat Treatment, v13, n3-4: 220-244, March-April.

Densit, www.densit.com. (2008). Data Sheet-Ultra High Performance Grout.

Dias W.P.S, Khoury G.A, Sullivan P.J.E. (1990). Mechanical properties of hardened cement paste exposed to temperatures up to 700°C. ACI Materials Journal, 87: 160-166.

Diederichs U, Jumppanen U.M, Penttala V. (1988). Material properties of highs strength concrete at elevated temperatures. IABSE 13th Congress, Helsinki, June.

Ding J, Wang Y.C. (2005). Finite element analysis of concrete filled steel columns in fire. Advances in steel structures, II:1053-1058.

Ding J, Wang Y.C. (2008). Realistic modeling of thermal and structural behavior of unprotected concrete filled tubular columns in fire. Journal of Constructional Steel Research 64:1086–1102.

Epsilon Technology Corp. (2000). Model 3548HI high temperature furnace extensometer installation and operation, Revision A, September.

Espinos A, Romero M.L, Hospitaler A. (2010). Advanced model for predicting the fire response of concrete filled tubular columns. Journal of Constructional Steel Research, 66: 1030-1046.

European Committee for Standardization. (1992). Tensile testing of metallic materials-Part 5: Method of test at elevated temperatures, EN 10002-5.

European Committee for Standardization. (1999). Fire resistance tests for loadbearing elements-Part 4: Columns, EN 1365-4.

European Committee for Standardization. (2002). Eurocode 0: Basis of structural design, EN 1990.

European Committee for Standardization. (2002). Eurocode 1: Actions on structures-Part 1-2: General actions-actions on structures exposed to fire, EN 1991-1-2.

226

European Committee for Standardization. (2004). Eurocode 2: Design of concrete structures-Part 1-2: General rules-structural fire design, EN 1992-1-2.

European Committee for Standardization. (2004). Hot rolled products of structural steels-Part 2: Technical delivery conditions for non-alloy structural steels, EN 10025-2.

European Committee for Standardization. (2005). Eurocode 3. Design of steel structures – Part 1-1: General rules and rules for buildings, EN 1993-1-1.

European Committee for Standardization. (2005). Eurocode 3: Design of steel structures-Part 1-2: General rules-structural fire design, EN 1993-1-2.

European Committee for Standardization. (2005). Eurocode 3: Design of steel structures-Part 1-8: Design of joints, EN 1993-1-8.

European Committee for Standardization. (2004). Eurocode 4: Design of composite steel and concrete structures-Part 1-1: General rules and rules for buildings, EN 1994-1-1.

European Committee for Standardization. (2005). Eurocode 4: Design of composite steel and concrete structures-Part 1-2: General rules-structural fire design, EN 1994-1-2.

European Committee for Standardization. (2007). Eurocode 3. Design of steel structures – Part 1-12: Additional rules for the extension of EN 1993 up to steel grades S700, EN 1993-1-12.

Felicetti R, Gambarova P.G, Rosati G.P, Corsi F, Giannuzzi G. (1996). Residual mechanical properties of high strength concretes subjected to high temperature cycles. Proceedings 4th International Symposium on Utilization of High Strength/High Performance Concrete, Paris France, 579-588.

Feng J.B, Han L.H, Jing J.S, Feng Y.C. (2001). Experimental study on the fire resistance of high strength concrete filled steel tube columns under axial load. Fire Science and Technology, 1st issue, 8-9.

Fessler H., Hyde T.H. (1978). Creep deformation of metals, creep of engineering materials. A journal of strain analysis monograph, Mechanical Engineering Publication Limited, 80-110.

Furumura F, Ave T, Okabe T, Kim W.J. (1986). A uniaxial stress-strain formula of structural steel at high temperature and its application to thermal deformation analysis of steel frames. Transportation of Architect Institute of Japan, 363:110-117.

Furumura F, Abe T, Shinohara Y. (1995). Mechanical properties of high strength concrete at high temperatures. Proceedings of the fourth Weimar workshop on high performance concrete: material properties and design, held at Hochschule fur Architectur und Bauwesen (HAB), Weimar, Germany, October 4th and 5th, 237-254.

Graham P. (2006). High strength steel use in Australia, Japan and the US. Structural Engineer, v 84, n 21, p 27-30, November 7.

Hadi M.N.S. (2007). Using fibres to enhance the properties of concrete columns. Construction and Building Materials, 21: 118-125.

Hammer T.A. (1995). High-strength concrete phase 3, compressive strength and elastic modulus at elevated temperatures. SP6 Fire resistance, Report 6.1, SINTEF Structure and concrete, STF70 A95023, February.

Han C.C., Hwang Y.S., Yang S.H., Gowripalan N. (2005). Performance of spalling resistance of high performance concrete with polypropylene fiber contents and lateral confinement. Cement and Concrete Research, 35: 1747-1753.

Han C.C., Han M.C., Heo Y.S. (2009). Improvement of residual compressive strength and spalling resistance of high-strength RC columns subjected to fire. Construction and Building Materials, 23: 107-116.

Han L.H, Huo J.S. (2002). Bearing capacity of concrete filled steel tubular columns after fire. China Civil Engineering Journal (Chinese), 35(4): 25-36.

Han L.H. (2004). Concrete filled steel tubular structure-Theory and Practice. Science Press (Chinese).

Han L.H, Yang Y.F. (2007) Structural technology for concrete filled steel tubular columns. China Architecture & Building Press (Chinese).

Harmathy T.Z. (1970). Thermal properties of concrete at elevated temperature. Journal of Materials, JMLSA, 5(1):47-74, March.

Harmathy T.Z. (1993). Fire safety design and concrete. Longman Scientific & Technical.

Hertz K. (1984). Heat induced explosion of dense concretes. Report No.166, Institute of Building Design, Technical University of Denmark.

Hertz K. (1991). Danish investigations on silica fume concrete at elevated temperatures. Proceedings, ACI spring convention, Boston, MA, March 17-22.

Hong S.D, Varma A.H. (2009). Analytical modeling of the standard fire behavior of loaded CFT columns. Journal of Constructional Steel Research, 65:54-69.

Ianizzi R, Schleich J.B. (1991). Mechanical properties of structural steel at elevated temperatures-comparisons by numerical simulations. RPS Rep.No.15/90, ARBED Researches, Luxembourg.

ISO 834-1. (1999). Fire-resistance tests-elements of building construction Part1: General requirements. International Standard ISO 834, Geneva.

Jeane D.C. (1985). Application of the computer in modeling fire endurance of structural steel floor systems. Fire Safety Journal, 9:119-135.

Kalifa P., Chene G., Galle C. (2001). High-temperature behavior of HPC with polypropylene fibers from spalling to microstructure. Cement and Concrete Research, 31:1487-1499.

Kelly F.S., Sha W. (1999). A comparison of the mechanical properties of fire-resistant and S275 structural steels. Journal of Constructional Steel Research 50: 223–233.

Khoury G.A. (1992). Compressive strength of concrete at high temperature: a reassessment. Magazine of Concrete Research, 44:291-309.

Kirby B.R., Preston R.R. (1988). High temperature properties of hot-rolled, structural steels for use in fire engineering design studies. Fire Safety Journal, 13:27-37.

Kirby B.R. (1995). The behavior of high-strength Grade 8.8 bolts in fire. Journal of Constructional Steel Research, 33:3-38.

Kodur V.K.R. Lie T.T. (1995). Performance of concrete-filled hollow steel columns. Journal of Fire Protection Engineering, Vol. 7, No. 3.

Kodur V.K.R. (1996). Factors affecting the fire resistance of square hollow steel columns filled with steel-fiber-reinforced concrete. National Research Council Canada, Internal Report, No.590.

Kodur V.K.R. (1996). Factors affecting the fire resistance of circular hollow steel columns filled with steel-fiber-reinforced concrete. National Research Council Canada, Internal Report, No.598.

Kodur V.K.R. (1996). Assessment of the fire resistance of steel hollow structural section columns filled with steel fiber reinforced concrete. National Research Council Canada, Internal Report No.731.

Kodur V.K.R. Lie T.T. (1997). Discussion: performance of concrete-filled hollow steel columns. Journal of Fire Protection Engineering, Vol. 8, No. 3.

Kodur V.K.R. (1998). Performance of high strength concrete-filled steel columns exposed to fire. Canadian Journal of Civil Engineering, 25:975-981.

Kodur V.K.R. Makinnon D.H. (2000). Design of concrete-filled hollow structural steel columns for fire endurance, Engineering Journal, AISC, Vol. 37, No. 1.

Kodur V.K.R, Dwaikat M., Fike R. (2010). High-temperature properties of steel for fire resistance modeling of structures. Journal of Materials in Civil Engineering, Vol.22, No. 5, May 1.

Lennon,T, Moore, D.B, Wang Y.C, Bailey C.G. (2007). Designers' guild to EN 1991-1-1, 1992-1-2, 1993-1-2 and 1994-1-2, Handbook for the fire design of steel, composite and concrete structures to the Eurocodes. Thomas Telford Publishing.

Li G.Q., Yin Y.Z., Li M.F. (2002). Experimental studies on the material properties of high-strength bolt connection at elevated temperatures. Steel and Composite Structures, Vol. 2, No. 4:247-258.

Li G.Q, Han L.H, Lou G.B, Jiang S.C. (2006). Fire resistance design of steel structures & steel-concrete composite structures. China Architecture & Building Press (Chinese).

Lie T.T, Allen D.E. (1974). Fire Resistance of Reinforced Concrete Columns. National Research Council of Canada, Division of Building Research, Research Paper NO. 622:245-254.

Lie T.T, Caron S.E. (1988). Fire resistance of circular hollow steel columns filled with siliceous aggregate concrete: Test Results. National Research Council Canada, Internal Report, No.570.

Lie T.T, Caron S.E. (1988). Fire resistance of circular hollow steel columns filled with carbonate aggregate concrete: Test Results. National Research Council Canada, Internal Report, No.573.

Lie T.T, Chabot M. (1990). A method to predict the fire resistance of circular concrete filled hollow steel columns. Journal of Fire Protection Engineering, 2(4):111-126.

Lie T.T, Iwin R.J, Chabot M. (1991). Factors affecting the fire resistance of circular hollow steel columns filled with plain concrete. National Research Council Canada, Internal Report, No.612.

Lie T.T. (1992). Structural fire protection: Manual of Practice, ASCE Manual and Reports on Engineering Practice No.78, American Society of Civil Engineers, New York.

Lie T.T, Chabot M. (1992). Experimental studies on the fire resistance of hollow steel columns filled with plain concrete. National Research Council Canada, Internal Report No. 611.

References

Lie T.T, Iwin R.J. (1992). Fire resistance of rectangular hollow steel columns filled with bar-reinforced concrete. National Research Council Canada, Internal Report, No.631.

Lie T.T, Dawod I. (1992). Factors affecting the fire resistance of square hollow steel columns filled with plain concrete. National Research Council Canada, Internal Report, No.633.

Lie T.T, Denham E.M.A. (1993). Factors affecting the fire resistance of square hollow steel columns filled with bar-reinforced concrete. National Research Council Canada, Internal Report, No.650.

Lie T.T, Denham E.M.A. (1993). Factors affecting the fire resistance of circular hollow steel columns filled with bar-reinforced concrete. National Research Council Canada, Internal Report, No.651.

Liew J.Y.R. (2004). Performance Based Fire Safety Design of Structures-A Multi-Dimensional Integration. Advances in Structural Engineering Vol. 7 No. 4.

Liew J.Y.R. (2004). Buildable design of multi-storey and large span steel structures. Journal of Steel Structures, Korean Society of Steel Structures, 4(2): 53–70.

Liew, J.Y.R, Xiong, D.X. (2009). Effect of preload on the axial capacity of concrete-filled composite columns. Journal of Constructional Steel Research, 65(3):709-722.

Lu H, Zhao X.L, Han L.H. (2009). Fire behaviour of high strength self-consolidating concrete filled steel tubular stub columns. Journal of Constructional Steel Research, 65: 1995-2000.

Lu H, Zhao X.L, Han L.H. (2010a). Testing of self-consolidating concrete-filled tubular stub columns exposed to fire. Journal of Constructional Steel Research, 66: 1069-1080.

Lu H, Han L.H, Zhao X.L. (2010b). Fire performance of self-consolidating concrete filled double skin steel tubular columns: experiments. Fire Safety Journal, 45: 106-115.

232

Malhotra H.L. (1956). The effect of temperature on the compressive strength of concrete. Magazine of Concrete Research, 8(22): 85-94.

Mao X.Y, Kodur V.K.R. (2011). Fire resistance of concrete encased steel columns under 3- and 4-side standard heating. Journal of Constructional Steel Research 67:270–280.

Menzel C.A. (1943). Tests of the fire resistance and thermal properties of solid concrete slabs and their significance. Proceedings, American Society for Testing and Materials (ASTM), 43:1099-1153.

Morita T, Saito H, Kumagai H. (1992). Residual mechanical properties of high strength concrete members exposed to high temperature-Part 1: Test on material properties. Summaries of Technical Papers of Annual Meeting, Architectural Institute of Japan, Niigata, August.

Naus D.J. (2006). The effect of elevated temperature on concrete material and structures-a literature review. Oak Ridge National Laboratory.

Ouedraogo E, Roosefid M, Prompt N, Deteuf C. (2011). Refractory concretes uniaxial compression behaviour under high temperature testing conditions. Journal of the European Ceramic Society, 31: 2763-2774.

Outinen J., Kaitila O., Mäkeläinen P. (2001). High-temperature testing of structural steel and modeling of structures at fire temperatures. Research Report. No. TKK-TER-23, Helsinki Univ. of Technology Laboratory of Steel Structures, Helsinki, Finland.

Patterson N.L, Zhao X.L, Wong M.B, Ghojel J, Grundy P. (1999). Elevated temperature testing of composite columns. Department of Civil Engineering, Monash University, Melbourne, Australia.

Poh K.W. (2001). Stress-strain-temperature relationships for structural steel. Journal of Materials in Civil Engineering, 13(5):371-379.

Purkiss J.A. (1988). Developments in the fire safety design of structural steelwork, Journal of Construction Steel Research, 11(1/3):149-173.

References

RILEM Technical Committee. (2007). Recommendation of RILEM TC 200-HTC: mechanical concrete properties at high temperatures – modeling and applications, Part 2: stress-strain relation. Materials and Structures, 40:855-864.

Romero M.L, Moliner V, Espinos A, Ibanez C, Hospitaler A. (2011). Fire behavior of axially loaded slender high strength concrete-filled tubular columns. Journal of Constructional Steel Research, 67: 1953-1965.

Rubert A, Schaumann P. (1988).Critical temperatures of steel columns exposed to fire. Fire Safety Journal, 13:39-44.

Saemann J.G, Washa G.W. (1957). Variation of motar and concrete properties and temperature. ACI Journal, Proceedings 54(5): 385-397, November.

Sakumoto Y, Okada T, Yoshida M, Tasaka S. (1994). Fire resistance of concrete-filled, fire-resistant steel-tube columns. Journal of Materials in Civil Engineering, 169-184.

Schaumann P, Bahr O, Kodur, V.K.R. (2006). Numerical studies on HSC-filled steel columns exposed to fire. Welding in the World, v50, SPEC. ISS.: 373-378.

Schaumanna P, Kodur V.K, Bahr O. (2009). Fire behaviour of hollow structural section steel columns filled with high strength concrete. Journal of Constructional Steel Research, 65: 1794-1802.

Schneider, R. (2010). Constitutive equations and empirical creep law of structural steel S460 at high temperatures. Structures in Fire-Proceedings of the Sixth International Conference, SiF'10, 703-710.

Sullivan P.J.E, Sharshar R. (1992). Performance of concrete at elevated temperatures (as measured by the reduction in compressive strength). Fire Technology, 28(3):240-250, August.

Tan K. H, Tang C. Y. (2004). Interaction model for unprotected concrete filled steel columns under standard fire conditions. Journal of Structural Engineering, 130(9):1405–1413.

Tanyildizi H, Coskun A. (2008). The effect of high temperature on compressive strength and splitting tensile strength of structural lightweight concrete containing fly ash. Construction and Build Materials, 22:2269-2275.

Tao W.C. (2006). Heat transfer. Northwestern Polytechnic University Press (Chinese).

Totten G.E. (2007). Steel heat treatment handbook-2nd Edition. CRC Press, Taylor & Francis Group.

Tubal C. (1984). Hardening, tempering and heat treatment for model engineers. Argus Books Ltd.

Wang C.M, Wang C.Y, Reddy J.N. (2004). Exact solutions for buckling of structural members. CRC Press.

Wang Y. C. (1997). Some Considerations in the Design of Unprotected Concrete-Filled Steel Tubular Columns under Fire Conditions. Journal of Constructional Steel Research, 44(3):203-223.

Wang Y.C. (2000). A simple method for calculating the fire resistance of concrete-filled CHS columns. Journal of Constructional Steel Research 54:365–386.

Wang Y.C. (2002). Steel and composite structures: behavior and design for fire safety. Spon Press, London and New York.

Webb J, Peyton J.J. (1990). Composite concrete filled steel tube columns. Proceedings of the Structural Engineering Conference, the Institute of Engineers, Australia, 181-185.

Xiao J.Z., Falkner H. (2006). On residual strength of high-performance concrete with and without polypropylene fibers at elevated temperatures. Fire Safety Journal, 41:115-121.

Yu M, Zha X.X, Ye J.Q, Li Y. (2010). Fire responses and resistance of concrete-filled steel tubular frame structures. International Journal of Structural Stability and Dynamics, Vol. 10, No. 2: 253-271.

Zeiml M., Leithner D., Lackner R., Mang H.A. (2006). How do polypropylene fibers improve the spalling behavior of in-situ concrete? Cement and Concrete Research, 36:929-942.

Zha X.X. (2003). FE analysis of fire resistance of concrete filled CHS columns. Journal of Constructional Steel Research, 59:769–779.